

Automatic classification of patient status based on ventilation data

P Marx



[orcid.org/ 0000-0002-6141-9943](https://orcid.org/0000-0002-6141-9943)

Dissertation accepted in fulfilment of the requirements for the
degree *Master of Engineering in Computer and Electronic
Engineering* at the North-West University

Supervisor: Prof H Marais

Co-supervisor: Prof MJ Grobler

Graduation: December 2023

Student number: 29703662

ABSTRACT

Mechanical ventilation therapy is a vital treatment for a myriad of pulmonary complications. Optimally administering it demands continuous expert supervision from pulmonologists due to the patient's dynamic health status and requirements. The pulmonologist adjusts the mechanical ventilator's settings to meet the patient's ventilation needs. The needs are derived from performing skilled, invasive manoeuvres to determine the status of the respiratory system parameters, such as airway resistance and static compliance. However, practicality and insufficient expertise lead to error-prone, periodical assessments, leading to suboptimal mechanical ventilation and resource management. Therefore, a need persists for continuously monitoring and logging a patient's pulmonary parameters in a way that allows limited pulmonologists to still supervise patients practically at scale. An automated solution is proposed that assesses the mechanical ventilation time-series data to classify the ventilation mode, derive the ventilator settings, extract informative features, and predict the status of the airway resistance and static compliance. The ventilation mode classifier produced prediction accuracies over 99%. After a breath's ventilation mode is predicted, its corresponding ventilator settings determined, and its informative features extracted, the airway resistance and static compliance are predicted with accuracies exceeding the capabilities of human experts at over 98%. These findings not only show that autonomous monitoring of a patient's health status is possible, but also that it could be done continuously with high accuracies. Logging the patient's health status on a per-breath-basis at scale can reduce unnecessary complications and improve the efficiency of pulmonologist-to-patient ratios in demanding circumstances (such as the Covid-19 pandemic).

Keywords: Mechanical Ventilation, Condition Monitoring, Airway Resistance, Static Compliance, Volume-Controlled Ventilation, Pressure-Controlled Ventilation, Automation

LIST OF ABBREVIATIONS AND ACRONYMS

A-a Gradient – Arterial Alveolar Gradient-

ABG – Arterial Blood Gas

ARDS – Acute Respiratory Distress Syndrome

AC – Assist Control

APC – Adaptive Pressure Control

APRV – Airway Pressure Release Ventilation

ASV – Adaptive Support Ventilation

ATP – Adenosine Triphosphate

AVAPS – Average Volume-Assured Pressure Support

BiPAP – Bi-Positive Airway Pressure

BNN – Bi-Layered Neural Network

CMV – Continuous Mandatory Ventilation

COPD – Chronic Obstructive Pulmonary Disease

COVID-19 – Coronavirus Disease of 2019

CPAP – Continuous Positive Airway Pressure

CPU – Central Processing Unit

CSV – Comma Separated Values

DB – Database

EPAP – Expiratory Positive Airway Pressure

ETT – Endotracheal Tube

F-V – Flow-Volume Loop

FDI – Fault Detection and Isolation

GB – Giga Byte

GPR – Gaussian Process Regression

GUI – Graphical User Interface

HFOV – High-Frequency Oscillatory Ventilation

HMI – Human-Machine Interface

ICU – Intensive Care Unit

IPAP – Inspiratory Positive Airway Pressure

IQR – Interquartile Range

IRV – Inverse Ratio Ventilation

kNN – k-Nearest Neighbours

M – Million

MB – Mega Byte

ML – Machine Learning

MMV – Mandatory Minute Ventilation

MNN – Medium Neural Network

MV – Mechanical Ventilator

MV-P – Mechanical Ventilator-Patient

NAVA – Neurally Adjusted Ventilatory Assist

NIPPV – Non-Invasive Positive Pressure Ventilation

NN – Neural Network

NNN – Narrow Neural Network

NWU – North-West University

Obs – Obstacles

P-V Loop – Pressure-Volume Loop

PAV – Proportional Assist Ventilation

PC – Pressure-Controlled

PDF – Probability Distribution Function

PEEP – Positive End-Expiratory Pressure

PID – Product-Integrator-Differentiator

PPV – Positive Pressure Ventilation

PRVC – Pressure Regulated Volume Control

PS – Pressure Support

PSV – Pressure Support Ventilation

RC – Resistor-Capacitor

RIC – Resistor-Inductor-Capacitor

RMSE – Root Mean Square Error

RR – Respiratory Rate

SARS-CoV-2 – Severe Acute Respiratory Syndrome Coronavirus 2

SIMV – Synchronous Intermittent Mandatory Ventilation

SVM – Support Vector Machine

TB – Tuberculosis

TNN – Tri-Layered Neural Network

UPS – Uninterruptable Power Supply

UUID – Universally Unique Identifier

VC – Volume-Controlled

VCC – Volume-Controlled Constant Flow

VCD – Volume-Controlled Decelerating Ramp Flow

WNN – Wide Neural Network

WOB – Work of Breathing

ZEEP – Zero End-Expiratory Pressure

LIST OF SYMBOLS

Age – Patient Age in Years

C – Capacitance

C – Compliance

C_b – Bronchial Compliance

C_{calc} – Calculated Compliance

C_D – Dynamic Compliance

C_e – Extrathoracic Compliance

C_g – Alveolar Compliance

C_i – Compliance of *i*th Branch

C_l – Lung Compliance

CO₂ – Carbon Dioxide

c_Q – Offset of Flow Rate Best Fit Line Function

C_{RS} – Respiratory System Compliance

C_S – Static Compliance

C_t – Tissue Compliance

C_{ve} – Viscoelastic Compliance

C_w – Chest Wall Compliance

E – Elastance

E_{RS} – Respiratory System Elastance

ERV – Expiratory Reserve Volume

ETT_{Size} – ETT Size

f – Frequency

FRC – Functional Residual Capacity

H_2O – Water

HCO_3 – Bicarbonate Level

$Height_{cm}$ – Height in Centimetres

I – Inertance

IBW_{Female} – Ideal Body Weight of Female

IBW_{kg} – Ideal Body Weight in Kilograms

IBW_{Male} – Ideal Body Weight of Male

IC – Inspiratory Capacity

I_{RS} – Respiratory System Inertance

IRV – Inspiratory Reserve Volume

K_1 – First Derivative Constant Coefficient

K_2 – Second Derivative Constant Coefficient

L – Characteristic Length or Pipe Inside Diameter

L – Inductance

L – Inertance

L_{aw} – Airway Inertance

L_t – Tissue Inertance

m_Q – Gradient of Flow Rate Best Fit Line Function

N – Number of Pressure Waveform Data Values

$n_{Transient_Breaths}$ – Number of Transient Breaths

O_2 – Oxygen

ρ – Fluid Density

P – Pressure

P_+ – Positive Pressure Relative to Baseline

P_0 – Baseline Pressure

P_1 – Lower Inflection Point

P_1 – Pressure in First State

P_2 – Pressure in Second State

P_2 – Upper Inflection Point

$PaCO_2$ – Arterial Blood Pressure of Carbon Dioxide

PAO_2 – Alveolar Blood Pressure of Oxygen

PaO_2 – Arterial Blood Pressure of Oxygen

P_{aw} – Airway Resistance

P_c – Compliance Pressure

PC_1 – First Pressure-Controlled Group

PC_2 – Second Pressure-Controlled Group

$P_{Driving}/\Delta P$ – Driving Pressure

P_I – Inertance Pressure

p_i – Pressure Waveform Data Value

PiO_2 – Pressure of Inspired Oxygen

P_{PIP} – Peak Inspiratory Pressure

$P_{Plateau}$ – Plateau Pressure

P_R – Resistance Pressure

P_{RS} – Respiratory System Pressure

Q – Flow Rate

q_{fit} – Flow Rate Best Fit Line Function

$q_{fit_corrected}$ – Corrected Flow Rate Best Fit Line Function

$q_{fit_corrected_i}$ – Corrected Flow Rate Best Fit Line Function Data Values

q_i – Flow Rate Waveform Data Values

Q_{max} – Peak Expiratory Flow

Q_{max} – Peak Inspiratory Flow

q_{Qmax} – Point of Initial Maximum Flow Rate

q_{Qzero} – Point of Zero-Flow Rate

Q_τ – Expiratory Flow at One Time Constant

Q_{TH} – Cut-Off Flow Threshold

R – Resistance

R^2 – Coefficient of Determination

R_{aw} – Airway Resistance

R_c – Central Resistance

$R_{circuit}$ – Mechanical Ventilator Circuit Resistance

R_e – Reynold's Number

R_{ETT} – Endotracheal Tube Resistance

R_{EXP} – Expiratory Resistance

R_i – Resistance of i^{th} Branch

R_{INSP} – Inspiratory Resistance

R_p – Peripheral Resistance

RR – Respiratory Rate

R_{RS} – Respiratory System Resistance

R_t – Tissue Resistance

RV – Residual Volume

R_{ve} – Viscoelastic Resistance

SaO_2 – Oxygen Saturation

STD – Standard Deviation

$Surface_{Data}$ – Area Above the Unit Data Curve

$Surface_{Reference}$ – Triangular Area

t – Time

TD_{Female} – Trachea Diameter of Female

TD_{Male} – Trachea Diameter of Male

TD_{mm} – Trachea Diameter in Millimetres

T_e – Expiratory Time

T_{EIHM} – End-Inspiratory Hold Manoeuvre Duration

T_i – Inspiratory Time

TLC – Total Lung Capacity

TL_{Female} – Trachea Length of Female

TL_{Male} – Trachea Length of Male

TL_{mm} – Trachea Length in Millimetres

T_{Period} – Breath Cycle Period

t_{Qmax} – Timestamp at Point of Initial Maximum Flow Rate

t_{Qzero} – Timestamp at Point of Zero-Flow Rate

τ_{RC} – RC Time Constant

t_{Trim} – Trim Time

μ – Dynamic Viscosity

μ – Mean of Pressure Waveform Data Values

μ_{data} – Mean of Waveform Data

$\mu_{fit_corrected}$ – Mean of Corrected Flow Rate Best Fit Line Function Data Values

μ_{q_fit} – Mean of Flow Rate Best Fit Line Function

u – Velocity of Airflow

V – Volume

v – Kinematic Viscosity

$V(t)$ – Volume Scalar

$\dot{V}(t)$ – First Derivative of Volume Scalar

$\ddot{V}(t)$ – Second Derivative of Volume Scalar

V_1 – Volume in First State

V_2 – Volume in Second State

VC – Vital Capacity

V_M – Minute Ventilation

V_T – Tidal Volume

X_C – Capacitive Reactance

X_L – Inductive Reactance

Z_C – Capacitive Impedance

Z_L – Inductive Impedance

Z_{L+C} – Inductive and Capacitive Impedance

Z_R – Resistive Impedance

Z_{Total} – Total Impedance

TABLE OF CONTENTS

ABSTRACT	I
LIST OF ABBREVIATIONS AND ACRONYMS.....	II
LIST OF SYMBOLS.....	VI
LIST OF TABLES.....	XX
LIST OF FIGURES.....	XX
CHAPTER 1 – INTRODUCTION.....	1
2.1 Problem Context.....	1
2.2 Problem Statement.....	2
2.3 Research Purpose.....	2
2.4 Project Objectives.....	3
2.4.1 Primary Objective	3
2.4.2 Secondary Objectives.....	3
2.5 Project Delimitations	3
2.5.1 Patient Delimitations	4
2.5.2 Mechanical Ventilation Use Cases.....	4
2.6 Thesis Structure	5
2.7 Chapter Summary.....	5
CHAPTER 2 – BACKGROUND	6
3.1 Basics of the Spontaneous Breathing Patient	6
3.1.1 The Respiration Process	6
3.1.2 The Respiratory Tract.....	7
3.1.3 Mechanics of Spontaneous Breathing	7
3.2 Modelling the Respiratory System	9
3.2.1 Respiratory System Analogies.....	9

3.2.2	Respiratory System Mechanical Parameters	10
3.2.3	Standard Respiratory System Models.....	11
3.2.4	Single-Compartment RC Model	14
3.3	Basics of Mechanical Ventilation.....	18
3.3.1	Reasons for Use	18
3.3.2	Mechanical Ventilator-Patient (MV-P) Circuit	18
3.3.3	Mechanics of Positive-Pressure Ventilation (PPV).....	19
3.3.4	The Breathing Cycle	20
3.3.5	Waveform Scalars	21
3.3.6	Hysteresis Loops	22
3.4	Ventilation Techniques	23
3.4.1	Types of Ventilation	23
3.4.2	Categories of Ventilation Modes	24
3.4.3	More on Primary Modes of Ventilation	25
3.4.4	More on Controlled Modes of Ventilation	26
3.5	Relevant Mechanical Ventilator-Patient (MV-P) Parameters	29
3.5.1	Patient Biological and Anthropometric Parameters	29
3.5.2	Pulmonary System Parameters	30
3.5.3	Ventilator Circuit Parameters	32
3.5.4	Mechanical Ventilator (MV) Parameters.....	33
3.6	Ventilated Patient Condition Monitoring	35
3.6.1	Chemical Data-Driven Indicators	35
3.6.2	MV Data-Driven Indicators.....	35
3.7	Machine Learning	42
3.7.1	The Machine Learning (ML) Process	42
3.7.2	Different ML Types	43
3.7.3	Different Machine Learning Techniques.....	43
3.7.4	Regression Algorithms.....	44

3.7.5	Validation Methods	45
3.7.6	Algorithm Performance Parameters.....	45
3.8	Chapter Summary.....	46
	CHAPTER 3 – DATA ACQUISITION.....	47
4.1	Acquiring Appropriate Datasets	47
4.2	Develop a MATLAB® Simulink® Model	48
4.2.1	Existing MATLAB® Simulink® MV-P Model Draft	49
4.2.2	Capturing Patient’s Biological and Anthropometric Parameters	50
4.2.3	Implementing the Endotracheal Tube (ETT)	52
4.2.4	Variable Baseline Pressure Expiratory Valve.....	53
4.2.5	Dynamic Patient Mechanical Parameters	54
4.2.6	Biting of the Endotracheal Tube (ETT).....	56
4.2.7	Implementing the Expiratory Hold Manoeuvre Option	57
4.2.8	Implementing the VC Flow Pattern Options	57
4.2.9	The Expanded MATLAB® Simulink® MV-P Model	59
4.3	Verify MATLAB® Simulink® MV-P Model	60
4.3.1	Qualitative Verification of the MV-P Model.....	60
4.3.2	Quantitative Verification of the MV-P Model.....	63
4.3.3	Sensitivity of the Model.....	66
4.4	Generate Appropriate Data Using the MATLAB® Simulink® MV-P Model	69
4.4.1	Scoping the Dataset	69
4.4.2	Normal Parameter Ranges	70
4.4.3	Defining the Dataset Spectrum	72
4.4.4	The Adapted Mechanical Ventilator (MV) Data Generator Application	73
4.4.5	Optimising the MV Data Generator Application.....	75
4.4.6	Data Generation Expedition.....	76
4.5	Chapter Summary.....	77

CHAPTER 4 – STATISTICS-BASED VENTILATION MODE CLASSIFIER	79
5.1 Identify Statistically Descriptive Shape Parameters	79
5.1.1 Extract the Standard Deviation (<i>STD</i>) Parameter from the Pressure Waveform	80
5.1.2 Extract the Coefficient of Determination Parameter from the Flow Rate Waveform	81
5.2 Analyse the Statistical Parameters to Develop a Ventilation Mode Classifier	82
5.2.1 Implement a Hard Decision Boundary Classifier	82
5.2.2 Implement a Kernel Probability Distribution Function Classifier	86
5.2.3 Implement a Hybrid Ventilation Mode Classifier.....	88
5.3 Evaluate the Classifier	91
5.3.1 Evaluating the 3D Distribution Graphs of the False Negative Predictions	91
5.3.2 Evaluating the Confusion Matrix	93
5.4 Chapter Summary.....	94
CHAPTER 5 – FEATURE EXTRACTION LAYER	95
6.1 Feature Extraction of the Independent Variables	95
6.1.1 Baseline Pressure Feature Extraction.....	96
6.1.2 Maximum Inspiratory Flow Feature Extraction	97
6.1.3 Tidal Volume Feature Extraction.....	98
6.1.4 Inspiratory Time Feature Extraction	99
6.1.5 Peak Inspiratory Pressure Feature Extraction.....	100
6.2 Feature Engineering of the Dependent Variables	101
6.2.1 Time Constant Feature Extraction	101
6.2.2 Expiratory Flow at One Time Constant	102
6.2.3 Flow-Volume Loop Scoop Gradient	102
6.2.4 Flow-Volume Loop Scoop Resistance Analysis	103
6.3 Storing the Extracted Features into a Database.....	105
6.4 Chapter Summary.....	106

CHAPTER 6 – MACHINE LEARNING REGRESSION MODELS	107
7.1 Training the Regression Models	108
7.2 Evaluating the Regression Models.....	110
7.2.1 Regression Models for Predicting Resistance for VCC	112
7.2.2 Regression Models for Predicting Resistance for VCD	114
7.2.3 Regression Models for Predicting Compliance for VCC	115
7.2.4 Regression Models for Predicting Compliance for VCD	116
7.2.5 Discussion of the Chosen Models.....	117
7.3 Deploying the Regression Models	118
7.4 Chapter Summary.....	119
CHAPTER 7 – CONCLUSION AND FUTURE WORK	120
8.1 Project Conclusions	120
8.1.1 Introduction.....	120
8.1.2 Background	121
8.1.3 Data Acquisition.....	122
8.1.4 Statistics-Based Ventilation Mode Classifier	123
8.1.5 Feature Extraction Layer	124
8.1.6 Machine Learning Regression Models.....	124
8.1.7 Project Final Result	125
8.2 Suggested Future Work.....	125
BIBLIOGRAPHY	126
ANNEXURE 1 – SIMULINK MODEL	131
ANNEXURE 2 – GITHUB REPOSITORY.....	132
ANNEXURE 3 – IFAC WC 2023 SUBMISSION 1589	132
ANNEXURE 4 – ENLARGED FIGURES.....	133

LIST OF TABLES

Table 2-1: Respiratory System Hydraulic-, Mechanical- and Electrical Analogies	9
Table 2-2: Lookup Table of Standard Endotracheal Tube (ETT) Sizes	32
Table 3-1: Lookup Table of Standard Endotracheal Tube (ETT) Sizes	51
Table 3-2: Results for Sweeping the Resistance During VCC.....	64
Table 3-3: Results for Sweeping the Compliance During VCC	65
Table 3-4: Resistance Range Results for the Inspiratory Phase Experiments	66
Table 3-5: Reynold's Number Values for Flow Rate Sweep	67
Table 3-6: Resistance Range Results for the Inspiratory Phase Experiments	68
Table 4-1: Summary of the Unidentified Tallies of Each Mode Before Implementing Decision Boundaries	82
Table 4-2: Summary of the Unidentified Tallies of Each Mode After Implementing the First Set of Hard Decision Boundaries.....	83
Table 4-3: Summary of the Unidentified Tallies of Each Mode After Implementing the Second Set of Hard Decision Boundaries.....	84
Table 4-4: Summary of the Unidentified Tallies of Each Mode After Implementing the Final Set of Hard Decision Boundaries.....	85
Table 4-5: Summary of the True Positive Accuracies for Each Ventilation Mode	87
Table 4-6: Summary of the True Positive Accuracies for Each Ventilation Mode	88
Table 4-7: Confusion Matrix for Training Results of the Proposed Hybrid Classifier	90
Table 4-8: Confusion Matrix for Training Results of the Proposed Hybrid Classifier	93
Table 4-9: True Positive and False Positive Accuracies for Each Ventilation Mode After Evaluation	93
Table 5-1: Root Mean Squared Error Summary for Baseline Pressure Feature Extraction per Ventilation Mode	96

Table 5-2: Root Mean Squared Error Summary for Maximum Inspiratory Flow Feature Extraction	97
Table 5-3: Root Mean Squared Error Summary for Tidal Volume Feature Extraction	98
Table 5-4: Root Mean Squared Error Summary for Inspiratory Time Feature Extraction	99
Table 5-5: Root Mean Squared Error Summary for Peak Inspiratory Pressure Feature Extraction	100
Table 6-1: Performance Summary of Regression Models for Predicting Resistance for VCC Mode.....	112
Table 6-2: Resulting Ranked Shortlist of Regression Models for Predicting Resistance for VCC Mode.....	112
Table 6-3: Performance Summary of Regression Models for Predicting Resistance for VCD Mode.....	114
Table 6-4: Resulting Ranked Shortlist of Regression Models for Predicting Resistance for VCD Mode.....	114
Table 6-5: Performance Summary of Regression Models for Predicting Compliance for VCC Mode.....	115
Table 6-6: Resulting Ranked Shortlist of Regression Models for Predicting Compliance for VCC Mode.....	115
Table 6-7: Performance Summary of Regression Models for Predicting Compliance for VCD Mode.....	116
Table 6-8: Resulting Ranked Shortlist of Regression Models for Predicting Compliance for VCD Mode.....	116
Table 6-9: Performance Summary of the Chosen Regression Models.....	117
Table 6-10: Local and Total Root Mean Square Error Percentages per Use Case	118
Table 6-11: Performance Summary of the Chosen Regression Models.....	119
Table 7-1: Performance Summary of the Chosen Regression Models.....	124

LIST OF FIGURES

Figure 1-1: Flow Diagram of the Delimitated Project Overview	3
Figure 1-2: Thesis Structure of the Chapters and Sections per Chapter	5
Figure 2-1: Composition of the Respiratory Tract	7
Figure 2-2: Spontaneous Breathing Process: Inhalation (a) and Exhalation (b)	8
Figure 2-3: Single-Compartment Models: RC (a), RIC (b) and Extended RIC Model (c)	11
Figure 2-4: Multi-Compartment: Series RC- (a), Parallel RC- (b) and Parallel RIC Bi-Compartmental Model (c)	12
Figure 2-5: Advanced Descriptive Models: Mead Model (a), Dubois Model (b) and Viscoelastic Model (c)	13
Figure 2-6: Single-Compartment RC Respiratory Tract Model: Hydraulic Representation (a), Mechanical Schematic (b) and Electrical Circuit (c)	14
Figure 2-7: Phasor Diagrams of Adding Impedance Components	15
Figure 2-8: Graph of the Charging and Discharging Curves for an RC Circuit	17
Figure 2-9: Schematic of the Mechanical Ventilator-Patient Circuit.....	18
Figure 2-10: Mechanical Ventilator-Patient Interfaces: Nasal Prongs (a), Tight-Fitting Face Mask (b), Endotracheal Tube (c) and Tracheostomy Tube (d)	19
Figure 2-11: Pressure Waveform Depicting the Breathing Cycle Phases: Initiation Phase (a), Inspiratory Phase (b), Plateau Phase (c) and Expiratory Phase (d)	20
Figure 2-12: Mechanical Ventilator-Patient Circuit with Pressure Annotations	20
Figure 2-13: Waveform Scalars: Proximal Airway Pressure, Flow Rate and Volume	21
Figure 2-14: Hysteresis Loops: Pressure-Volume Loop (a) and Flow-Volume Loop (b)	22
Figure 2-15: Pressure Waveform Scalars of CPAP (a) and BiPAP (b)	23
Figure 2-16: Pressure Waveform Scalars of the Primary Ventilation Modes: Control Mode (a), AC/CMV Mode (b) and SIMV Mode (c)	25

Figure 2-17: The Flow Patterns of Volume-Controlled Ventilation: Constant Flow (a), Sinusoidal Flow (b), Accelerating Ramp Flow (c), Decelerating Ramp Flow (d), Exponential Increasing Flow (e) and Exponential Decreasing Flow (f).....	27
Figure 2-18: The Three Most Common Modes for Controlled Ventilation: Volume-Controlled Constant Flow Mode (a), Volume-Controlled Decelerating Ramp Flow Mode (b) and Pressure-Controlled Mode (c).....	28
Figure 2-19: Volume Waveform Depicting Pulmonary System Volumes and Capacities.....	31
Figure 2-20: Example Illustration of the Mechanical Ventilator's Human-Machine Interface	34
Figure 2-21: Pressure Waveform Scalar of Ineffective Triggering Effort	36
Figure 2-22: Pressure Waveform Scalar of Auto-Triggering/Auto-Cycling	37
Figure 2-23: Pressure Waveform Scalar of Delayed Triggering	37
Figure 2-24: Pressure Waveform Scalar of Reverse Triggering.....	37
Figure 2-25: Pressure Waveform Scalar of Flow Starvation/Insufficient Pressurization	37
Figure 2-26: Pressure Waveform Scalar of Delayed Cycling	38
Figure 2-27: Pressure Waveform Scalar of Premature/Short Cycling	38
Figure 2-28: The Three Waveform Scalars of Double-Triggering/Breath Stacking.....	38
Figure 2-29: Pressure-Volume Loop of Inflection Points	39
Figure 2-30: Volume Waveform Scalar of Air Leak	39
Figure 2-31: Flow-Volume Loop of Secretion Build Up: Normal Case (a), Inspiratory Tube Secretions (b) and Expiratory Tube Secretions (c)	39
Figure 2-32: Pressure Waveform Scalar of Increasing Compliance	40
Figure 2-33: Varying Compliance Loops: Pressure-Volume (a) and Flow-Volume Loop (b)....	41
Figure 2-34: Pressure Waveform Scalar of Increasing Resistance	41
Figure 2-35: Varying Resistance Loops: Pressure-Volume (a) and Flow-Volume Loop (b).....	41
Figure 2-36: Diagram of the Machine Learning Process	42

Figure 3-1: Drafted Simulink® Medical Ventilator with Lung Model Schematic Diagram	49
Figure 3-2: Graphical User Interface (GUI) for Specifying the Patient’s Simulation Parameters for the Mechanical Ventilator-Patient Simulink® Model	50
Figure 3-3: Settings Recorded in ET Tube Block Parameters.....	51
Figure 3-4: Settings Recorded in Trachea Block Parameters	52
Figure 3-5: Settings Recorded in Lungs Block Parameters.....	52
Figure 3-6: Settings Recorded in Y-Piece Block Parameters	52
Figure 3-7: Recorded Expiratory Valve’s Pressure Reference Block Parameter Settings	53
Figure 3-8: Graphical User Interface (GUI) for Specifying the Mechanical Ventilator Simulation Parameters for the Mechanical Ventilator-Patient Simulink® Model.....	53
Figure 3-9: The Schematic Diagram of The RC Subsystem Block.....	54
Figure 3-10: Graphical User Interface (GUI) for Specifying the Patient’s Mechanical Parameters for the Mechanical Ventilator-Patient Simulink® Model: Parameters for Configuring the Control Signals: Resistance (a) and Compliance (b).....	54
Figure 3-11: Waveform Scalars Resulting from Simulated Dynamic Lung Resistance.....	55
Figure 3-12: Waveform Scalars Resulting from Simulated Dynamic Lung Compliance.....	55
Figure 3-13: The Schematic Diagram of The Teeth Subsystem Block	56
Figure 3-14: Graphical User Interface (GUI) for Specifying the Patient’s Bite Intensity Parameters for the Mechanical Ventilator-Patient Simulink® Model (a) and Waveform Scalars Resulting from Simulated Dynamic Biting Intensity (b).....	56
Figure 3-15: Schematic Diagram of The Constant Flow Mechanical Ventilator Control Signal Subsystem.....	57
Figure 3-16: Schematic Diagram of The Decelerating Flow Mechanical Ventilator Control Signal Subsystem.....	57
Figure 3-17: Graphical User Interface for Specifying the Mechanical Ventilator Parameters for the Simulink® Model: Constant (a) and Decelerating Ramp Flow Pattern (b)	58

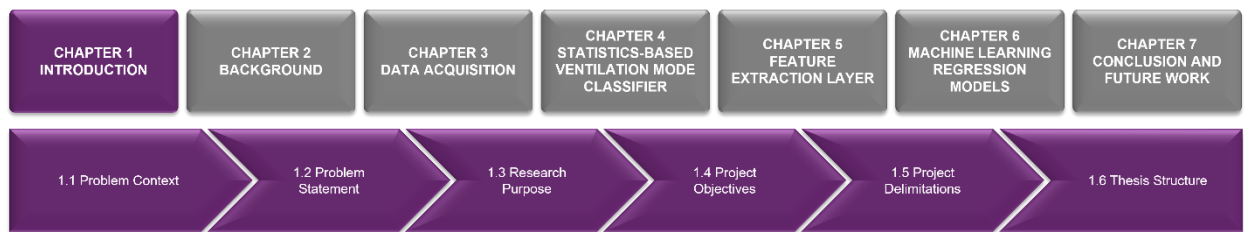
Figure 3-18: Waveform Scalars Resulting from Simulated Volume-Controlled Modes: Constant Flow Pattern (a) and Decelerating Flow Pattern (b)	58
Figure 3-19: The Schematic Diagram of the Expanded Simulink® Mechanical Ventilator-Patient Model	59
Figure 3-20: Graphical User Interface (GUI) for Specifying the Patient's Parameters, Mechanical Ventilator Settings and Complication Parameters for Simulating a Session Instance of the Mechanical Ventilator-Patient Simulink® Model	59
Figure 3-21: Pressure Waveform of Isolated Pressure Component due to Resistance	60
Figure 3-22: Pressure Waveform of Isolated Pressure Component due to Compliance	60
Figure 3-23: Waveform Scalars for Varying Resistance.....	61
Figure 3-24: Waveform Scalars for Varying Compliance	61
Figure 3-25: VCC Waveform Scalar Comparison of Actual Mechanical Ventilator Data with the Simulated Data.....	62
Figure 3-26: VCD Waveform Scalar Comparison of Actual Mechanical Ventilator Data with the Simulated Data.....	62
Figure 3-27: Mechanical Ventilator Settings and Resulting Waveform Output for VCC.....	63
Figure 3-28: Mechanical Ventilator Settings and Resulting Waveform Output for VCD	63
Figure 3-29: GUI of the Input Parameters for Sweeping the Resistance during VCC	64
Figure 3-30: Waveform Scalar and Complication Signal Outputs for Sweeping Resistance in VCC.....	64
Figure 3-31: GUI of the Input Parameters for Sweeping the Compliance during VCC	65
Figure 3-32: Waveform Scalar and Complication Signal Outputs for Sweeping Compliance in VCC.....	65
Figure 3-33: Graphical User Interface (GUI) for Specifying the Patient's Parameters, Mechanical Ventilator Settings and Complication Parameters for Simulating a Sweep of Session Instances of the Mechanical Ventilator-Patient Simulink® Model	73

Figure 3-34: Photo of Data Generation Expedition Utilising 60 Machines in the NWU's Computer Laboratory	76
Figure 4-1: Waveform Scalars' Generalised Shapes per Ventilation Mode: Volume-Controlled Constant Flow Pattern Ventilation (a), Volume-Controlled Decelerating Flow Pattern Ventilation (b) and Pressure-Controlled Ventilation (c).....	79
Figure 4-2: Graphical Illustrations of the Inspiratory Phase Standard Deviation Feature Extraction from Each Ventilation Mode's General Pressure Waveform Scalar Shapes.....	80
Figure 4-3: Graphical Illustrations of the Inspiratory Phase Coefficient of Determination Feature Extraction from Each Ventilation Mode's General Flow Rate Waveform Scalar Shapes.....	81
Figure 4-4: Boxplots of the Coefficient of Determination (a) and Standard Deviation (b) for Each Mode.....	82
Figure 4-5: Boxplots of the Coefficient of Determination (a) and Standard Deviation (b) for Each Mode After Implementing the First Set of Hard Decision Boundaries.....	83
Figure 4-6: Boxplots of the Coefficient of Determination (a) and Standard Deviation (b) for the Remaining Modes of Ventilation After Implementing the Second Set of Hard Decision Boundaries.....	84
Figure 4-7: Boxplots of the Coefficient of Determination (a) and Standard Deviation (b) for the Remaining Modes of Ventilation After Implementing the Final Set of Hard Decision Boundaries.....	85
Figure 4-8: Kernel Fitted Functions of the Coefficient of Determination Statistical Parameter for the VCC (a), VCD (b) and PC (c) Ventilation Modes	86
Figure 4-9: Kernel Fitted Functions of the Standard Deviation Statistical Parameter for the VCC (a), VCD (b) and PC (c) Ventilation Modes.....	86
Figure 4-10: Graph of the Kernel Probability Distribution Functions for Ventilation Mode Classification Given the Coefficient of Determination	87
Figure 4-11: Graph of the Kernel Probability Distribution Functions for Ventilation Mode Classification Given the Standard Deviation	87

Figure 4-12: Graph of the Kernel Probability Distribution Functions Given the Coefficient of Determination	88
Figure 4-13: Graph of the Kernel Probability Distribution Functions Given the Standard Deviation	88
Figure 4-14: 3D Distribution Graphs of the False Negative Predictions for the VCC Mode	89
Figure 4-15: 3D Distribution Graphs of the False Negative Predictions for the VCD Mode	89
Figure 4-16: 3D Distribution Graphs of the False Negative Predictions for the VCD Mode	90
Figure 4-17: 3D Distribution Graphs of the False Negative Predictions for the VCC Mode	91
Figure 4-18: 3D Distribution Graphs of the False Negative Predictions for the VCD Mode	92
Figure 4-19: 3D Distribution Graphs of the False Negative Predictions for the PC Mode.....	92
Figure 5-1: Boxplots of Baseline Pressure Feature for VCC (a), VCD (b) and PC (c)	96
Figure 5-2: Boxplots of Maximum Inspiratory Flow Feature for VCC (a) and VCD (b).....	97
Figure 5-3: Boxplots of Tidal Volume Feature for VCC (a) and VCD (b)	98
Figure 5-4: Boxplots of Inspiratory Time Feature for PC	99
Figure 5-5: Boxplots of Peak Inspiratory Pressure Feature for Baseline Pressures of 0 cmH ₂ O (a), 5 cmH ₂ O (b), 10 cmH ₂ O (c) and 15 cmH ₂ O (d)	100
Figure 5-6: Flow-Volume Loops of Varying Compliance for VCC (a) and VCD (b).....	102
Figure 5-7: Expiratory Segments of Flow-Volume Loops of Varying Compliance for VCC (a) and VCD (b)	102
Figure 5-8: Flow-Volume Loops of Varying Resistance for VCC (a) and VCD (b)	103
Figure 5-9: Expiratory Segments of Flow-Volume Loops of Varying Resistance for VCC (a) and VCD (b)	103
Figure 5-10: Normalised Segments of Flow-Volume Loops of Varying Resistance for VCC (a) and VCD (b)	103
Figure 5-11: Illustration of the Data Surface (Grey) and the Reference Surface (Blue)	104

Figure 5-12: Illustration of the Data Point Distribution Transformation: Original (a) and Interpolated (b)	104
Figure 5-13: Entity Relationship Diagram of the Database	105
Figure 6-1: Diagram of the Machine Learning Process	107
Figure 6-2: Photo of Training Machine Learning Regression Models in the NWU's Computer Laboratory	109
Figure 6-3: Boxplots of the RMSE Percentage for VCC (a) and VCD (b)	110
Figure 6-4: Boxplots of the Training Speed for VCC (a) and VCD (b)	110
Figure 6-5: Boxplots of the Overfitting Index for VCC (a) and VCD (b)	111
Figure 6-6: Boxplots of the Prediction Speed for VCC (a) and VCD (b)	111
Figure 6-7: Boxplots of the Model Size for VCC (a) and VCD (b)	111
Figure 6-8: Response Plots for Bi-Layered Neural Network (a), Medium Tree (b) and Linear SVM (c)	113
Figure 6-9: Predicted vs Actual Plots for Bi-Layered Neural Network (a), Medium Tree (b) and Linear SVM (c)	113
Figure 6-10: Residual Plots for Bi-Layered Neural Network (a), Medium Tree (b) and Linear SVM (c)	113
Figure 6-11: Residual Plots for Predicting the Resistance for VCC (a) and VCD (b)	117
Figure 6-12: Residual Plots for Predicting the Compliance for VCC (a) and VCD (b)	117
Figure 6-13: Predicted vs Actual Resistance Results for VCC (a) and VCD (b)	118
Figure 6-14: Predicted vs Actual Compliance Results for VCC (a) and VCD (b)	118
Figure 7-1: Flow Diagram of the Delimitated Project Overview	120
Figure 7-2: Project Final Result Diagram	125

CHAPTER 1 – INTRODUCTION



In this chapter, an overview of the project and the context behind it is introduced to the reader. First, the context of the problem is conveyed to clarify why the problem is worthwhile and relevant. Second, the project's problem statement is defined, representing the macro mission this project attempts to address. Third, the research purpose is stated, which should attempt to contribute to solving the problem. Fourth, the project's objectives are stipulated, leading to the methodology of this project's proposed solution. After that, the project is scoped to keep the solution focused and effective. Finally, a brief overview of the thesis structure is conveyed.

1.1 Problem Context

Mechanical ventilation is a form of breath support administered to a patient experiencing respiratory distress caused by a pulmonary complication [1]. These complications comprise diseases and protection against secretion build-up that could suffocate the patient, for example, during sedation, where the patient cannot clear their throats as needed [1], [2]. Pulmonary diseases are vast and can lead to respiratory failure. Some of the most prevalent respiratory diseases include acute respiratory distress syndrome (ARDS), chronic obstructive pulmonary disease (COPD), and tuberculosis (TB), which all form part of the world's top ten leading causes of death, independent of the countries' developmental status [3]. Another recent example is the SARS-CoV-2 virus, which led to the ongoing Coronavirus pandemic (COVID-19) [4]. When respiratory diseases severely flare up, mechanical ventilation therapy becomes vital and, unfortunately, unavailable to many people due to insufficient resources (hospital housing space, mechanical ventilators (MVs) and oxygen tanks are limited) [4].

A pulmonologist ensures appropriate MV settings, which control the ventilation protocol to meet the patient's ventilatory demands [5]. Pulmonologists derive these demands with their analytical expertise regarding the standard waveform scalar data, hysteresis loops, and other tests [6]. However, the patient's health status is dynamic [7] and requires frequent check-ups to ensure optimal ventilation, which could reduce unnecessary complications, improve recovery rates, and improve resource management. However, limited human experts inevitably lead to errors (hospital pulmonary physicians are finite and have limited time, energy, and memory) [8].

During a respiratory examination of the patient's health status, pulmonologists either use accurate, invasive manoeuvres [9] or rely on expensive MVs with non-invasive technology that produces approximation parameters [6] (dynamic vs static indicators) to determine the patient's health status. Since the pulmonologists likely have multiple patients in different rooms, these check-ups are done periodically. Logs of the patient's respiratory status are not automatically performed and are either memorised by the pulmonologists or manually recorded into some logging system. Since pulmonologists are still human, overwhelming numbers of assigned patients or even human negligence could lead to mishaps. These include impaired memory, misplacing logs, faulty manual calculations, estimated measurements, and omitted/irregular inspections. These mishaps can lead to suboptimal recovery rates and inefficient equipment, resources, and hospitalisation space management.

Therefore, a need persists to automatically monitor and log a patient's pulmonary parameters automatically and continuously while allowing the limited pulmonologists to supervise patients practically at scale. Such a solution would optimise resource management, reduce unnecessary complications, and allow remote monitoring for future pandemics of contagious diseases.

1.2 Problem Statement

The main gap this project attempts to address is to empower pulmonologists with a monitoring tool and not automatically adjust the ventilator's settings since doing so will require high-level ethical approval and could lead to severe adverse effects if unforeseen scenarios occur [10]. Therefore, the project's problem statement is defined below.

Mechanical ventilation of patients can be vital yet unattainable or trivial when expertise, utilities or other resources are temporarily exhausted due to inefficient management or availability thereof. Can mechanical ventilator waveform data be used to automatically classify patient health statuses to improve the sustainability of these limited resources and possibly prevent avoidable deaths?

1.3 Research Purpose

The research purpose of this project is to develop improved management of limited expertise, utilities, and other resources to improve efficiency in attending to ventilated patients.

Fulfilling the research purpose could, in turn, lead to fewer mishaps regarding monitoring and logging the patient's respiratory health status. If implemented at scale, it could also help pulmonologists prioritise patients requiring more immediate attention, increase recovery rates, and effectively increase the turnover capabilities of hospitals in future pulmonary pandemics.

1.4 Project Objectives

To fulfil the research purpose and, in turn, contribute to solving the problem, the project objectives are stipulated, which will guide the methodology for the project. These objectives are divided into the primary objective and secondary objectives. The primary objective takes priority, and the secondary objectives are optional if time allows attempting to address them.

1.4.1 Primary Objective

Using simulated, real-time, mechanically ventilated, patient waveform data as input, develop a continuous, health-status monitoring, fault detection and isolation (FDI) expert system.

1.4.2 Secondary Objectives

- Develop a continuous, quantified health-status parameter indicator.
- Develop a scalable one-to-many version of the system.

1.5 Project Delimitations

The delimitations of the project need to be stipulated to keep the scope from creeping. Since the project requires access to mechanical waveform data, the first constraint placed on the project is to minimise the tasks leading up to the data acquisition. Therefore, either existing datasets will be used, or new datasets will be created, i.e., developing the hardware (MV and sensors) falls outside this project's scope. Also, the project need not surpass the point of developing a continuous, quantified health-status parameter indicator. After obtaining the time-series MV waveform data, the other main steps are to develop an independent MV settings analyser, a health indication analyser that utilises the dependent patient interaction, and a respiratory status FDI quantifier. The pulmonologist will then interpret the quantified outputs and arrive at their expert conclusion of the patient's health status classification (see Figure 1-1).

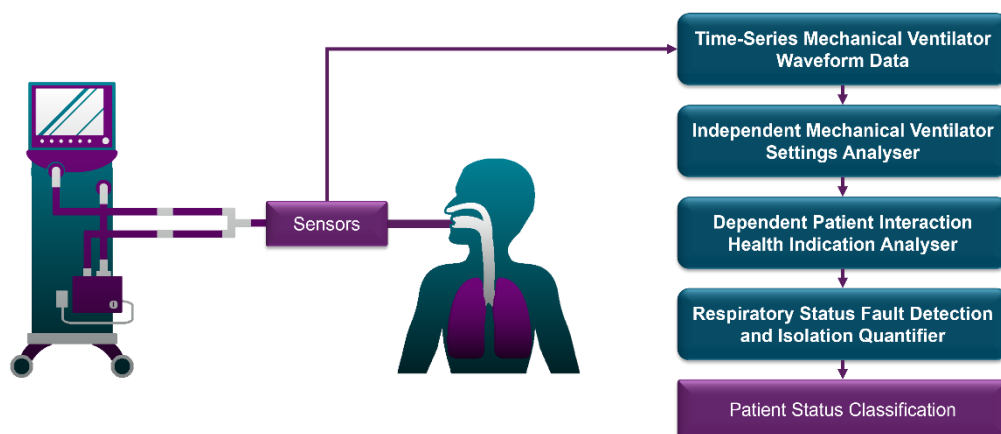


Figure 1-1: Flow Diagram of the Delimited Project Overview

1.5.1 Patient Delimitations

A patient's biological and anthropometric data considerably affect the mechanical ventilation parameters [11]–[14] and, thus, the ventilation protocol. It would be sensible to attempt to keep the patient's identity as deterministic as possible to solidify the project's findings for at least a specific patient identity and state.

A census of the Americas was done in 2019, which showed that the age-standardised deaths per population were higher for men than for women (42.2 deaths vs 31.0 deaths per 100 000 population) [15]. Therefore, the generic patient's sex is chosen as male for this project.

The median ages per country increase as technology and infrastructure advance [16]. Africa has the lowest age median at 18 years, and Europe has the highest median at 42 years. The other countries have medians ranging from 31 to 35 years [17]. Since this research purpose will be more appropriate in countries where the population is large and hospital resource management suffers most, an age closer to that of Africa's median age is appropriate. Therefore, the age chosen for the patient identity in this project is 25 years.

Also, the normal height distribution of adult men aged 18 between 2008 and 2012 was done based on large group studies and concluded a median height of 178.4 cm with a standard deviation of 7.1 cm [18]. The height data are for 18-year-olds, which does not matter, since this age is post full growth. As the patient's height increases above the median, the project's findings will become more inclusive but less accurate for the average case. Therefore, one standard deviation above average (84th percentile) is chosen as the patient's height (186 cm).

Since pulmonologists will benefit from this technology's contribution most in severe cases, such as ICU patients who cannot communicate their discomfort and optimal mechanical ventilation is most desired, the patient is assumed to be sedated, intubated and supine [19].

Hence, the chosen patient is a 25-year-old male 186 cm in height, sedated, intubated and supine.

1.5.2 Mechanical Ventilation Use Cases

A cursory study showed that many different mechanical ventilation techniques and modes exist [13], [20]–[22]. Since this project only requires an answer to whether the automatic classification of a patient's health status is possible using ventilation data, at most, three modes are considered.

Finally, possible faults handleable by the proposed solution need not include the identification of secretions, condensation, or inappropriate ventilator settings. Only the patient's respiratory health status must be classified automatically.

1.6 Thesis Structure

The thesis comprises seven chapters (investigate Figure 1-2 for the detailed chapter layout). Chapter 1 is the current introductory chapter, where the project's problem, objectives and delimitations are provided. Chapter 2 provides the background for the chapter in the form of a literature study on the spontaneous breathing patient, mechanical ventilation theory and an overview of machine learning. Chapter 3 deals with how this project's dataset was acquired and why it is deemed appropriate. Chapter 4 describes the developmental process for the proposed statistics-based ventilation mode classifier. Chapter 5 discusses the feature extraction layer. Chapter 6 conveys how the machine learning regression models were trained and evaluated. Finally, Chapter 7 delivers the project conclusions and the suggested future work.

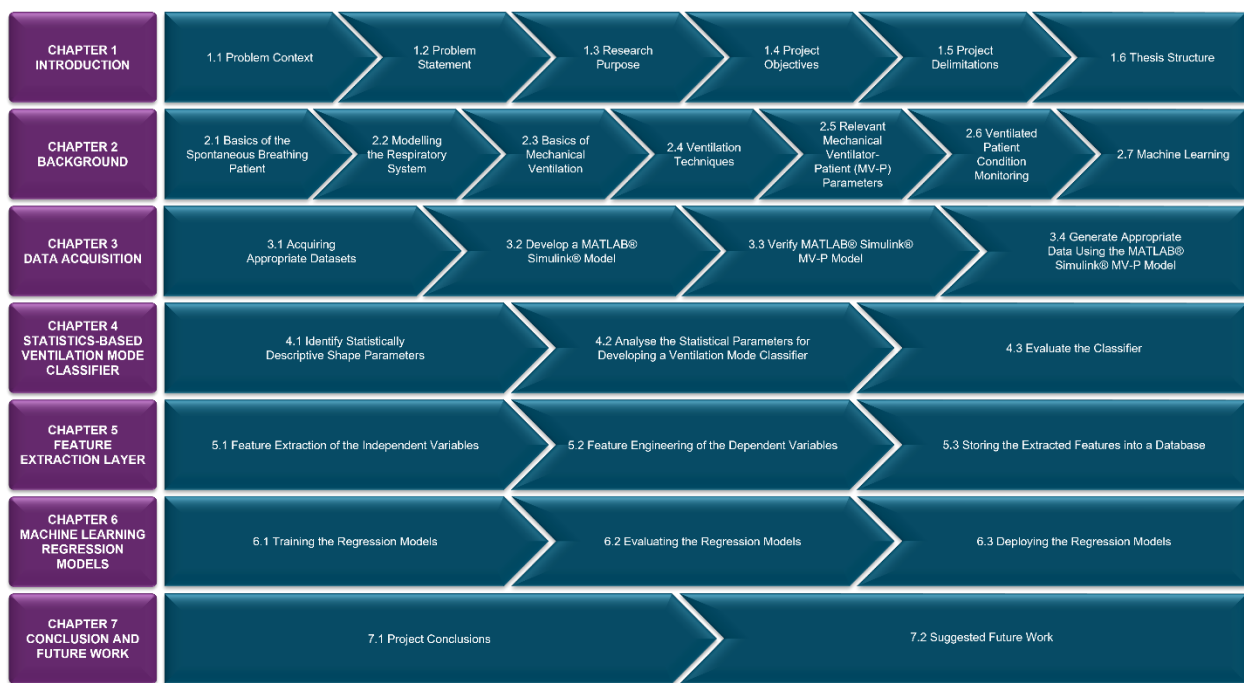
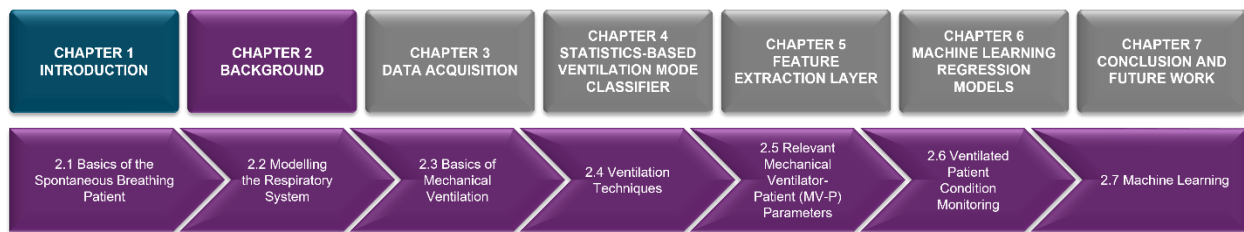


Figure 1-2: Thesis Structure of the Chapters and Sections per Chapter

1.7 Chapter Summary

This chapter was an introduction to the project reported throughout this thesis. Firstly, the problem context was portrayed; a need persists in monitoring and logging a patient's pulmonary parameters automatically and continuously to mainly optimise resource management. After that, the problem statement and research purpose were clearly depicted. This was followed by the project's objectives that would guide the methodology proposed to solve the problem. The delimitations of the project were also provided; the chosen patient identity is a 25-year-old male of 186 cm in height, sedated, intubated and supine, and at most, only three ventilation modes must be considered for this project. Finally, a description of the thesis' structure was provided to acquaint the reader with what could be expected in this thesis.

CHAPTER 2 – BACKGROUND



This chapter is a literature study on the human respiratory system and other mechanical ventilation process topics. The first section provides a background on the basics of the spontaneous breathing patient. The second section deals with modelling the respiratory system. The third section is about understanding the basics of mechanical ventilation for better comprehension of the following section, which explains the different ventilation techniques. After grasping the basics of the respiratory system and the ventilation process separately, another section describes the relevant mechanical ventilator-patient (MV-P) parameters to explain their interaction. After obtaining the background on how an MV-P system works and how to set it up, the subsequent section discusses the condition monitoring techniques. The final background section briefly overviews relevant machine learning literature for this project.

2.1 Basics of the Spontaneous Breathing Patient

This section discusses the basic knowledge of spontaneous breathing patients. Firstly, the respiration process, its necessity, and its consequences are mentioned. Secondly, an overview of the respiratory tract is provided. Finally, the spontaneous breathing mechanics are reviewed.

2.1.1 The Respiration Process

Aerobic respiration is the chemical process during which an organism converts oxygen (O_2) and glucose into carbon dioxide (CO_2), water and energy (see equation (2-1)) [23]. The resulting energy is stored on a cellular level as adenosine triphosphate (ATP). When appropriate, the organism uses ATP to sustain life processes such as transmitting nerve impulses, contracting muscles, generating cells, and synthesising protein [24]. Therefore, respiration is a vital process for maintaining a living organism. However, one of the by-products of this process is CO_2 , which could cause carbon dioxide poisoning (side effects include convulsions, coma, or death) if concentrations remain high ($>10\%$) for prolonged periods [25]. Therefore, the organism must properly regulate its gas composition concentrations (O_2 and CO_2) to survive.



Regulating the gas composition concentrations of a respiratory system that continually performs aerobic respiration involves supplying the system with O₂ and removing CO₂, referred to as ventilation [1]. When an organism performs ventilation without aid, it is called spontaneous breathing [26]. Spontaneous breathing relies on the organism's respiratory tract, diaphragm and other muscles in and around the thorax (the intercostal muscles or chest muscles) [21], [27].

2.1.2 The Respiratory Tract

The respiratory tract acts as a channel (for gas transmission) and a dispersed container (for temporarily storing a breath during the dynamic respiratory process). The respiratory tract is thus the interface between the organism and the environment for gas exchange. Figure 2-1 illustrates that the tract comprises the nasal cavity (a), oral cavity (b), pharynx (c), larynx (d), trachea (e), bronchi (f) and lungs (g). The lungs, in turn, include the bronchiole and alveoli. The latter are small inflatable containers where aerobic respiration occurs on a cellular level, interfacing with the bloodstream (gas diffusion) through microscopic capillaries [10], [21], [27].

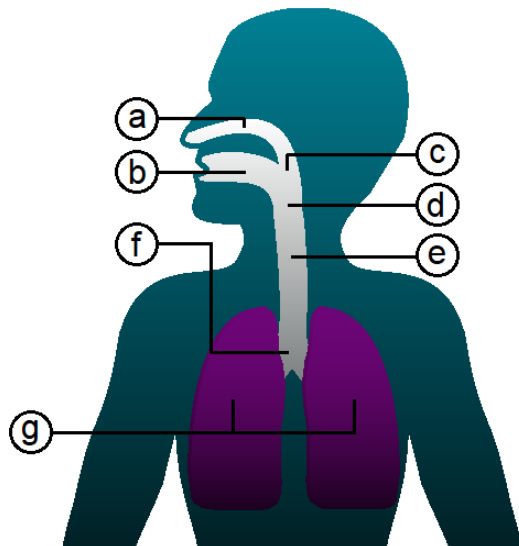


Figure 2-1: Composition of the Respiratory Tract

2.1.3 Mechanics of Spontaneous Breathing

The respiratory tract needs to receive (inhale) O₂ and expel (exhale) CO₂ during the respiratory process. During spontaneous breathing, inhalation by the organism is achieved through the activation of muscles (specifically the diaphragm and the intercostal muscles) [21], [27]. When the diaphragm contracts, it expands the volume capacity occupied by the respiratory tract (thoracic cavity) in a vertical direction. When the external intercostal muscles contract, the ribcage rises and extends the thoracic cavity's horizontal circumference. Both movements cause an increase in the housing volume of the respiratory system [28].

According to Boyle's law (equation (2-2)) [29], a confined gas with constant temperature (deviation effects are negligible during breathing) has a constant product between volume and pressure.

$$P_1 V_1 = P_2 V_2 \quad (2-2)$$

Therefore, volume is inversely proportional to the pressure (equation (2-3)).

$$P \propto \frac{1}{V} \quad (2-3)$$

Since the housing volume of the thoracic cavity increases during inhalation, the pressure inside the respiratory system (P_{RS}) decreases. When the reduced P_{RS} becomes less than the end-expiratory pressure (baseline pressure – P_0), equilibrium of the pressures will commence the moment the containers become connected, i.e., no obstructions between the environment and the lungs (patent airway). Equilibrium of the pressures is achieved as airflow commences into the lungs (Figure 2-2 (a)). This gas inhalation procedure is called negative-pressure ventilation [1], [30] and can also be mimicked by enclosing the thoracic cavity inside a negatively pressurised chamber [20].

Spontaneous exhalation (exhalation by the organism) can be active or passive. The former is achieved by utilising additional muscles to force the gas out of the lungs [13], [27], and the latter, by simply relaxing the muscles that extend the thorax [13], [27]. In either case, the thoracic capacity decreases, and P_{RS} increases. When P_{RS} exceeds P_0 , the flow rate is reversed (air flows in the opposite direction, i.e., out of the patient's lungs, as illustrated in Figure 2-2 (b)).

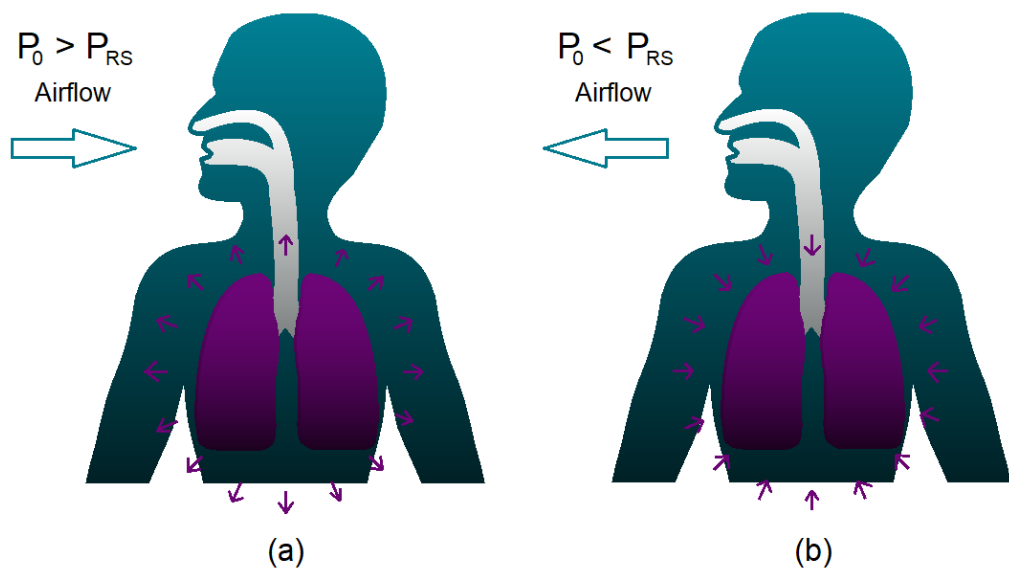


Figure 2-2: Spontaneous Breathing Process: Inhalation (a) and Exhalation (b)

2.2 Modelling the Respiratory System

This section discusses standard models of the respiratory system. Thus, it is a critical review of previously published existing solutions for pulmonary models, which is important for later ventilation data generation purposes. Firstly, analogies are presented for a more intuitive understanding of the respiratory system. Secondly, the mechanical parameters that characterise the system are mentioned. Thirdly, the most common models are investigated. Finally, the single-compartment RC model and its equations are conveyed.

2.2.1 Respiratory System Analogies

As mentioned in Section 2.1.2, the respiratory system can be interpreted as a channel for gas transmission and a dispersed container to store a breath temporarily. When a change in pressure occurs between two points within the guided system, air flows from the point of higher pressure to the point of lower pressure. Therefore, air (the substance) flows through a pipe (the channel) with a resulting resistance. Since the air is comprised of matter, an inertial, lagging effect to the change in velocity (change in flow rate) is present – the inertance. Also, a lung (the container) stores a certain amount of air at a given pressure, which means that the volume of the lungs and the pressure is directly proportional to each other – an elastic characteristic [6].

As air is stored in the hydraulic domain, so is a charge stored in the electrical domain. Pressure differences drive airflow, as do potential differences drive current. Just as the pipes introduce resistance to the airflow, the conductors introduce resistance to the current. Also, as the air lags during sudden changes in flow rate (inertance), so does current (inductance). Finally, the air is stored in an elastic container, and the charge is stored in a capacitor (inspect Table 2-1) [7], [31].

Table 2-1: Respiratory System Hydraulic-, Mechanical- and Electrical Analogies

	Hydraulic Domain	Mechanical Translatory Domain	Electrical Domain
	Air	Matter	Charge
	Pressure	Force	Voltage
	Flow Rate	Velocity	Current
Parasitic Element	Resistance	Resistance	Resistance
	Inertance	Mass	Inductance
	Elastance	Spring	Capacitance

2.2.2 Respiratory System Mechanical Parameters

Section 2.2.1 describes how a respiratory system can be characterised by its mechanical properties [7], [32], represented by the parasitic elements [33]. These elements are:

- Resistance (R – measured in $\text{cmH}_2\text{O}\cdot\text{s/L}$)
- Elastance (E – measured in $\text{cmH}_2\text{O/L}$) or its inverse – Compliance (C – measured in $\text{L}/\text{cmH}_2\text{O}$)
- Inertance (I – measured in $\text{cmH}_2\text{O}\cdot\text{s}^2/\text{L}$)

Since the respiration process is cyclical with a dynamic supply of air (flow rate is time-variant), the frequency and shape of the flow rate's cycles cause compliance and inertance to add to the respiratory system's total impedance [7]. Electrical literature [33] can be leveraged in its complementary electrical domain to inspect the effects of these parasitic elements on the system.

The impedance from the resistive component in the electrical domain is independent of frequency, and thus, the magnitude stays the same. The magnitude of airway resistance can range from normal levels (around $1 \text{ cmH}_2\text{O}\cdot\text{s/L}$) to high levels (more than $18 \text{ cmH}_2\text{O}\cdot\text{s/L}$) [13].

Compliance's effects on the system can be compared to the impedance caused by an equivalent capacitive component. The impedance from the capacitance is given by equation (2-4) [33]. The magnitude of an active patient's static lung compliance differs from that of a positive pressure ventilated (PPV) patient. For an active patient, normal ranges are from 0.1 to $0.4 \text{ L}/\text{cmH}_2\text{O}$ [34]. For a mechanically ventilated patient, it can range from 0.01 to $0.1 \text{ L}/\text{cmH}_2\text{O}$ [13].

$$(2-4) \quad |Z_C| = X_C = \frac{1}{2\pi f C}$$

Inertance's effect on the respiratory system can be derived from the impedance generated by the inductance of an equivalent electrical circuit and is calculable by equation (2-5) [33]. The magnitude of airway inertance can range from about 0.1 to $0.2 \text{ cmH}_2\text{O}\cdot\text{s}^2/\text{L}$ [35].

$$(2-5) \quad |Z_L| = X_L = 2\pi f L$$

For a sedated PPV patient, the respiratory rate (RR) is rarely set to more than 30 breaths/min, although standard mechanical ventilators can reach frequencies of up to 60 breaths/min [13]. Therefore, assuming a RR range of 10 – 30 breaths/min, the elements' impedance ranges are as follows: $Z_R = 1.0$ to 18.0Ω , $|Z_C| = 5.8$ to 17.4Ω , and $|Z_L| = 0.2$ to 0.5Ω . The effects of inertance for PPV patients are low enough that many models regard it as negligible [7].

2.2.3 Standard Respiratory System Models

Knowing that the respiratory system can be represented by the components of resistance, compliance and inertance, studies show that different models can be created by configuring these components in numerous ways. Some configuration possibilities arise, such as the number of compartments necessary, which components should be present in which compartments and if the models have appropriate representative complexity for the application at hand. A discussion of some of the most prevalent respiratory system models follows.

2.2.3.1 Single-Compartment Models

Since effective pulmonary mechanical properties are the leading interest for many applications, a simplistic approach by utilising only a single compartment is prevalent. These models all have one thing in common; they have a single storage component representing the lungs. They also share a common resistive component that represents airway resistance. The most simplistic version is the RC model (Figure 2-3 (a)), represented as a series RC circuit in the electrical domain [7]. This model is a good fit for normal ventilation with an RR of less than 30 breaths/min. However, it starts to deviate for patients with narrow airways (neonates or intubated patients) and those undergoing high-frequency oscillatory ventilation (HFOV) [7]. It is possible to compensate for this flaw by introducing a component of inertance. This implementation leads to the RIC model (Figure 2-3 (b)). Further improvement for more accurate representation can be accomplished by extending the model with a resistive component (R_p – the smaller airways) in parallel with the container (see Figure 2-3 (c)).

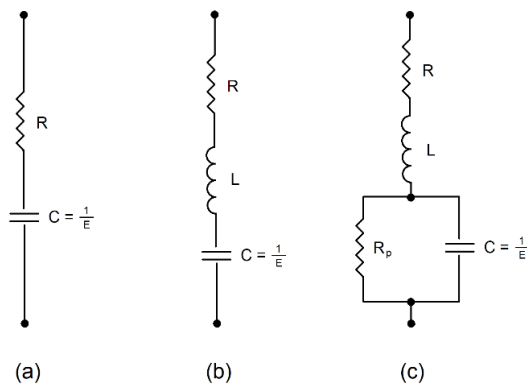


Figure 2-3: Single-Compartment Models: RC (a), RIC (b) and Extended RIC Model (c)

The mathematical equivalent for the models above follows the equation of motion, where a pressure differential is a driving component for airflow through the system [26]. The pressures comprising the total airway pressure (P_{aw} or P_{RS}) are pressure due to resistance (P_R), pressure due to compliance (P_C), pressure due to inertance (P_I), and the baseline pressure (P_0). Therefore, the airway pressure (at any given time, t) can be calculated by equation (2-6) [7], [34], [36].

(2-6)

$$P_{aw}(t) = P_I(t) + P_R(t) + P_C(t) + P_0$$

When considering these models, the mechanical parameters are assumed to be constant during a breath. Therefore, the respiratory model can be represented as a dynamic linear model solvable by differential equations (as represented by equation (2-7)) [7].

(2-7)

$$P_{aw}(t) = I_{RS} \cdot \ddot{V}(t) + R_{RS} \cdot \dot{V}(t) + E_{RS} \cdot V(t) + P_0$$

However, two variations of these models exist that introduced the concept of possible non-linearity regarding the parameters of resistance and elastance for the respiratory model [37]. These variations are the flow-dependent resistance model (equation (2-8)) and the volume-dependent elastance model (equation (2-9)), which are obtained by replacing the relevant pressure component with quadratic functions [7].

(2-8)

$$P_{aw}(t) = I_{RS} \cdot \ddot{V}(t) + [K_1 \cdot \dot{V}(t) + K_2 \cdot \dot{V}(t) \cdot |\dot{V}(t)|] + E_{RS} \cdot V(t) + P_0$$

(2-9)

$$P_{aw}(t) = I_{RS} \cdot \ddot{V}(t) + R_{RS} \cdot \dot{V}(t) + [E_1 \cdot V(t) + E_2 \cdot V^2(t)] + P_0$$

These variations are helpful when the scenario calls for models where the resistance changes significantly due to changes in the flow (as with turbulent cases) and where elastance changes significantly with changes in volume inside the lungs (as in the case of alveolar recruitment).

2.2.3.2 Multi-Compartment Models

The multi-compartment models incorporate the idea that each lung could have an independent resistance and elastance as denoted by R_i and C_i , respectively, where i is the number identifying the RC branch. Figure 2-4 (a) represents a series RC bi-compartmental model [7]. Figure 2-4 (b) is its parallel counterpart with R_{aw} 's additional component representing airway resistance [7]. Figure 2-4 (c) has the additional component L_{aw} representing the airway inertance [31].

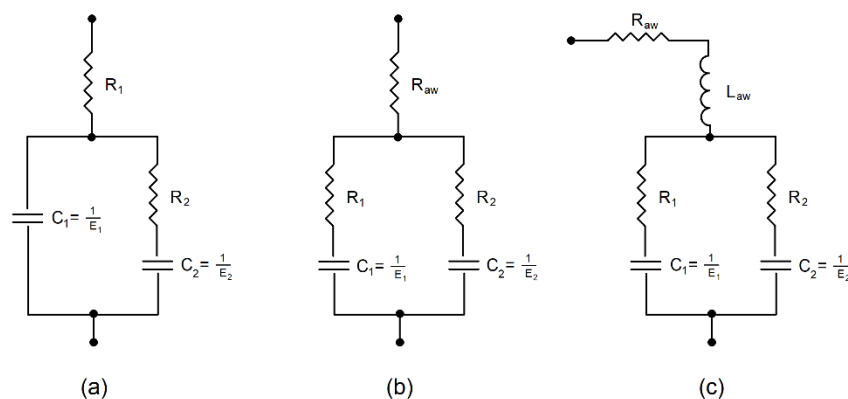


Figure 2-4: Multi-Compartment: Series RC- (a), Parallel RC- (b) and Parallel RIC Bi-Compartmental Model (c)

2.2.3.3 Advanced Descriptive Models

Some applications of pulmonary models require more descriptive characterization, which could aid in more elaborate condition monitoring opportunities.

2.2.3.3.1 The Mead Model

The Mead model comprises seven mechanical parameters. These include central resistance (R_c), Inertance (L), peripheral resistance (R_p), extrathoracic compliance (C_e), bronchial compliance (C_b), lung compliance (C_l) and chest wall compliance (C_w). This model is represented by Figure 2-5 (a) [31].

2.2.3.3.2 Dubois Model

Another model is used to characterise the pulmonary system's tissue mechanical parameters. This model is represented by Figure 2-5 (b) and is called the Dubois model, which has parameters for airway resistance (R_{aw}), airway inertance (L_{aw}), tissue resistance (R_t), tissue inertance (L_t), tissue compliance (C_t) and alveolar compliance (C_g) [31].

2.2.3.3.3 Viscoelastic Model

The tissue of the pulmonary system has viscous as well as elastic properties. Therefore, the viscoelastic model can prove helpful for occasions where such behaviour needs to be analysed (see Figure 2-5 (c)). The model comprises the airway resistance (R_{aw}), static compliance (C_s), viscoelastic resistance (R_{ve}) and viscoelastic compliance (C_{ve}) of the tissue [7], [31].

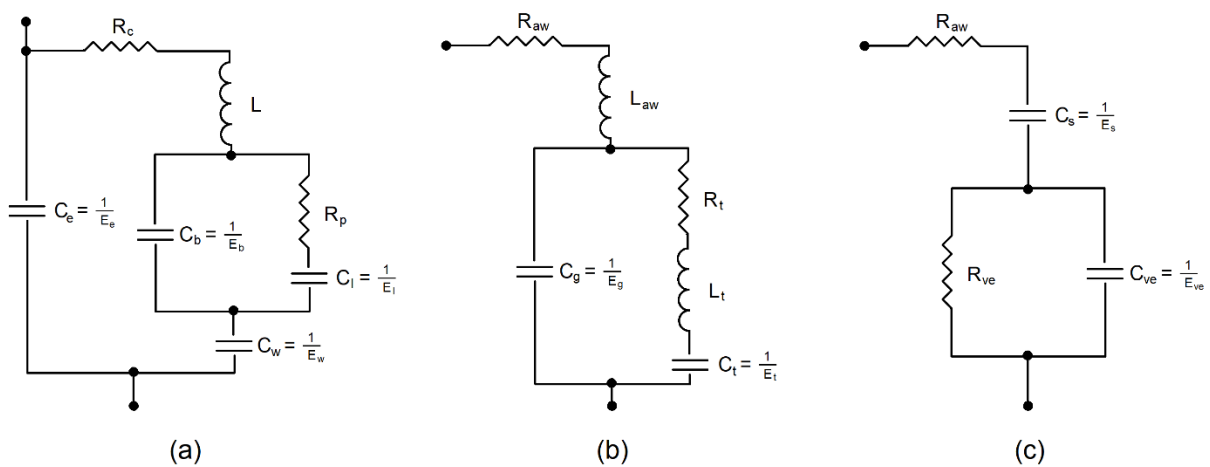


Figure 2-5: Advanced Descriptive Models: Mead Model (a), Dubois Model (b) and Viscoelastic Model (c)

2.2.4 Single-Compartment RC Model

As mentioned in Section 2.2.3.1, the single-compartment RC model is an electrical-based equivalent of the respiratory tract. It represents the airways (trachea and bronchi) with a single resistance and the lungs with a capacitor (hence, single-compartment model). The resistance and capacitor are placed in a series configuration. The mechanical equivalent can be represented by a spring (for elastance) and dashpot (for resistance). The respiratory tract's equivalent analogies are depicted in Figure 2-6 (a) the hydraulic representation, Figure 2-6 (b) the mechanical schematic, and Figure 2-6 (c) the electrical circuit [7], [31].

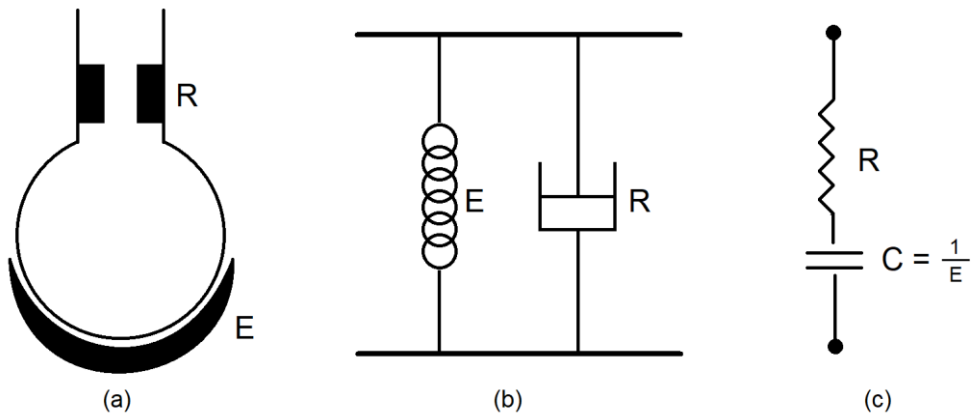


Figure 2-6: Single-Compartment RC Respiratory Tract Model: Hydraulic Representation (a), Mechanical Schematic (b) and Electrical Circuit (c)

2.2.4.1 Investigating the Significance of Inertance

The single-compartment RC model has good representative complexity in specific scenarios. When a mechanically ventilated patient's health condition is monitored in practice at the bedside, the equivalent resistance and compliance are the only mechanical parameters of interest to pulmonologists. However, that does not mean that the inertance of the patient's lungs is unimportant. In specific setups and test cases, the inertance of a patient's lungs can be used to monitor the condition of other pulmonary complications the patient might suffer.

The following equations are relevant when investigating the effect of inertance on the total impedance of the respiratory system [33].

$$Z_R = R \quad (2-10)$$

$$Z_L = j \cdot 2\pi f L \quad (2-11)$$

$$Z_C = -j \cdot \frac{1}{2\pi f C} \quad (2-12)$$

To calculate the total impedance of a RIC circuit, equation (2-13) is used.

$$(2-13) \quad Z_{Total} = Z_R + Z_L + Z_C$$

Figure 2-7 is a graphical representation of how the components contribute to the total impedance. It should be noted that Z_L is purely imaginary and positive (equation (2-11)) and that Z_C is also purely imaginary but negative (equation (2-12)) and is represented as such by Figure 2-7 (a). Therefore, adding these two components can only lead to a total imaginary component smaller or equal to the component with the larger magnitude. Thus, the presence of both components relatively increases the contribution of the real component (Figure 2-7 (b)). Finally, the superposition of the resulting phasors is Z_{Total} resulting in both a real and imaginary component when $|Z_L| \neq |Z_C|$ and $Z_R \neq 0$ (see Figure 2-7 (c)).

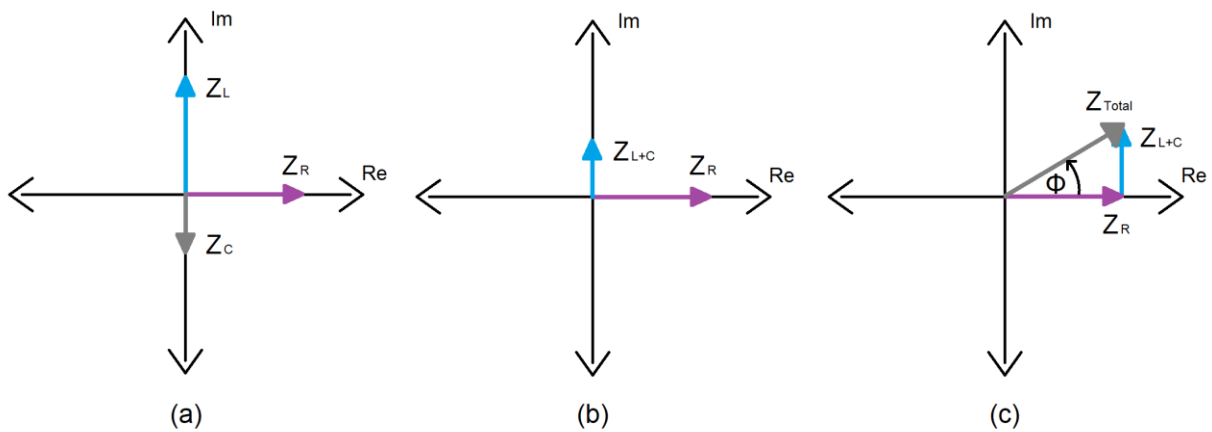


Figure 2-7: Phasor Diagrams of Adding Impedance Components

When the passive component's phasors are summed up and equals zero, Z_{Total} will only have a real component. However, when this is not the case, Z_{Total} will have real and imaginary components that follow equation (2-14).

$$(2-14) \quad Z_{Total} = Re(Z_{Total}) + j \cdot Im(Z_{Total})$$

The resulting magnitude of Z_{Total} is calculated with equation (2-15).

$$(2-15) \quad |Z_{Total}| = \sqrt{Re(Z_{Total})^2 + Im(Z_{Total})^2}$$

Since Z_R is purely real and both Z_L and Z_C are purely imaginary (reactance), equation (2-15) can be rewritten as equation (2-16).

$$(2-16) \quad |Z_{Total}| = \sqrt{Re(Z_R)^2 + Im(|Z_L| - |Z_C|)^2}$$

Therefore, when using the values of the usual ranges for each component of impedance from Section 2.2.2 ($Z_R = 1.0$ to 18.0Ω , $|Z_C| = 5.8$ to 17.4Ω , and $|Z_L| = 0.2$ to 0.5Ω), the relevance of the inertial component reduces even more when being mindful of equation (2-16).

However, it should be clear from this phenomenon that inertance can become more relevant in some cases. These cases are generally when the impedances change – the impedance of compliance decreases, and the impedance of inertance increases [7]. From equations (2-10) to (2-16), it can be derived that this will be the case when frequency increases (above 30 breaths/min become significant), when the compliance of the lungs decreases and when the inertance of the lungs increases. Some practical cases are that of neonates (short breaths with low compliance), HFOV procedures [38] or patients suffering from severe Acute Respiratory Distress Syndrome (ARDS) – low compliance.

It should also be mentioned that the inertance of the total patient-ventilator system increases and thus become more relevant when the patient is intubated. However, this is because of the presence of the endotracheal tube (ETT) and not a change in the patient's lung inertance. Studies show that the effects of inertance in an intubated patient-ventilator system are dominantly due to the ETT and not the patient [7]. Therefore, if an RC model is to be implemented in a patient-ventilator setup, including an ETT in the setup will increase the representative complexity at higher frequencies and render the effect of the absent inertance component of the lungs negligible [7].

2.2.4.2 Inevitable Drawbacks of Single-Compartment RC Model

Recall from Section 2.2.3 that other standard models were designed for specific applications requiring higher representative complexity.

One of the ideas implemented by these models was for the mechanical parameters to be non-linear (dynamic during a single breath). The single-compartment RC model is based on linear dynamic equations of motion and does not adhere to this requirement.

Another idea the other models were designed around is to allow multiple components for any mechanical parameter (such as multiple branches or compartments). This idea increases the resolution of area-specific investigable complications.

Since standard bedside monitoring of mechanically ventilated patients acquires a single reading for effective resistance and compliance of a breath, these drawbacks are irrelevant. The dynamic component of other models and any area-specific simulatable complication will be reduced to a single scalar reading for resistance and compliance. Therefore, the single-compartment RC model has sufficient representative complexity for such applications.

2.2.4.3 The RC Time Constant

In electrical theory, a characteristic parameter called the RC constant (τ_{RC}) becomes relevant when applying a step voltage differential input to an RC circuit. This parameter describes an RC circuit's time to charge or discharge by 63.2%. Since charging or discharging an RC circuit has a non-linear response (exponential), τ_{RC} is conveniently used to describe the five significant markers of the curve at stages 63.2%, 86.5%, 95.0%, 98.2% and 99.3% [33]. These stages are reached at multiples of the RC time constant (see Figure 2-8 for a graphical representation of the charging (purple curve) and discharging (blue curve) rates).

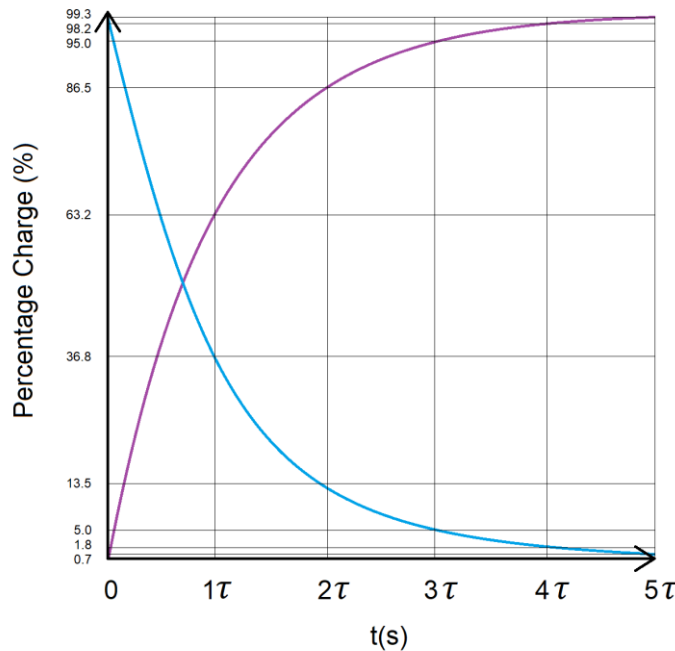


Figure 2-8: Graph of the Charging and Discharging Curves for an RC Circuit

Since the single-compartment RC model is based on the RC circuit in the electrical domain, these charge and discharge curves also apply to the respiratory system for a step pressure differential (ΔP) input. Therefore, these curves will result in the volume waveform for an instant pressure change held constant for at least five time constants.

The dynamic analysis of the volume delivered at a specific time is calculable by equations (2-17) and (2-18) during inspiration and exhalation, respectively [6], [33].

$$V(t) = C \cdot \Delta P \cdot e^{t/\tau_{RC}} \quad (2-17)$$

$$V(t) = C \cdot \Delta P \cdot e^{-t/\tau_{RC}} \quad (2-18)$$

2.3 Basics of Mechanical Ventilation

This section discusses the basic knowledge of mechanical ventilation. It covers the reasons for its use, the composition of the MV-P circuit, the mechanics behind PPV, the phases of the breathing cycle, the three waveform scalars and the hysteresis loops.

2.3.1 Reasons for Use

Mechanical ventilation is administered when a person cannot adequately control their muscles (inadequate work of breathing – WOB) to breathe spontaneously [1]. Typical cases are when a patient is sedated for the following reasons [19]:

- Respiratory Failure – Hypoxemic/Hypercapnic (Oxygenation- / Mechanical Complications)
- Airway Protection
- Imaging Agitated Patients or those Incapable of Laying Still

Not sedating a patient during these complications may cause them to become intolerable to the endotracheal tube or laying still in the supine position for extended periods. It may also cause ventilator desynchrony, suboptimal oxygenation and increased risk for patient safety [10]. Also, not intubating a patient under sedation could lead to secretion build-up in the airways or respiratory depression. The latter is possible since the neuromuscular control of the pharyngeal segment (upper airway) becomes impaired and could cause a collapse during negative-pressure ventilation [39]. MV, therefore, is a vital supportive procedure where the ventilator acts as a surrogate for performing artificial WOB.

2.3.2 Mechanical Ventilator-Patient (MV-P) Circuit

Referring to Figure 2-9, an MV-P circuit comprises the mechanical ventilator (MV) (a), patient (b), inhalation tube (c) with check valve (d), exhalation tube (e) with check valve (f), y-piece (g), patient interfacing component (h), airways (i) and lungs (j) [27].

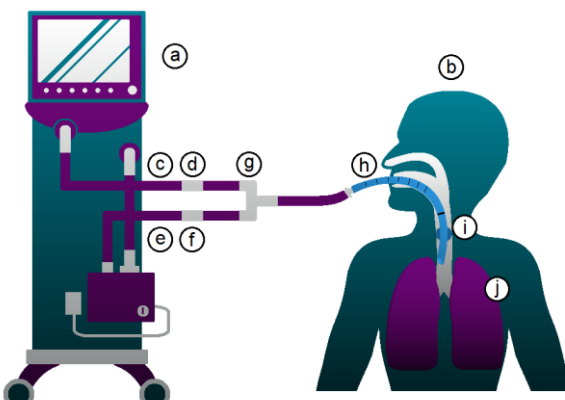


Figure 2-9: Schematic of the Mechanical Ventilator-Patient Circuit

The patient interfacing component can be any of the following options (Figure 2-10) [1], [40]:

- a) Nasal Prongs
- b) Tight-Fitting Face Mask
- c) Endotracheal Tube (ETT)
- d) Tracheostomy Tube

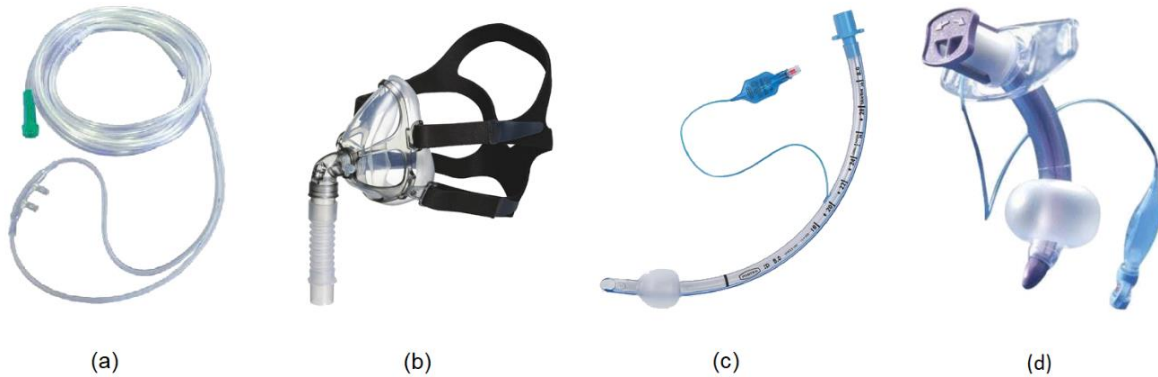


Figure 2-10: Mechanical Ventilator-Patient Interfaces: Nasal Prongs (a), Tight-Fitting Face Mask (b), Endotracheal Tube (c) and Tracheostomy Tube (d)

Nasal prongs and tight-fitting face masks are used for non-invasive ventilation, whereas endotracheal- and tracheostomy tubes are used for invasive ventilation procedures. The later cases are administered with a distribution of 75% and 25% to sedated patients.

2.3.3 Mechanics of Positive-Pressure Ventilation (PPV)

PPV is a type of mechanical ventilation procedure where an external air source with positive pressure (a relatively higher-pressure level than the resting respiratory pressure – P_{RS}) is applied to a patient [1], [30]. Here, the main driving component for ventilation is the increased external pressure rather than the vacuum caused by the decreased internal pressure (P_{RS}) generated by the respiratory muscles during spontaneous breathing. Due to the external pressure being higher than that of the respiratory system (once again), the same reasoning follows for gas flowing into the patient's lungs.

For exhalation to commence in the case of a sedated, mechanically ventilated patient whose respiratory muscles are inactive, P_{RS} must be higher than the applied ventilation pressure. Therefore, at the start of the exhalation phase, the applied external pressure must be decreased to accomplish a relatively higher pressure inside the patient's lungs. It can be accomplished by reducing the positive pressure source to baseline (passive exhalation) or generating a negative pressure (active). For almost all standard ventilation use cases, the passive method is utilised, and the resulting negative flow waveform depends on the RC constant [34] and MV circuit's properties.

2.3.4 The Breathing Cycle

Section 2.3.3 already described the procedure behind mechanical air flow during inspiration and expiration for PPV. The breathing cycle (depicted in Figure 2-11), comprises of four phases [10]:

- Initiation Phase
- Inspiratory Phase
- Plateau Phase
- Expiratory Phase

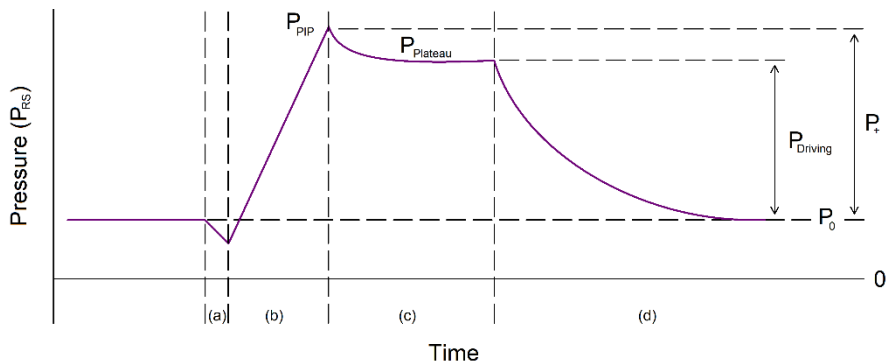


Figure 2-11: Pressure Waveform Depicting the Breathing Cycle Phases: Initiation Phase (a), Inspiratory Phase (b), Plateau Phase (c) and Expiratory Phase (d)

The initiation phase (triggered by an active patient) is identifiable by a slight pressure drop resulting from the negative pressure differential (w.r.t. baseline or end-expiratory pressure – P_0) generated by an active patient at the start of a breath. The MV senses the drop and enters the inspiratory phase by opening the inspiratory tube's check valve (1 in Figure 2-12) and closing the expiratory tube's check valve (2 in Figure 2-12). A pressure differential exists between P_+ and P_{RS} , causing air to flow into the patient's lungs until P_{RS} reaches the peak inspiratory pressure (P_{PIP}). The plateau phase is optional and is performed by an end-inspiratory hold manoeuvre, during which airflow is stopped by closing both valves [9]. The P_{RS} drops to $P_{Plateau}$ since the pressure in the tubes caused by airflow is eliminated. Finally, during the expiratory phase, check valve 1 remains closed and check valve 2 opens. This causes a pressure differential where P_{RS} decreases passively in an exponential pattern until equalling P_0 .

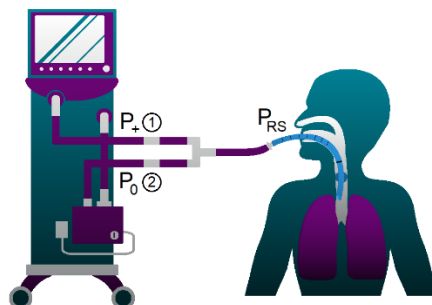


Figure 2-12: Mechanical Ventilator-Patient Circuit with Pressure Annotations

2.3.5 Waveform Scalars

During the administration of PPV, the MV conveys three important output variables as waveforms to the pulmonologist via the human-machine interface (HMI). These waveforms (sometimes referred to as waveform scalars) are [9], [36]:

- a) Proximal Airway Pressure (cmH₂O)
- b) Flow Rate (L/min)
- c) Volume (L)

Figure 2-13 depicts an example of how the waveforms coincide during the breathing cycle [10]. At the initiation phase, pressure drops, but the MV provides no flow, and the volume delivered to the patient by the MV remains unchanged. The MV senses the trigger for a breath and enters the inspiratory phase. The MV opens the inspiratory check valve, and flow commences due to the change in pressure, which leads to the volume waveform increasing over time. When the plateau phase is reached, airflow ceases because both check valves are closed, and the volume inside the patient's lungs remains constant (tidal volume - V_T). When the expiratory phase occurs, the expiratory check valve opens, and air flows out of the patient's lungs (negative flow) in an exponentially decaying fashion. The volume waveform also decays exponentially if a pressure differential exists between P_{RS} and P_0 .

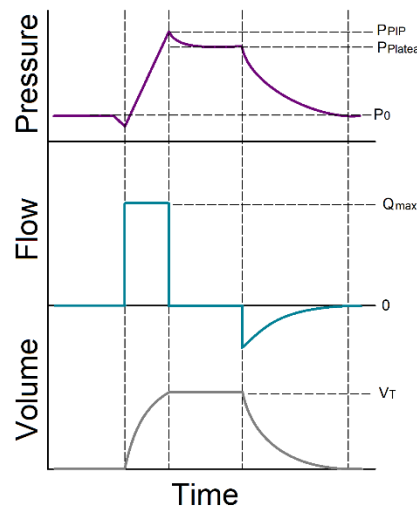


Figure 2-13: Waveform Scalars: Proximal Airway Pressure, Flow Rate and Volume

The set of waveform scalars generally follows this pattern, apart from the inspiratory phase. Different PPV techniques exist with different protocols for executing the inspiratory phase. Either the pressure- or flow waveforms are controlled by the MV settings chosen by the pulmonologist (and is called the independent/target waveform). The remaining waveform is measured and is, therefore, the dependent/conditional waveform [26]. The volume waveform is derived from the flow waveform through integration and technically conveys no new information [9].

2.3.6 Hysteresis Loops

The waveform scalars mentioned in Section 2.3.5 are the standard screening outputs of most mechanical ventilators. However, other output formats exist that convey the same data from another perspective. Leveraging these formats sometimes help pulmonologists to detect easier complications than using the original waveform scalars. These formats are obtained by graphing two of the three waveform scalars over each other synchronously [9], [36]. Lagging/leading effects observed in an MV-P system make graphing a fully cycled breath follow different paths for inspiration and expiration, causing a loop shape when returning to the origin point. Thus, changes in the hysteresis loop's shape contain information on the changing mechanical parameters of the MV-P system. This is further discussed in Section 2.6.2.3.

2.3.6.1 The Pressure-Volume Loop

One of the loop formats is the pressure-volume loop (see Figure 2-14 (a)). This loop is the plot of the volume over pressure and typically results in a leaf or S-shape [9], [36]. Inspiration starts at the lower pressure point (P_0) and then follows the lower path of the loop until P_{PIP} is reached (V_T is delivered). During expiration, the upper path is followed until pressure returns to P_0 .

2.3.6.2 The Flow-Volume Loop

The other standard loop format is the flow-volume loop (depicted in Figure 2-14 (b)). The flow rate is plotted on the y-axis, and the volume on the x-axis [9]. The flow rate's sign changes as the airflow direction changes. Therefore, the positive range of the flow rate indicates inspiration and the negative range, expiration. The inspiratory phase starts at the volume equal to zero and ends when the tidal volume (V_T) is delivered. A peak negative flow is reached during expiration before the breath cycles back to zero volume.

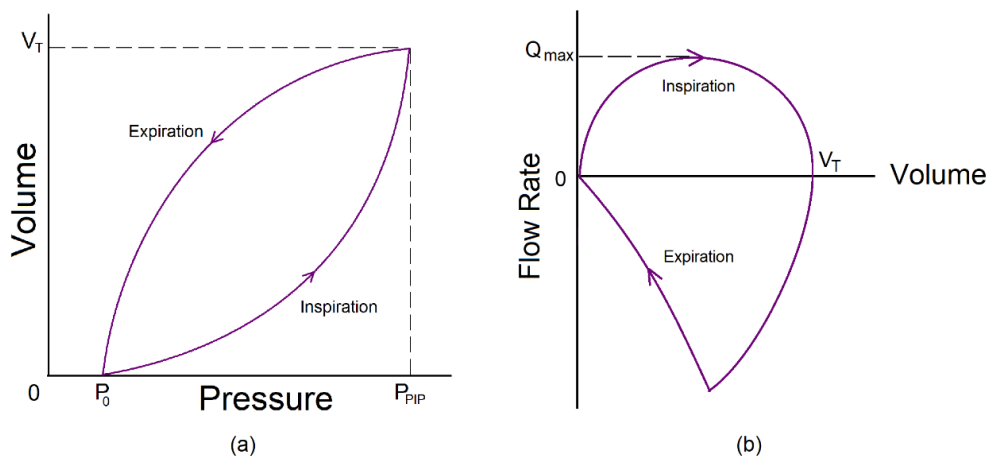


Figure 2-14: Hysteresis Loops: Pressure-Volume Loop (a) and Flow-Volume Loop (b)

2.4 Ventilation Techniques

This section conveys more detail about the standard ventilation techniques. It covers the types of ventilation, the different ventilation modes, then elaborates more on the different primary modes of ventilation and, finally, more on the controlled-ventilation modes.

2.4.1 Types of Ventilation

PPV can be invasive (usage of ETT or tracheostomy tube) or non-invasive (usage of nasal prongs or tight-fitting face mask) [37], [41]. Invasive types of ventilation require experts to insert the MV-P interface into the patient in the safest way possible. The section hereafter will focus more on the invasive types of mechanical ventilation. Non-invasive positive pressure ventilation (NIPPV) can be administered without a high skill level (unlike invasive ventilation [42]) since interfacing the patient with the MV poses no safety risks [1].

NIPPV can be divided into two subtypes of ventilation:

- Continuous Positive Airway Pressure (CPAP)
- Bi-Positive Airway Pressure (BiPAP)

CPAP supplies the patient with continuous positive airway pressure throughout the breathing cycle to reduce the work of breathing (WOB) required by the patient to breathe (depicted by the purple flat line in Figure 2-15 (a)). Some machines have advanced techniques to adjust this constant, continuous pressure in different circumstances automatically.

BiPAP, on the other hand, has two alternating positive airway pressure levels, a high (inspiratory positive airway pressure – IPAP) and slightly lower (expiratory positive airway pressure – EPAP) pressure level exercised during the inspiratory and expiratory phase (inspect Figure 2-15 (b)). BiPAP alleviates the discomfort of patients that struggles to adjust to CPAP.

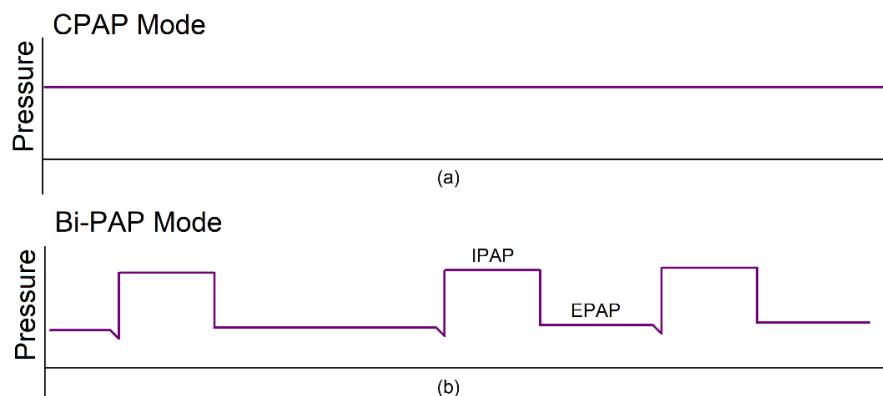


Figure 2-15: Pressure Waveform Scalars of CPAP (a) and BiPAP (b)

2.4.2 Categories of Ventilation Modes

The three main categories of ventilation modes are the primary, spontaneous breathing, and secondary- or unconventional modes. All the primary modes contain an aspect of a mandatory breath protocol, i.e., they can deliver a breath to the patient without being triggered by the patient to do so [26], [43]. The spontaneous breathing modes are those modes that only support spontaneous breathing attempts by the patient and have no mandatory aspect to the protocol[43]. Secondary or unconventional ventilation modes are a set of less common or advanced ventilator techniques recommended only to be administered with the assistance of a pulmonologist for short periods [1], [44]. Below is a list of the three main categories of ventilation modes with some examples of each.

2.4.2.1 Primary Ventilation Modes

- Control Mode
- Assist Control (AC) or Continuous Mandatory Ventilation (CMV) Mode
- Synchronous Intermittent Mandatory Ventilation (SIMV) Mode

2.4.2.2 Spontaneous Breathing Modes

- Continuous Positive Airway Pressure (CPAP) Mode
- Bi-Positive Airway Pressure (BiPAP) Mode
- Pressure Support Ventilation (PSV) Mode
- Volume Support Mode

2.4.2.3 Secondary or Unconventional Modes

- Adaptive Pressure Control (APC)
- Airway Pressure Release Ventilation (APRV)
- Adaptive Support Ventilation (ASV)
- Automatic Tube Compensation (ATC)
- Average Volume-Assured Pressure Support (AVAPS)
- High-Frequency Oscillatory Ventilation (HFOV)
- Inverse Ratio Ventilation (IRV)
- Mandatory Minute Ventilation (MMV)
- Neutrally Adjusted Ventilatory Assist (NAVA)
- Proportional Assist Ventilation (PAV)
- Pressure Regulated Volume Control (PRVC)

2.4.3 More on Primary Modes of Ventilation

The primary modes of ventilation are the control mode, assist control (AC) or continuous mandatory ventilation (CMV) mode, and synchronous intermittent mandatory ventilation (SIMV) mode [1]. Each of these three modes' protocols differs in how much WOB alleviation they offer.

2.4.3.1 Control Mode

The control mode offers no alleviation of the WOB. However, this mode delivers full support in breath delivery according to the settings on the MV as set by the pulmonologist. Inspecting Figure 2-16 (a) clarifies that no breath is delivered when a pressure drop occurs during the initiation phase. Only when the period ($T_{Period} = 60/RR$ – resulting from the respiratory rate setting) has elapsed will a fully supported breath be delivered (mandatory breath) [26].

2.4.3.2 AC/CMV Mode

The AC/CMV mode can deliver mandatory breaths (such as the control mode), but this mode can also deliver assisted breaths [32]. These breaths are fully supported, just like the mandatory breaths, but can be triggered by the patient at any time outside the inspiratory phase. It should be noted that although a breath can be triggered at any time when a trigger does not occur within T_{Period} , a mandatory breath will be delivered (illustrated in Figure 2-16 (b) [36]).

2.4.3.3 SIMV Mode

The SIMV mode is very similar to the AC/CMV mode but has the added weaning functionality of choosing the support level for the triggered assisted breaths. Figure 2-16 (c) demonstrates how an assisted breath delivers less support to encourage increased WOB from the patient [45].

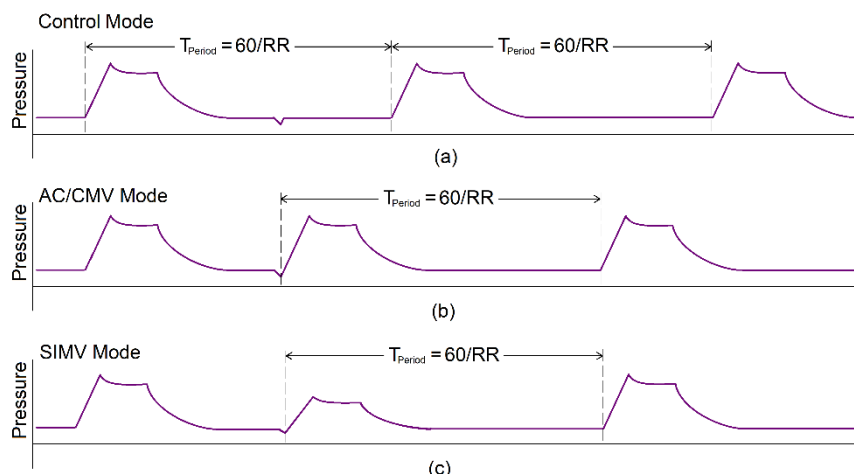


Figure 2-16: Pressure Waveform Scalars of the Primary Ventilation Modes: Control Mode (a), AC/CMV Mode (b) and SIMV Mode (c)

2.4.4 More on Controlled Modes of Ventilation

Controlled ventilation modes follow a protocol where the ventilator operator chooses and sets a target variable to be controlled by the ventilator during breath delivery. The options for target variables are pressure, volume, flow, and time. The most common procedures are the volume-controlled (VC) and pressure-controlled (PC) ventilation modes. These controlled modes also use the phase variables to construct further the breathing cycle described in Section 2.3.4.

2.4.4.1 The Phase Variables

The phase variables determine the conditions for breath delivery to a patient and, in return, the shape of the breathing cycle. The phase variables are the trigger, limit, and cycle variables [30], [34], [43].

2.4.4.1.1 The Trigger Variable

The trigger variable depicts the protocol for the MV to determine when the inspiration phase of the breathing cycle should start [9].

- Time Triggering – The MV triggers a breath according to the set respiratory rate.
- Patient Triggering – The patient triggers a breath whenever they exert acceptable WOB.
- Flow Triggering – The patient triggers a breath when the flow dips below the threshold.
- Volume Triggering - The patient triggers a breath when a drop in volume is detected.

2.4.4.1.2 The Limit Variable

The limit variable restricts breath delivery in a way that could promote patient safety [9].

- Pressure Limiting – The pressure in the circuit is restricted from exceeding this value.
- Volume Limiting – The MV interrupts further gas delivery when this volume is achieved.
- Flow Limiting – The MV restricts the air flow in the circuit to exceed this delivery speed.

2.4.4.1.3 The Cycle Variable

The cycle variable depicts the protocol for the MV to determine when the inspiration phase of the breathing cycle should be terminated [9], [46].

- Volume-Cycled Ventilation – End of inspiration is achieved by delivering a specific volume.
- Time Cycled Ventilation – End of inspiration is achieved at the elapsed inspiratory time.
- Flow-Cycled Ventilation – End of inspiration is achieved by detecting a sub-threshold flow.
- Pressure-Cycled Ventilation – End of inspiration is achieved by obtaining a set pressure.

2.4.4.2 Volume-Controlled Ventilation (VC)

The VC protocol for delivering a breath utilises time triggering, per the set respiratory rate (RR), with volume-cycled ventilation to deliver a predefined tidal volume (V_T) [32]. During VC, the flow rate waveform scalar is controlled (independent/target waveform), and the pressure waveform is measured (dependent/conditional waveform) [30]. The volume waveform is derived mathematically with integration techniques from the flow waveform [9]. The other ventilation parameters that must be set to fully constrain the flow waveform's shape are the baseline pressure (P_0), peak inspiratory flow (Q_{max}) and the flow pattern. The flow pattern determines the flow waveform's shape during the inspiratory phase. Each shape is scaled vertically according to Q_{max} and horizontally along the time axis by calculating the time needed to deliver the set V_T , given the flow rate waveform's shape function. The six possible options for the flow rate pattern are [1], [34]:

- Constant / Square / Rectangular Flow (VCC) – Figure 2-17 (a)
- Sinusoidal Wave Flow – Figure 2-17 (b)
- Ramp / Saw-Tooth (Accelerating or Decelerating (VCD)) Flow – Figure 2-17 (c) and (d)
- Exponential (Increasing or Decreasing) Flow – Figure 2-17 (e) and (f)

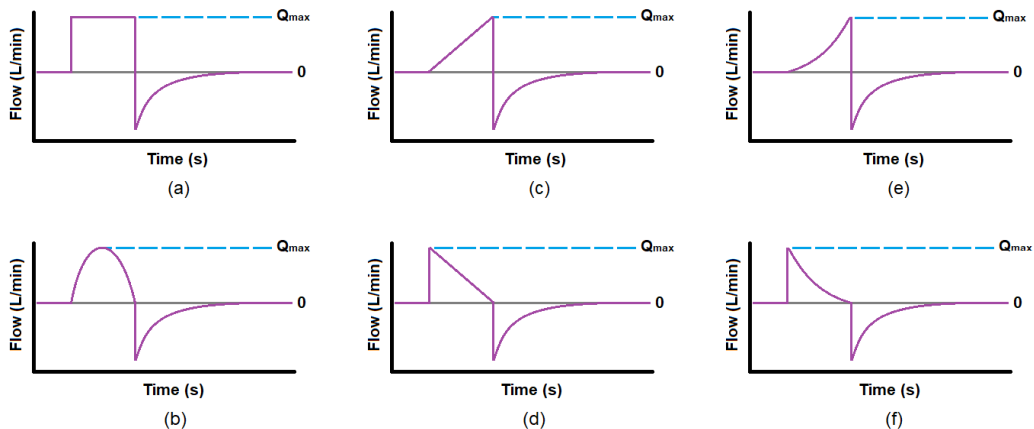


Figure 2-17: The Flow Patterns of Volume-Controlled Ventilation:
Constant Flow (a), Sinusoidal Flow (b), Accelerating Ramp Flow (c), Decelerating Ramp Flow (d),
Exponential Increasing Flow (e) and Exponential Decreasing Flow (f)

2.4.4.3 Pressure-Controlled Ventilation (PC)

The PC protocol for breath delivery utilises time triggering (per the set RR) with time-cycled ventilation at a predefined peak inspiratory pressure (P_{PIP}). The other ventilation parameters that must be set to fully constrain the pressure waveform's shape are P_0 and the inspiratory time (T_i). During PC, the pressure waveform scalar is controlled (independent/target waveform), and the flow rate waveform is measured (dependent/conditional waveform) [30], [32]. The volume waveform is derived mathematically with integration techniques from the flow waveform.

2.4.4.4 Comparing VC and PC Ventilation

At the onset, the pulmonologist chooses the ventilator settings to be appropriate given the patient's expected needs and health state. In the case of sedated patients, the pulmonologist can initially set up any ventilation mode appropriately. However, as time progresses, the patient's pulmonary mechanical properties may change as the health state of the patient improves or deteriorates. When this happens, the MV-P system changes; therefore, the dependent waveform scalar will also change accordingly.

In the case of VC ventilation, changes in the patient's health status may cause changes in the respiratory system's pressure (P_{RS}). When resistance increases and compliance decreases, the pressure will reach higher levels and could lead to barotrauma if left unchecked with no pressure limiting phase variable. Also, implementing a pressure limit will lead to reduced tidal volumes, which can lead to hypoventilation if the respiratory rate is not adjusted to achieve the required minute ventilation. In extreme cases, decreased resistance and increased compliance will cause the alveoli to collapse (atelectasis), which will restrict respiration and cause inflammation [1], [9], [32], [47], [48].

PC ventilation and changes in the patient's health status may cause changes in the delivered tidal volume (V_T). This mode is much more susceptible to hyperventilation and hypoventilation since the minute ventilation changes as the mechanical parameters of the patient change [1], [9], [32], [47], [48].

Therefore, both VC and PC have advantages and disadvantages when left unchecked. Both control modes are currently standard, specifically VCC, VCD and PC [1], [32], [34], [47], [49], [50]. The typical shapes of the three waveform scalars for each mode are illustrated in Figure 2-18 [34].

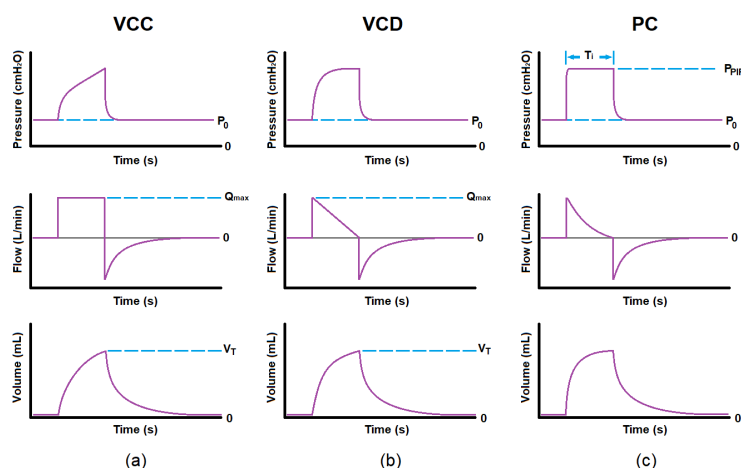


Figure 2-18: The Three Most Common Modes for Controlled Ventilation: Volume-Controlled Constant Flow Mode (a), Volume-Controlled Decelerating Ramp Flow Mode (b) and Pressure-Controlled Mode (c)

2.5 Relevant Mechanical Ventilator-Patient (MV-P) Parameters

This section discusses the relevant mechanical ventilator-patient (MV-P) parameters. It covers the parameters of the patient's biological and anthropometric data, the pulmonary system, the ventilator circuit, and the mechanical ventilator.

2.5.1 Patient Biological and Anthropometric Parameters

One of the parameter groups that influences the characteristics of the MV-P system is the patient's biological and anthropometric data. It should be noted that these parameters are just used to make estimations on physical characteristics describing the respiratory system later. It is possible that multiple patients with the same biological and anthropometric data (those easier to measure) could very well have different respiratory system characteristics. However, since those physical characteristics are impractical to measure, this parameter group is used instead as input to prediction heuristic functions. Below is a list of the biological and anthropometric parameters that play a role in respiratory system characterization. Age, height, sex, and ideal body weight (IBW_{kg}) are most important; the rest are either impractical to measure or are unclear to what extent they contribute. The IBW_{kg} is used instead of actual weight since the respiratory system dimensions does not correlate with body fat percentage. IBW_{kg} (in kilograms), is dependent on height (in centimetres), and sex (see equations (2-19) and (2-20)) [29], [37].

- Most Important Parameters

- Age
- Height ($Height_{cm}$)
- Sex
- Ideal Body Weight (IBW_{kg})

(2-19)

$$IBW_{Male} = 50 + [0.9055 \times (Height_{cm} - 152.4)]$$

(2-20)

$$IBW_{Female} = 45.5 + [0.9055 \times (Height_{cm} - 152.4)]$$

- Other Parameters

Other less studied parameters that contribute to the characterization of the respiratory system are the circadian rhythms, menstrual cycle, social and healthcare choices, environmental factors, lifestyle, chronic diseases, and genetics [4], [51]. The magnitude of effect these parameters have on the respiratory system is impractical to model since obtaining quantified measurements isolating these events is complex.

2.5.2 Pulmonary System Parameters

The two main hydraulic components of the lungs are the airways (trachea) and the lungs (discussed in Section 2.2). These two components' dimensions depend on the patient's biological and anthropometric data from Section 2.5.1.

2.5.2.1 Trachea Dimensions

The trachea can be represented as a pipe with a specific inside diameter and length. Assuming the trachea's dimensions need only depend on the sex and height of the patient, multiple sources can be used in conjunction with each other to estimate the inside diameter and length of the trachea in millimetres [52]–[56]. These heuristic equations are represented by equations (2-21) and (2-24).

- Trachea Length (TL_{mm})

$$TL_{Male} = 0.612 \times Height_{cm} + 9.18 \quad (2-21)$$

$$TL_{Female} = 0.606 \times Height_{cm} + 9.09 \quad (2-22)$$

- Trachea Diameter (TD_{mm})

$$TD_{Male} = 0.0934 \times Height_{cm} + 1.40 \quad (2-23)$$

$$TD_{Female} = 0.0925 \times Height_{cm} + 1.39 \quad (2-24)$$

2.5.2.2 Capacity Dimensions

The total volume of the respiratory tract comprises four sub-volumes and the dead space [29]:

- Residual Volume (RV) – The remaining volume in the lungs after expelling a breath forcefully.
- Expiratory Reserve Volume (ERV) – The volume expelled forcefully from the resting level.
- Tidal Volume (V_T) – The volume inhaled from the resting level without forceful WOB.
- Inspiratory Reserve Volume (IRV) – The remaining volume inhalable by forceful WOB.
- Dead Space – The total volume of the nasal cavity, oral cavity, and airways (~ 30% of V_T).

These volumes are used to define the four capacity parameters of the lungs [29]:

- Total Lung Capacity (*TLC*) – The total volume storables inside a lung.

$$(2-25) \quad TLC = RV + ERV + V_T + IRV$$

- Vital Capacity (*VC*) – The lungs' total capacity controllable by WOB.

$$(2-26) \quad VC = ERV + V_T + IRV$$

- Inspiratory Capacity (*IC*) – The lungs' total capacity dedicated for full inspiration.

$$(2-27) \quad IC = V_T + IRV$$

- Functional Residual Capacity (*FRC*) – Total capacity of the lungs at resting expiratory level.

$$(2-28) \quad FRC = RV + ERV$$

Figure 2-19 is a graph of the volume waveform scalar with annotations indicating the different volume levels, volume ranges and capacities of the lungs. During mechanical ventilation, before and after the breathing cycle, the lungs should remain at the resting expiratory level at *FRC* and deliver breaths with *V_T*, typically 5 to 8 mL/kg (*IBW_{kg}*) [1], [5]. *V_T* has a minimum and maximum range of 4 to 10 mL/kg (*IBW_{kg}*). *FRC* can be estimated as 30 mL/kg (*IBW_{kg}*).

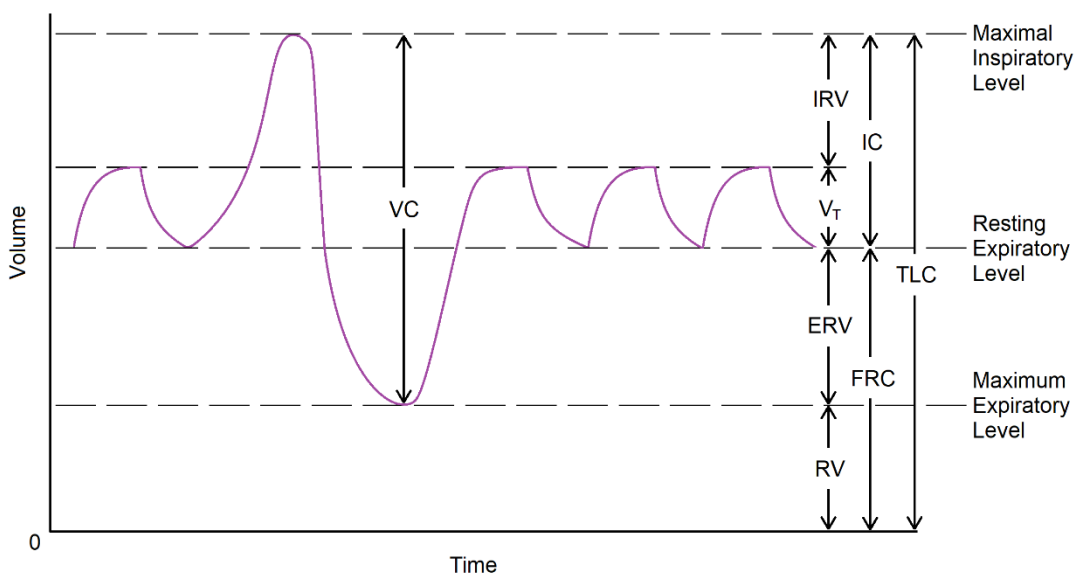


Figure 2-19: Volume Waveform Depicting Pulmonary System Volumes and Capacities

2.5.3 Ventilator Circuit Parameters

The ventilator circuit consists of an inspiratory, expiratory, and endotracheal tube (ETT). The physical dimensions of these components influence the impedance added to the MV-P system.

2.5.3.1 Inspiratory and Expiratory Tube Dimensions

The inspiratory and expiratory tubes are identical. The standard size for these tubes is one metre in length and ten millimetres in diameter [57].

2.5.3.2 Endotracheal Tube (ETT)

The ETT is inserted into the trachea of the mechanically ventilated patient and could harm the patient if not selected appropriately. The ETT comes in 17 sizes and is usually inserted halfway into the trachea [58]. The sizes come in six different lengths, from 230 to 302 mm, of which only the shortest and longest sizes have more than one inside diameter as an option. The inside diameter ranges from 2.0 mm to 10.0 mm. See Table 2-2 for the list of ETT length-inside diameter combinations [59], [60].

For an adult male, the heuristic used by pulmonologists is to select an ETT size with at least an 8.0 mm inside diameter and, for women, at least a 7.0 mm inside diameter [61], [62].

The heuristic used for selecting the approximate ETT inside diameter is given by equation (2-29) [29], [62]–[64] for paediatric patients. The standard is to select the ETT with an inner diameter less than ETT_{Size} .

$$ETT_{Size} = \frac{Age + 16}{4} \quad (2-29)$$

Table 2-2: Lookup Table of Standard Endotracheal Tube (ETT) Sizes

ETT Length (mm)	ETT Inner Diameter (mm)
230	2.0, 2.5, 3.0, 3.5, 4.0, 4.5, 5.0
260	5.5
270	6.0
280	6.5
290	7.0
302	7.5, 8.0, 8.5, 9.0, 9.5, 10.0

2.5.4 Mechanical Ventilator (MV) Parameters

The MV has an HMI (Figure 2-20) for setting different MV parameters, which act as inputs to the breath delivery protocol of the chosen PPV mode [1], [29], [32], [37].

2.5.4.1 Respiratory Rate (RR)

The respiratory rate is one of the most important parameters and is always set by the pulmonologist during mechanical ventilation. It is measured in breaths/min (equation (2-30)).

$$RR = \text{Number of Breaths}/1 \text{ Minute} \quad (2-30)$$

Recommended RR ranges are 30 to 50 breaths/min for infants, 18 to 30 breaths/min for children, and 8 to 18 breaths/min for adults.

2.5.4.2 Breath Cycle Period (T_{Period})

The breath cycle period is the time allotted for completing one cycle of breath (in seconds).

$$T_{Period} = 60/RR \quad (2-31)$$

2.5.4.3 Inspiratory Time (T_i)

The inspiratory time is the time duration of the inspiratory phase.

2.5.4.4 Baseline Pressure / End-Expiratory Pressure (P_0)

P_0 is the pressure level at rest after expiration. When P_0 equals 0 cmH₂O, it is called zero end-expiratory pressure (ZEEP); when P_0 is positive, it is called positive end-expiratory pressure (PEEP). It is prevalent to only refer to the baseline pressure as PEEP.

2.5.4.5 Peak Inspiratory Pressure (P_{PIP})

The peak inspiratory pressure is the highest pressure achieved during the inspiratory phase.

2.5.4.6 Plateau Phase ($P_{Plateau}$)

$P_{Plateau}$ is the steady state pressure level achieved after the inspiratory phase during no airflow.

2.5.4.7 Driving Pressure ($P_{Driving}/\Delta P$)

The driving pressure is the pressure difference generated before the expiratory phase is entered.

$$P_{Driving} = P_{Plateau} - P_0 \quad (2-32)$$

2.5.4.8 Peak Inspiratory Flow (Q_{max})

The peak inspiratory flow is a parameter settable by a pulmonologist during VC modes. It represents the maximum flow rate during the inspiratory phase and is measured in L/min.

2.5.4.9 Tidal Volume (V_T)

The tidal volume is the air (in litres) delivered to a patient during inspiration. The equation for V_T changes according to the chosen ventilation mode and flow pattern. When using PC mode, equation (2-33) is appropriate.

$$V_T = C \cdot \Delta P \cdot e^{T_i/\tau_{RC}} \quad (2-33)$$

When using VCC mode, the flow rate is constant, and V_T is thus given by equation (2-34).

$$V_T = \frac{Q_{max} \times T_i}{60} \quad (2-34)$$

When using VCD mode, the flow rate is a decelerating ramp function from Q_{max} to some cut-off threshold (Q_{TH}) over T_i . Therefore, equation (2-36) calculates the tidal volume.

$$V_T = \frac{\left(\frac{1}{2} \times Q_{max} \times T_i\right) + (Q_{TH} \times T_i)}{60} \quad (2-35)$$

2.5.4.10 Minute Ventilation (V_M)

Minute ventilation is the total volume of air delivered to the patient within a minute of ventilation.

$$V_M = RR \times V_T \quad (2-36)$$

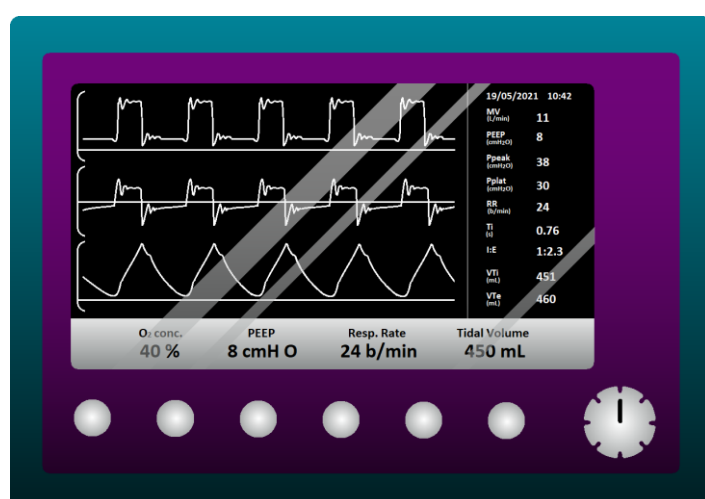


Figure 2-20: Example Illustration of the Mechanical Ventilator's Human-Machine Interface

2.6 Ventilated Patient Condition Monitoring

After a patient has been intubated, the ventilation mode specified, and the appropriate initial MV parameters set, the patient's health condition needs to be monitored. Continually monitoring the patient's condition could indicate any need to adjust the ventilator parameters appropriately to optimise patient recovery. Condition monitoring can be performed using data-driven techniques or model-based techniques [65]–[70]. In practice, pulmonologists use data by performing tests or by examining the MV outputs as indicators of the patient's health status. The goal is to look for indicators of respiratory failure, being hypoxemic or hypercapnic (oxygenation- or mechanical complications) and apply the appropriate treatment to ensure adequate respiration.

2.6.1 Chemical Data-Driven Indicators

One data-driven approach is in the chemical domain [1], [4]. Two standard tests are used to monitor the oxygenation levels of the patient. These are the arterial blood gas (ABG) test and the arterial alveolar gradient (A-a gradient).

2.6.1.1 Arterial Blood Gas (ABG) Test

The ABG test assesses the following parameters [71]:

- pH Level of the Blood – Normal is 7.35 to 7.45
- Arterial Blood Pressure of Carbon Dioxide (PaCO_2) – Normal is 35 to 45 mmHg
- Arterial Blood Pressure of Oxygen (PaO_2) – Normal is 80 to 100 mmHg
- Bicarbonate Level (HCO_3) – Normal is 22 to 26 mEq/L
- Oxygen Saturation (SaO_2) – Normal is 95 to 100%

The results will determine if the patient exhibits signs of respiratory- and metabolic acidosis or alkalosis, which could indicate to the pulmonologist how ventilation should be adjusted.

2.6.1.2 Arterial Alveolar Gradient (A-a Gradient)

The A-a gradient uses the ABG test to further analyse the patient for combined oxygenation-ventilation complications (equation (2-37) [29]). PiO_2 is the pressure of inspired oxygen.

$$\text{A-a Gradient} = \text{PAO}_2 - \text{PaO}_2 = (\text{PiO}_2 - \text{PaCO}_2/0.8) - \text{PaO}_2 \quad (2-37)$$

2.6.2 MV Data-Driven Indicators

The other data-driven approach is by examining the MV's graphical output. As previously mentioned, the MV has two different output formats:

- The Waveform Scalars (Section 2.3.5)
- The Hysteresis Loops (Section 2.3.6)

These outputs can be used to perform fault detection and isolation (FDI) on the MV-P system at three different stages:

- Inappropriate Ventilator Settings
- Ventilator Circuit Malfunctioning
- Respiratory System Condition Monitoring

2.6.2.1 Inappropriate Ventilator Settings

The initial settings chosen by the pulmonologist for the MV (controller) can be inappropriate when the condition of the ventilator circuit or patient (plant) changes over time. These issues are mainly identifiable by noticing MV-P asynchronies on the HMI (sensor) when the patient is active (closed loop via neural response and MV sensors to HMI). However, when the patient is sedated, the chemical-data-driven results from Section 2.6.1 become the indicators of inappropriate ventilator settings (closed loop via chemical-data-driven tests). Some indicators of inappropriate ventilator settings identifiable via the HMI are discussed below [9], [19], [32], [34], [36], [72]–[74].

1. Ineffective Triggering Effort – The MV does not identify the patient's triggering effort as sufficient and fails to deliver a breath as requested (Figure 2-21).

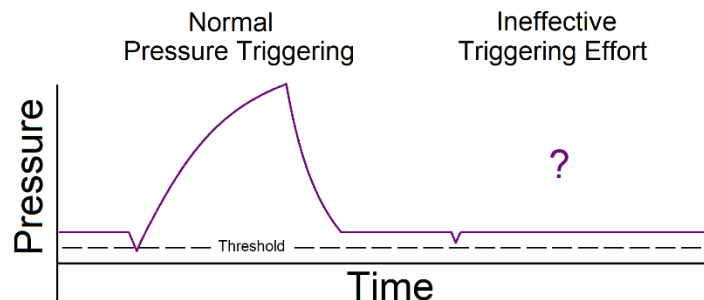


Figure 2-21: Pressure Waveform Scalar of Ineffective Triggering Effort

2. Auto-Triggering/Auto-Cycling – The MV identifies an artefact that is a non-patient trigger effort as sufficient and continues to deliver an unwanted breath (Figure 2-22).

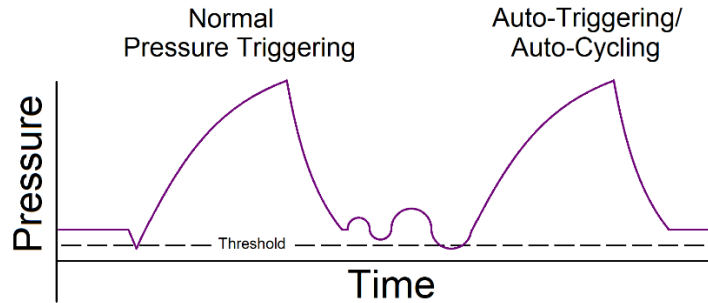


Figure 2-22: Pressure Waveform Scalar of Auto-Triggering/Auto-Cycling

3. Delayed Triggering – The MV breath delivery lags the patient triggering effort (Figure 2-23).

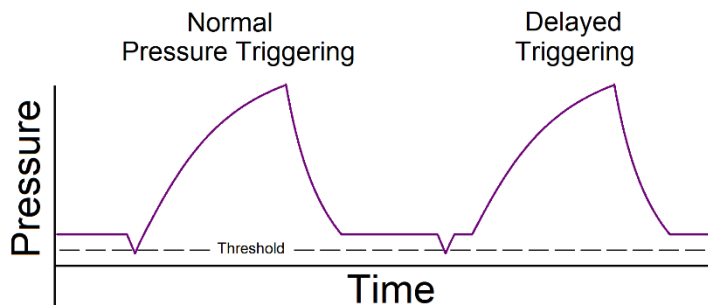


Figure 2-23: Pressure Waveform Scalar of Delayed Triggering

4. Reverse Triggering – Patient trigger effort lags mandatory MV breath delivery (Figure 2-24).

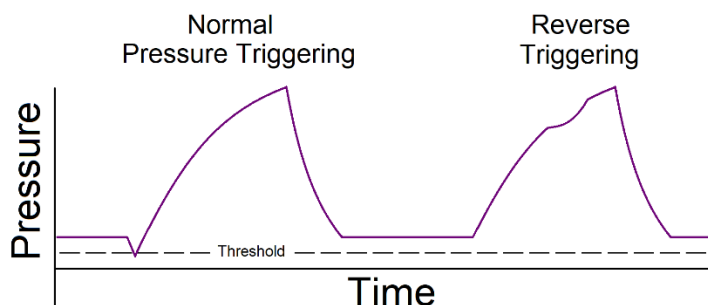


Figure 2-24: Pressure Waveform Scalar of Reverse Triggering

5. Flow Starvation/Insufficient Pressurization – The patient's breath flow rate demand during the inspiratory phase is greater than provided by the MV (Figure 2-25).

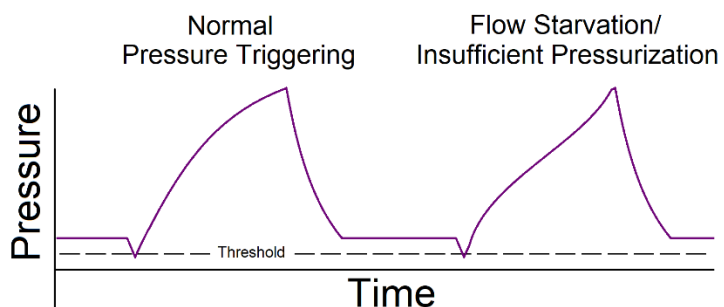


Figure 2-25: Pressure Waveform Scalar of Flow Starvation/Insufficient Pressurization

6. Delayed Cycling – The inspiratory time is longer than the neural cycling time (Figure 2-26).

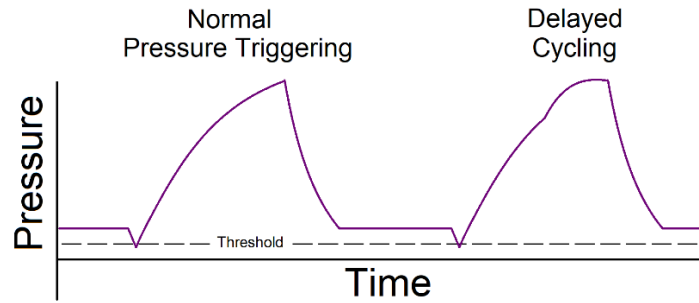


Figure 2-26: Pressure Waveform Scalar of Delayed Cycling

7. Premature/Short Cycling – The neural time of the inspiratory effort is longer than the inspiratory time (Figure 2-27).

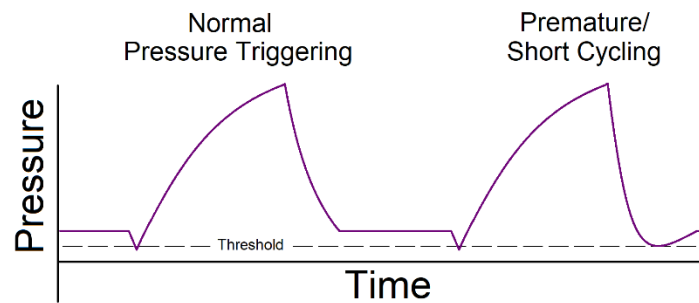


Figure 2-27: Pressure Waveform Scalar of Premature/Short Cycling

8. Double-Triggering/Breath Stacking – The inspiratory phase is initiated before sufficient expiratory time has elapsed (Figure 2-28).

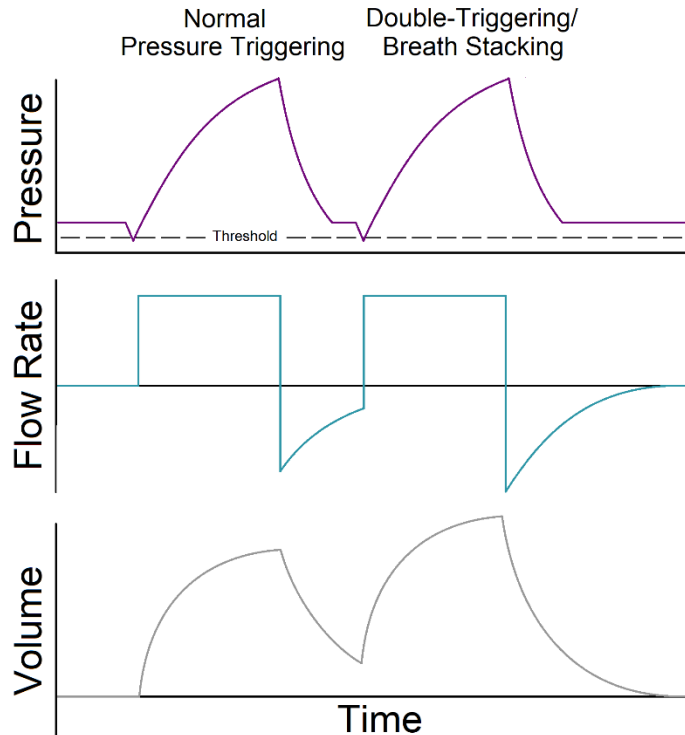


Figure 2-28: The Three Waveform Scalars of Double-Triggering/Breath Stacking

9. Alveolar Collapse – When the lower inflection point (P_1 from Figure 2-29) has a higher-pressure level than P_0 , the alveoli collapse and cause atelectasis.
10. Alveolar Overdistension – When the upper inflection point (P_2 from Figure 2-29) has a lower-pressure level than P_{PIP} , the alveoli become overdistended and cause barotrauma.

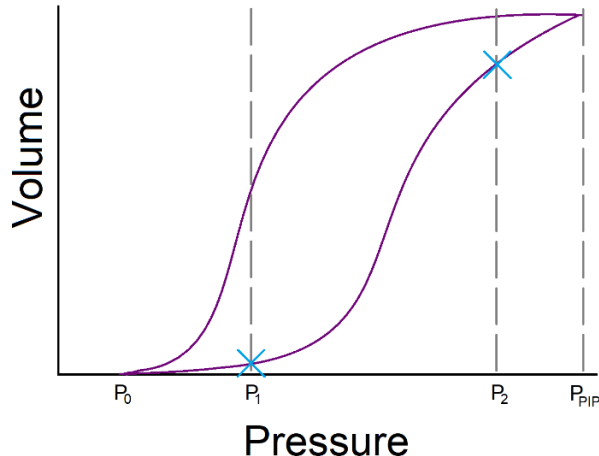


Figure 2-29: Pressure-Volume Loop of Inflection Points

2.6.2.2 Ventilator Circuit Malfunctioning

1. Air Leak – The tidal volume does not return to the *FRC* level (Figure 2-30) [9], [32].

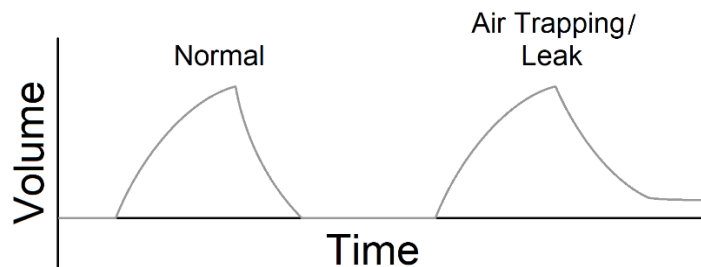


Figure 2-30: Volume Waveform Scalar of Air Leak

2. Secretions – Secretion build-up or condensation inside the tubes causes oscillation artefacts. Figure 2-31 (a) is a normal case of a flow-volume loop as a reference. Figure 2-31 (b) shows secretion build-up in the inspiratory tube (oscillations on the inspiratory curve). Figure 2-31 (c) shows secretion build-up in the expiratory tube (oscillations on the expiratory curve) [36].

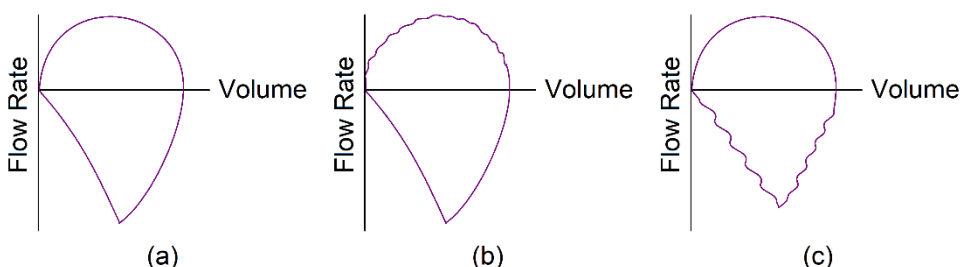


Figure 2-31: Flow-Volume Loop of Secretion Build Up: Normal Case (a), Inspiratory Tube Secretions (b) and Expiratory Tube Secretions (c)

2.6.2.3 Respiratory System Condition Monitoring

As mentioned in Section 2.2.4.1, the inertance of a respiratory system is negligible at respiratory rates lower than 30 breaths/min and is dominated by the inertance of the artificial airways (endotracheal tube). Thus, pulmonologists are only interested in the patient's resistance and compliance in practice, as the inertance does not change significantly over time.

2.6.2.3.1 Compliance

The compliance of the respiratory system is the amount of volume delivered into the lungs (V_T) per change in pressure at the start of the expiratory phase. Figure 2-32 indicates how the pressure waveform scalar changes as compliance increases (P_{PIP} and $P_{Plateau}$ decreases) [36].

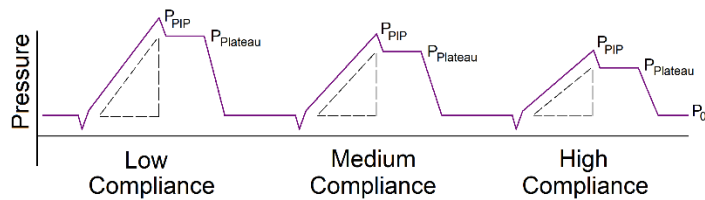


Figure 2-32: Pressure Waveform Scalar of Increasing Compliance

Referring to the equation of motion from Section 2.2.3.1, the elastic component is not the only contributor to change in pressure but also resistance due to airflow (equation (2-38)).

$$P_{aw}(t) = P_I(t) + P_R(t) + P_C(t) + P_0 = I_{RS} \cdot \ddot{V}(t) + R_{RS} \cdot \dot{V}(t) + E_{RS} \cdot V(t) + P_0 \quad (2-38)$$

The static compliance (C_S) is the reciprocal of E_{RS} and is calculated using equation (2-39) [29], [34], [37].

$$C_S = \frac{V_T}{P_{Plateau} - P_0} \quad (2-39)$$

However, $P_{Plateau}$ is only measurable during an expiratory hold manoeuvre, a manual manoeuvre performed by the pulmonologist [9]. During this manoeuvre, the pulmonologist must estimate the V_T and $P_{Plateau}$ values. Therefore, logging each breath is impractical, prone to human error and inaccurate. Many high-end MVs calculate an approximation of C_S without performing an expiratory hold manoeuvre. This approximation is called dynamic compliance (C_D), which inaccurately correlates to the resistance's pressure component. $P_{Plateau}$ is replaced by P_{PIP} , as indicated by equation (2-40) when using this approximation method [29], [37].

$$C_D = \frac{V_T}{P_{PIP} - P_0} \quad (2-40)$$

However, when diagnosing patients' status, pulmonologists and experimental researchers use C_S and not C_D ; since C_D 's accuracy depends on the resistance.

Another way to monitor the changes in compliance is to utilize the loops. Using the pressure-volume loop (P-V loop), the change in compliance is represented by a change in the gradient of the hysteresis loop. This gradient is C_D . Figure 2-33 (a) shows how the P-V loop's gradient changes for changing compliance [34], [36]. The flow-volume loop (F-V loop) also changes as compliance changes (see Figure 2-33 (b)) [34]. The grey curve has the highest compliance, the purple curve has normal compliance, and the blue curve has the lowest compliance.

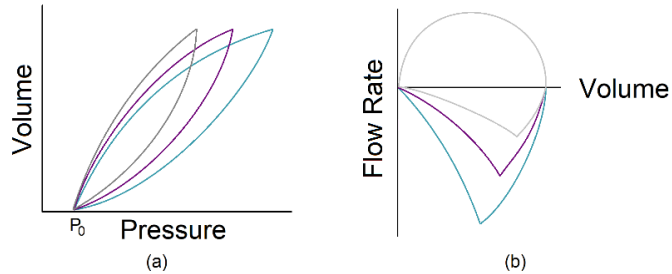


Figure 2-33: Varying Compliance Loops: Pressure-Volume (a) and Flow-Volume Loop (b)

2.6.2.3.2 Resistance

According to equation (2-41), the resistance (R_{INSP}) due to the inspiratory circuit (inspiratory tube, endotracheal tube, and airways) is the change in pressure (due to the airflow component) divided by the flow rate (Q) [29], [34], [37]. Figure 2-34 indicates how the pressure waveform scalar changes as the resistance increases (P_{PIP} increases and $P_{Plateau}$ stays the same [9]) [36].

$$R_{INSP} = \frac{P_{PIP} - P_{Plateau}}{Q} \quad (2-41)$$

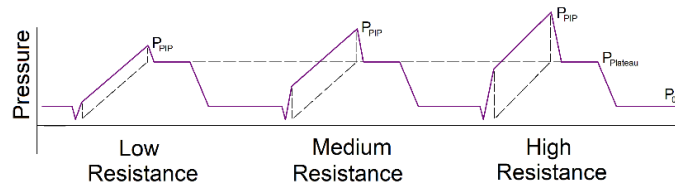


Figure 2-34: Pressure Waveform Scalar of Increasing Resistance

Again, determining the resistance is dependent on $P_{Plateau}$. The P-V loop's width increases with the resistance (Figure 2-35 (a)) [9], and the F-V loop's expiratory scoop becomes more concave (Figure 2-35 (b)) [9].

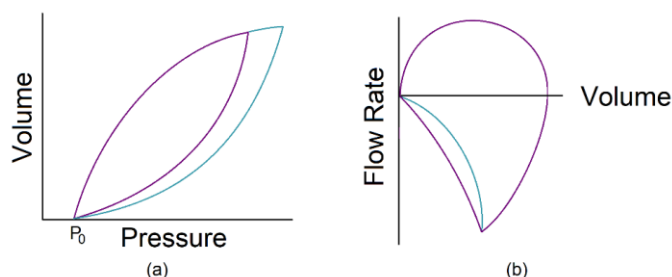


Figure 2-35: Varying Resistance Loops: Pressure-Volume (a) and Flow-Volume Loop (b)

2.7 Machine Learning

Machine learning (ML) is the process of creating prediction models using statistics-based algorithms and data [75]–[77]. The resulting models resemble patterns recognised from the data, which can solve problems than are too complex for traditional programming techniques. In this section, we will briefly discuss the ML process, ML's different types, its different techniques, a few regression algorithms, and the performance parameters necessary for evaluating the models.

2.7.1 The Machine Learning (ML) Process

ML is a statistics-based process and, therefore, relies on the statistical information of the data. The data acquired for ML must be appropriate to improve the accuracy of the statistical information derived from the data. The dataset must be acceptable, have a suitable range and spread, and be clean and complete. After the data has been acquired, it needs to be pre-processed to ensure it is clean and complete. Also, the data can be manipulated at this stage to present in another format if necessary. Next, the data is inspected for informative characteristics that can be extracted as informative features (feature engineering). After that, the training set of the dataset is used to build (train) a model based on a specified algorithm. After obtaining a trained model, it is validated and tested using the hold-out sets (validation and test sets). If the model's performance is acceptable, the model is deployed. Otherwise, another iteration is performed, as indicated by the diagram in Figure 2-36 [42], [75]–[78].

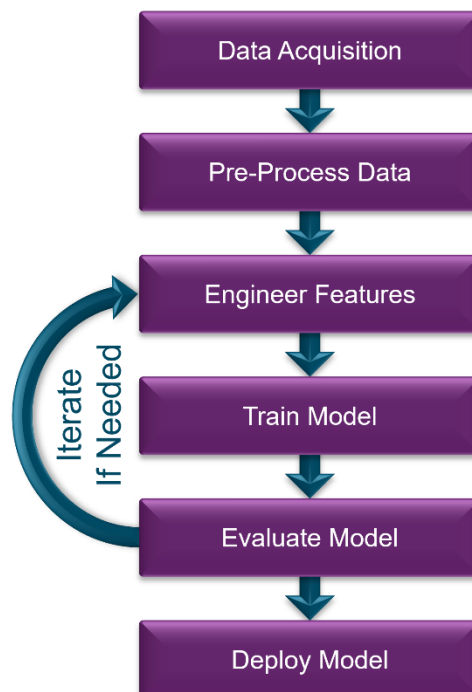


Figure 2-36: Diagram of the Machine Learning Process

2.7.2 Different ML Types

ML has different learning types, characterised by the type of data used (labelled or unlabelled) and the general goal to achieve. These types are supervised-, semi-supervised-, unsupervised- and reinforcement learning [75]–[77], [79].

2.7.2.1 Supervised Learning

A model is trained with a dataset containing only labelled feature vectors, which is implemented to deduce labels for unlabelled feature vectors.

2.7.2.2 Semi-Supervised Learning

A model is trained with a dataset containing labelled and unlabelled feature vectors (the latter is usually the larger sample), which is implemented to deduce labels for unlabelled feature vectors.

2.7.2.3 Unsupervised Learning

A model is trained with a dataset containing only unlabelled feature vectors, which is implemented to transform the unlabelled feature vectors into either another vector or a value that can be used to solve practical problems.

2.7.2.4 Reinforcement Learning

A model (policy) is learned by allowing a machine to execute actions in different states of a “perceivable environment”, which is only a feature vector. Rewards and penalties are used to identify which actions are optimal to perform in the different states. The idea is to obtain an optimised policy for sequential decision-making problem contexts.

2.7.3 Different Machine Learning Techniques

2.7.3.1 Classification

Classification techniques assign labels to feature vectors (the label is a class attribute) [75], [76].

2.7.3.2 Regression

Regression techniques predict values for feature vectors (the label is a value attribute) [75], [76].

2.7.3.3 Clustering

Clustering techniques recognise probable clusters (the label set is unlabelled classes) [75], [76].

2.7.4 Regression Algorithms

2.7.4.1 Linear Regression Algorithms

An algorithm category that uses a linear combination of the feature vectors to minimise the cost function for the hyperplane to represent the data points as accurately as possible. Examples of this category are normal linear regression, interactions linear regression, robust linear regression and stepwise linear regression [75], [76], [79]–[81].

2.7.4.2 Decision Tree Algorithms

An algorithm category that uses acyclic decision-making graphs where the feature vectors dictate which branches to follow until a leaf node determines the prediction. Examples of this category are fine trees, medium trees and coarse trees [75], [76], [79]–[81].

2.7.4.3 k-Nearest Neighbours (kNN) Algorithm

The kNN algorithm uses the principle of probability by taking the average value of a k-amount of the nearest neighbours in the region of interest. Examples include Euclidean, negative cosine similarity, Chebyshev, Mahalanobis and Hamming [75], [76], [79]–[81].

2.7.4.4 Support Vector Machine (SVM) Algorithms

An algorithm category that uses kernel functions for complex hyperplane modelling. Examples include linear SVM, quadratic SVM, cubic SVM, fine gaussian SVM, medium gaussian SVM and coarse gaussian SVM [75], [76], [79]–[81].

2.7.4.5 Gaussian Process Regression (GPR) Algorithms

An algorithm category that uses kernel functions for complex hyperplane modelling, like SVMs, additionally providing highly calibrated probabilities and estimated uncertainties. E.g., exponential GPR, squared exponential GPR, Matern 5/2 GPR and rational quadratic GPR [75], [81].

2.7.4.6 Ensemble Algorithms

Combination algorithms such as boosted trees and bagged trees [75], [76], [79]–[81].

2.7.4.7 Neural Networks (NN)

An algorithm category that uses nested functions (layers of neurons) to manipulate the input layer to obtain an output layer. Examples are narrow-, medium-, wide-, bi-layered- and tri-layered NN [75], [76], [79]–[81].

2.7.5 Validation Methods

When creating models using ML, the training set is used to determine the model directly. Therefore, the training set cannot be used to test the validity of the model's accuracy since no evidence for generalisation can be provided. A model is validated using held-out data from the training set (validation set obtained from the methods below) during training as proof of the generalisation performance level. It is used to find and optimise the best model from a specified algorithm while keeping in mind the model's validity [75], [77], [82], [83].

2.7.5.1 K-Fold Cross Validation

Validating a model by using the training dataset for both training and validation. The data is partitioned into k number of subsets (folds) so that k separate learning experiments can be performed by picking one subset for validation and the rest for training. The average of the k different accuracy results represents the final validation result of the model [75], [76], [84]–[86].

2.7.5.2 Hold-Out Validation

When a large dataset is available, a simple hold-out method can be used to validate the model. This is done by splitting the training set into two parts with sizes correlating to the specified hold-out percentage and using the subsets exclusively (training and validation).

2.7.5.3 Resubstitution Validation

The whole dataset is used for training and validation by evaluating the error rate. Thus, no protection against overfitting is implemented.

2.7.6 Algorithm Performance Parameters

- RMSE – The root mean squared error of the predictions versus the target values (an indication of the model's accuracy).
- Training Speed – The time it takes to train a model using the specified algorithm.
- Overfitting Index – An indication of the quality of generalization. It is derived from the validation and test RMSE results. The closer these RMSE results are to each other, the smaller the likelihood is that the model is overfitted [86].
- Prediction Speed – The number of predictions an ML model can generate within a specific time, which can significantly affect the deployment cost.
- Size of Model – The storage space or memory needed to host an instance of the model on a machine, which can also significantly affect the deployment cost.

2.8 Chapter Summary

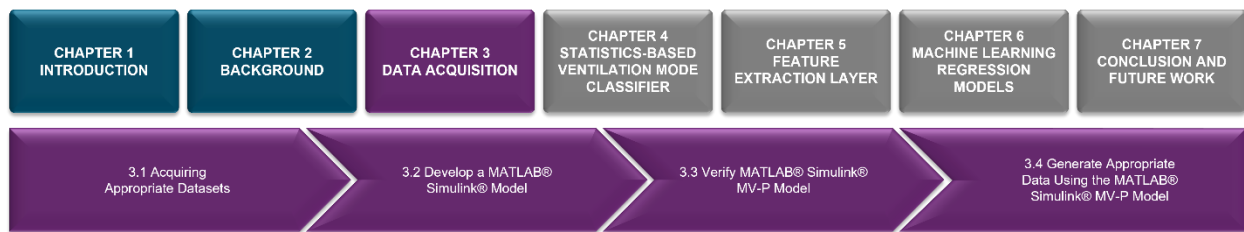
This chapter started with an overview of the essential background knowledge of the spontaneous breathing patient and how to model the respiratory system. One of the essential takeaways was that ventilation is achieved through pressure differentials following Boyle's law. The second important conclusion was that modelling a respiratory system with a single-compartmental RC model has sufficient representative complexity for the project since the patient will be sedated, an ETT will be used, relatively low respiratory rates will be administered (sub 30 breaths per minute), and scalar values for the airway resistance and static compliance are all that is necessary for mechanically describing the state of a respiratory system (as in practice).

Subsequently, the basics and techniques of mechanical ventilation were investigated to scope the relevant ventilation modes for the project. The components of the MV-P circuit were conveyed. The mechanics behind PPV and the phases of the breathing cycle were discussed. Also, the standard monitoring outputs (the three waveform scalars of proximal airway pressure, flow rate and volume over time, and the hysteresis loops, i.e., the pressure-volume and flow-volume loops) were determined. Finally, the most prevalent ventilation modes appropriate for the project (VCC, VCD and PC) were identified out of the wide range of ventilation techniques.

After that, the relevant parameters and heuristics, for appropriately setting up the MV-P system, were identified, followed by a discussion of how the dependent feedback could be used for condition monitoring of the patient's health status. The relevant patient parameters identified were age, height, and sex. From these parameters, dependent parameters were predicted, such as the trachea's length and diameter, the lungs' dead space and functional residual capacity, ETT size, and the recommended ventilator settings. The necessary ventilator settings are the mode of ventilation, respiratory rate, baseline pressure, maximum inspiratory flow, tidal volume, peak inspiratory pressure, and inspiratory time. Finally, the techniques used for respiratory system condition monitoring using the three waveform scalars and hysteresis loops were discussed.

Finally, a summary of machine learning and the appropriate algorithms expected to be useful for the project was conveyed. Since the respiratory system's health status can be sufficiently described with the values of the airway resistance and static compliance, automatically performing classification of the patient's status from ventilation data becomes a regression problem. Therefore, machine learning algorithms expected to be used for this project are linear regression algorithms, decision tree algorithms (assuming high label resolution), support vector machine algorithms, gaussian process regression algorithms, ensemble algorithms, and neural networks.

CHAPTER 3 – DATA ACQUISITION



In this chapter, the process used for acquiring the labelled mechanical ventilation data is chosen and described. First, the requirements for the labelled mechanical ventilation dataset are conveyed, and a dataset survey's results are mentioned. After that, a MATLAB® Simulink® model of a mechanical ventilator-patient (MV-P) system is developed (and verified) to meet the required representative complexity and can adjust the relevant parameters for this project, as discussed in Chapter 2. Finally, said model is utilised to generate the required labelled dataset.

3.1 Acquiring Appropriate Datasets

In order to automate the classification of a patient's status based on ventilation data, artificial knowledge must be recognised by inspecting the data using statistical or machine learning methods. Both methods require data examples of the different types of instances from which the automatic classification types should be identified. Chapter 2 discusses the mechanical ventilation process as a multivariate issue; thus, a myriad of variables is to be considered throughout the setup. This includes the biological and anthropometric parameters of the patient, the mechanical characteristics of the patient's respiratory system, the choice of interface used to ventilate the patient (and its variations), the mechanical ventilator (MV) circuit's dimensions, and finally, the protocol and settings specified by the pulmonologist for the MV to deliver the breaths. Not only do these parameters need to be known to properly label the specific instance of the MV-P setup, but also the time-variate waveform scalars (pressure, flow rate and volume) need to be logged at an appropriate sampling frequency for proper information resolution for feature extraction later.

First, it should be determined if a dataset with data fidelity appropriate to the multivariate nature of the problem is readily available for use. A dataset survey was done to locate any such datasets available for research purposes, and usage permission was requested. Unfortunately, all available datasets found [87]–[95], which were available for research purposes by students, did not meet the requirements (as previously mentioned) for solving the problem. These datasets contained information on the anthropometric and biological parameters of the patient, as well as the protocols used to ventilate those patients. However, the ventilator settings, mechanical parameter logs per breath and the time-series data of the waveforms were unavailable.

Solving this problem meant that a dataset needed to be created. Since generating the dataset by recording empirical data at the bedside would be time-consuming and deliver a small dataset and raise ethical issues, a synthetic dataset is apparent. Using a pipe-balloon experimental setup or the HAL® S3201 programmable patient puppet has its use-case limitations and would require an MV, which was also unavailable for the project.

Considering all the points mentioned for why a physical solution for creating a dataset with high enough fidelity is impossible, it was agreed upon that the synthetic dataset had to be generated using simulation model-based techniques.

A few MV-P simulation models were found [89], [96]–[98]. However, none of the models were versatile enough to meet all the requirements for creating such a high-fidelity dataset. Therefore, the most eloquent existing model was chosen to be further developed to meet said requirements. The chosen model used as a draft was the MATLAB® Simulink® Medical Ventilator with Lung Model from The MathWorks®, Inc.

3.2 Develop a MATLAB® Simulink® Model

As previously mentioned, the simulation model should be able to generate synthetic waveform scalar data of the pressure, flow rate and volume variables from a versatile set of options for setting up the MV-P system. The findings from Chapter 2 are used to determine the specific requirements (listed below) that the simulation model should meet.

- Patient's biological and anthropometric parameters (age, sex, height and ideal body weight) should be specifiable and automatically used by the model to calculate and implement the dead space of the MV-P system, the functional residual capacity (*FRC*) of the lungs, dimensions of the trachea (i.e., length and inside diameter) and the appropriate endotracheal tube (ETT) to be used (from the set of size combinations).
- The patient-interface component should be an endotracheal tube (ETT) since the assumptions from Chapter 1 dictate that the patient is fully sedated.
- The MV should incorporate a variable pressure valve at the expiratory tube for the model to simulate a variable baseline pressure [99].
- The patient's mechanical parameters (lung resistance and lung compliance) should be variable during simulation to simulate the changing health status of the patient.
- The patient biting the endotracheal tube (ETT) at variable intensity should be simulatable.
- The model should be able to simulate an expiratory hold manoeuvre for verification.
- The MV should support the volume-control (VC) mode and the choice of flow pattern protocol – options should be between constant flow (VCC) and decelerating flow (VCD).

3.2.1 Existing MATLAB® Simulink® MV-P Model Draft

The existing model used for functionality expansion was drafted from The MathWorks®, Inc. at the time of developing the simulation model [57]. The Simulink® model's diagram is conveyed in Figure 3-1.

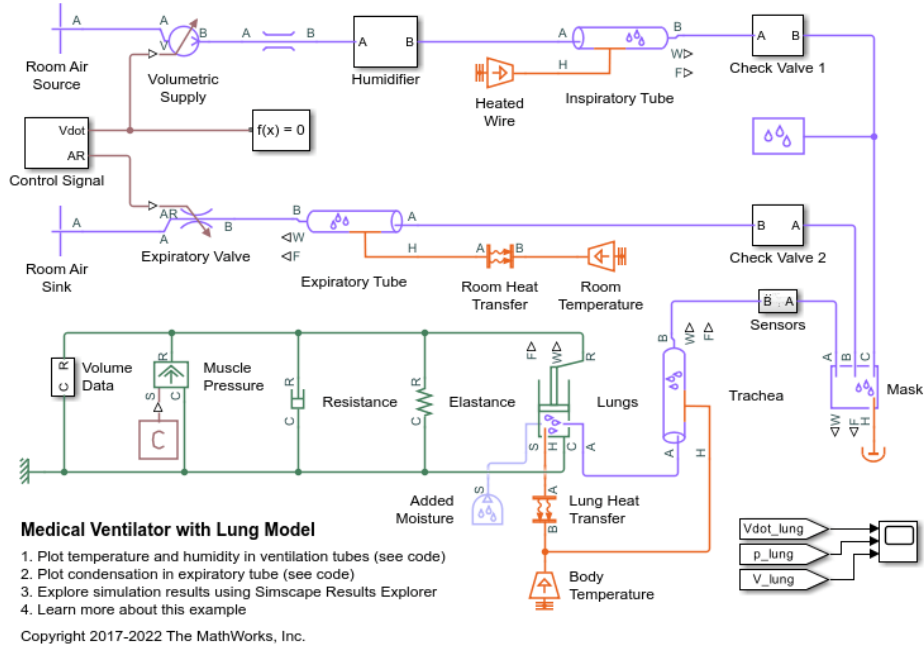


Figure 3-1: Drafted Simulink® Medical Ventilator with Lung Model Schematic Diagram

Upon inspection, the lungs (green area) resembled an RC model, the control signal component uses volume-controlled (VC) mode protocols, humidification and temperatures of the air are simulatable, control of the work of breathing (WOB) of the patient is possible (only used for active patients), and the model outputs the three waveform scalars of interest. However, the model deviates from the required solution in the following aspects and, thus, needs expansion:

- The model does not dynamically adjust the dead space, FRC , trachea dimensions or patient-interface component since no input methods exist to specify the patient's parameters.
- The patient-interface component is not an ETT, but a tight-fitting face mask, which is inappropriate for fully sedated patients.
- No variable pressure valve is incorporated at the expiratory tube; thus, the model cannot simulate a variable baseline pressure.
- The patient's mechanical parameters (lung resistance and lung compliance) are static during the simulation and can, therefore, not simulate the changing health status of the patient.
- No components are implemented to resemble the patient biting the ETT.
- The model is incapable of simulating an expiratory hold manoeuvre.
- The MV supports the VC mode but only the constant flow (VCC) pattern.

3.2.2 Capturing Patient's Biological and Anthropometric Parameters

MATLAB® App Designer was used to interface the Simulink® model with a graphical user interface (GUI) to capture the parameters used when simulating the MV-P model. The user can select an existing patient from the database (DB) or add a new patient with their biological and anthropometric parameters to the DB. These parameters include the patient's name, surname, sex, date of birth (automatically calculates the age of the patient at simulation), and height ($Height_{cm}$) recorded at simulation (see Figure 3-2).

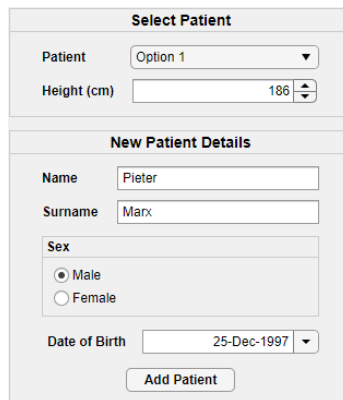


Figure 3-2: Graphical User Interface (GUI) for Specifying the Patient's Simulation Parameters for the Mechanical Ventilator-Patient Simulink® Model

These parameters are used to calculate the ideal body weight (IBW_{kg}), dead space, FRC and trachea dimensions (trachea length (TL_{mm}) and trachea diameter (TD_{mm})), as well as to determine the appropriate ETT size to use. These methods are discussed in Chapter 2, and the relevant equations are briefly mentioned below as a reminder.

$$IBW_{Male} = 50 + [0.9055 \times (Height_{cm} - 152.4)] \quad (3-1)$$

$$IBW_{Female} = 45.5 + [0.9055 \times (Height_{cm} - 152.4)] \quad (3-2)$$

$$V_T = 7 \text{ mL}/IBW_{kg} \quad (3-3)$$

$$\text{Dead Space} = 30\% \text{ of } V_T \quad (3-4)$$

$$FRC = 30 \text{ mL}/IBW_{kg} \quad (3-5)$$

(3-6)

$$TL_{Male} = 0.612 \times Height_{cm} + 9.18$$

(3-7)

$$TL_{Female} = 0.606 \times Height_{cm} + 9.09$$

(3-8)

$$TD_{Male} = 0.0934 \times Height_{cm} + 1.40$$

(3-9)

$$TD_{Female} = 0.0925 \times Height_{cm} + 1.39$$

For an adult male, the heuristic used by pulmonologists is to select an ETT size with at least an 8.0 mm inside diameter and an ETT size with at least a 7.0 mm inside diameter for adult women.

The heuristic used for selecting the approximate ETT inside diameter is given by equation (3-10) for paediatric patients. The standard is to select the ETT with an inner diameter less than ETT_{Size} from the list of 17 ETT size combinations in Table 3-1.

(3-10)

$$ETT_{Size} = \frac{Age + 16}{4}$$

Table 3-1: Lookup Table of Standard Endotracheal Tube (ETT) Sizes

ETT Length (mm)	ETT Inner Diameter (mm)
230	2.0, 2.5, 3.0, 3.5, 4.0, 4.5, 5.0
260	5.5
270	6.0
280	6.5
290	7.0
302	7.5, 8.0, 8.5, 9.0, 9.5, 10.0

After determining the parameters, the ETT size combination (Figure 3-3), trachea dimensions (Figure 3-4), dead space and *FRC* parameters (Figure 3-5) are automatically fed into the MATLAB® Simulink® MV-P model's settings before simulation commences.

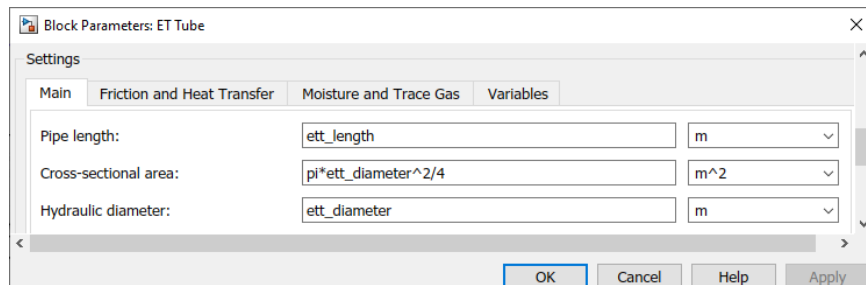


Figure 3-3: Settings Recorded in ET Tube Block Parameters

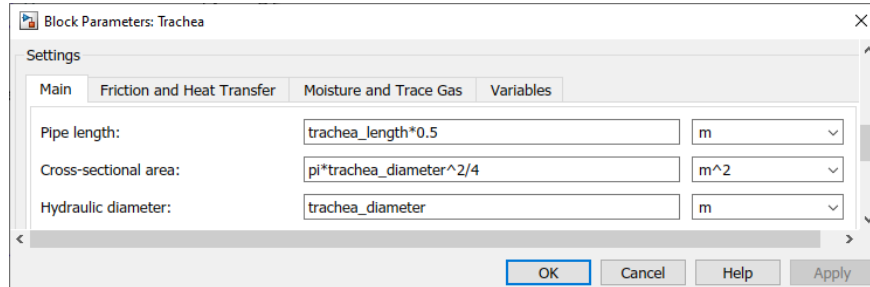


Figure 3-4: Settings Recorded in Trachea Block Parameters

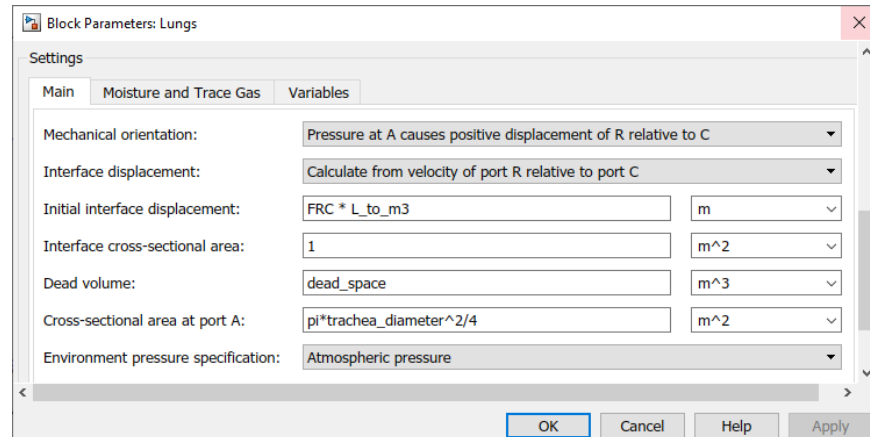


Figure 3-5: Settings Recorded in Lungs Block Parameters

3.2.3 Implementing the Endotracheal Tube (ETT)

The patient-interfacing component in the drafted Simulink® model is a tight-fitting face mask. This is appropriate for non-invasive positive pressure ventilation (NIPPV) such as continuous positive airway pressure (CPAP), bi-positive airway pressure (BiPAP) and pressure support (PS) modes. In these cases, the patient is active and can breathe spontaneously. For sedated patients, a tight-fitting face mask can cause secretions to build up in the trachea. Therefore, implementing an ETT for sedated patients is vital for airway protection.

To implement an ETT in the Simulink® model, the tight-fitting face mask's block parameters are replaced with that of a Y-piece since both components can be modelled as constant volume chambers (Figure 3-6). The Y-piece connects the tubes of the ventilator with the ETT.

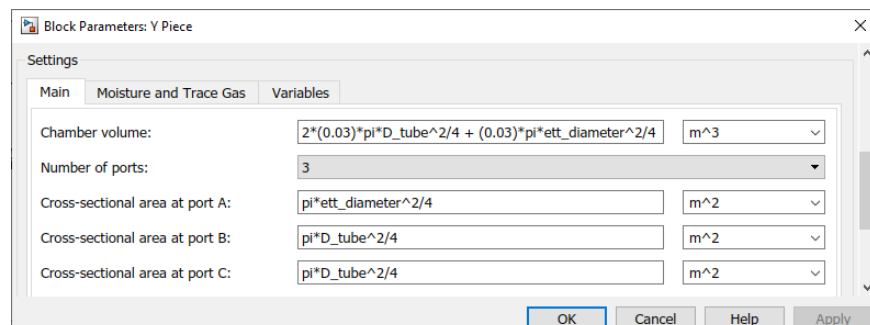


Figure 3-6: Settings Recorded in Y-Piece Block Parameters

3.2.4 Variable Baseline Pressure Expiratory Valve

The baseline pressure (end-expiratory pressure) is sometimes greater than atmospheric pressure (positive end-expiratory pressure – PEEP). This technique is commonly used to keep the alveoli pressurised (even at expiration), preventing the alveoli from collapsing. Frequent collapsing alveoli not only cause restricted gas exchange but also leads to inflammation, which prolongs ventilation therapy.

To implement the variable baseline pressure functionality, the expiratory valve's pressure reference needs only be configured with a variable that will update at the start of each ventilation session (reservoir pressure in Figure 3-7). The variable is retrieved from the simulation app's GUI (see the PEEP spinner component in Figure 3-8).

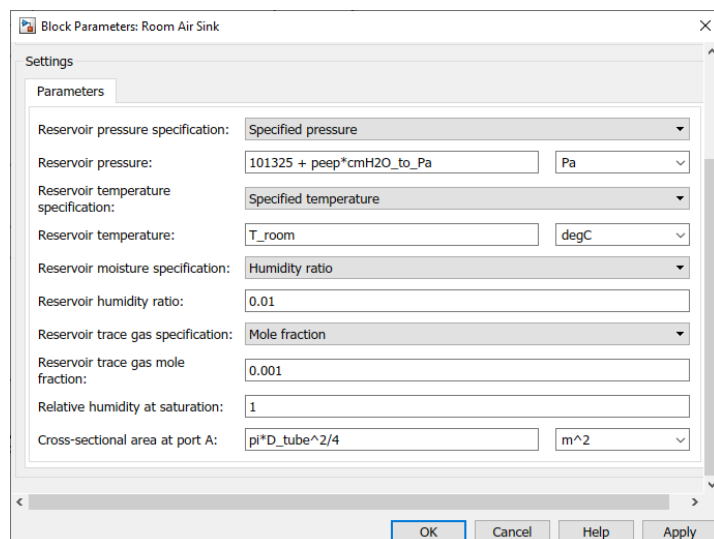


Figure 3-7: Recorded Expiratory Valve's Pressure Reference Block Parameter Settings

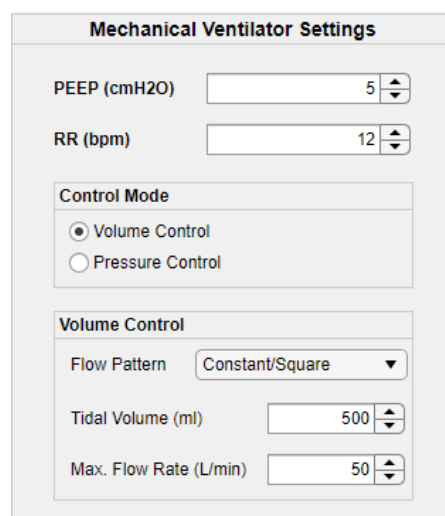


Figure 3-8: Graphical User Interface (GUI) for Specifying the Mechanical Ventilator Simulation Parameters for the Mechanical Ventilator-Patient Simulink® Model

3.2.5 Dynamic Patient Mechanical Parameters

The lungs in the drafted Simulink® model are represented by the single-compartment RC model discussed in Section 2.2.4. This is an appropriate respiratory system model choice since the respiratory rate used during positive pressure ventilation (PPV) is below 30 breaths/min. The ETT is modelled separately to represent the dominating, constant inertance component.

However, the resistance and elastance components (represented by the dashpot and spring) have constant input parameters, which disables the Simulink® model to simulate time-variant patient health conditions. These components are replaced by their counterpart variable component blocks, which can control the mechanical parameters of the patient's respiratory system and, therefore, the patient's health status during a simulation. This is accomplished by sending a variable control signal during the simulation from the MATLAB® workspace. Figure 3-9 is the schematic diagram of the RC status subsystem block that retrieves and sends the control signals to the varying component blocks.

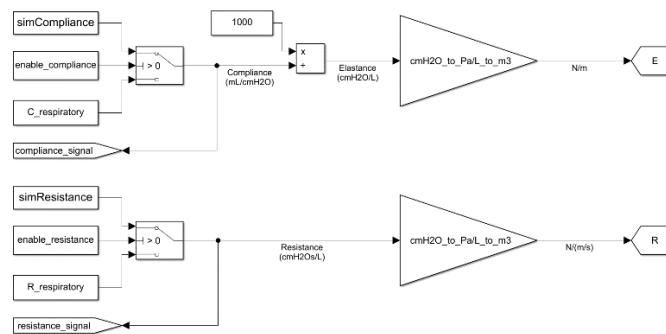


Figure 3-9: The Schematic Diagram of The RC Subsystem Block

The variable control signals are configured from the input parameters retrieved from the data generation app's GUI (see Figure 3-10 (a) for controlling resistance and (b) for controlling compliance).

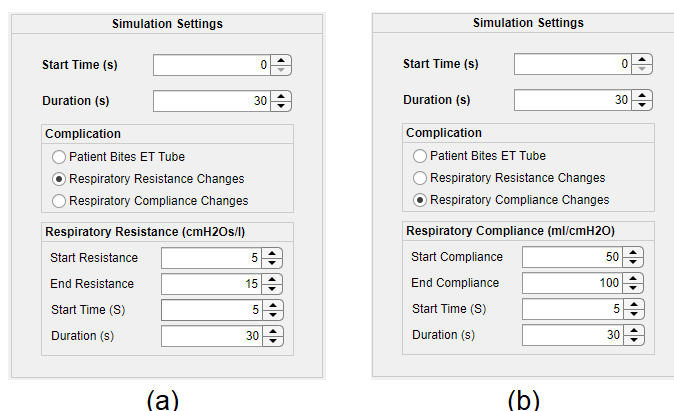


Figure 3-10: Graphical User Interface (GUI) for Specifying the Patient's Mechanical Parameters for the Mechanical Ventilator-Patient Simulink® Model: Parameters for Configuring the Control Signals: Resistance (a) and Compliance (b)

Figure 3-11 shows the resulting waveform scalars (left-hand side) during VCC as the resistance complication signal increases with $5 \text{ cmH}_2\text{O} \cdot \text{s/L}$ for each breath (right-hand side). The first breath is transient since *FRC* must be established first, but the second and third breath is steady and resembles increasing resistance traits (constant $P_{Plateau}$ and increased P_{PIP}).

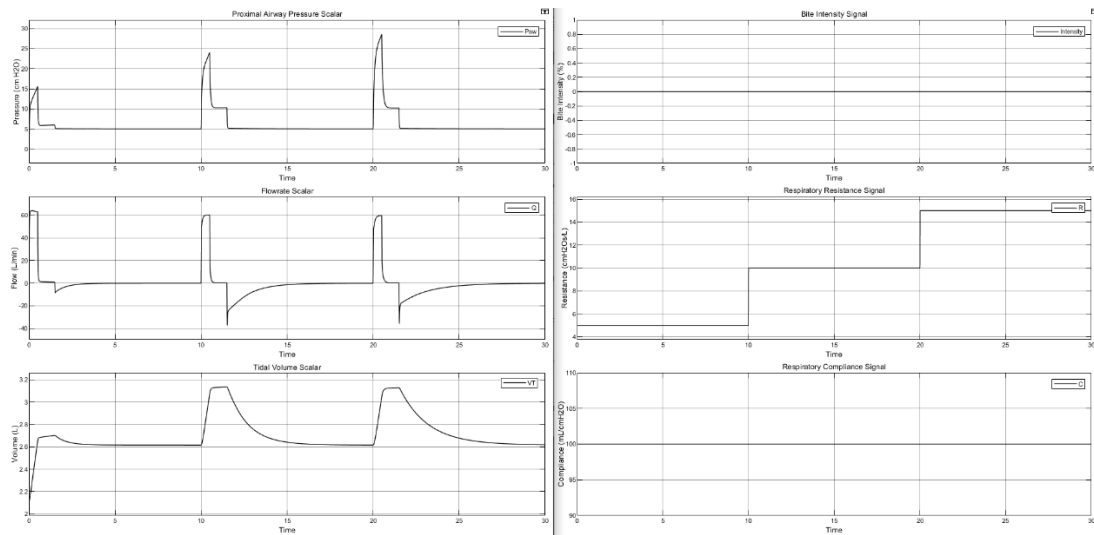


Figure 3-11: Waveform Scalars Resulting from Simulated Dynamic Lung Resistance

Figure 3-12 shows the resulting waveform scalars (left-hand side) during VCC as the compliance complication signal increases with $25 \text{ mL/cmH}_2\text{O}$ for each breath (right-hand side). The first breath is transient since *FRC* need to be established first. However, the second and third breath is in a steady state and resembles traits of increasing compliance (decreasing $P_{Plateau}$, constant pressure drop from P_{PIP} to $P_{Plateau}$ and increasing baseline volume). The baseline volume increases since more volume is stored at the constant baseline pressure for increased compliance (units being mL/cmH₂O).

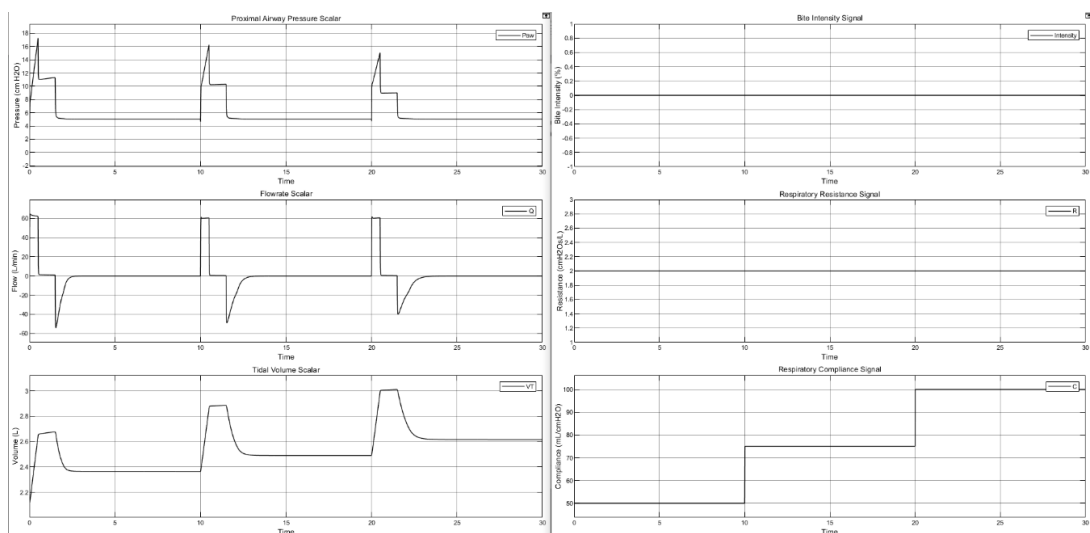


Figure 3-12: Waveform Scalars Resulting from Simulated Dynamic Lung Compliance

3.2.6 Biting of the Endotracheal Tube (ETT)

Although the patient is assumed to be sedated, the patient is still able to experience muscle contractions during medical complications or kinking of the pipes can still occur. Some methods for obstructing the flow in the pipes are needed to implement this complication as an option. Therefore, a variable local restriction is implemented between the ETT and the sensors. This component can resemble the teeth of the patient or a kink in the ventilator circuit. The restriction area is controlled in the same manner that the variable mechanical parameters of the patient's lungs are controlled (by implementing a variable control signal during the simulation from the MATLAB® workspace). Figure 3-13 is the schematic diagram of the teeth subsystem block that retrieves and sends the control signals to the varying local resistance block.

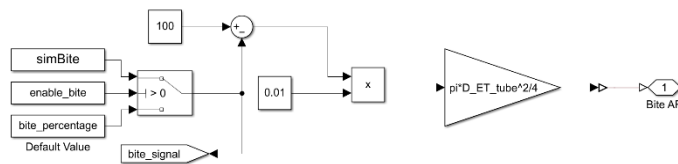


Figure 3-13: The Schematic Diagram of The Teeth Subsystem Block

The variable control signal for bite intensity is configured from the input parameters retrieved from the data generation app's GUI (see Figure 3-14 (a)).

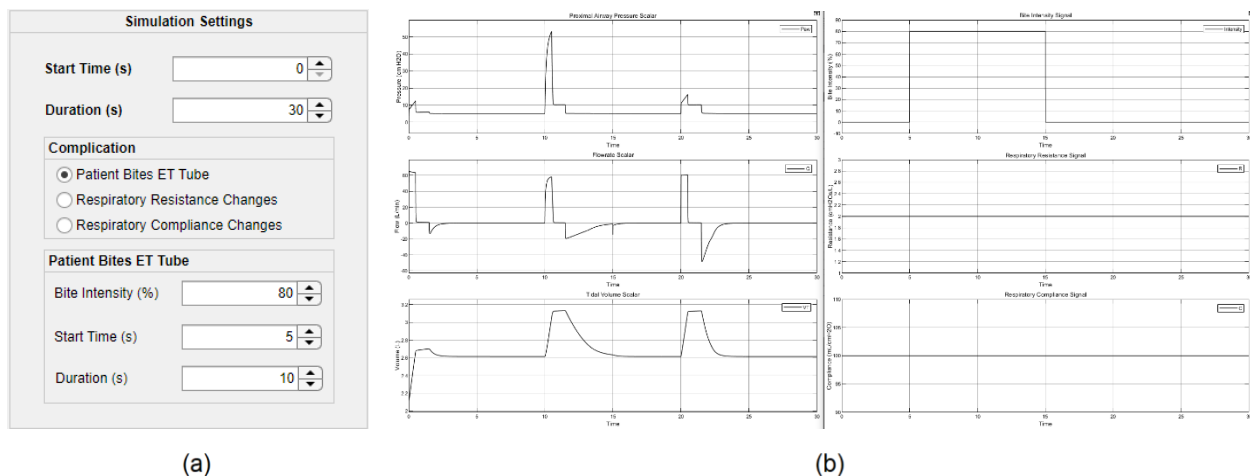


Figure 3-14: Graphical User Interface (GUI) for Specifying the Patient's Bite Intensity Parameters for the Mechanical Ventilator-Patient Simulink® Model (a) and Waveform Scalars Resulting from Simulated Dynamic Biting Intensity (b)

Biting the ETT or bending the tube to form a kink are just specific examples of increased resistance within the ventilator circuit. Figure 3-14 (b) shows the resulting waveform scalars (left-hand side) during VCC as the biting intensity is present from the 5 to 15 second interval at 80% intensity. The first breath is transient since *FRC* needs to be established first, but the second breath resembles the biting period, and the third breath is normal. During the second breath, traits of increased resistance are present (constant $P_{Plateau}$ and increased P_{PIP}).

3.2.7 Implementing the Expiratory Hold Manoeuvre Option

As discussed in Section 2.6.2.3, the pulmonologist uses the expiratory hold manoeuvre to quantitatively evaluate the mechanical parameters, during which no airflow is present at the end of the inspiratory phase. As mentioned, this manual manoeuvre is too invasive to perform at each breath. Logging the results is time-consuming for pulmonologists (wasting resources) and is prone to human error. However, this manoeuvre is implemented into the model only to verify the mechanical parameters later. This manoeuvre is achievable by implementing pulse generator logic and a parameter that specifies the duration of the manoeuvre. This is done in the backend of the model since there is no need to implement this manoeuvre for dataset generation purposes using the GUI. Evidence of this added feature's implementation can be noticed in Figure 3-11, Figure 3-12 and Figure 3-14 (b) by the plateau phase lasting one second each time.

3.2.8 Implementing the VC Flow Pattern Options

From Section 2.4.4.4, the VC mode has different variations of flow patterns for the inspiratory phase, of which the constant flow (VCC) and decelerating ramp flow (VCD) patterns are the most common. Figure 3-15 (VCC) and Figure 3-16 (VCD) are the schematic diagrams for implementing these breath delivery protocols using control signals.

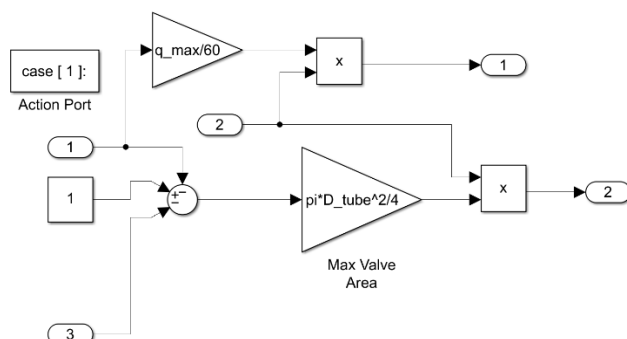


Figure 3-15: Schematic Diagram of The Constant Flow Mechanical Ventilator Control Signal Subsystem

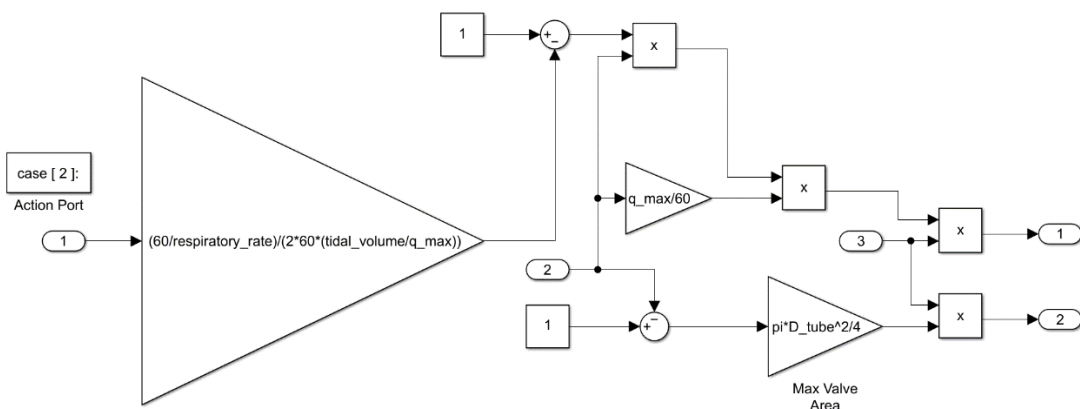


Figure 3-16: Schematic Diagram of The Decelerating Flow Mechanical Ventilator Control Signal Subsystem

The control signals used to manipulate the flow rate during the inspiratory phase are configured from the input parameters retrieved from the data generation app's GUI (see Figure 3-17 (a) for controlling VCC and (b) for controlling VCD).

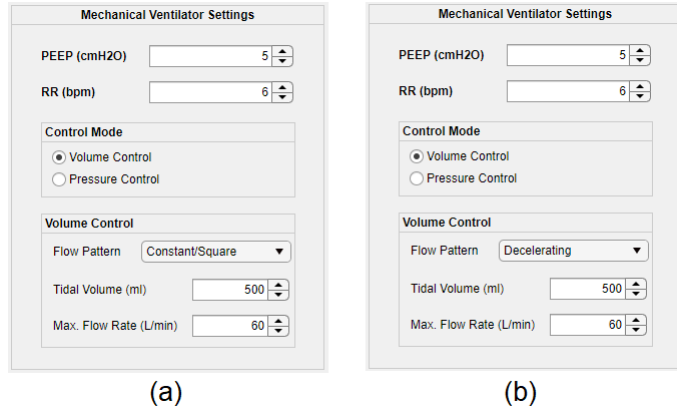


Figure 3-17: Graphical User Interface for Specifying the Mechanical Ventilator Parameters for the Simulink® Model: Constant (a) and Decelerating Ramp Flow Pattern (b)

Rewriting equations (2-34) and (2-35) from Section 2.5.4.9 results in the equations used to determine the inspiratory time (T_i) required for delivering a breath with a specified tidal volume (V_T in litres) and peak inspiratory flow rate (Q_{max} in litres per minute). Equations (3-11) and (3-12) are used to calculate T_i for VCC and VCD, respectively.

$$T_i = \frac{60 \times V_T}{Q_{max}} \quad (3-11)$$

$$T_i = \frac{60 \times V_T}{\frac{1}{2} \times Q_{max} + Q_{TH}} \quad (3-12)$$

When V_T is set to 0.5 L, Q_{max} to 60 L/min and Q_{TH} to 0 L/min, the resulting T_i should be 0.5 s for VCC and 1.0 s for VCD. Inspecting the waveform scalars from the simulations shows that this is the case (Figure 3-18 (a) is VCC, and Figure 3-18 (b) is VCD).

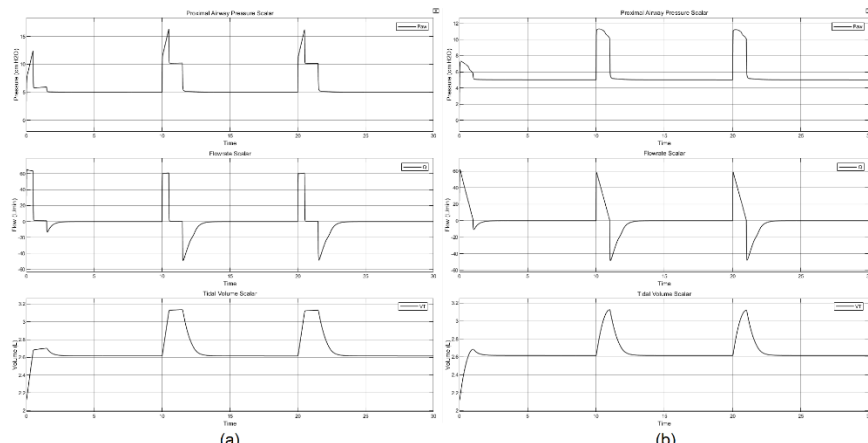


Figure 3-18: Waveform Scalars Resulting from Simulated Volume-Controlled Modes: Constant Flow Pattern (a) and Decelerating Flow Pattern (b)

3.2.9 The Expanded MATLAB® Simulink® MV-P Model

After expanding the functionality of the MATLAB® Simulink® MV-P model to meet the requirements mentioned in Section 3.2, the new schematic diagram is resembled by Figure 3-19. The differences include the conversion of the tight-fitting face mask into a Y-piece, adding a local resistance block to resemble the teeth, the ETT, the pattern option functionality for the VC mode and replacing the static mechanical parameter components with their variable counterparts. Also, the trachea, ETT and expiratory valve pressure reference settings have been modified to update automatically from the MV data generator application's input parameters (Figure 3-20).

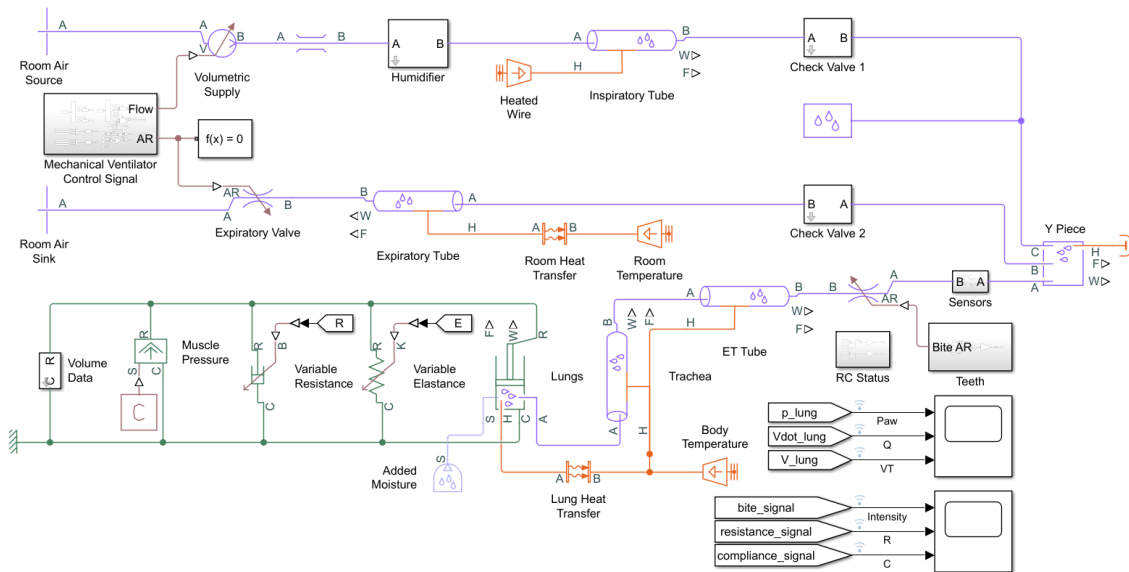


Figure 3-19: The Schematic Diagram of the Expanded Simulink® Mechanical Ventilator-Patient Model

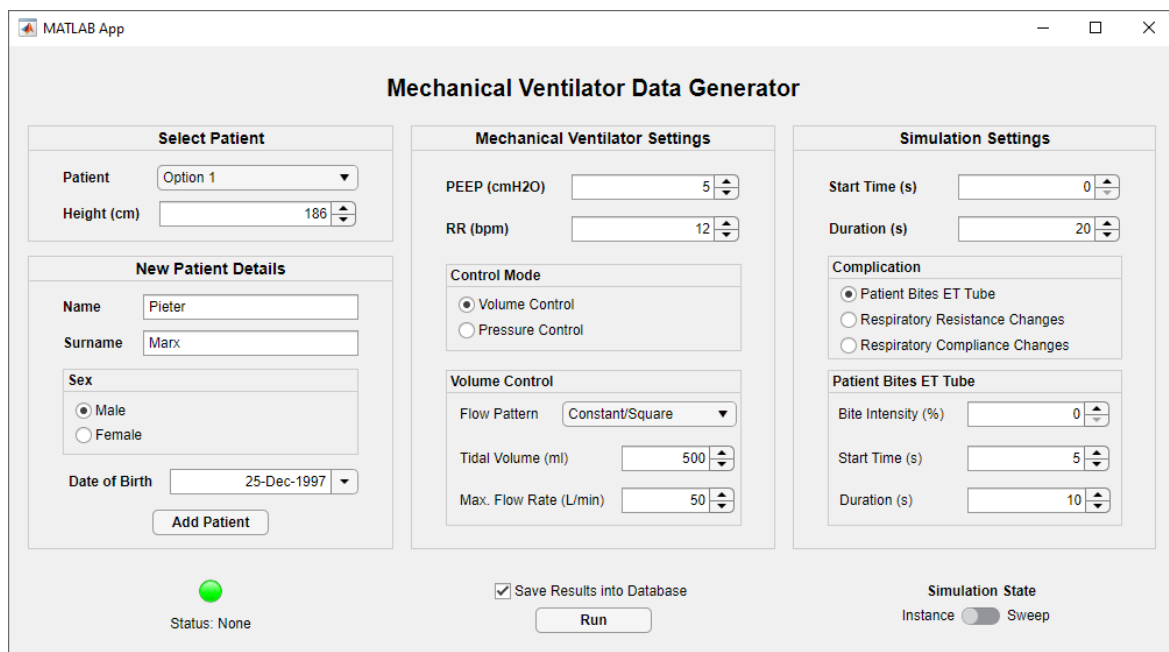


Figure 3-20: Graphical User Interface (GUI) for Specifying the Patient's Parameters, Mechanical Ventilator Settings and Complication Parameters for Simulating a Session Instance of the Mechanical Ventilator-Patient Simulink® Model

3.3 Verify MATLAB® Simulink® MV-P Model

In this section, the developed MATLAB® Simulink® MV-P model is verified qualitatively and quantitatively, and the model's sensitivity is inspected. Qualitatively verifying the model comprises analysing the pressure component behaviours and the effects of varying the mechanical parameters and comparing the shapes of the simulated waveform scalars to actual examples. Quantitatively verifying the model comprises varying the settable parameters and analysing the results for appropriate corresponding outputs.

3.3.1 Qualitative Verification of the MV-P Model

Qualitatively verifying the MV-P model is accomplished by inspecting the pressure component behaviours, examining the change in waveform shape as the mechanical parameters are varied and comparing the shapes of the waveform scalar data with actual data.

3.3.1.1 Pressure Component Behaviours

Referring to the equation of motion from Section 2.2.3.1 (evoked below for convenience by equation (3-13)), the resistance and elastance of the respiratory model are responsible for two separate pressure components ($P_R(t)$ and $P_C(t)$, respectively). These components can be exploited for verification purposes. Only implementing the resistive component in the MV-P model for a constant flow (VCC) should cause the pressure waveform to instantly increase to a constant value (verified by Figure 3-21) [10]. Also, only implementing the elastic component in the MV-P model should cause the pressure waveform to increase proportionally to the volume (linearly) due to the constant flow pattern when implementing VCC (verified by Figure 3-22) [10].

(3-13)

$$P_{aw}(t) = P_I(t) + P_R(t) + P_C(t) + P_0 = I_{RS} \cdot \dot{V}(t) + R_{RS} \cdot \dot{V}(t) + E_{RS} \cdot V(t) + P_0$$

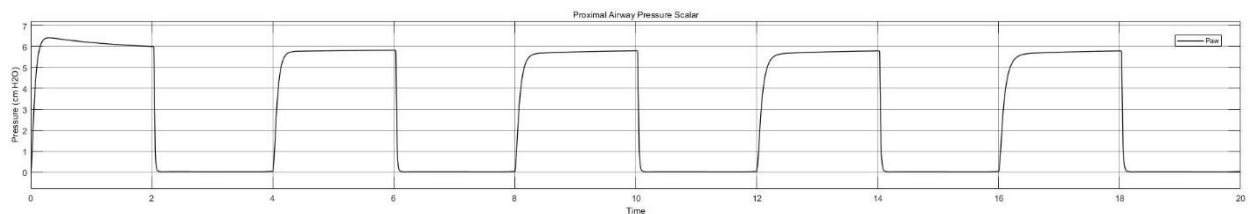


Figure 3-21: Pressure Waveform of Isolated Pressure Component due to Resistance

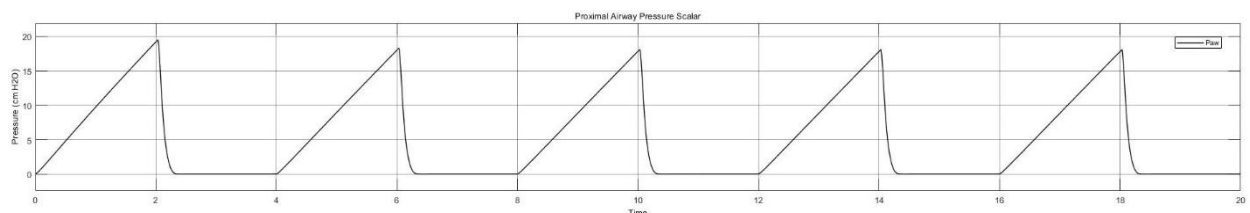


Figure 3-22: Pressure Waveform of Isolated Pressure Component due to Compliance

3.3.1.2 Verifying Effect of Changing Mechanical Parameters

Increasing the mechanical resistance parameter should result in the same effect illustrated by Figure 2-34 from Section 2.6.2.3.2. The effect is a constant plateau pressure with increasing peak pressure as the resistance increases (verified by Figure 3-23).

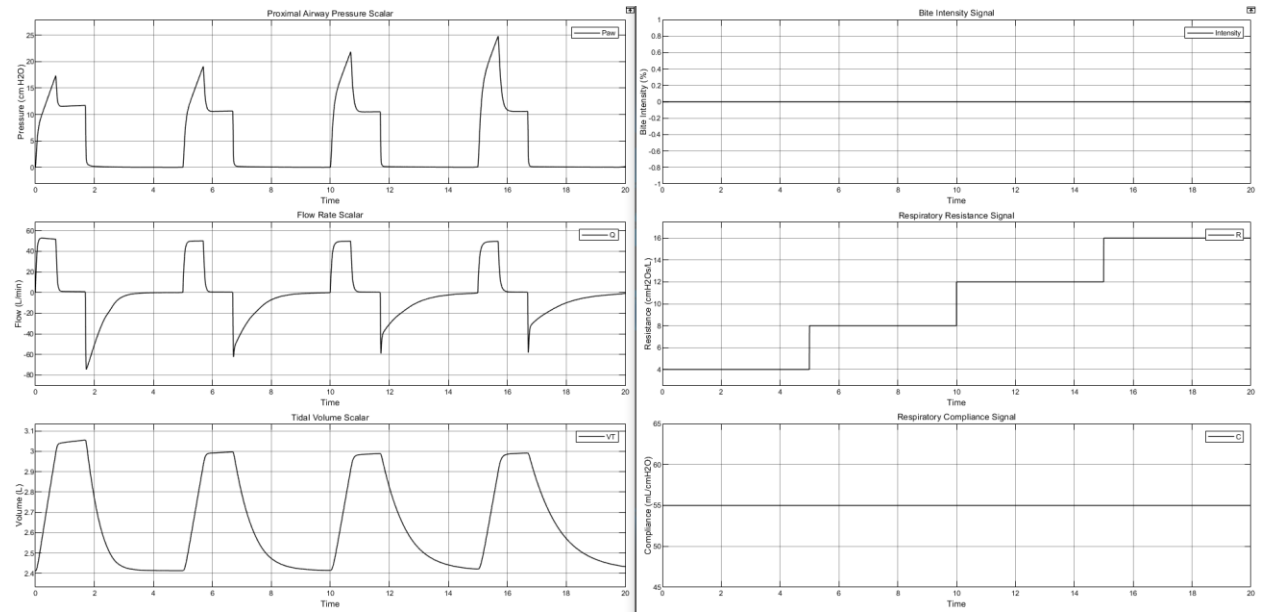


Figure 3-23: Waveform Scalars for Varying Resistance

Increasing the mechanical compliance parameter should result in the same effect illustrated by Figure 2-32 from Section 2.6.2.3.1. The effect is a constant pressure drop from peak pressure to plateau pressure with a decreasing plateau pressure as compliance increases (verified by Figure 3-24).

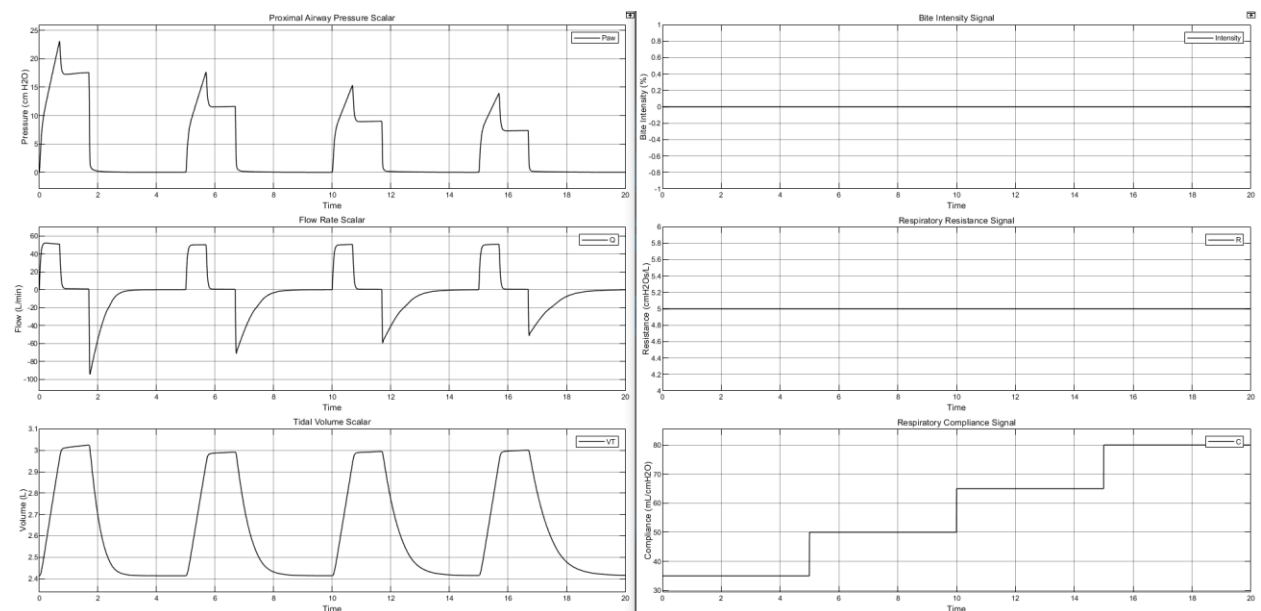


Figure 3-24: Waveform Scalars for Varying Compliance

3.3.1.3 Comparing Shapes of the Waveform Scalar Data

The waveform scalars of a simulation instance for VCC are compared to actual mechanical ventilation data in Figure 3-25 [6]. Overall, the curves match each other well. However, some noticeable differences are that the simulated pressure deviates at the start and end of the inspiratory phase. This is due to the delay in the opening and closing of the valves. The delays are kept since other examples of actual mechanical ventilation data exist with even longer delays (it depends on the mechanics of the physical MV). Furthermore, details on the exact setup (patient's mechanical parameters and the size of the ETT) for the actual data curves are not available. Therefore, matching the expiratory phase curves for the simulated and actual data is complex, and some settings had to be presumed.

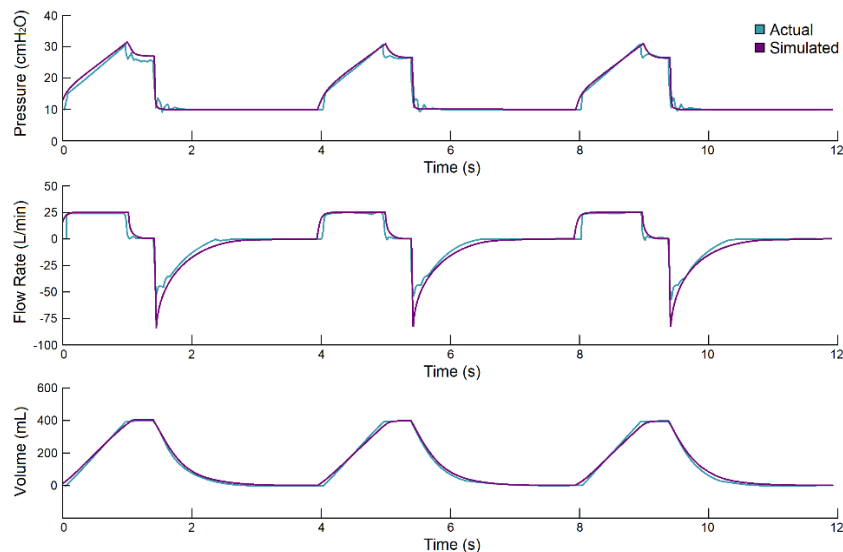


Figure 3-25: VCC Waveform Scalar Comparison of Actual Mechanical Ventilator Data with the Simulated Data

The same procedure was repeated for qualitatively verifying the VCD mode (results are conveyed in Figure 3-26) [6]. Since the MV-P system remained the same, the same deviations transpired. Delays in the opening and closing of the valves caused the pressure waveform scalar to reach the peak pressure at a later stage. The actual data curves came from the same source, and therefore, the details regarding the patient's mechanical parameters and the ETT size were undisclosed, resulting in another presumed setup.

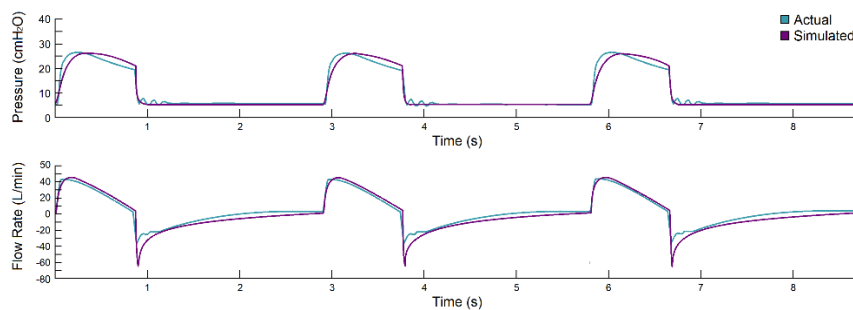


Figure 3-26: VCD Waveform Scalar Comparison of Actual Mechanical Ventilator Data with the Simulated Data

3.3.2 Quantitative Verification of the MV-P Model

Quantitatively verifying the MV-P model is accomplished by analysing the waveform scalars to verify that the MV settings have correctly been executed by the simulation and by performing the expiratory hold manoeuvre to verify the set mechanical parameter values analytically.

3.3.2.1 Verifying the MV Settings

Figure 3-27 and Figure 3-28 convey the relationship between the input parameters for the MV settings and the resulting waveform scalar outputs for VCC and VCD, respectively. The baseline pressure was set at 5 cmH₂O for VCC (measured 5.017 cmH₂O) and at 10 cmH₂O for VCD (measured 10.03 cmH₂O). The respiratory rate was set at 12 bpm for VCC (measured 12.0 bpm) and at 15 bpm for VCD (measured 15.0 bpm). The maximum inspiratory flow was set at 50 L/min for both VCC (measured at 49.91 L/min) and VCD (measured at 48.86 L/min). The tidal volume was set at 550 mL for VCC (measured at 522.9 mL) and VCD (measured at 527.3 mL). The cause for the noticeable tidal volume deviation is the lagging valves [100].

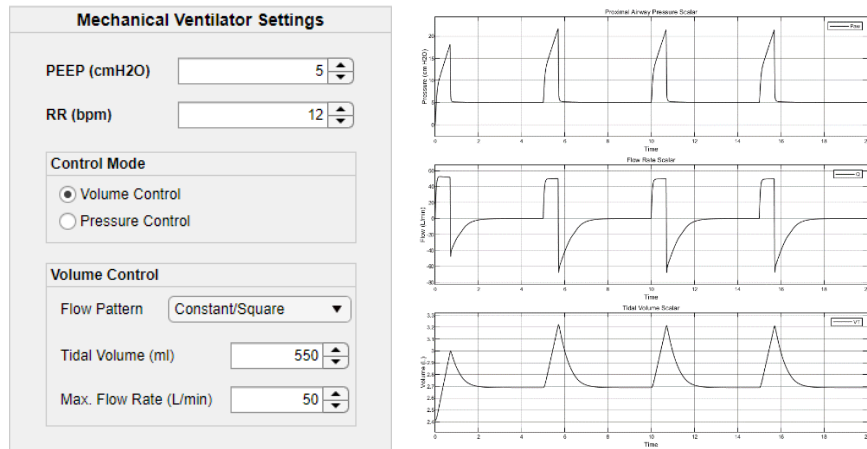


Figure 3-27: Mechanical Ventilator Settings and Resulting Waveform Output for VCC

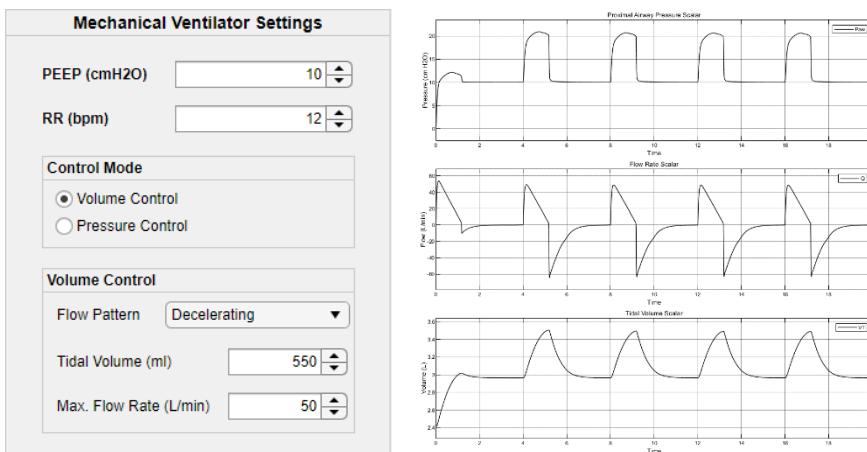


Figure 3-28: Mechanical Ventilator Settings and Resulting Waveform Output for VCD

3.3.2.2 Verifying the Resistance Mechanical Parameter's Values

Referring to the inspiratory resistance (R_{INSP}) equation from Section 2.6.2.3.2 (evoked below for convenience by equation (3-14)), R_{RS} can be approximated by performing the expiratory hold manoeuvre to acquire the plateau pressure. R_{RS} was swept for four breaths from 4 to 16 $\text{cmH}_2\text{O}\cdot\text{s/L}$. The mode is VCC, the tidal volume is 550 mL, and Q is 50 L/min (Figure 3-29). R_{INSP} was calculated from the output waveforms of Figure 3-30 (evaluated in Table 3-2).

$$R_{RS} \approx R_{INSP} = R_{RS} + R_{Circuit} = \frac{P_{PIP} - P_{Plateau}}{Q} \quad (3-14)$$

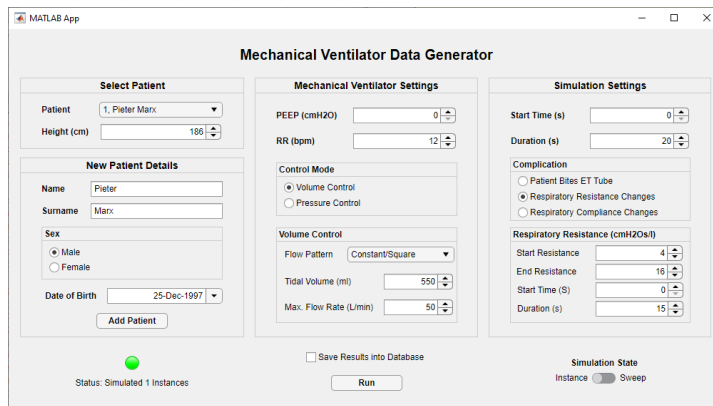


Figure 3-29: GUI of the Input Parameters for Sweeping the Resistance during VCC

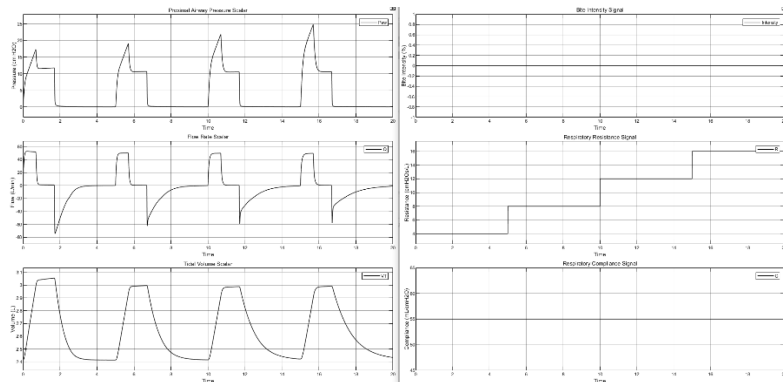


Figure 3-30: Waveform Scalar and Complication Signal Outputs for Sweeping Resistance in VCC

Table 3-2: Results for Sweeping the Resistance During VCC

R_{RS} [$\text{cmH}_2\text{O}\cdot\text{s/L}$]	P_{PIP} [cmH_2O]	$P_{Plateau}$ [cmH_2O]	Q [L/min]	R_{INSP} [$\text{cmH}_2\text{O}\cdot\text{s/L}$]	Inaccuracy [%]
4.00	17.34	11.72	52.82	6.38	59.60
8.00	19.10	10.65	50.14	10.11	26.40
12.00	21.85	10.53	49.82	13.63	13.61
16.00	24.82	10.60	49.64	17.19	7.42

3.3.2.3 Verifying the Compliance Mechanical Parameter's Values

Referring to the static compliance (C_S) equation from Section 2.6.2.3.1 (evoked below for convenience by equation (3-15)), the compliance can be calculated by performing the expiratory hold manoeuvre to acquire the plateau pressure. The compliance (C_{RS}) was swept for four breaths from 35 to 80 mL/cmH₂O. The mode is VCC, volume is 550 mL, and Q is 50 L/min (Figure 3-31). C_{RS} was calculated (C_{Calc}) from the output waveforms of Figure 3-32 (evaluated in Table 3-3).

$$(3-15) \quad C_S = \frac{V_T}{P_{Plateau} - P_0}$$

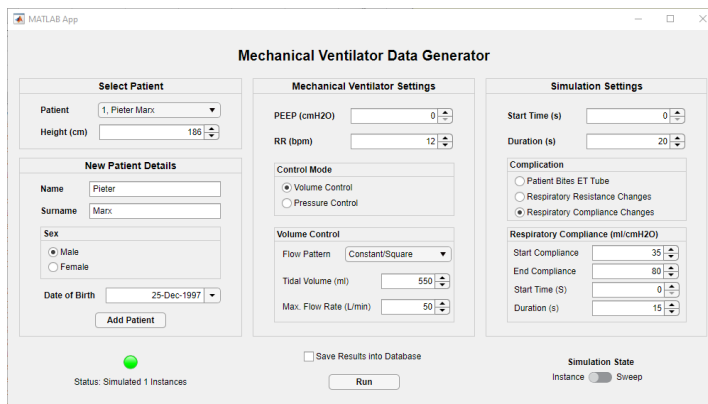


Figure 3-31: GUI of the Input Parameters for Sweeping the Compliance during VCC

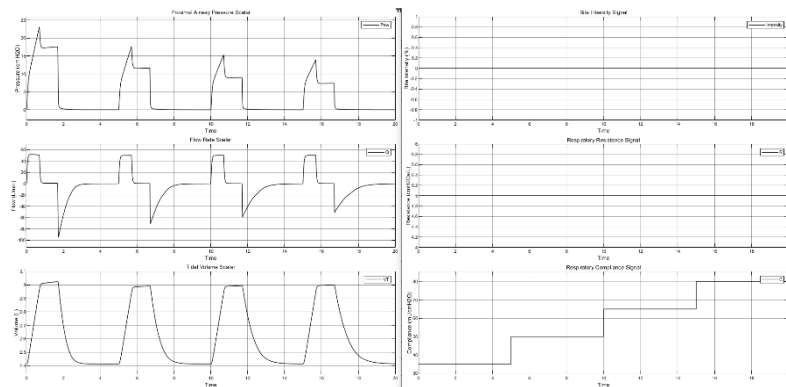


Figure 3-32: Waveform Scalar and Complication Signal Outputs for Sweeping Compliance in VCC

Table 3-3: Results for Sweeping the Compliance During VCC

C_{RS} [mL/cmH ₂ O]	V_T [mL]	$P_{Plateau}$ [cmH ₂ O]	P_0 [cmH ₂ O]	C_{Calc} [mL/cmH ₂ O]	Inaccuracy [%]
35.00	612.20	17.52	0.02	34.98	0.05
50.00	578.40	11.60	0.02	49.95	0.10
65.00	581.40	8.98	0.02	64.89	0.17
80.00	586.60	7.38	0.02	79.70	0.37

3.3.3 Sensitivity of the Model

The sensitivity of the MV-P model can be investigated by changing the parameters of the component blocks or by neglecting component blocks altogether. The components of interest are the inspiratory circuit (inspiratory tube and check valve), the expiratory circuit (expiratory tube and check valve), the endotracheal tube, the trachea and the expiratory valve.

3.3.3.1 Inspiratory Phase Related Circuit Parameter Sensitivity Analysis

The expiratory circuit and its parameters can be discounted by investigating the inspiratory phase behaviour independently. Twelve maximum inspiratory flow rates (10 to 120 L/min) were simulated for instances with and without an ETT. Equation (3-14) was then used to calculate R_{INSP} for both cases. The difference in R_{INSP} for the cases with and for those without the ETT is effectively R_{ETT} . Since the resistance inside a tube depends on the flow through the tube, the resistance values were recorded corresponding to the minimum and the maximum flow as an indication of the resistance range. This was done for R_{INSP} without the ETT and for R_{ETT} . R_{RS} was kept constant at 5 cmH₂O·s/L throughout the simulations.

This method was repeated for different setups of the MV-P model. The first case is the normal setup with all the components present in the model. The second case had no inspiratory circuit, i.e., no inspiratory tube or check valve. The third case was similar to the second case, but with the addition of no trachea. The results obtained were recorded in Table 3-4.

Table 3-4: Resistance Range Results for the Inspiratory Phase Experiments

Setup Description	R_{INSP} w/o ETT [cmH ₂ O·s/L]			R_{ETT} [cmH ₂ O·s/L]	
Flow (L/min)	10	120	Avg.	10	120
All Components	4.74	4.86	4.83	0.90	6.97
No Insp. Circuit	5.16	5.03	5.12	0.90	7.24
No Insp. Circuit or Trachea	5.16	4.94	5.06	0.90	7.24

The ETT's resistance (R_{ETT}) ranged from 0.90 to 7.24 cmH₂O·s/L. R_{INSP} without the ETT was relatively constant, with averages ranging from 4.83 to 5.12 cmH₂O·s/L (dominated by R_{RS}). Upon further inspection, the trachea contributes about 0.04 cmH₂O·s/L of R_{INSP} , and the inspiratory tube with its check valve contributes about 0.29 cmH₂O·s/L.

The ETT's resistance varies significantly and depends on the flow rate. This is attributable to the Eddy currents during turbulent flow through a pipe [101]. During turbulent flow, the pressure and velocity of airflow are random, and a higher pressure-differential is required to maintain the flow rate, i.e., the resistance to airflow increases [37].

To verify that the ETT does cause a turbulent flow state, a unitless parameter called Reynold's Number (R_e) can be assessed using equation (3-15). This formula is specifically appropriate for determining the state of airflow through a pipe.

$$R_e = \frac{\rho u L}{\mu} = \frac{uL}{\nu} \quad (3-16)$$

R_e – Reynold's Number

ρ – Fluid Density (kg/m³) – 1.164 kg/m³ [102]

u – Velocity of Airflow (m/s)

L – Characteristic Length or Pipe Inside Diameter (m)

μ – Dynamic Viscosity (kg/m·s)

ν – Kinematic Viscosity (m²/s)

Since the humidifier's temperature is set to 40 °C during simulation, the kinematic viscosity of the air is 1.702×10^{-5} m²/s [102]. The inside diameter of the ETT is 8 mm, and the flow rate was swept from 10 to 120 L/min. If R_e is below 2 000, the air flows in a laminar state. If R_e is between 2 000 and 4 000, the air flows in a transitional state. When R_e surpasses 4 000, the turbulent state is achieved. Using these parameters together with equation (3-16), R_e was calculated over the airflow sweep and summarised in Table 3-5.

Table 3-5: Reynold's Number Values for Flow Rate Sweep

Flow Rate (L/min)	10.00	12.83	25.67	30.00	75.00	120.00
u (m/s)	3.32	4.25	8.51	9.95	24.87	39.79
R_e	1 558.51	1 999.57	4 000.69	4 675.53	11 688.82	18 702.11

Since the specified ETT exceeds 2 000 at relatively low flow rates (at approximately 12.83 L/min), the airflow through the pipe is non-laminar for most of the flow range. Thus, Eddy currents occur at greater flow rates, causing the increase in resistance reflected in Table 3-4.

3.3.3.2 Expiratory Phase Related Circuit Parameter Sensitivity Analysis

In order to inspect the expiratory phase-related parameters, the time constant (τ_{RC}) and C_S (using equation (3-15)) were leveraged. First, C_S was calculated by analysing the expiratory phase waveforms using the same simulation settings discussed in the previous section. C_S had more than 99% accuracy each time (hold manoeuvre analysis works well for C_S). τ_{RC} was measured from the volume waveform and used with equation (3-17) to get R_{EXP} [29], [37].

$$\tau_{RC} = R_{EXP} \times C_S \quad (3-17)$$

Different MV-P setups were evaluated to isolate each component's effects on the outputs. The first case is the normal setup with all the components inside the model. The second case was a set of simulations where the expiratory valve's discharge coefficient was swept from 0.6 to 1.0. The third case was also a set of simulations, but the expiratory valve's minimum restriction area parameter was swept from 0.8 to 1.0. The fourth case had no expiratory circuit, i.e., no expiratory tube or check valve. The results obtained were recorded in Table 3-6.

Table 3-6: Resistance Range Results for the Inspiratory Phase Experiments

Setup Description	Avg. R_{EXP} [cmH ₂ O·s/L]	R_{EXP} w/o R_{RS}	
		Statistic	[cmH ₂ O·s/L]
All Components	7.76	Avg.	2.76
Valve Discharge Coef. (0.6 to 1.0)	7.75	Std.	0.01
Valve Min. Restriction Area (0.8 to 1.0)	7.77	Std.	0.04
No Exp. Circuit (Only ETT)	7.44	Avg.	2.44

R_{EXP} without R_{RS} had a relatively large average (2.76 cmH₂O·s/L) due to the ETT forming part of the expiratory circuit. Sweeping both parameters of the expiratory valve (the discharge coefficient and the minimum restriction area) had negligible effects on the system, with standard deviations in the resistance respectively being 0.01 and 0.04 cmH₂O·s/L. The expiratory tube with its check valve only contributed 0.32 cmH₂O·s/L, which is very similar to that of the inspiratory circuit.

3.3.3.3 Discussion and Conclusion on Model Sensitivity

The MV circuit and trachea have negligible effects (totalling around 0.3 cmH₂O·s/L). Thus, finetuning is unnecessary for the representative complexity required for this project. However, the ETT dominates the system's resistance, even at low flow rates, with an ETT suitable for adults. Proving that using traditional analytical techniques for approximating R_{RS} is inadequate.

3.4 Generate Appropriate Data Using the MATLAB® Simulink® MV-P Model

In this section, the dataset generation process is discussed. Firstly, some assumptions are made to scope the theoretically unlimited dataset for the project. A discussion follows the typical parameter ranges, which are used as the rationale for the chosen dataset spectrum. After that, the MV data generator is adapted to support the parameter sweep functionality and is optimised with parallel computing techniques. Finally, the generated dataset and its format are discussed.

3.4.1 Scoping the Dataset

The objective of this project (investigating the possibility of automatically classifying the health status of a mechanically ventilated patient) allows a dataset from a single patient identity to be sufficient. However, strategic parameter sweeping can generate a more inclusive dataset.

Recall from Section 3.2.2 that the patient's identity determines some parameters considered for this project. These parameters are the dead space, *FRC*, trachea dimensions and ETT size.

The dead space and *FRC* parameters are only significant during the transient ventilation state. These parameters become irrelevant if the recorded data is only captured from the steady state. The steady state is reached after the cumulative volume delivered to the patient exceeds the sum volume of *FRC* and dead space and after the established baseline pressure.

The trachea dimensions and ETT size choice affect only the overall flow-dependent resistance of the MV-P system. Therefore, the resistances contributed by these two components are dynamic and cannot simply be accounted for by sweeping the mechanical resistance parameter over a greater range, since the latter resembles static behaviour for a varying flow rate. Thus, the set of waveform shapes simulatable for one ETT will be unique from other ETT options. Recall from Section 3.3.3.3 that the ETT's resistance contribution dominates that of the trachea, and the latter's effect can therefore be considered negligible.

The typical ranges for the resistance (R_{RS}) and compliance (C_{RS}) depend on patient age, height and sex. However, the per-breath static behaviour of these pulmonary parameters means that increasing the sweeping ranges will effectively encompass a larger set of patient identities.

Therefore, the generatable dataset for a single MV-P setup can only represent the patient identities deemed appropriate for interfacing with the chosen ETT. Choosing a 25-year-old male (186 cm in length) results in an 8.0 mm inside diameter ETT. However, sweeping R_{RS} and C_{RS} over extensive ranges will effectively result in a dataset representing any patient interfaceable with said ETT (Section 3.2.2 implies any man and woman over 16).

3.4.2 Normal Parameter Ranges

The MV can be set up to deliver air in different ways using different modes. Regardless of the mode set, a few parameters need to be set in such a way as to ventilate the patient properly. The first parameter is the respiratory rate, which should be set in such a way as to allow for full inhalation and exhalation of each breath. The other parameters are discussed below: baseline pressure, maximum inspiratory flow, tidal volume, peak inspiratory pressure, and inspiratory time. Also, the patient has a certain health status characterizable by the respiratory system's resistance and compliance. A discussion of the practical ranges for all these parameters follows below.

3.4.2.1 Baseline Pressure

The baseline pressure is typically implemented to prevent alveolar collapse, thus keeping the patient's respiratory process uninterrupted. Also, in the case of active patients, an increased baseline pressure could relieve the work of breathing.

The appropriate level of baseline pressure depends on the scenario. However, a good heuristic is to initially apply low positive baseline pressures (positive end-expiratory pressure (PEEP) of sub 5 cmH₂O) and increase it by 3 to 5 cmH₂O [37]. Pulmonologists widely agreed that the plateau (maximum alveolar pressure) should not exceed 30 cmH₂O [1], [37]. Since the difference between the plateau pressure and PEEP is the pressure range driving the ventilation process, PEEP can theoretically be set to any value below 30 cmH₂O. However, more practical values range from low PEEP (less than 5 cmH₂O for normal lungs [1]) to intermediate (5 to 10 cmH₂O for COPD cases) and high (greater than 10 cmH₂O for ARDS [1], [5]). PEEP rarely exceeds 15 cmH₂O.

3.4.2.2 Maximum Inspiratory Flow (Q_{max})

The flow rate is essential for patient comfort and for meeting respiratory demand. MVs can accomplish maximum flow rates (Q_{max}) from 10 to 180 L/min [1]. However, flow rates rarely exceed 100 L/min.

3.4.2.3 Tidal Volume (V_T)

The tidal volume (V_T) is the per-breath volume delivered to the patient. The accepted heuristic was 10 to 15 mL/kg of ideal body weight at one stage [1]. However, it has been reduced to 6 to 8 mL/kg of ideal body weight [37]. Some sources still recommend V_T ranges of 4 to 8 mL/kg ideal body weight [1], [5], [32], [47]. For a man with a height of 186 cm, this translates to V_T ranges of 322 to 643 mL.

3.4.2.4 Peak Inspiratory Pressure (P_{PIP})

The peak inspiratory pressure (P_{PIP}) is the maximum pressure achieved during the inspiratory phase and should never be too high to result in a plateau pressure exceeding 30 cmH₂O [1], [37]. A P_{PIP} value that would lead to such dangerous levels depends greatly on the inspiratory resistance and cannot be deduced to an absolute maximum without first knowing more about the MV-P setup. However, if the inspiratory resistance exceeds 20 cmH₂O·s/L, P_{PIP} could reach levels as high as 100 cmH₂O. Nonetheless, when working with more practical cases (no chronic ETT biting or bent pipes), P_{PIP} rarely exceeds 40 cmH₂O [1], [47].

3.4.2.5 Inspiratory Time (T_i)

Inspiratory time (T_i) is the duration of the inspiratory phase in seconds. The inspiratory time for VCD mode will be double that for the VCC mode set to deliver the same V_T at the same Q_{max} . As a general idea, the lower end of T_i for VCD and PC modes is about 0.5 s (V_T of 322 mL and relatively fast Q_{max} of 80 L/min). Also, the upper end of T_i for VCD and PC modes is about 1.9 s (V_T of 643 mL and relatively low Q_{max} of 40 L/min).

3.4.2.6 Resistance (R_{RS})

For an active, spontaneously breathing patient, normal respiratory resistance (R_{RS}) ranges from 0.6 to 2.4 cmH₂O·s/L at flow rates of 0.5 L/s [37]. For abnormalities such as emphysema and asthma patients, it can increase to ranges around 13 to 18 cmH₂O·s/L [32], [89], [103], [104]. The resistance measured by ventilators is of the total respiratory tract (R_{INSP} – including the ETT and other ventilator components). This approximation parameter was discussed in Section 3.3.2.2, showing that it is not an adequate representation of R_{RS} since flow-dependent resistances vary greatly depending on the choice of ETT. Therefore, R_{INSP} is higher for intubated patients; its normal range is 5 to 10 cmH₂O·s/L [34], [37] and higher for MV-P abnormalities.

3.4.2.7 Compliance (C_S)

Spontaneously breathing patients have normal lung compliance of 60 to 400 mL/cmH₂O [34]. The positioning of the patient affects lung compliance considerably. The patient lies supine when mechanically ventilated, and the normal lung compliance decreases to lower ranges. Adult men have a normal static compliance of 40 to 50 mL/cmH₂O [32], [89], [103], [104]; for adult women, it is 35 to 45 mL/cmH₂O. For hyper-compliance abnormalities, static compliance can increase up to 100 mL/cmH₂O [37]. Low static compliance is around 40 mL/cmH₂O (ARDS or cardiogenic pulmonary oedema), and high compliance is around 66 mL/cmH₂O (COPD and asthma). Normal static lung compliance decreases for younger patients (5.79 to 17.65 mL/cmH₂O for neonates).

3.4.3 Defining the Dataset Spectrum

For this project, the patient identity specified for the simulation is a 25-year-old male at 186 cm height. Recall from Section 3.4.1 that this means the ETT size must have an inside diameter of 8.0 mm. The section also explains that, theoretically, by extensively sweeping the MV setting parameters and the patient's mechanical parameters of resistance and compliance, the dataset will contain waveform data representative of a more extensive set of patient identities. By extensively sweeping the parameters for an MV-P setup with an ETT size of 8.0 mm, the patient identity group represented by the simulatable dataset can be increased to any man or woman older than 16 and promotes good generalisation [105]. The chosen sweeping ranges (discussed below) are based on this group identity set and the practical ranges discussed in Section 3.4.2.

The MV can operate in three modes of ventilation: volume-controlled constant flow pattern ventilation (VCC), volume-controlled decelerating flow pattern ventilation (VCD) and pressure-controlled ventilation (PC). All three modes require a set baseline pressure.

- Baseline pressure (P_0) – Swept from 0 to 15 cmH₂O (4 levels linearly spaced).

The tidal volume and maximum inspiratory flow are specified for the volume-controlled modes. The MV uses these parameters to calculate the inspiratory time automatically, and the peak inspiratory pressure is a resulting dependent variable.

- Tidal Volume (V_T) – Swept from 180 to 750 mL (20 levels linearly spaced).
- Maximum Inspiratory Flow (Q_{max}) – Swept from 10 to 105 L/min (20 levels linearly spaced).

The peak inspiratory pressure (P_{PIP}) and inspiratory time are specified for the pressure-controlled mode. The MV uses these parameters to manipulate the flow waveform to achieve the set P_{PIP} as quickly as possible and to maintain this pressure during inspiration for the specified inspiratory time. The resulting dependent variables for this ventilation mode are the tidal volume and maximum inspiratory flow.

- Peak Inspiratory Pressure (P_{PIP}) – Swept from $P_0 + 5$ to 35 cmH₂O (20 levels linearly spaced).
- Inspiratory Time (T_i) – Swept from 0.5 to 2.4 seconds (20 levels linearly spaced).

The patient's mechanical parameters (respiratory resistance and static compliance) are swept extensively to encapsulate said identity group.

- Respiratory Resistance (R_{RS}) – Swept from 1 to 20 cmH₂O·s/L (20 levels linearly spaced).
- Static Compliance (C_S) – Swept from 10 to 105 mL/cmH₂O (20 levels linearly spaced).

3.4.4 The Adapted Mechanical Ventilator (MV) Data Generator Application

The MV data generator application was adapted to incorporate a sweeping simulation state. When enabled, the Parameter Sweep Settings panel appears on the right-hand side (as illustrated in Figure 3-33) for simulating a sweep of session instances.

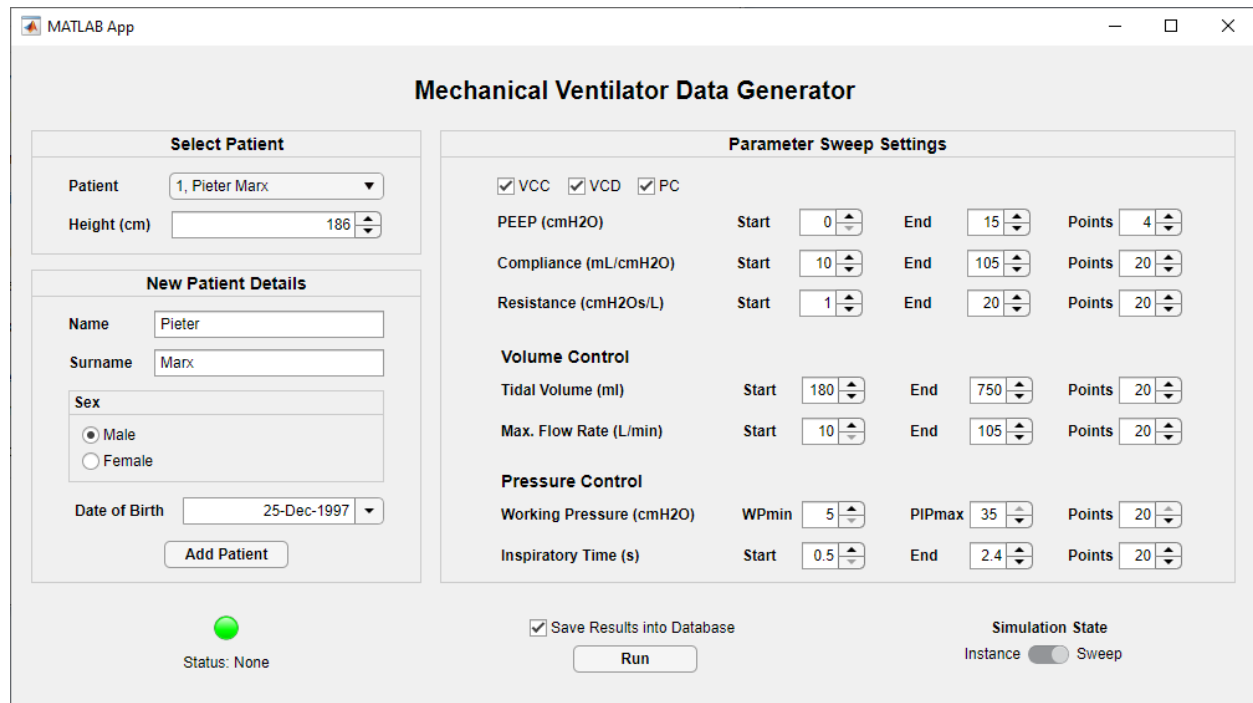


Figure 3-33: Graphical User Interface (GUI) for Specifying the Patient's Parameters, Mechanical Ventilator Settings and Complication Parameters for Simulating a Sweep of Session Instances of the Mechanical Ventilator-Patient Simulink® Model

By selecting the checkboxes next to VCC, VCD and PC, the respective modes will be simulated using the parameter sweep settings underneath these options. The appropriate ventilation mode utilises each parameter according to the description in Section 3.4.3. Also, each parameter has three numeric spinner components. The first is the starting value, the second is the terminating value, and the third is the number of linearly swept points across the specified range.

The adapted MV data generator application runs the simulations in a specific way. Each simulation instance has a constant baseline pressure, compliance, ventilation mode, and control parameters. The only parameter swept during a single simulation is the resistance. This method proves sensible since changing other parameters during a single simulation could lead to inappropriate initial respiratory rates or introduce intermittent transient states. A respiratory rate that is too fast will result in incomplete cycling of breaths, and a respiratory rate that is too slow will result in unnecessary simulation time and wasted storage.

The respiratory rate (RR) is set dynamically to a constant value per simulation. This value is calculated using equations (3-18) to (3-22). T_{EIHM} is the duration of the end-inspiratory hold manoeuvre, which is set to zero since this manoeuvre is not used on a per-breath basis in practice. T_e is the expiratory time and is chosen as six times the time constant (ample time according to Section 2.2.4.3 for proper expiration). R_{EXP} is the total resistance during expiration and is calculated by summing the maximum R_{RS} value and an overestimated circuit resistance ($R_{Circuit}$). The latter is chosen as 10 cmH₂O·s/L to accommodate high resistances when small ETTs are chosen for simulation. The chosen ETTs inside diameter is on the larger side of the spectrum as it was determined to have an average resistance of around 2.76 cmH₂O·s/L (mentioned in Section 3.3.3.2). Therefore, the constant respiratory rate for a single simulation is deliberately overestimated to ensure proper cycling of each simulated breath.

$$RR = \frac{60}{T_{Period}} \quad (3-18)$$

$$T_{Period} = ceiling(T_i + T_{EIHM} + T_e) \quad (3-19)$$

$$T_e = 6 \times \tau_{RC} \quad (3-20)$$

$$\tau_{RC} = C_s \times R_{EXP} \quad (3-21)$$

$$R_{EXP} = R_{RS} + R_{Circuit} \quad (3-22)$$

At the start of each simulation, a transient state occurs. Each recorded breath should be of a steady state to ensure accurately represented breaths. Therefore, the number of breaths that must be simulated and omitted before reaching the steady state (appropriate start for recording data) is crucial. The transient state occurs since the initial pressure inside the patient's lungs does not necessarily equal the baseline pressure. This mismatch will lead to an imbalance of inspired and expired volumes and, thus, unacceptable waveforms. During the steady state, the volume inspired should equal the volume expired. To determine the number of breaths to exclude from recordings ($n_{Transient_Breaths}$), equation (3-23) is used. Unit addition and flooring ensure that at least one breath is always omitted. Sweeping of R_{RS} only occurs during the steady state; thus, the number of recorded breaths will always equal the specified number of R_{RS} sweeping points.

$$n_{Transient_Breaths} = floor\left(\frac{C_s \times P_0}{V_T} + 1\right) \quad (3-23)$$

3.4.5 Optimising the MV Data Generator Application

The first version of the MV data generator application simulated the instances in series (single core processing). When a simulation is completed, the settings used to run the simulation are stored in a database table as a single record using an insert-stored procedure. After that, the recorded waveform scalar data (pressure, flow and volume waveforms) were sampled at 200 Hz and further analysed by the application. The analyses are comprised of a peak detection method suitable for all three different modes of ventilation, isolation of each breath, trimming of deadtime (pre- and post-breath cycles), and per-beath feature extraction of what the MV's settings might have been. These extracted features are stored in a different database table as a single record per breath using an insert-stored procedure. A single breath's isolated and trimmed time-series waveform data is also stored in another database table using a multiple-row insert query.

Therefore, this first version of the MV data generator application ran simulations serially and analysed and stored the relevant data and features on a per-breath basis. A rough sweep test (covering the same parameter ranges mentioned in Section 3.4.3) was performed with 1 500 simulations. The simulation set was simulated with four levels of baseline pressure, five levels of compliance, all three modes of ventilation, five levels for each of the two relevant parameters per mode, and 20 levels of resistance per simulation – equating to 30 000 breaths). The average time to simulate, process and store the results in the database was 8.55 seconds per breath.

Recall from Section 3.4.3 that the desired resolution is much higher. The desired simulation set has four levels of baseline pressure, 20 levels of compliance and resistance, and three ventilation modes. Each mode has two relevant parameters; each swept across 20 levels. This results in the total desired number of simulated breaths being 1.92 million. If the performance of the first version is accepted, it will result in a total data generation time of about 190 days. Since this predicted total data generation time is impractical, optimization methods for the application were investigated, which resulted in two other versions of the application.

The second version of the MV data generation application leveraged parallel computing techniques. This was accomplished by utilising the parsim function, which creates a parallel pool in the Simulink® environment that simultaneously runs each simulation on a different core. The storage and analysis methods of the generated data required utilising a universally unique identifier (UUID). Given the parallel nature of this solution, the UUID was implemented to ensure proper data reference tracking between the database tables for each breath. This reduced the per-breath processing time to 4.03 seconds (89.56 days).

An analysis of the allocated processing time per task indicated that much time was spent on data storage. MATLAB® and MySQL™ reference manuals suggested utilising queries that write multiple records per query execution. There is, however, an optimisation limit to this method when writing more than ten million records into the database for a single query.

This resulted in the final optimised version of the data generation application utilising matrices representing the database tables. After analysis of a breath, the results are appended to these matrices. The lengths of the matrices are monitored for reaching more than ten million rows, after which the respective matrix is stored as a CSV file. After all the simulations are executed and all breaths are analysed, all remaining matrices (not exceeding ten million rows) are stored as CSV files. These CSV files are then loaded into the database one at a time using the LOAD query. This version further reduced the per-breath processing time to 3.35 seconds (74.44 days).

3.4.6 Data Generation Expedition

A request was made to book one of the NWU's clusters or to rent other online clusters to generate all the required data at even faster speeds. This, however, did not realise, and another option was considered. At the time, the NWU had a vacant computer laboratory with sixty computers (G22 in building N1), each with approximately the same processing power as the machine used for performance testing up until now. The laboratory was booked for a weekend, and all sixty computers were given a segment of the sweeping set to simulate, process and store into CSV files (see Figure 3-34). This only took about two days, and the CSV files were downloaded from each computer. This resulted in about 168 GB of CSV data files. After trimming the dead time from the results, the total storage required for the CSV files was 66.7 GB. After loading the CSV files into the database, the table storing all the time-series data had a size of about 49 GB. The table storing the session setting parameters was about 16 MB. Finally, the table storing the extracted MV settings features was about 152 MB.



Figure 3-34: Photo of Data Generation Expedition Utilising 60 Machines in the NWU's Computer Laboratory

3.5 Chapter Summary

This chapter describes how the labelled MV dataset was obtained and why it was synthetically generated using MATLAB® Simulink® model-based simulations.

The chapter started with a discussion of the fidelity requirements of an appropriately labelled MV dataset and the reasons for having to simulate one. A dataset survey was done to gain permission to use existing empirical datasets generated by hospitals. However, these datasets were found to need more fidelity or denied access for research purposes by students. The next option was to create an empirical dataset; however, this would be time-consuming, low-resolution use cases and ethical clearance would have had to be obtained. The third option was to create synthetical empirical datasets using a pipe-balloon experimental setup or HAL® S3201 programmable patient puppet emulator; however, it would also prove to be time-consuming, limit the mechanical parameter sweep range and requires a mechanical ventilator, which was unobtainable at the time. Finally, the last option was to generate synthetical datasets using MATLAB® Simulink® model-based simulations. This option would grant full fidelity, unlimited use cases, and clean data and would be much faster to record; however, such a model must be verified.

Subsequently, the MATLAB® Simulink® model of the MV-P system was developed to meet the fidelity and representative complexity necessary for this project. These were to capture and apply the patient's biological identity (i.e., age, sex, and height) and anthropometric data (trachea dimensions, *FRC*, dead space, and appropriate ETT size) to the MV-P model. The model had to implement an ETT as the patient-interface component, variable baseline pressure valve, variable patient mechanical parameters of airway resistance and static compliance, the variable intensity of the patient biting the ETT or a kink forming in the tubes, a means of performing the end-inspiratory hold manoeuvre, and input options for selecting the ventilation mode (VCC, VCD and PC) and their corresponding parameter settings (respiratory rate, baseline pressure, maximum inspiratory flow, tidal volume, peak inspiratory pressure and inspiratory time).

After that, the MATLAB® Simulink® MV-P model was verified qualitatively and quantitatively, and its sensitivity was inspected. The model was qualitatively verified by analysing the pressure component behaviours and the effects of varying the mechanical parameters and by comparing the shapes of the simulated waveform scalars to actual examples. The model was quantitatively verified by varying the parameters and analysing the results for appropriate corresponding outputs. The model's sensitivity was inspected by changing the parameters of the components and by comparing deviations when omitting components during certain use cases. The ETT proved to be the only point of significant sensitivity due to turbulent flow, as is the practice case.

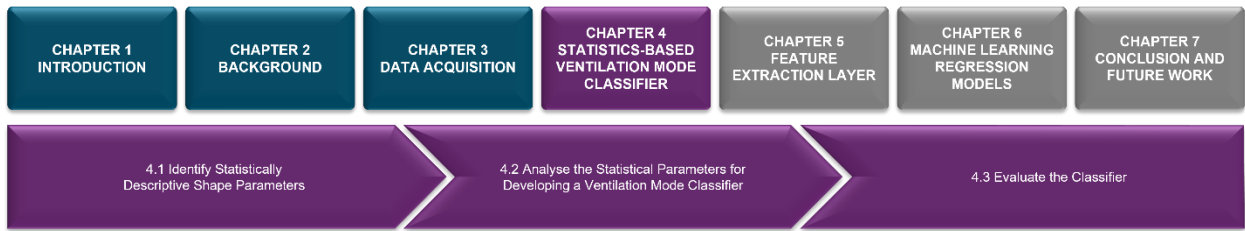
After the MATLAB® Simulink® MV-P model was developed and verified, some assumptions were made to scope the theoretically unlimited dataset for the project whilst representing an extensive patient identity set. The assumptions concluded that the generatable dataset for a single MV-P setup could only represent the patient identities deemed appropriate for interfacing with the chosen ETT. Since a 25-year-old male (186 cm in length) was chosen as the identity to be simulated, it resulted in an 8.0 mm inside diameter ETT. The represented patient identity set expanded by sweeping R_{RS} and C_S over extensive ranges, including any patient deemed appropriate to interface with said ETT. Section 3.2.2 implies any man or woman over 16.

The typical ranges of the parameters for the specified patient identity set were determined:

- Baseline Pressure (P_0) – Swept from 0 to 15 cmH₂O (4 levels linearly spaced).
- Tidal Volume (V_T) – Swept from 180 to 750 mL (20 levels linearly spaced).
- Maximum Inspiratory Flow (Q_{max}) – Swept from 10 to 105 L/min (20 levels linearly spaced).
- Peak Inspiratory Pressure (P_{PIP}) – Swept from $P_0 + 5$ to 35 cmH₂O (20 levels linearly spaced).
- Inspiratory Time (T_i) – Swept from 0.5 to 2.4 seconds (20 levels linearly spaced).
- Airway Resistance (R_{RS}) – Swept from 1 to 20 cmH₂O·s/L (20 levels linearly spaced).
- Static Compliance (C_S) – Swept from 10 to 105 mL/cmH₂O (20 levels linearly spaced).

Finally, the model was optimised to generate the required labelled mechanical ventilation dataset. The MV data generator application was adapted to support the parameter sweep functionality. Initially, the average time to simulate, process and store the results was 8.55 seconds per breath. Considering that the sweep mentioned above's ranges result in 1.92 M breaths, this would have taken 190 days to acquire. A second, improved model version was developed using parallel computing techniques, which decreased the time per breath to 4.03 seconds (which would take 89.56 days for all breaths). Further improvements were made to store the data more efficiently from the model into the database by uploading CSV files of about ten million records at a time. This further decreased the time per breath to 3.35 seconds (which would take 74.44 days for all breaths). These computational speeds could further be increased by utilising faster or more machines. Since no access was granted to use one of the NWU's clusters or to rent other online clusters, one of the NWU's vacant computer laboratories (G22 in building N1, which houses 60 machines) was booked for data generation using the model. It took about two days for all 1.92 M breaths and generated about 168 GB of data. After trimming the data, it resulted in 66.7 GB of CSV data files, and further conversion to the data types used by the database reduced the storage to 49 GB. The table that stored the session settings was 16 MB, and the table that stored the extracted MV setting features was 152 MB.

CHAPTER 4 – STATISTICS-BASED VENTILATION MODE CLASSIFIER



Since the solution must be autonomous, it is necessary for the solution to automatically determine from the available waveform data what the ventilator's settings are. In this chapter, a statistics-based method is developed to analyse the waveform scalars of a single breath for classifying which ventilation mode was performed by the mechanical ventilator (MV). First, the generalised shapes of the waveforms are considered to identify statistical shape characteristic parameters that could be utilised to describe ventilation mode class probabilities quantitatively. After that, the statistical parameters are investigated to obtain classification intelligence using different techniques. Finally, the proposed ventilation mode classifier is evaluated by employing per-mode graphical parameter sensitivity analysis and the classification confusion matrix.

4.1 Identify Statistically Descriptive Shape Parameters

When considering the waveform scalars of pressure, flow rate and volume, the latter is derived from the flow rate waveform using integration. Therefore, the volume waveform is redundant. Considering each mode's generalised waveform scalar shapes, the inspiratory phase is the only mode-dependent phase (see Figure 4-1). Therefore, only the pressure and flow rate waveforms' inspiratory phase shapes will be necessary to identify statistically descriptive shape parameters.

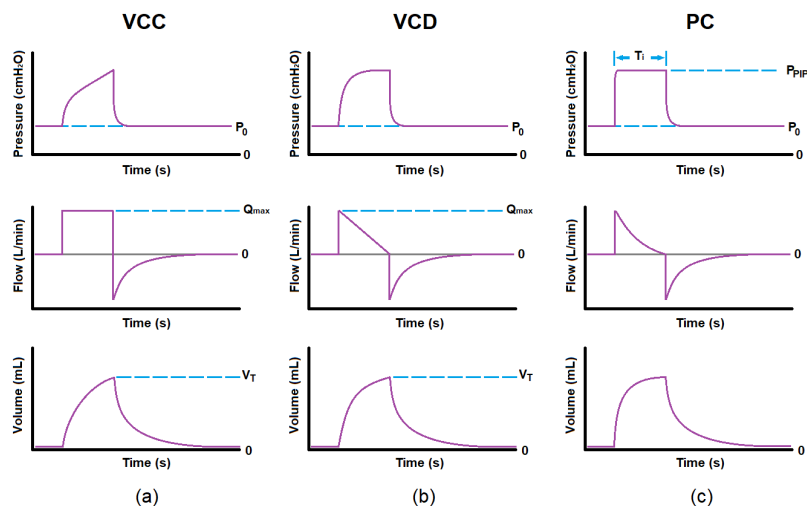


Figure 4-1: Waveform Scalars' Generalised Shapes per Ventilation Mode: Volume-Controlled Constant Flow Pattern Ventilation (a), Volume-Controlled Decelerating Flow Pattern Ventilation (b) and Pressure-Controlled Ventilation (c)

4.1.1 Extract the Standard Deviation (*STD*) Parameter from the Pressure Waveform

Considering only the pressure waveform's inspiratory phase's shapes, the volume-controlled constant flow pattern ventilation mode (VCC) has a triangular shape, the volume-controlled decelerating flow pattern ventilation mode (VCD) has a curved shape, and the pressure-controlled ventilation mode (PC) has a square waveform. One way to quantitatively describe these shapes is to determine the standard deviation (*STD*) of the actual waveform data during the inspiratory phase with the average over the same data. This leads to the VCC mode having a high *STD*, the PC mode having a low *STD* and the VCD mode having an *STD* somewhere in between. Some MVs perform PC ventilation by manipulating the flow rate through a PID controller, as in control theory. A typical indication of this is an overshoot in pressure with some settling time at the initial part of the inspiratory phase. This artefact's prominence differs from model to model and could affect the classification performance of this descriptive parameter. Therefore, a trim time (t_{Trim}) of 50 ms is implemented at the start of inspiration to minimise this artefact's influence and ensure a good classification performance of this descriptive parameter.

The waveform data during inspiration is pre-processed to ensure that the standard deviations of the pressure waveforms are comparable across all different breaths. First, the waveform is offset to the same reference by subtracting the baseline pressure (P_0), then scaled to the same reference by dividing it with the resulting maximum pressure. This ensures that all pressure waveform data of every breath range from 0 to 1 across the inspiratory phase.

Thereafter, the *STD* of the waveform data is calculated using equation (4-1), where p_i is the processed pressure waveform data values, μ is the mean of these values and N is the number of these values [106].

$$STD = \sqrt{\frac{\sum(p_i - \mu)^2}{N}} \quad (4-1)$$

Figure 4-2 graphically illustrates the *STD* feature extraction method.

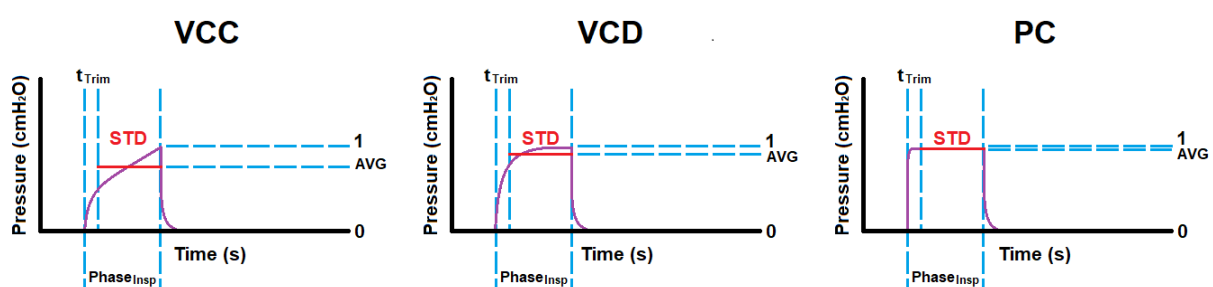


Figure 4-2: Graphical Illustrations of the Inspiratory Phase Standard Deviation Feature Extraction from Each Ventilation Mode's General Pressure Waveform Scalar Shapes

4.1.2 Extract the Coefficient of Determination Parameter from the Flow Rate Waveform

Considering only the flow rate waveform's inspiratory phase's shapes, the VCC mode has a square waveform, the VCD mode has a triangular shape, and the PC mode has an exponentially decaying shape. One way to quantitatively describe these shapes is to fit a straight line from the point of initial maximum flow rate (q_{Qmax}) to the zero-flow point (q_{Qzero} at the end of the inspiratory phase) and calculate its coefficient of determination (R^2) with respect to the actual inspiratory phase waveform data. This leads to the VCC mode having a bad fit ($R^2 \approx 0$), the VCD mode having a good fit ($R^2 \approx 1$) and the PC mode having an average fit (R^2 somewhere in-between). Equations (4-2) to (4-4) are used to determine the equation for the straight line of best fit.

$$q_{fit}(t) = m_Q \times t + c_Q \quad (4-2)$$

$$m_Q = \frac{q_{Qzero} - q_{Qmax}}{t_{Qzero} - t_{Qmax}} \quad (4-3)$$

$$c_Q = q_{Qmax} - m_Q \times t_{Qmax} \quad (4-4)$$

After obtaining $q_{fit}(t)$, it must be corrected ($q_{fit_corrected}(t)$) by minimising its standard deviation. This is accomplished by ensuring that both the average of the waveform data (μ_{data}) and the average of $q_{fit}(t)$ (μ_{q_fit}) are the same. This is accomplished using equation (4-5).

$$q_{fit_corrected}(t) = m_Q \times t + c_Q - \mu_{q_fit} + \mu_{data} \quad (4-5)$$

Finally, R^2 of the waveform data is calculated using equation (4-6) [107], where q_i is the flow rate waveform data values, $q_{fit_corrected_i}$ is the data values of the fit line, and $\mu_{fit_corrected}$ is its mean.

$$R^2 = 1 - \frac{\sum (q_{fit_corrected_i} - q_i)^2}{\sum (q_{fit_corrected_i} - \mu_{fit_corrected})^2} \quad (4-6)$$

Figure 4-3 graphically illustrates the R^2 feature extraction method.

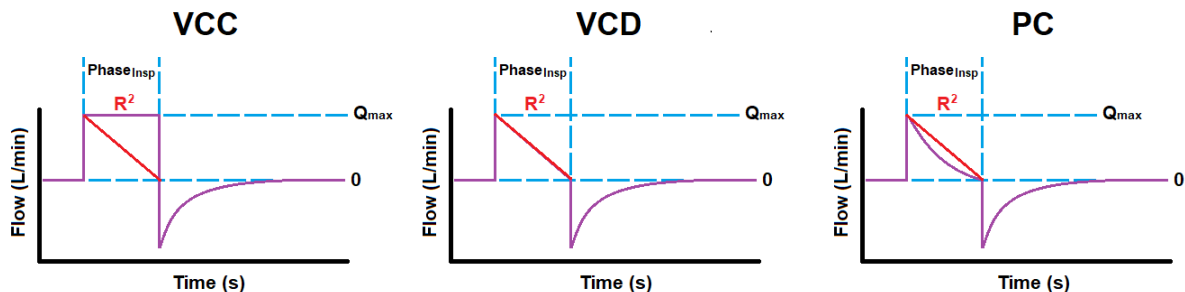


Figure 4-3: Graphical Illustrations of the Inspiratory Phase Coefficient of Determination Feature Extraction from Each Ventilation Mode's General Flow Rate Waveform Scalar Shapes

4.2 Analyse the Statistical Parameters to Develop a Ventilation Mode Classifier

Recall from Section 3.4.5 that a relatively small dataset acquired 30 000 unique breaths. In this section, the statistical descriptive shape parameters discussed in Section 4.1 (the coefficient of determination (R^2) from the flow waveform and the standard deviation (STD) from the pressure waveform) are calculated from said dataset. This section analyses the spreads of these statistical parameters per ventilation mode to acquire information on how these parameters could be utilised for classifying any breath as VCC, VCD, or PC delivered. First, the spreads are inspected for hard decision boundaries (non-overlapping spectra). After that, kernel probability distribution functions (PDFs) are leveraged to attempt to classify the remaining breaths with overlapping parameter spectra.

4.2.1 Implement a Hard Decision Boundary Classifier

One way to visually inspect the statistical parameters' spectra is to leverage boxplots. Figure 4-4 conveys the spectra for each mode of ventilation's R^2 (a) and STD (b). Upon first inspection, the R^2 spectra seem to have less overlap than that of the STD . VCC's R^2 is almost fully discriminative (apart from the outliers). The interquartile ranges (IQRs) of VCD's and PC's R^2 are mutually exclusive. On the other hand, the STD spectra only have PC's IQR not overlapping with that of the other modes.

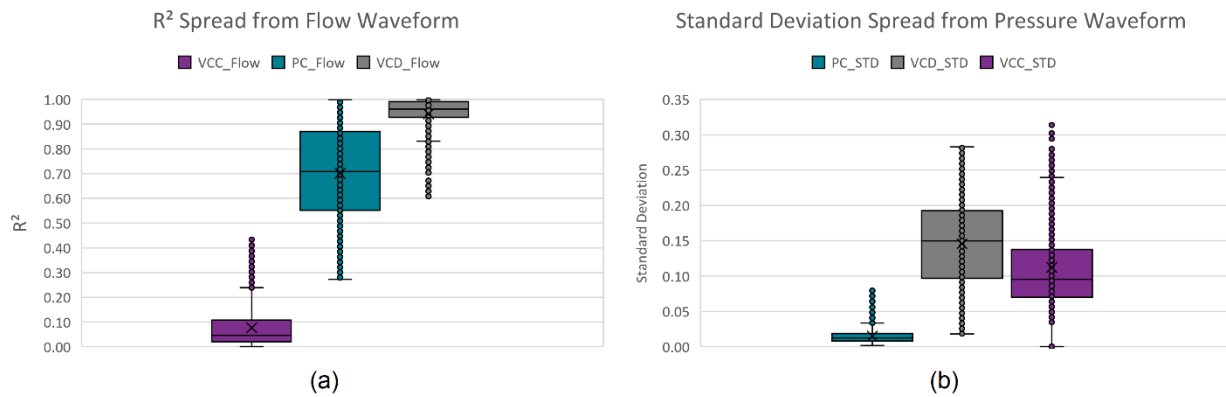


Figure 4-4: Boxplots of the Coefficient of Determination (a) and Standard Deviation (b) for Each Mode

At this stage, no decision boundaries have been implemented, and therefore, the unidentified tallies per mode are summarised in Table 4-1.

Table 4-1: Summary of the Unidentified Tallies of Each Mode Before Implementing Decision Boundaries

Breath Modes	VCC	VCD	PC
Unidentified Breaths	10 000	10 000	10 000

When implementing the following hard decision boundaries, the spectra of the remaining unidentified breaths can be visually represented by Figure 4-5.

- Classify all breaths with $R^2 < 0.27215$ (minima of PC's R^2) as VCC breaths.
- Classify all remaining breaths with $0.44558 < R^2 < 0.60865$ (maxima of VCC's R^2 and minima of VCD's R^2 , respectively) as PC breaths.
- Classify all remaining breaths with $R^2 > 0.99862$ (maxima of PC's R^2) as VCD breaths.

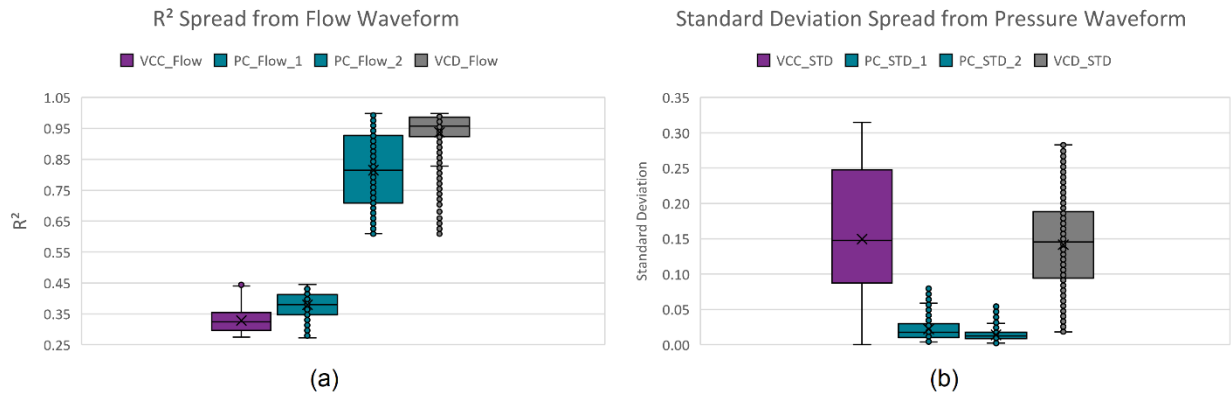


Figure 4-5: Boxplots of the Coefficient of Determination (a) and Standard Deviation (b) for Each Mode After Implementing the First Set of Hard Decision Boundaries

After implementing the first set of hard decision boundaries, the R^2 spectrum for PC is divided into two ranges. The first range overlaps with VCC and the second with VCD. These will further be referred to as PC_1 and PC_2 , respectively. It also causes two separate spectra of STD for PC, corresponding to the two separate spectra of R^2 . Thus, all PC breaths described by PC_1 's R^2 are also described by PC_1 's STD spectrum. The same relationship counts for PC_2 . By implementing nested decision boundaries beyond this point, the split in PC's R^2 allows for further handling of the unidentified breaths as two separate problems.

- Discriminating VCC breaths from PC_1 breaths.
- Discriminating VCD breaths from PC_2 breaths.

The summary for the tallies of unidentified breaths is updated and conveyed in Table 4-2. Most VCC breaths have been identified at this stage, which is understandable given that the R^2 analysis method from Section 4.1.2 conveyed that the straight-line fit would be the worst for this mode.

Table 4-2: Summary of the Unidentified Tallies of Each Mode After Implementing the First Set of Hard Decision Boundaries

Breath Modes	VCC	PC ₁	PC ₂	VCD
Unidentified Breaths	314	1 290	6 682	9 372

No hard decision boundaries for the STD parameter have been implemented at this stage. After implementing the following nested hard decision boundaries, the spectra of the remaining unidentified breaths can be visually represented by Figure 4-6.

Given that $0.27215 \leq R^2 \leq 0.44558$:

- Classify all breaths with $STD < 0.00412$ (minima of PC_1 's STD) as VCC breaths.
- Classify all remaining breaths with $STD > 0.08465$ (maxima of PC_1 's STD) as VCC breaths.

Otherwise, given that $0.60865 \leq R^2 \leq 0.99862$:

- Classify all breaths with $STD < 0.01825$ (minima of VCD 's STD) as PC_2 breaths.
- Classify all remaining breaths with $STD > 0.05516$ (maxima of PC_2 's STD) as VCD breaths.

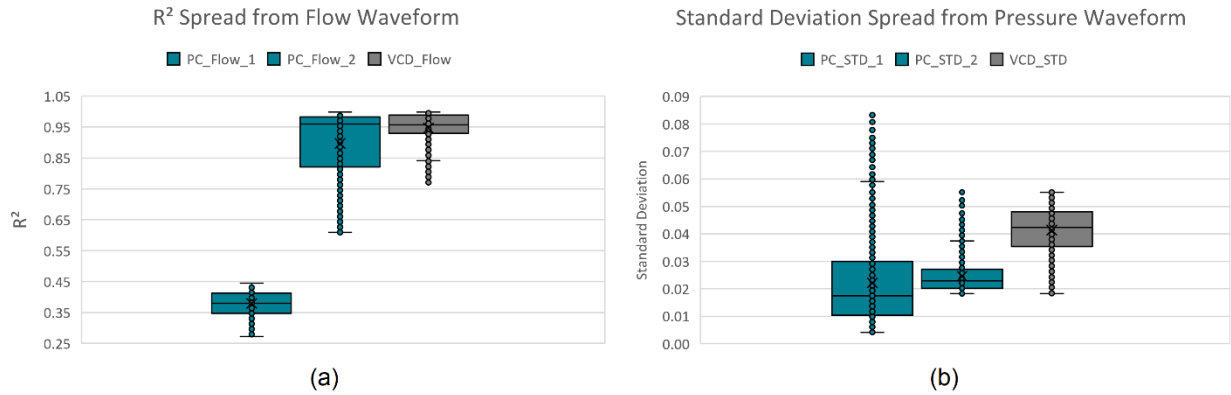


Figure 4-6: Boxplots of the Coefficient of Determination (a) and Standard Deviation (b) for the Remaining Modes of Ventilation After Implementing the Second Set of Hard Decision Boundaries

After implementing the second set of hard decision boundaries, all the VCC breaths have been identified since there were no instances where the STD of the VCC breaths fell within the range of the remaining PC_1 STD spectrum. All the instances were either below or above the PC_1 STD spectrum values. This means that PC_1 's remaining breaths are the only unidentified breaths, given that $0.27215 \leq R^2 \leq 0.44558$.

The summary for the tallies of unidentified breaths is updated and conveyed in Table 4-3. At this point, the unidentified breaths for PC_2 and VCD have decreased noticeably, which is understandable given the discriminative nature of the STD analysis method from Section 4.1.1.

Table 4-3: Summary of the Unidentified Tallies of Each Mode After Implementing the Second Set of Hard Decision Boundaries

Breath Modes	VCC	PC_1	PC_2	VCD
Unidentified Breaths	0	1 290	1 514	1 075

Finally, as described below, the last round of hard decision boundaries on the remaining unidentified breaths are implemented to capitalise on the last bit of remaining leverage this classification technique can provide. This results in the remaining unidentified breaths being only of the PC₂ and VCD breaths, which is understandable, given how close these waveforms' shapes are to one another. The spectra for these remaining breaths are conveyed in Figure 4-7.

Given that $0.27215 \leq R^2 \leq 0.44558$:

- Classify all remaining breaths as PC₁ breaths.

Otherwise, given that $0.60865 \leq R^2 \leq 0.99862$:

- Classify all breaths with $R^2 < 0.77049$ (minima of VCD's R^2) as PC₂ breaths.
- Classify all remaining breaths with $R^2 > 0.99846$ (maxima of VCD's R^2) as PC₂ breaths.

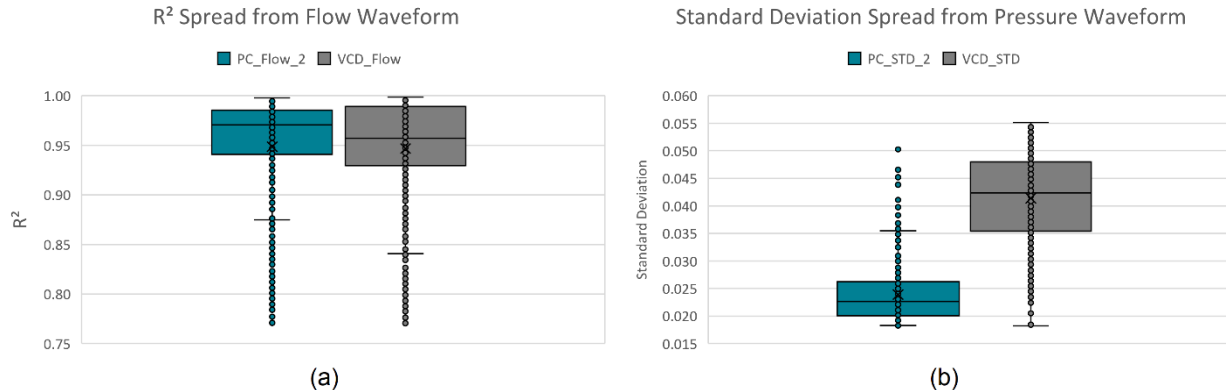


Figure 4-7: Boxplots of the Coefficient of Determination (a) and Standard Deviation (b) for the Remaining Modes of Ventilation After Implementing the Final Set of Hard Decision Boundaries

The summary for the tallies of unidentified breaths is updated and conveyed in Table 4-4. At this stage, the classification performance (using hard decision boundaries) has been exhausted from a significance standpoint. Other classification techniques must further be implemented since the remaining unidentified breaths have overlapping statistical parameter spectra.

Table 4-4: Summary of the Unidentified Tallies of Each Mode After Implementing the Final Set of Hard Decision Boundaries

Breath Modes	VCC	PC ₁	PC ₂	VCD
Unidentified Breaths	0	0	1 217	1 075

The remaining unidentified breaths make up 7.64% due to overlapping ranges. We could assume that the remaining unidentified breaths are PC₂ breaths (given the similarity between the shapes), which would conclude a classifier with an accuracy of 96.42%.

4.2.2 Implement a Kernel Probability Distribution Function Classifier

In this section, a classification technique involving probability prediction is investigated to attempt to identify the remaining overlapping breaths. This technique uses kernel probability distribution functions [108]. These functions are kernel fitted and take on the shape of the histograms that describe the tallies per bin of the statistical parameter's spread. Figure 4-8 conveys the kernel-fitted functions for the coefficient of determination (R^2) for the VCC mode (a), for the VCD mode (b) and for the PC mode (c). Figure 4-9 conveys the kernel-fitted functions for the STD for the VCC mode (a), for the VCD mode (b) and for the PC mode (c).

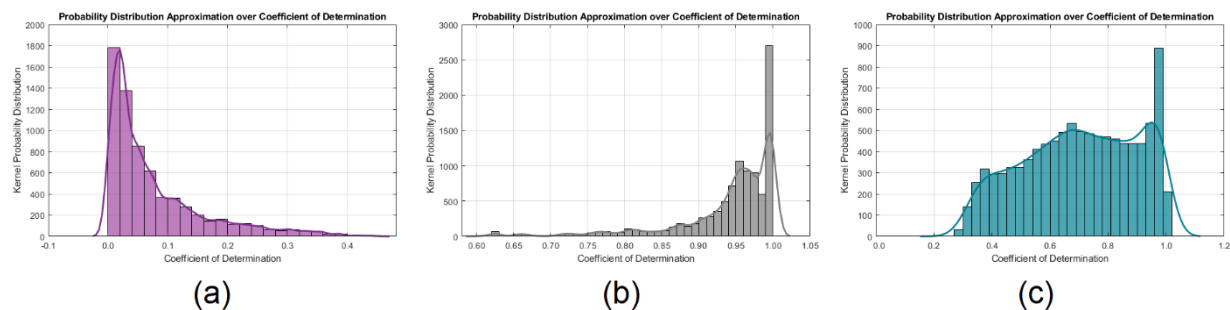


Figure 4-8: Kernel Fitted Functions of the Coefficient of Determination Statistical Parameter for the VCC (a), VCD (b) and PC (c) Ventilation Modes

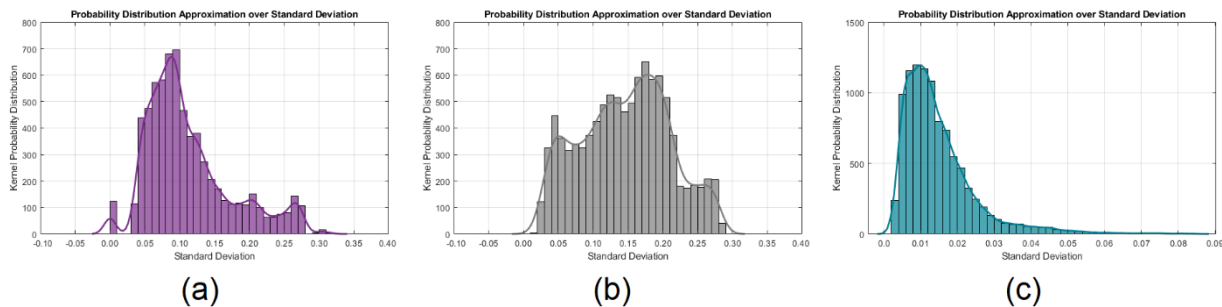


Figure 4-9: Kernel Fitted Functions of the Standard Deviation Statistical Parameter for the VCC (a), VCD (b) and PC (c) Ventilation Modes

When these kernel functions are scaled so that the integral over the range of these functions equates to unity, these functions are called probability distribution functions (PDFs). The function can then be used to calculate a prediction scoring value that indicates, given the corresponding statistical parameter's value, what the likelihood is that the breath is of the corresponding ventilation mode. When the three functions of the modes (per statistical parameter) are applied simultaneously to a breath, these calculated likelihoods that a breath belongs to the different modes are compared. The higher prediction value indicates to which ventilation mode the breath most probably belongs. Summing the prediction scores of both PDFs (that of R^2 and STD) for each mode adds complexity to the probability scoring method, which could increase the classification performance of this method.

Figure 4-10 and Figure 4-11 depict the kernel PDFs for each mode given the coefficient of determination and the standard deviation statistical parameter values, respectively.

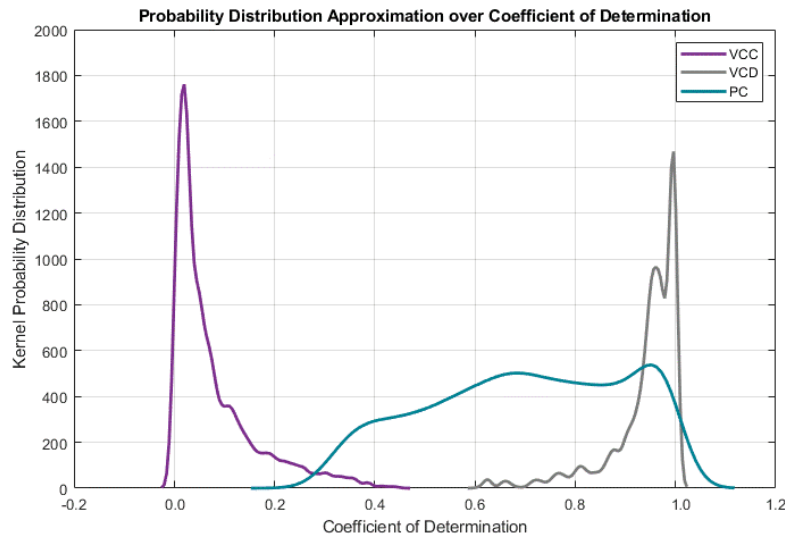


Figure 4-10: Graph of the Kernel Probability Distribution Functions for Ventilation Mode Classification Given the Coefficient of Determination

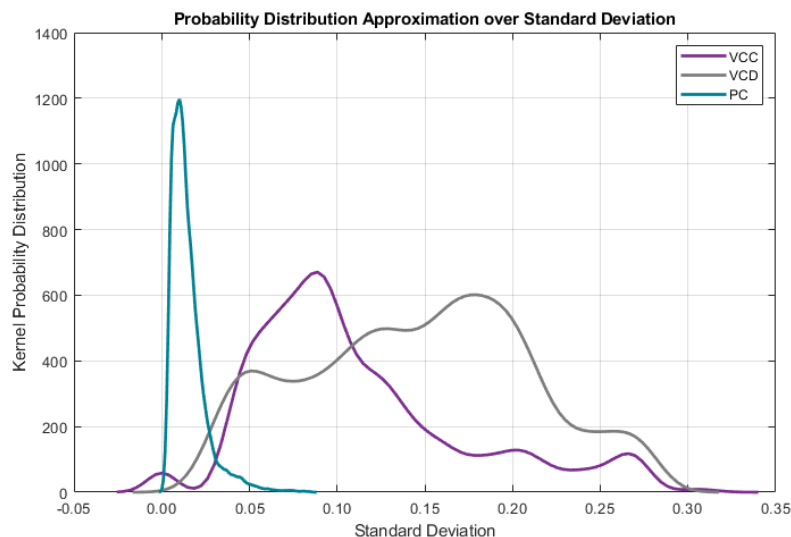


Figure 4-11: Graph of the Kernel Probability Distribution Functions for Ventilation Mode Classification Given the Standard Deviation

When applying these functions to all 30 000 breaths without any prior decision boundary implementation, the true positive prediction accuracies result in 94.98% for VCC, 93.66% for VCD and 94.09% for PC. This results in a classifier with overall prediction accuracy of 94.24%.

Table 4-5: Summary of the True Positive Accuracies for Each Ventilation Mode

Breath Modes	VCC	VCD	PC
Acc. True Positive [%]	94.98	93.66	94.09

4.2.3 Implement a Hybrid Ventilation Mode Classifier

Although the PDF classification technique is more elegant, the accuracy (94.24%) of the classifier is less than that of the hard decision boundary classification technique (96.42%). Therefore, a hybrid method is proposed. This method leverages the hard decision boundaries discussed in Section 4.2.1, thereafter, applying the kernel PDF technique to the remaining 7.64% of unidentified breaths. Since these breaths are either VCD or PC, only the PDFs of these modes are considered. Figure 4-12 and Figure 4-13 convey the PDFs given R^2 and STD , respectively.

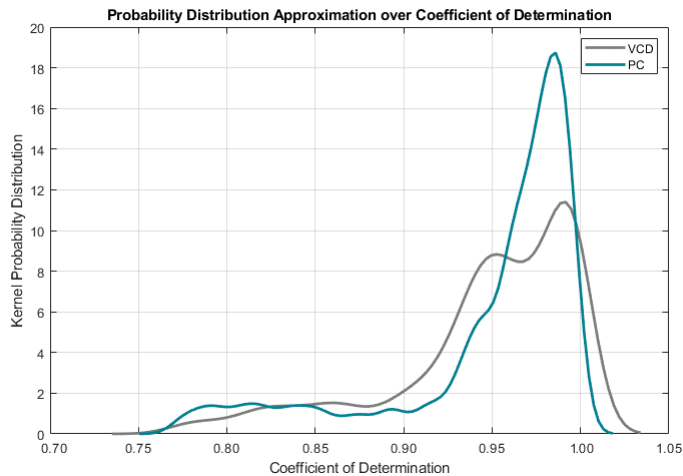


Figure 4-12: Graph of the Kernel Probability Distribution Functions Given the Coefficient of Determination

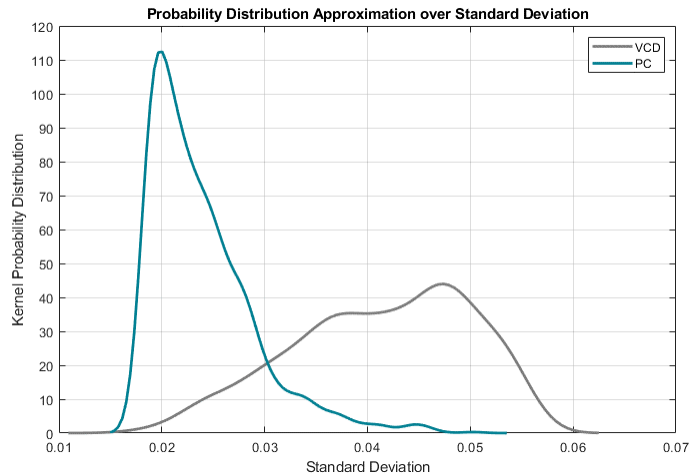


Figure 4-13: Graph of the Kernel Probability Distribution Functions Given the Standard Deviation

Table 4-6 conveys that the true positive accuracies per mode increased to 100.00%, 98.67% and 98.86% for the proposed hybrid method. The classifier's overall accuracy is 99.18%.

Table 4-6: Summary of the True Positive Accuracies for Each Ventilation Mode

Breath Modes	VCC	VCD	PC
Acc. True Positive [%]	100.00	98.67	98.86

Figure 4-14 depicts the resulting 3D distribution graphs of the false negative predictions for the VCC mode. However, since all VCC breaths were classified as such, these graphs had no instances of false negatives, hence the empty graphs.

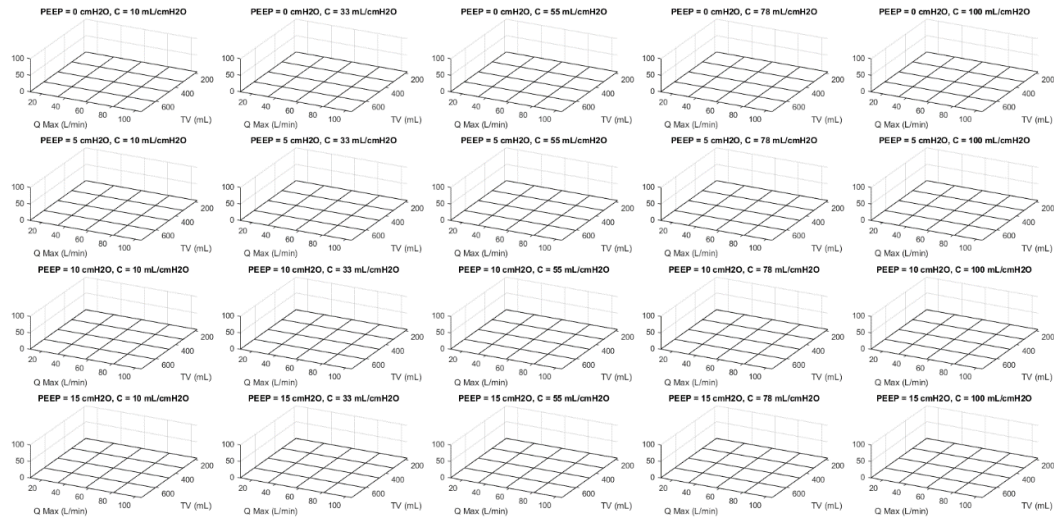


Figure 4-14: 3D Distribution Graphs of the False Negative Predictions for the VCC Mode

Figure 4-15 depicts the resulting 3D distribution graphs of the false negative predictions for the VCD mode. Here, all the blue areas are instances where VCD breaths were misclassified as PC breaths. Each column has a different static compliance (C_S) level (10 to 100 mL/cmH₂O), and each row has a different baseline pressure level (PEEP of 0 to 15 cmH₂O). The tidal volume (V_T) and maximum inspiratory flow (Q_{max}) are varied along the horizontal axes, and the z-axis is the percentage of false negatives across the resistance sweep. From inspection, it looks like the proposed hybrid classifier is less sensitive to changes in baseline pressure than changes in compliance. Also, it does not seem like changes in V_T and Q_{max} contribute any significant relationship to misclassifications.

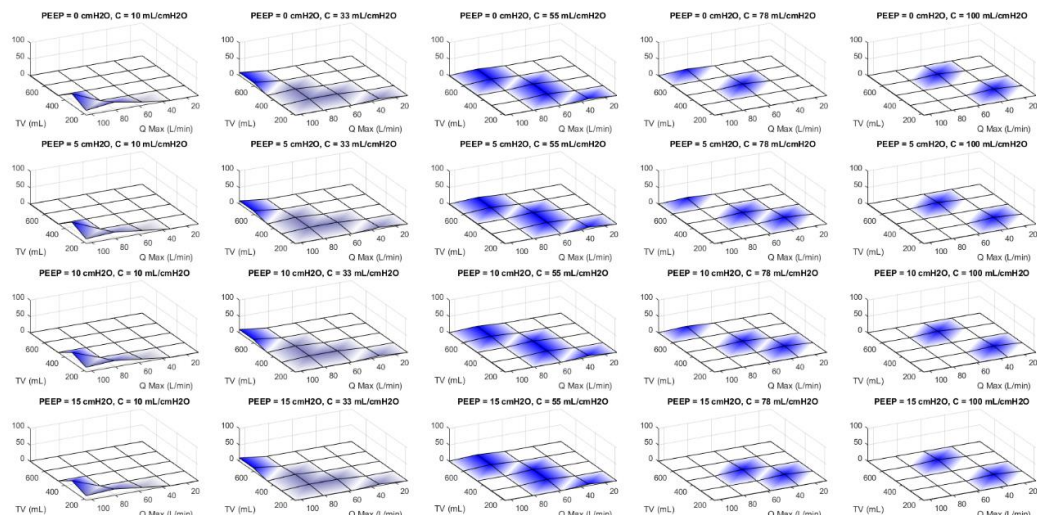


Figure 4-15: 3D Distribution Graphs of the False Negative Predictions for the VCD Mode

Figure 4-16 depicts the resulting 3D distribution graphs of the false negative predictions for the PC mode. All the green and red areas are instances where PC breaths were misclassified as VCD and VCC breaths, respectively. Each column has a different compliance level (10 to 100 mL/cmH₂O), and each row has a different baseline pressure level (PEEP of 0 to 15 cmH₂O). The peak inspiratory pressure (P_{PIP}) and inspiratory time (T_i) are varied along the horizontal axes, and the z-axis is the percentage of false negatives across the resistance sweep. The proposed hybrid classifier tends to make misclassifications from inspection when the P_{PIP} is set relatively close to the PEEP. Also, the classifier tends to make misclassifications at low T_i for compliance of around 33 mL/cmH₂O.

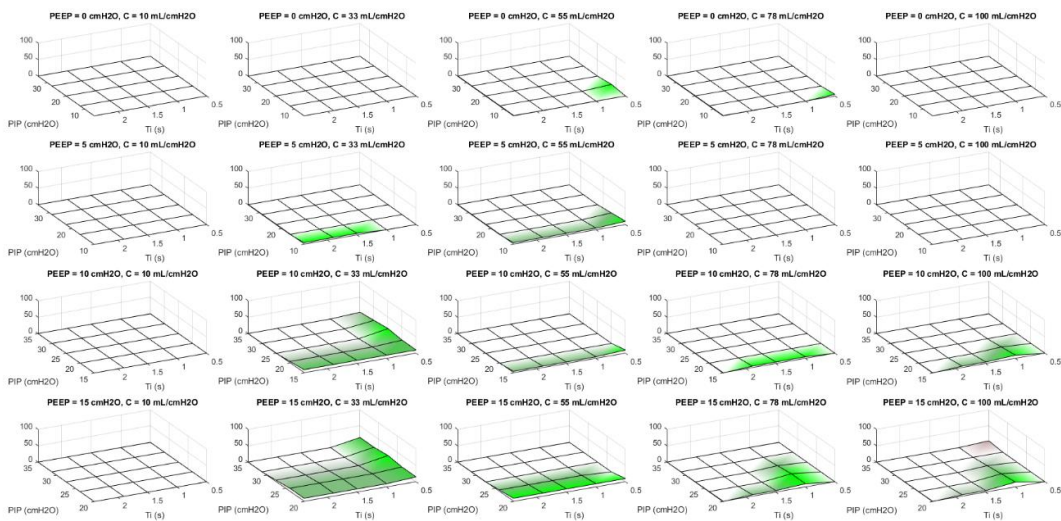


Figure 4-16: 3D Distribution Graphs of the False Negative Predictions for the VCD Mode

Table 4-7 is the resulting confusion matrix for the proposed hybrid classifier. Here, we see that all VCC breaths were correctly classified, 133 VCD breaths were misclassified as PC breaths, 1 PC breath was misclassified as VCC, and 113 PC breaths were misclassified as VCD breaths. The misclassification of a PC breath as a VCC breath raises concern since the proposed method indicated only confusion between VCD and PC breaths. However, further inspection showed that this is one of possibly several cases where the hard decision boundaries' significant figures do not match the decimal length formatting during analysis, causing edge cases to be misclassified.

Table 4-7: Confusion Matrix for Training Results of the Proposed Hybrid Classifier

Modes	Predicted	VCC	VCD	PC
Actual	Total = 30 000	10 001	9 980	10 019
VCC	10 000	10 000	0	0
VCD	10 000	0	9 867	133
PC	10 000	1	113	9 886

4.3 Evaluate the Classifier

The proposed hybrid classifier needs to be evaluated for appropriate generalisation by analysing a larger dataset containing unobserved breaths. Recall that the classifier was developed using a smaller dataset of 30 000 breaths. Evaluation will be performed on the total generated dataset described in Section 3.4.3 (1.92 M breaths) using the proposed hybrid classifier described in Section 4.2.3.

4.3.1 Evaluating the 3D Distribution Graphs of the False Negative Predictions

The expanded dataset has a higher sweeping resolution along all parameters except for the resistance and baseline pressure. Therefore, the resolutions of the grids also increase for the 3D distribution graphs of false negative predictions. Since fitting 20 graphs horizontally on a page (depicting the levels of compliance) is impractical, only the graphs with compliances closest to those mentioned in Section 4.2.3 is shown for conserving comparison. All three modes' 3D distribution graphs have different compliance levels per column (10 to 100 mL/cmH₂O), and different baseline pressure levels per row (PEEP of 0 to 15 cmH₂O). Each coordinate on the horizontal planes' values represents the percentage of false negatives that occurred across the resistance sweep for those parameter settings.

Figure 4-17 depicts the resulting 3D distribution graphs of the false negative predictions for the VCC mode. All blue areas are instances where VCC breaths were misclassified as PC breaths. The V_T and Q_{max} are varied along the horizontal axes. From comparison, the expanded dataset resulted in misclassifications for the VCC mode, which was not the case during development. However, the tally of instances is low. From inspection, the proposed hybrid classifier tends to make misclassifications for VCC breaths when the V_T is low, and Q_{max} is high for increased C_S , which is a practically unlikely combination during sedated mechanical ventilation.

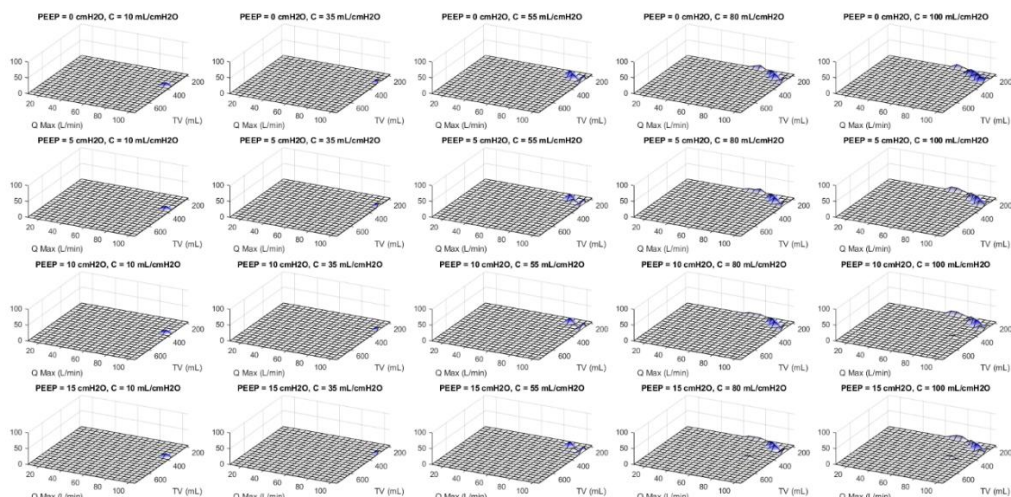


Figure 4-17: 3D Distribution Graphs of the False Negative Predictions for the VCC Mode

Figure 4-18 depicts the resulting 3D distribution graphs of the false negative predictions for the VCD mode. All blue areas are instances where VCD breaths were misclassified as PC breaths. The V_T and Q_{max} are varied along the horizontal axes. From comparison, the expanded dataset resulted in similar misclassification tendencies, which dictates good generalisation. From inspection, the proposed hybrid classifier tends to make misclassifications for VCD breaths linearly from low V_T and low Q_{max} to high V_T and high Q_{max} . Also, this trend changes at low C_s (10 mL/cmH₂O), and misclassification occurs at low V_T and high Q_{max} , which is a practically unlikely combination during sedated mechanical ventilation.

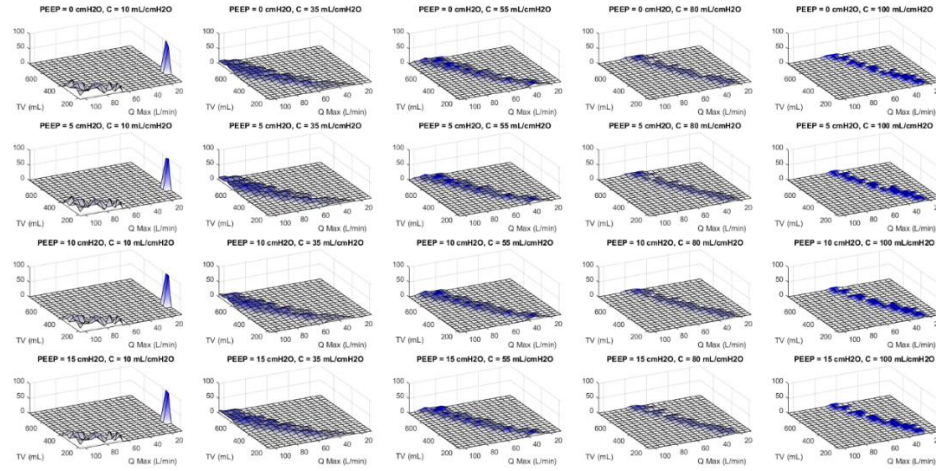


Figure 4-18: 3D Distribution Graphs of the False Negative Predictions for the VCD Mode

Figure 4-19 depicts the resulting 3D distribution graphs of the false negative predictions for the PC mode. All the green and red areas are instances where PC breaths were misclassified as VCD and VCC breaths, respectively. P_{PIP} and T_i are varied along the horizontal axes. From comparison, the expanded dataset resulted in similar misclassification tendencies, which dictates good generalisation. The phenomenon of misclassifications for P_{PIP} close to PEEP could indicate that breaths simulated with these settings need attending to. If this issue is solvable, regeneration of the PDFs could also improve VCD prediction performance.

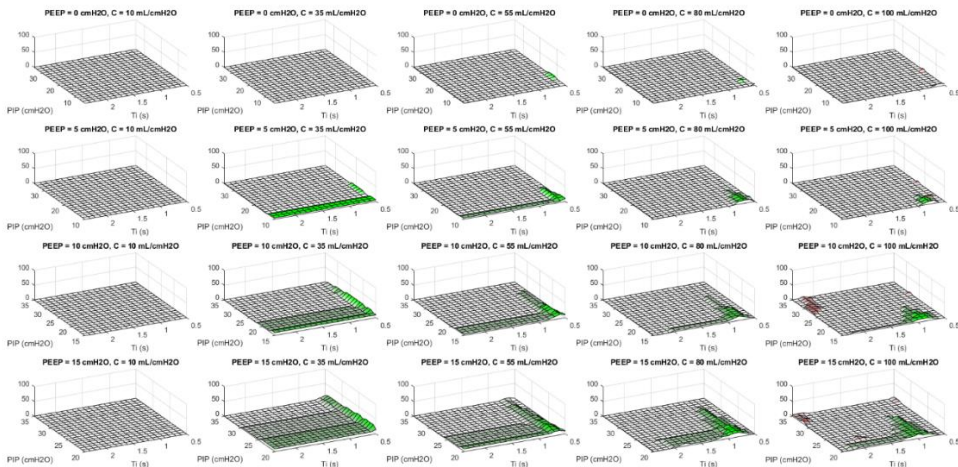


Figure 4-19: 3D Distribution Graphs of the False Negative Predictions for the PC Mode

4.3.2 Evaluating the Confusion Matrix

Table 4-8 is the confusion matrix for the proposed hybrid classifier applied to the extended dataset. Each ventilation mode consists of 640 000 simulated breaths for the extended dataset. Here, we see that 819 of the VCC breaths were misclassified as PC breaths, 8 032 VCD breaths were misclassified as PC breaths, 160 PC breaths were misclassified as VCC breaths, and 8 094 PC breaths were misclassified as VCD breaths.

The misclassified 819 VCC breaths increased from 0.00% to 0.13%, which could be interpreted as bad generalisation. However, the increase is insignificant. Also, as previously established from the 3D distribution graphs of the false negative predictions, these new misclassified breaths are all from impractical setting combinations for a sedated patient. The misclassified VCD breaths decreased from 1.33% to 1.26% (0.08% difference), showing good generalisation for VCD breath predictions. The misclassified PC breaths increased from 1.14% to 1.29% (0.15%), about double the difference for VCD. However, this difference is still insignificant, and therefore, good generalisation is achieved.

Table 4-8: Confusion Matrix for Training Results of the Proposed Hybrid Classifier

Modes	Predicted	VCC	VCD	PC
Actual	Total = 1.92 M	639 341	640 062	640 597
VCC	640 000	639 181	0	819
VCD	640 000	0	631 968	8 032
PC	640 000	160	8 094	631 746

Table 4-9 conveys that the true positive accuracies changed from 100.00% to 99.87% for VCC, from 98.67% to 98.75% for VCD, and from 98.86% to 98.71% for PC after performing the evaluation. False positives for each mode are 0.03%, 1.26% and 1.38%, respectively. The classifier's overall accuracy decreased from 99.18% to 99.11% after evaluation on an increased dataset size of 6 400%, indicating that the proposed hybrid classifier generalises well.

Table 4-9: True Positive and False Positive Accuracies for Each Ventilation Mode After Evaluation

Breath Modes	VCC	VCD	PC
True Positive [%]	99.87	98.75	98.71
False Positive [%]	0.03	1.26	1.38

4.4 Chapter Summary

This chapter discussed how the statistics-based ventilation mode classifier was developed to identify whether a mechanically ventilated breath belongs to the VCC, VCD, or PC mode.

First, the classifier calculates two statistically descriptive shape parameters (the standard deviation and the coefficient of determination), by analysing the breath cycle's pressure and flow waveform scalar data, respectively. These two statistical parameters were calculated for a smaller dataset of 30 000 breaths with the same parameter sweep ranges of the complete dataset.

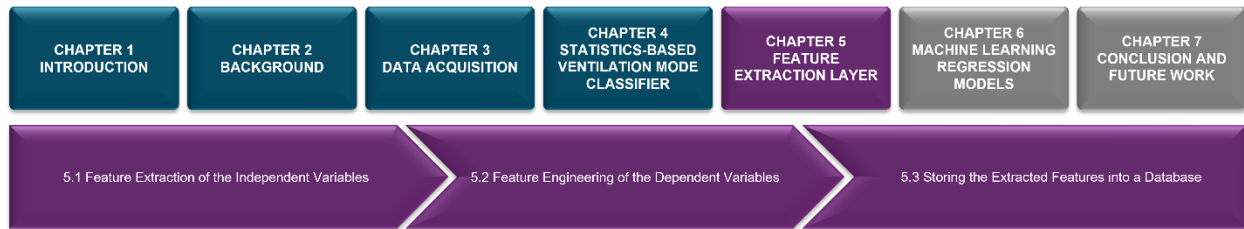
The first investigated classification technique leveraged insight into the spread of these statistical parameters' ranges (obtained through boxplots) to identify hard decision boundaries. Since both parameters' boxplots conveyed classification knowledge that could help eliminate possible confusion of its counterpart and, thus, lead to set-up better hard decision boundary sets, a nested decision boundary approach was implemented. This ensured that the classification knowledge of both statistical parameters' spread was optimally leveraged, resulting in only 7.64% of the 30 000 breaths remaining unclassified. All VCC breaths were correctly classified using this technique, and only 1 075 of the VCD breaths and 1 217 of the PC breaths remained unclassified. Assuming the remainder of the unclassified breaths belonged to the larger unidentified ventilation mode class (i.e., PC breaths), this classification technique resulted in an overall accuracy of 96.42%.

The second investigated option for classifying the ventilation modes was to leverage PDFs fitted with Kernel functions. The idea was to evaluate the likelihood that a breath belonged to a ventilation mode by comparing the probability scores that result from applying the statistical parameters' values to these Kernel PDFs. Implementing these PDFs resulted in classification accuracies of 94.98% for VCC, 93.66% for VCD, and 94.09% for PC. Therefore, the overall accuracy for this classification technique was 94.24%.

Finally, a hybrid approach was considered where the hard decision boundary technique is first leveraged. If the classifier's result was undefined (7.64% of the cases), Kernel PDFs are utilised to identify the breaths as either VCD or PC. This hybrid solution resulted in classification accuracies of 100.00% for VCC, 98.67% for VCD, and 98.86% for PC. The overall accuracy for this approach was 99.18% for the 30 000 breaths.

The proposed hybrid classifier was evaluated by testing the total dataset of 1.92 M breaths, which resulted in classification accuracies of 99.87% for VCC, 98.75% for VCD, and 98.71% for PC. The overall accuracy is 99.11%, which shows that the proposed hybrid classifier generalises well.

CHAPTER 5 – FEATURE EXTRACTION LAYER



In this chapter, a feature extraction layer is developed to translate the time-series data into informative feature vectors. Since the mechanical ventilator-patient (MV-P) setup can be seen as a controller (ventilator) interacting with a plant (ventilator circuit and patient) which is monitored by sensors, independent and dependent information becomes relevant for describing the process. The pulmonologist sets the mechanical ventilator (MV) parameters describing the ventilation protocol prior to ventilation and is, therefore, the independent features needing extraction. The MV performs the ventilation protocol on the patient, and the sensors log the resulting time-series data. The logged data depends on the parameters of the respiratory system, i.e., the patient's health status. The mode of ventilation (one of the independent features) depicts which waveforms (pressure waveform or flow rate waveform in the case of volume-controlled or pressure-controlled ventilation, respectively) will incorporate the dependent features needing extraction. Some dependent features have already been discussed in previous sections. However, additional informative, dependent features need to be identified and quantified. This process is called feature engineering [77]. The independent features form the baseline (or carrier data), which is used to interpret the resulting dependent features for enabling predictions on the health status of the patient. The combination of the dependent and independent features (extracted per breath) is called a feature vector. Each breath's feature vector is then paired with its target labels (resistance and compliance target values), to be used later to develop machine learning regression models.

5.1 Feature Extraction of the Independent Variables

The independent features needing extraction is the parameters set by the pulmonologist on the MV to define the ventilation protocol. Recall from Section 4.3.2 that the accuracy of the mode feature extraction is 99.11%. Baseline pressure (P_0 or PEEP – cmH₂O) is the first independent feature needing extraction. The other independent features are mode-specific. For the volume-controlled modes (VCC for constant flow pattern and VCD for decelerating flow pattern), the mode-specific independent features are the tidal volume (V_T – mL) and the maximum inspiratory flow (Q_{max} – L/min). For the pressure-controlled (PC) mode, the mode-specific independent features are the peak inspiratory pressure (P_{PIP} – cmH₂O) and the inspiratory time (T_i – seconds).

5.1.1 Baseline Pressure Feature Extraction

The baseline pressure feature is a setting on all three ventilation modes and was swept across four levels from 0 to 15 cmH₂O. After simulating the larger dataset (1.92 M breaths), the baseline pressure was extracted from all breaths using an algorithm that first identifies the expiratory phase and then determines the average pressure. Figure 5-1 illustrates the statistical spread of the root mean squared error (RMSE) for the extracted baseline pressure feature values. The first set of boxplots (Figure 5-1 (a)) is the spread for the VCC mode, (b) is of the VCD mode, and (c) is of the PC mode. PC has the fewest outliers, and the upper whiskers become shorter as the set baseline level increases. This is due to the decreasing required settling time as the range from the peak inspiratory pressure to the baseline pressure decreases.

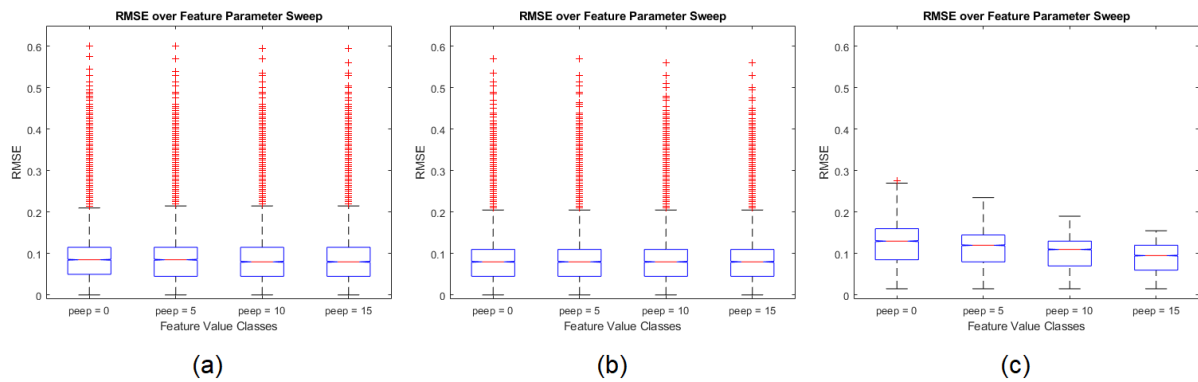


Figure 5-1: Boxplots of Baseline Pressure Feature for VCC (a), VCD (b) and PC (c)

Table 5-1 conveys the average RMSE for the baseline pressures of all three modes and the total averages. All three modes' RMSE are similar, as are the averages of the different levels' RMSE. This shows that the feature extraction method performs the same regardless of the set level and the chosen ventilation mode. The overall average RMSE across all modes and levels are 0.11 cmH₂O. For an average set value of 7.5 cmH₂O, this is a percentage error of 1.47%.

Table 5-1: Root Mean Squared Error Summary for Baseline Pressure Feature Extraction per Ventilation Mode

PEEP [cmH ₂ O]	VCC [RMSE]	VCD [RMSE]	PC [RMSE]	Average [RMSE]
0.00	0.11	0.10	0.14	0.12
5.00	0.11	0.10	0.13	0.11
10.00	0.11	0.10	0.12	0.11
15.00	0.11	0.10	0.10	0.11
Average	0.11	0.10	0.12	0.11

5.1.2 Maximum Inspiratory Flow Feature Extraction

The maximum inspiratory flow feature (Q_{max}) is a VCC and VCD mode setting. It was swept across 20 levels from 10 to 105 L/min. The breaths were analysed using an algorithm that determines the maximum flow. Figure 5-2 illustrates the statistical spread of the RMSE for the extracted Q_{max} feature values. Figure 5-2 (a) is the spread for the VCC mode and (b) is of the VCD mode. Recall from Section 3.3.1.3 that the simulation incorporates mechanical valves, which introduce flow delays at the onset of ventilation. This initial flow lagging phase causes the simulated Q_{max} to not necessarily reach the set Q_{max} . The RMSE for Q_{max} of the VCD mode is larger than for the VCC mode because Q_{max} is supposed to be achieved during this lagging phase for VCD and not necessarily for VCC. The RMSE gets noticeably larger for higher levels of Q_{max} , which is also due to the valves not fully opening before small target tidal volumes have already been delivered (180 mL at 105 L/min takes about 0.10 s).

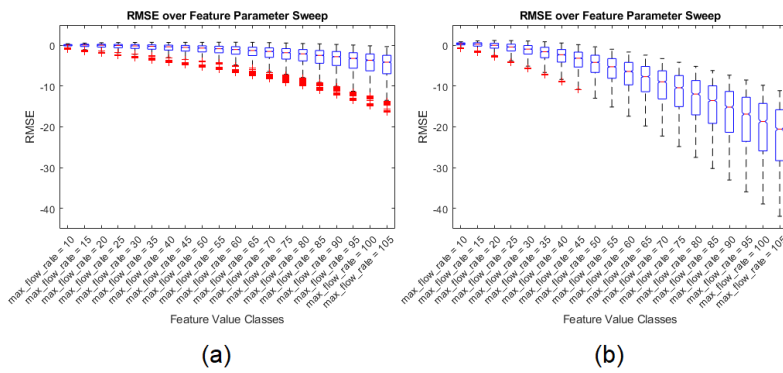


Figure 5-2: Boxplots of Maximum Inspiratory Flow Feature for VCC (a) and VCD (b)

Table 5-2 conveys the RMSE averages for Q_{max} for both volume-controlled (VC) modes. The overall average RMSE across all modes and levels is 5.33 L/min, or 7.57% error. This is due to the mechanical valve's flow-lagging phenomena, as is the practice case.

Table 5-2: Root Mean Squared Error Summary for Maximum Inspiratory Flow Feature Extraction

Q_{max} [L/min]	VCC [RMSE]	VCD [RMSE]	Error [%]
10.00	0.25	0.45	3.52
40.00	0.92	3.08	5.00
70.00	2.24	10.37	9.01
100.00	4.79	20.84	12.81
Average	2.03	8.63	7.57

5.1.3 Tidal Volume Feature Extraction

The tidal volume feature (V_T) is a VCC and VCD mode setting. It was swept across 20 levels from 180 to 750 mL. The breaths were analysed using an algorithm that determines the maximum volume. Figure 5-3 illustrates the statistical spread of the RMSE for the extracted V_T feature values. Figure 5-3 (a) is the spread for the VCC mode and (b) is of the VCD mode. Recall from Section 5.1.2 that the simulated Q_{max} never reached the set values in many cases. However, the allocated time of inspiration was calculated from set V_T and Q_{max} with the equation appropriate for the flow pattern shape. This means that in all cases where Q_{max} was not met, the allocated time was too short to deliver set V_T . Therefore, as a result, the extracted V_T is less for all those cases, and the RMSE averages will follow the same trends as that of the extracted Q_{max} feature.

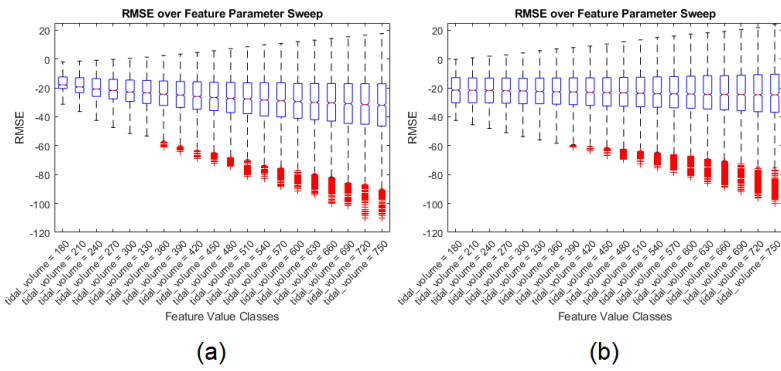


Figure 5-3: Boxplots of Tidal Volume Feature for VCC (a) and VCD (b)

Table 5-3 conveys the RMSE averages for V_T for both volume-controlled modes. The average RMSE across all modes and levels is 26.67 mL, or 6.40% error. This is due to the mechanical valve's flow-lagging phenomena, as is the case in practice.

Table 5-3: Root Mean Squared Error Summary for Tidal Volume Feature Extraction

V_T [mL]	VCC [RMSE]	VCD [RMSE]	Error [%]
180.00	18.33	21.84	11.16
360.00	26.18	22.77	6.80
540.00	31.47	25.18	5.24
720.00	36.09	28.31	4.47
Average	28.82	24.52	6.40

5.1.4 Inspiratory Time Feature Extraction

The inspiratory time feature (T_i) is a setting of the PC mode. It was swept across 20 levels from 0.5 to 2.4 s. The breaths were analysed using an algorithm that determines the inspiratory time from the flow waveform by subtracting the timestamp at the start of the inspiratory phase from that at the end of the inspiratory phase. The starting timestamp is determined by finding the timestamp at Q_{max} and then assessing the flow at prior timestamps until the flow diminishes below a flow threshold at 1.00% of Q_{max} . Similarly, the end timestamp is determined by finding the timestamp at Q_{-max} (the maximum expiratory flow) and then assessing the flow at prior timestamps until the negative flow diminishes below a flow threshold at 1.00% of Q_{-max} . Figure 5-4 illustrates the statistical spread of the RMSE for the extracted T_i feature values.

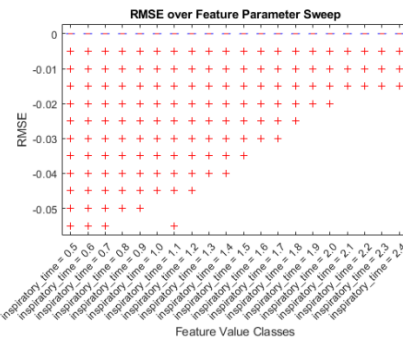


Figure 5-4: Boxplots of Inspiratory Time Feature for PC

Table 5-4 conveys the RMSE averages for T_i for the PC mode. The overall average RMSE across the levels is 0.01 s, or 0.85% error.

Table 5-4: Root Mean Squared Error Summary for Inspiratory Time Feature Extraction

T_i [s]	PC [RMSE]	Error [%]
0.50	0.01	1.60
0.80	0.01	1.54
1.10	0.01	1.27
1.40	0.01	0.91
1.70	0.01	0.51
2.00	0.00	0.22
2.30	0.00	0.08
Average	0.01	0.85

5.1.5 Peak Inspiratory Pressure Feature Extraction

The peak inspiratory pressure feature (P_{PIP}) is a setting of the PC mode. It was swept across 20 levels from 5 cmH₂O above baseline pressure to 35 cmH₂O. The breaths were analysed using an algorithm that determines the average pressure between the timestamp at 50 ms after Q_{max} and at the end of the inspiratory flow. Figure 5-5 illustrates the RMSE statistical spread for the extracted P_{PIP} feature values at 0 cmH₂O (a), 5 cmH₂O (b), 10 cmH₂O (c) and 15 cmH₂O (d).

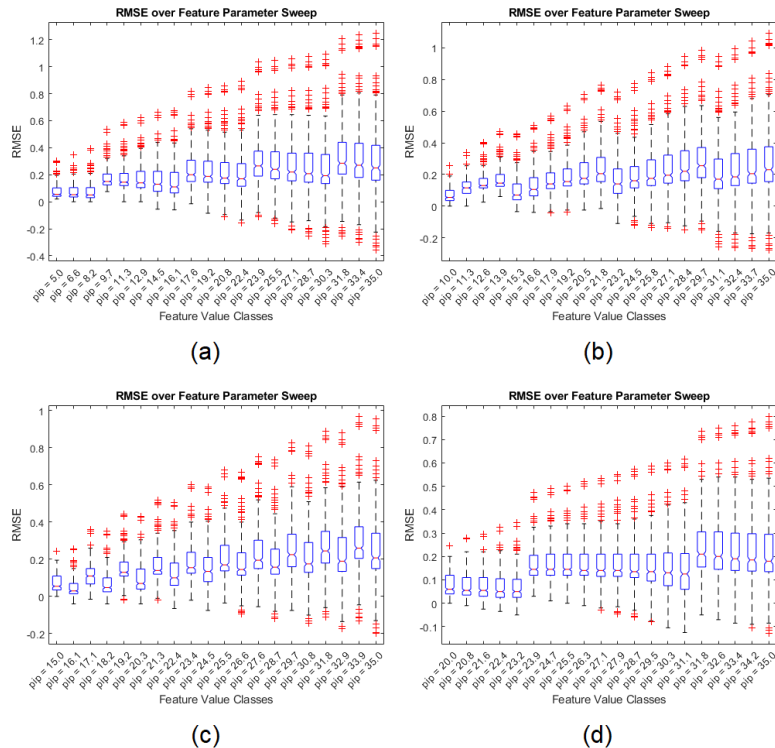


Figure 5-5: Boxplots of Peak Inspiratory Pressure Feature for Baseline Pressures of 0 cmH₂O (a), 5 cmH₂O (b), 10 cmH₂O (c) and 15 cmH₂O (d)

Table 5-5 conveys the RMSE averages for P_{PIP} for the PC mode. The overall average RMSE across the levels is 0.27 cmH₂O, or 1.53% error.

Table 5-5: Root Mean Squared Error Summary for Peak Inspiratory Pressure Feature Extraction

P_{PIP} [cmH ₂ O]	PC [RMSE]	Error [%]
5.00	0.13	2.52
14.47	0.22	1.52
23.95	0.35	1.48
35.00	0.38	1.07
Average	0.27	1.53

5.2 Feature Engineering of the Dependent Variables

The independent features extracted give information on the protocol used to deliver the breath, which must be known since it can be interpreted as the initiating input signal to the system (patient). The health status of the respiratory system (resistance and compliance levels) is applied to these signals, and dependent signals are measured as a result. These resulting signals embed information on the resistance and compliance levels, which need to be quantitatively extracted to predict these values using regression machine learning methods later.

Recall from sections 2.3.3 and 2.3.4 that the expiratory phase's protocol is the same for all three ventilation modes (for a sedated patient), which is that exhalation is achieved passively by controlling the valves of the MV circuit and the driving pressure. This suggests that if an informatively suitable combination of dependent features with appropriate representative complexity could be extracted from only the expiratory phase, the methods used to extract these features would be mode-independent (simplifying the analysis of the multivariate system).

Below is a list of the dependent features that were extracted. These features are deemed useful since they are derived from the waveform analysis techniques discussed in Section 2.2.4.3 (time constants) and Section 2.6.2.3 (loops).

- Time Constant (τ_{RC}) – seconds
- Expiratory Flow at One Time Constant (Q_τ) – L/min
- Flow-Volume Loop Scoop
 - Gradient
 - Surface Ratio
 - Skewness
 - Kurtosis

5.2.1 Time Constant Feature Extraction

As mentioned in Section 2.2.4.3, the volume is passively exhaled exponentially and follows equation (5-1). Also, τ_{RC} is calculated using equation (5-2) from Section 3.3.3.2. R_{EXP} is the sum resistance of the respiratory system (R_{RS}) and the expiratory circuit's resistance. Therefore, extracting the timestamp at which the tidal volume decreases to 36.8% (τ_{RC}), a feature encapsulating information on both R_{RS} and C_S is already engineered.

$$V(t) = C \cdot \Delta P \cdot e^{-t/\tau_{RC}} \quad (5-1)$$

$$\tau_{RC} = R_{EXP} \times C_S \quad (5-2)$$

5.2.2 Expiratory Flow at One Time Constant

As mentioned in Section 5.2.1, R_{EXP} is the sum resistance of R_{RS} and the expiratory circuit's resistance. The latter has flow-dependent resistance components. Therefore, extracting the flow rate at τ_{RC} could be useful since it encapsulates information necessary to predict the portion of R_{EXP} due to the flow-dependent resistances.

5.2.3 Flow-Volume Loop Scoop Gradient

Recall from Section 2.6.2.3.1 that the flow-volume loop's shape can be inspected for indications of changes in compliance (see Figure 5-6 (a) for VCC and (b) for VCD). The qualitative indication for different compliance levels is that the maximum negative flow during the expiratory phase (the lower segment of the loop) varies, as well as the volume at which it occurs. Low compliance showed higher maximum negative flow at lower volumes, and high compliance showed lower maximum negative flow at higher volumes (as indicated by Figure 5-7 (a) for VCC and (b) for VCD). However, as seen in the following section, the scoop's shape can interfere with calculating the average gradient. Note that the gradient remains stable after halfway exhalation. This means that the flow-volume loop's gradient (calculated from the halfway exhalation point to the point of full exhalation) conveys information about C_S and should be extracted as a feature.

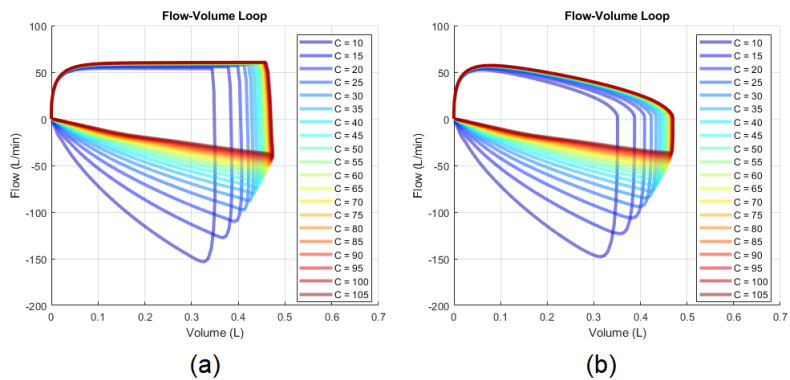


Figure 5-6: Flow-Volume Loops of Varying Compliance for VCC (a) and VCD (b)

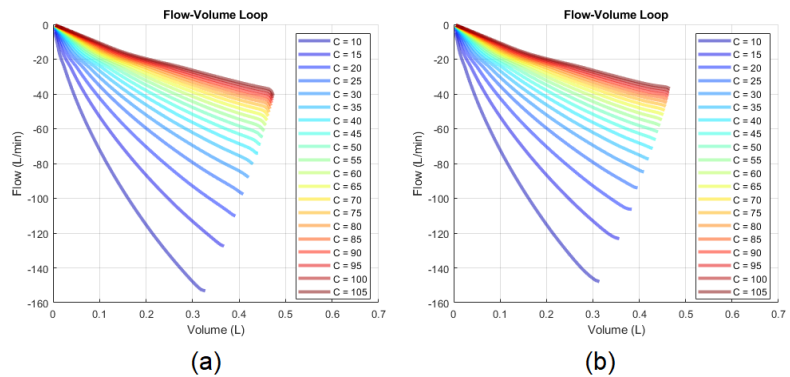


Figure 5-7: Expiratory Segments of Flow-Volume Loops of Varying Compliance for VCC (a) and VCD (b)

5.2.4 Flow-Volume Loop Scoop Resistance Analysis

Recall from Section 2.6.2.3.2 that the flow-volume loop's shape can also be inspected for indications of changes in resistance (see Figure 5-8 (a) for VCC and (b) for VCD). The qualitative indication for different resistance levels is that the concavity of the scoop during the expiratory phase (the lower segment of the loop) varies. A low resistance showed less concavity (sometimes even being convex), and a high resistance showed more concavity (as indicated by Figure 5-9 (a) for VCC and (b) for VCD). This means that the shape of the expiratory phase's scoop of the flow-volume loop conveys information about R_{RS} and should be analysed for features. The ranges of the segments are normalised to unity (Figure 5-10 (a) for VCC and (b) for VCD) to improve the compatibility of the features for any breath.

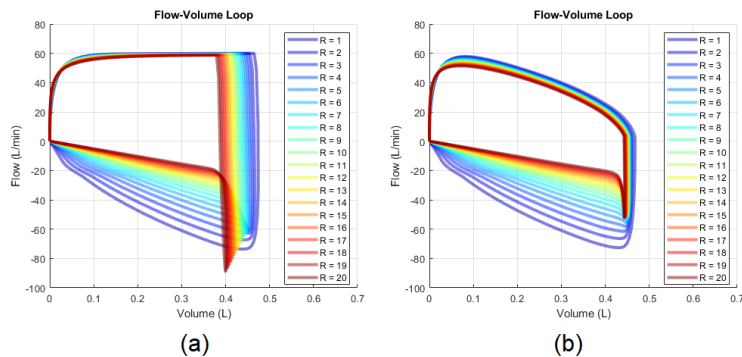


Figure 5-8: Flow-Volume Loops of Varying Resistance for VCC (a) and VCD (b)

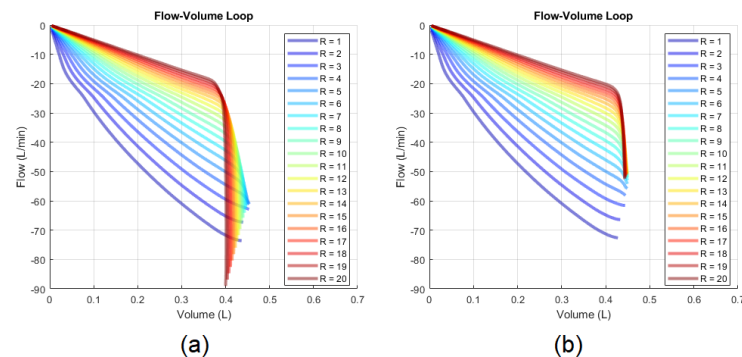


Figure 5-9: Expiratory Segments of Flow-Volume Loops of Varying Resistance for VCC (a) and VCD (b)

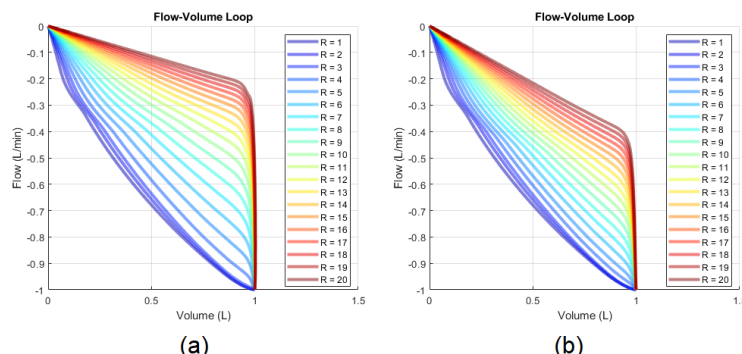


Figure 5-10: Normalised Segments of Flow-Volume Loops of Varying Resistance for VCC (a) and VCD (b)

5.2.4.1 Flow-Volume Loop Scoop Resistance Analysis Using Surface Ratio

One way of quantitatively describing the degree of concavity is to calculate a surface ratio. This can be accomplished by dividing the grey area ($Surface_{Data}$ – area above the unit data curve) by the blue area ($Surface_{Reference}$ – triangular area) as conveyed by equation (5-3) and clarified by Figure 5-11. $Surface_{Data}$ can be calculated using the Riemann sum algorithm (equation (5-4)).

$$Surface \text{ Ratio} = \frac{Surface_{Data}}{Surface_{Reference}} \quad (5-3)$$

$$Surface_{Data} = \sum_{k=0}^{n-1} \frac{f(x_k) + f(x_{k+1})}{2} \times (x_{k+1} - x_k) \quad (5-4)$$

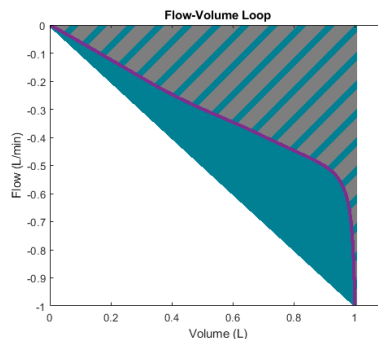


Figure 5-11: Illustration of the Data Surface (Grey) and the Reference Surface (Blue)

5.2.4.2 Flow-Volume Loop Scoop Resistance Analysis Using Skewness and Kurtosis

The data points were sampled at 200 Hz (time-dependent). Therefore, the original data point distribution is irregular when omitting the time dimension to plot the flow-volume loop (see Figure 5-12 (a) as an example). The skewness and kurtosis functions in MATLAB® only accept the value array as input (flow values). Therefore, to conserve representative information, the points need to be resampled (interpolated) over the same curve concerning the parameter array (volume values), as illustrated by Figure 5-12 (b). After that, the skewness and kurtosis of the resampled flow data points are extracted as features to describe the shape of the scoop further quantitatively.

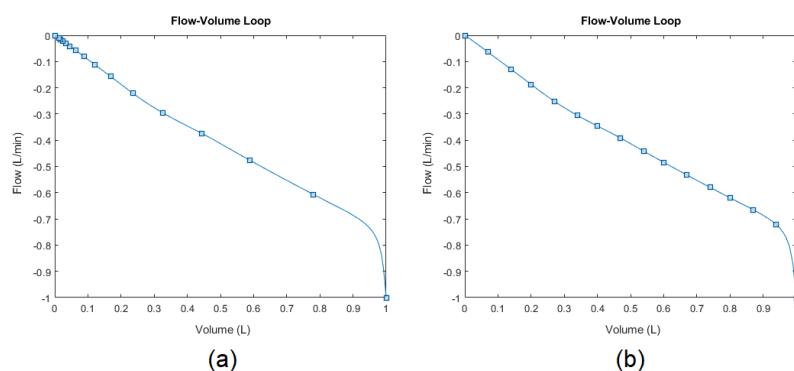


Figure 5-12: Illustration of the Data Point Distribution Transformation: Original (a) and Interpolated (b)

5.3 Storing the Extracted Features into a Database

A database was designed to store all the generated data from the simulations and the extracted features for later access. The entity relationship diagram (Figure 5-13) conveys the schematic of the database, dictating all tables, relationships and dependencies. Firstly, the patient table (*tbl_patient*) stores each patient's name, surname, sex and date of birth indexed by a primary key. One patient can undergo many sessions, hence the one-to-many relationship with the sessions table (*tbl_session*). Each entry of the sessions table comprises the session primary key, patient identity, the height of the patient at the time of admission, date of the session, ventilator settings and universally unique identifier (UUID). The sessions table also has two foreign keys; one indicating the identity of the patient and the other the mode used for ventilation listed in the modes table (*tbl_mode*). The modes table lists all existing modes (“vc_con” for VCC, “vc_dec” for VCD and “pc” for PC) with primary keys. Since many sessions can run the same ventilation mode, the relationship is one too many. Each session may perform multiple breath deliveries, therefore, the breaths table (*tbl_breath*) is linked to the sessions table with a one-to-many relationship. The breaths table comprises the session identity, extracted features, patient health status during each breath (resistance and compliance) and UUID. The breaths table also has two foreign keys; one indicating the session identifier and the other the mode identifier indicating the predicted mode the breath was performed with. Lastly, the time-series data sampled at 200 Hz was stored in the breaths data table. One breath consists of many data points and, thus, has a one-to-many relationship with the breaths table. Each record includes the breath identity, timestamp and pressure values, flow rate and volume at said timestamp.

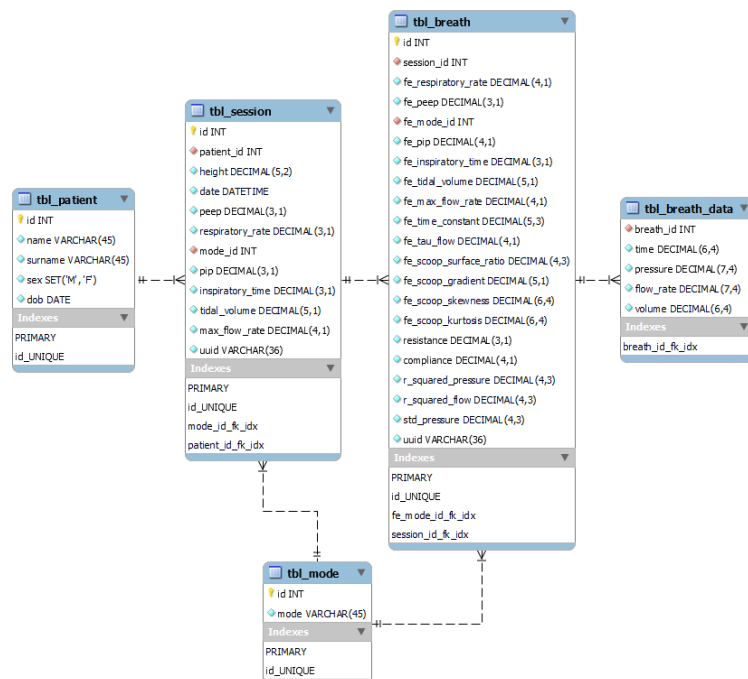


Figure 5-13: Entity Relationship Diagram of the Database

5.4 Chapter Summary

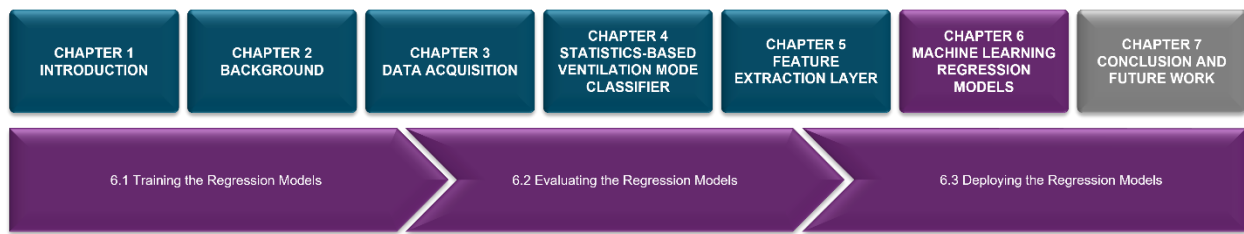
This chapter described the features that need to be extracted per breath before creating the models for predicting the patient's health status. These features are explicitly chosen to contain information on independent and dependent waveform scalar data. These features were then labelled with their mechanical parameter target values to form the labelled-feature vector pairs, which were stored in a database for machine learning later.

First, the three waveform scalars were analysed to determine the pulmonologist's settings for the mechanical ventilator to perform the mechanical ventilation protocol. These features are considered independent since they are assumed to convey no information on the patient's health status. Knowing these independent features' values constrains the inspiratory phase's shape of either the pressure waveform scalar (in the case of the PC mode) or the flow rate waveform scalar (in the case of the VCC or VCD mode). Since Chapter 4 already extracts the first independent feature (the ventilation mode) with an accuracy of 99.11%, this chapter focussed only on extracting the baseline pressure (1.47% extraction error) and the mode-specific features. The mode-specific features for the volume-controlled modes are the maximum inspiratory flow (7.57% extraction error) and the tidal volume (6.40% extraction error), and the peak inspiratory pressure (1.53% extraction error) and inspiratory time (0.85% extraction error) for the pressure-controlled mode. The chapter concluded that the relatively higher extraction errors for the volume-controlled modes were due to the flow-lagging effects of the mechanical valves implemented in the model as the practice case.

Subsequently, feature engineering was performed to identify and extract features that convey information on the patient's health status (the dependent features). These features were extracted from the expiratory phase and are, thus, mode-independent since all three modes' expiration protocol is to shut the inspiratory tube's valve and allow passive exhalation by opening the expiratory tube's valve. The time constant is a dependent feature extracted from the volume waveform scalar, which is leveraged to extract another dependent feature – the flow rate at said time constant. The remaining four dependent features were all extracted from the flow-volume loop's expiratory scoop. These were the gradient, surface ratio, skewness, and kurtosis parameters. These features convey information on the shape of the scoop, which conveys information on the patient's respiratory mechanical parameters (referring to Chapter 2 Sections 2.6.2.3.1 and 2.6.2.3.2).

Finally, a database was developed to store all the relevant data generated and extracted during this project. This database comprises tables with the patient's details, ventilation modes, session details, time-series data, and per-breath details such as the extracted features.

CHAPTER 6 – MACHINE LEARNING REGRESSION MODELS



Chapter 3 (Data Acquisition), 4 (Statistics-Based Ventilation Mode Classifier) and 5 (Feature Extraction Layer) delivered a labelled-feature vector dataset of 1.92 M breath examples. According to the machine learning process diagram (Figure 6-1), the next step is to start training models. This chapter uses the labelled-feature vector pairs to develop machine learning regression models to predict the respiratory resistance (R_{RS}) and static compliance (C_S) for the volume-controlled modes. Recall from Section 2.4.4.2 that these modes are the volume-controlled constant flow pattern ventilation (VCC) mode and the volume-controlled decelerating flow pattern ventilation (VCD) mode. Firstly, the regression algorithms on which the machine learning models are based are specified. After that, the labelled-feature vector pairs are randomly and equally divided into training and testing sets. The training set is then used to train machine learning regression models, which are cross-validated using k-fold methods. After acquiring the models, they are tested using the testing set. The performance of the models is then evaluated to determine the best models per use case. Finally, the best models are deployed and executed on typical mechanical ventilation sessions to validate the project.

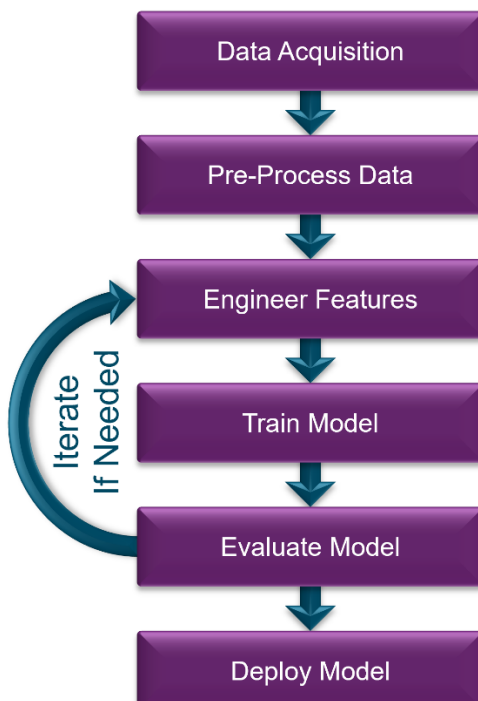


Figure 6-1: Diagram of the Machine Learning Process

6.1 Training the Regression Models

Recall from Section 2.7.4 that many different regression algorithms exist for training machine learning models, which were briefly discussed in said section. Below is a list of all algorithms considered for this project (further referred to as the regression algorithm set).

- Linear Regression Algorithms
 - Normal Linear Regression
 - Interactions Linear Regression
 - Robust Linear Regression
 - Stepwise Linear Regression
- Decision Tree Algorithms
 - Fine Trees
 - Medium Trees
 - Coarse Trees
- Support Vector Machine (SVM) Algorithms
 - Linear SVM
 - Quadratic SVM
 - Cubic SVM
 - Fine Gaussian SVM
 - Medium Gaussian SVM
 - Coarse Gaussian SVM
- Gaussian Process Regression (GPR) Algorithms
 - Exponential GPR
 - Squared Exponential GPR
 - Matern 5/2 GPR
 - Rational Quadratic GPR
- Ensemble Algorithms
 - Boosted Trees
 - Bagged Trees
- Neural Networks (NN)
 - Narrow Neural Network
 - Medium Neural Network
 - Wide Neural Network
 - Bi-Layered Neural Network
 - Tri-Layered Neural Network

The regression algorithm set was leveraged to train models for the four use cases. These four use cases are to predict R_{RS} and C_S for both VCC and VCD breaths. Since the regression algorithm set consists of 24 different algorithms, 96 regression models were trained for this project. Again, multiple machines of the NWU's computer laboratory (G22 in building N1) were leveraged to minimise training time (see Figure 6-2). At the time of training the models, Eskom implemented load-shedding multiple times a day nationally. Although the NWU has their own backup generators for these types of circumstances, the temporary shutdown of electricity before the backup generators take effect will cause the machines to shut down as well, and any unsaved progress will be lost. Therefore, an uninterruptable power supply (UPS) was used to prevent any loss of unsaved work. However, this meant that the number of machines utilisable at a time was limited to the capacity of the UPS. Therefore, only four machines were used to generate the models for the four use cases (one use case's model per machine). Parallel pools were used once more to minimise the training times further.



Figure 6-2: Photo of Training Machine Learning Regression Models in the NWU's Computer Laboratory

The regression learning tool of MATLAB® [109] was used together with the appropriate training datasets to train the models. Since the regression learning tool trains 24 different algorithms, hyperparameter tuning for six cases (144 models) could be a whole different project. Therefore, the default settings of the regression learning tool were accepted.

The datasets were first divided as per the predicted ventilation mode (about 640 000 breaths per mode). The datasets were then divided randomly and equally into training and testing sets. Each feature vector comprises the extracted baseline pressure (cmH_2O), tidal volume (mL), maximum inspiratory flow (L/min), time constant (s), signed flow at said time constant (L/min), and the surface ratio, gradient, skewness [110], and kurtosis [111] of the flow-volume loop's scoop. The type of label (R_{RS} or C_S) paired with the feature vector was that appropriate to the use case handled by the machine. All trained models were validated using the k-fold cross-validation method with five folds. All trained models for this project is available on a GitHub repository for repeatability.

6.2 Evaluating the Regression Models

The testing datasets (held-out dataset) were used to make predictions, which were compared to the target values to determine the accuracies of the models (root mean squared error (RMSE)). Furthermore, performance indicators such as the training speed, overfitting index, prediction speed and size of the models were compared to identify the best overall performing model per use case.

Subsequent is a summary of each performance indicator's description and the resulting absolute ranges over all four use cases. These ranges are then used to set up filters (cut-off limits) to create shortlists of the best-performing models. Finally, a weighted scoring system ranks the resulting models from the shortlists.

- Root Mean Squared Error (RMSE) Percentage

The root mean squared error of the predictions versus the target values (an indication of the model's accuracy). The absolute percentage range is 0.413 to 9.815% for R_{RS} and 0.5562 to 11.166% for C_S . Figure 6-3 is the boxplots of the RMSE percentage spread for the cases. The cut-off limit for the RMSE percentage is chosen as 5.000%.

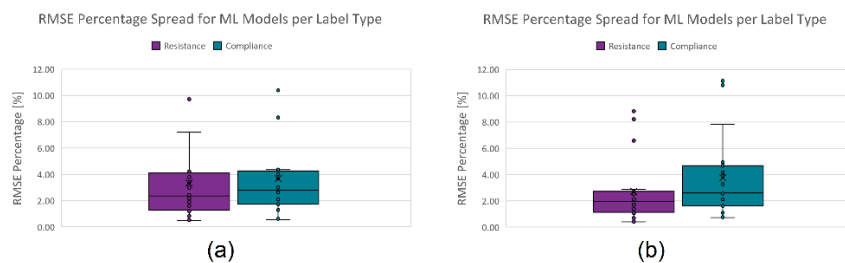


Figure 6-3: Boxplots of the RMSE Percentage for VCC (a) and VCD (b)

- Training Speed

The time it takes to train a model using the specified algorithm. The absolute range is 0.000 to 20.844 days for R_{RS} and 0.000 to 11.015 days for C_S . Figure 6-4 is the boxplots of the training speed spread for the cases. The cut-off limit for the training speed is chosen as 4.000 days. Since training is done infrequently, this performance indicator's scoring weight is decreased ten-fold.



Figure 6-4: Boxplots of the Training Speed for VCC (a) and VCD (b)

- Overfitting Index

An indication of the quality of generalization. It is derived from the validation and test RMSE results. The closer these RMSE results are, the smaller the likelihood that the model is overfitted. The absolute range is 0.012 to 287.940% for R_{RS} and 0.085 to 136.708% for C_S . Figure 6-5 is the boxplots of the overfitting index spread for the cases. The cut-off limit for the overfitting index is chosen as 10.000%.

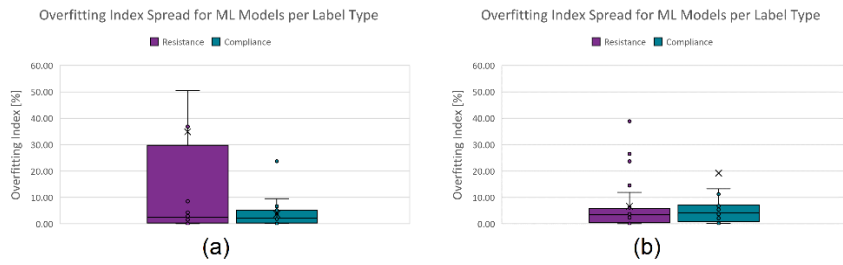


Figure 6-5: Boxplots of the Overfitting Index for VCC (a) and VCD (b)

- Prediction Speed

The number of predictions a model can generate within a certain amount of time, which can greatly affect the deployment cost. The absolute range is 87 to 990 000 obstacles/s (Obs/s) for R_{RS} and 90 to 1 100 000 obstacles/s for C_S . Figure 6-6 is the boxplots of the prediction speed spread for the cases. The cut-off limit for the prediction speed is chosen as 300 000 obstacles/s.

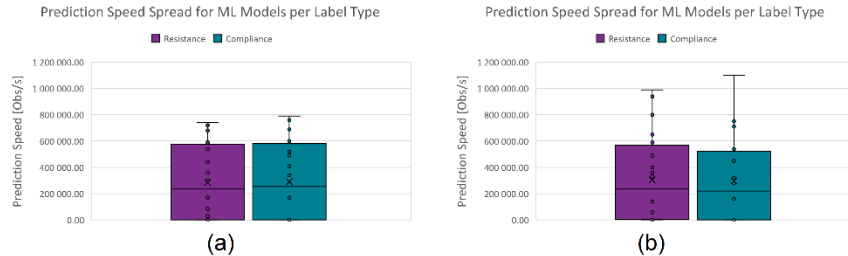


Figure 6-6: Boxplots of the Prediction Speed for VCC (a) and VCD (b)

- Model Size

The storage space or memory needed to host an instance of the model on a machine, which can also greatly affect the deployment cost. The absolute range is 25.036 to 238.944 MB for R_{RS} and 25.135 to 239.063 MB for C_S . Figure 6-7 is the boxplots of the model size spread for the cases. The cut-off limit for the model size is chosen as 55.000 MB.



Figure 6-7: Boxplots of the Model Size for VCC (a) and VCD (b)

6.2.1 Regression Models for Predicting Resistance for VCC

Training the models of the regression algorithm set for predicting R_{RS} for the VCC mode resulted in the below performance summary (Table 6-1).

Table 6-1: Performance Summary of Regression Models for Predicting Resistance for VCC Mode

Algorithm	RMSE Percentage [%]	Training Speed [Days]	Overfitting Index [%]	Prediction Speed [Obs/s]	Size of Model [MB]
Linear	9.721	0.000	0.216	680 000	55.892
Interactions Linear	4.207	0.001	0.049	300 000	238.876
Robust Linear	9.777	0.001	0.215	690 000	62.680
Stepwise Linear	4.207	0.124	0.049	320 000	235.313
Fine Tree	2.996	0.002	2.911	440 000	27.018
Medium Tree	3.054	0.002	3.143	540 000	26.763
Coarse Tree	3.395	0.002	4.262	590 000	25.923
Linear SVM	9.815	0.972	0.260	83 955	66.581
Quadratic SVM	3.788	2.187	0.091	720	48.794
Cubic SVM	1.891	1.289	0.447	30 000	39.505
Fine Gaussian SVM	2.440	0.584	1.838	3 100	40.698
Medium Gaussian SVM	2.186	0.637	1.583	9 200	39.218
Coarse Gaussian SVM	3.473	0.780	2.118	540	45.275
Boosted Trees	7.211	0.786	0.544	170 000	81.728
Bagged Trees	2.300	0.794	4.488	19 000	119.884
Squared Exponential GPR	0.567	6.805	0.737	170	175.975
Matern 5/2 GPR	0.535	2.325	36.848	93	175.524
Exponential GPR	0.492	7.947	8.525	160	176.062
Rational Quadratic GPR	2.260	4.830	287.940	87	175.906
Narrow Neural Network (NNN)	1.198	2.341	106.657	540 000	25.036
Medium Neural Network (MNN)	0.829	2.368	50.546	720 000	25.042
Wide Neural Network (WNN)	1.804	2.466	111.992	360 000	25.061
Bi-Layered Neural Network (BNN)	1.610	2.421	3.742	610 000	25.042
Tri-Layered Neural Network (TNN)	0.530	2.454	208.033	740 000	25.045

Applying the filters and weighted scoring system, Table 6-2 is the resulting ranked shortlist. The bi-layered neural network (BNN) trained the best model for predicting R_{RS} for the VCC mode.

Table 6-2: Resulting Ranked Shortlist of Regression Models for Predicting Resistance for VCC Mode

Algorithm	Attributed Score	Accuracy [%]
Bi-Layered Neural Network (BNN)	26.359	98.390
Medium Tree	25.486	96.946
Fine Tree	24.579	97.004
Coarse Tree	23.575	96.605

Figure 6-8 conveys the response plots for the BNN (a), medium tree (b) and linear SVM (c) algorithms. The linear SVM's results are also inspected as a reference for the worst-performing algorithm. The more distinguishable the horizontal levels, the better the model's performance at that target level. Figure 6-9 is the predicted vs actual plots for the same respective algorithm set. The closer the blue dots are to the black line, the better performance of the model at the target level. Figure 6-10 shows the residual plots for the same models. These boxplots show the statistical spread of the error at each target level. The amount of overlap at the response plot, large deviations from the reference line at the predicted vs actual plot, and the large boxplot ranges at the residual plot for the linear SVM model are all indicators of poor prediction performance. A clear performance difference is discovered using these plots for the two top-performing models. The tree model has a more evident target-level performance bias. This is the case for all tree algorithms since the target level is categorised discretely. This means that the total number of wrong predictions is less, and the size of errors is proportional to the resolution of the target levels, which are relatively large in this case. Thus, no tree algorithms will be considered.

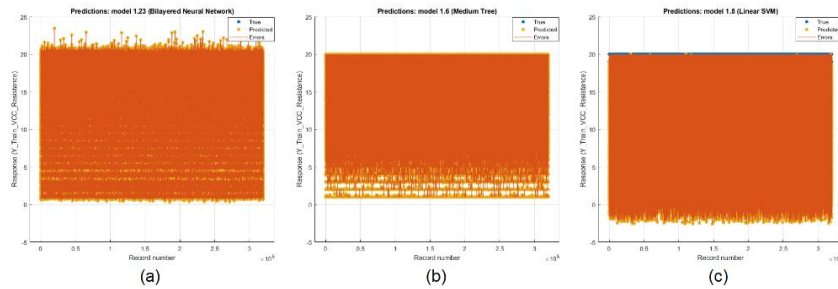


Figure 6-8: Response Plots for Bi-Layered Neural Network (a), Medium Tree (b) and Linear SVM (c)

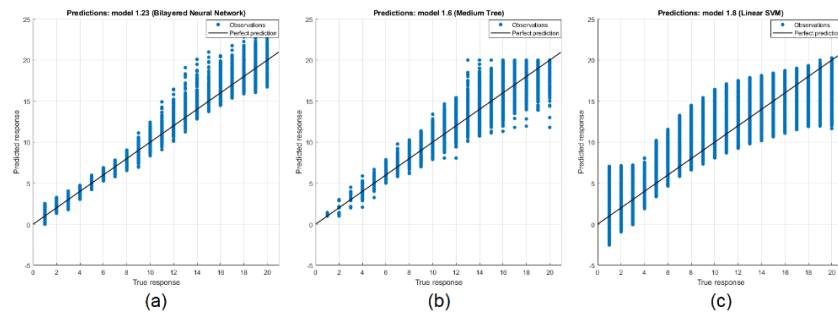


Figure 6-9: Predicted vs Actual Plots for Bi-Layered Neural Network (a), Medium Tree (b) and Linear SVM (c)

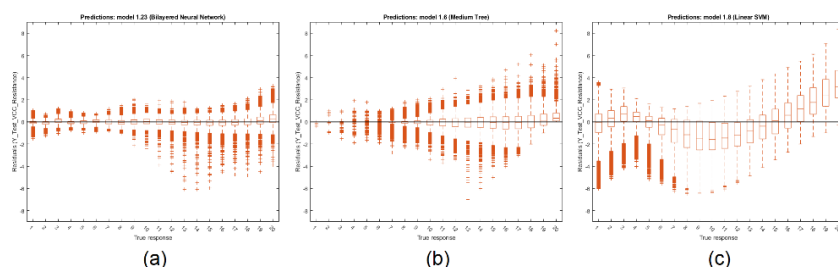


Figure 6-10: Residual Plots for Bi-Layered Neural Network (a), Medium Tree (b) and Linear SVM (c)

6.2.2 Regression Models for Predicting Resistance for VCD

Training the models of the regression algorithm set for predicting R_{RS} for the VCD mode resulted in the below performance summary (Table 6-3).

Table 6-3: Performance Summary of Regression Models for Predicting Resistance for VCD Mode

Algorithm	RMSE Percentage [%]	Training Speed [Days]	Overfitting Index [%]	Prediction Speed [Obs/s]	Size of Model [MB]
Linear	8.219	0.001	0.299	590 000	55.895
Interactions Linear	2.734	0.001	0.181	330 000	238.944
Robust Linear	8.825	0.001	0.375	800 000	62.540
Stepwise Linear	2.734	0.135	0.181	360 000	227.626
Fine Tree	2.501	0.002	2.527	400 000	26.447
Medium Tree	2.540	0.002	3.207	490 000	26.285
Coarse Tree	2.880	0.002	4.165	500 000	25.747
Linear SVM	8.404	1.124	0.376	290	62.923
Quadratic SVM	2.545	1.888	0.012	3 700	42.865
Cubic SVM	1.421	1.202	2.368	59 000	38.702
Fine Gaussian SVM	2.111	0.447	3.785	3 900	40.356
Medium Gaussian SVM	1.710	0.470	3.441	23 000	38.804
Coarse Gaussian SVM	2.325	0.537	3.398	1 500	41.340
Boosted Trees	6.581	0.546	0.068	140 000	81.451
Bagged Trees	1.800	0.554	4.460	20 000	104.682
Squared Exponential GPR	0.427	15.175	38.865	210	176.119
Matern 5/2 GPR	0.569	3.231	23.666	91	172.391
Exponential GPR	0.439	7.968	6.164	130	176.047
Rational Quadratic GPR	0.413	20.844	26.527	110	176.098
Narrow Neural Network (NNN)	1.747	3.242	14.510	990 000	25.042
Medium Neural Network (MNN)	1.076	3.269	11.934	650 000	25.048
Wide Neural Network (WNN)	0.698	3.364	3.746	370 000	25.064
Bi-Layered Neural Network (BNN)	1.390	3.386	0.781	940 000	25.043
Tri-Layered Neural Network (TNN)	1.265	3.418	3.701	660 000	25.047

Table 6-4 shows that the best model for predicting R_{RS} for the VCD mode is the BNN.

Table 6-4: Resulting Ranked Shortlist of Regression Models for Predicting Resistance for VCD Mode

Algorithm	Attributed Score	Accuracy [%]
Bi-Layered Neural Network (BNN)	24.250	98.610
Tri-Layered Neural Network (TNN)	17.118	98.735
Wide Neural Network (WNN)	15.830	99.302
Fine Tree	14.735	97.499
Medium Tree	14.714	97.460
Coarse Tree	13.352	97.120

6.2.3 Regression Models for Predicting Compliance for VCC

Training the models for predicting C_S for the VCC mode resulted in Table 6-5.

Table 6-5: Performance Summary of Regression Models for Predicting Compliance for VCC Mode

Algorithm	RMSE Percentage [%]	Training Speed [Days]	Overfitting Index [%]	Prediction Speed [Obs/s]	Size of Model [MB]
Linear	10.399	0.001	0.165	600 000	55.991
Interactions Linear	4.355	0.001	0.085	340 000	238.975
Robust Linear	10.473	0.001	0.155	700 000	62.779
Stepwise Linear	4.355	0.139	0.085	340 000	235.472
Fine Tree	3.014	0.002	4.651	410 000	27.220
Medium Tree	3.186	0.002	5.171	490 000	26.885
Coarse Tree	3.754	0.002	5.089	520 000	26.092
Linear SVM	10.521	0.868	0.263	200	70.995
Quadratic SVM	3.925	2.225	0.177	570	51.221
Cubic SVM	1.872	1.622	0.270	14 000	39.929
Fine Gaussian SVM	2.111	0.598	2.635	2 600	41.121
Medium Gaussian SVM	1.722	0.653	2.245	5 900	39.629
Coarse Gaussian SVM	3.706	0.846	3.556	390	49.275
Boosted Trees	8.329	0.852	0.995	170 000	82.218
Bagged Trees	2.309	0.860	3.853	19 000	122.450
Squared Exponential GPR	0.649	7.115	6.614	170	176.194
Matern 5/2 GPR	0.627	2.334	1.312	90	174.925
Exponential GPR	0.556	7.828	6.940	150	176.113
Rational Quadratic GPR	0.682	8.700	2.051	110	176.101
Narrow Neural Network (NNN)	4.019	2.347	9.542	780 000	25.135
Medium Neural Network (MNN)	1.963	2.373	1.791	790 000	25.142
Wide Neural Network (WNN)	1.294	2.468	2.024	340 000	25.160
Bi-Layered Neural Network (BNN)	2.629	2.490	23.736	760 000	25.142
Tri-Layered Neural Network (TNN)	1.826	2.522	5.795	690 000	25.145

Table 6-6 shows that the best model for predicting C_S for the VCC mode is the MNN.

Table 6-6: Resulting Ranked Shortlist of Regression Models for Predicting Compliance for VCC Mode

Algorithm	Attributed Score	Accuracy [%]
Medium Neural Network (MNN)	19.590	98.037
Wide Neural Network (WNN)	15.827	98.706
Tri-Layered Neural Network (TNN)	15.028	98.174
Medium Tree	13.064	96.814
Fine Tree	12.910	96.986
Coarse Tree	12.773	96.246
Narrow Neural Network (NNN)	10.808	95.981

6.2.4 Regression Models for Predicting Compliance for VCD

Training the models for predicting C_S for the VCD mode resulted in Table 6-7.

Table 6-7: Performance Summary of Regression Models for Predicting Compliance for VCD Mode

Algorithm	RMSE Percentage [%]	Training Speed [Days]	Overfitting Index [%]	Prediction Speed [Obs/s]	Size of Model [MB]
Linear	10.813	0.000	0.159	470 000	55.994
Interactions Linear	4.682	0.001	0.740	280 000	239.044
Robust Linear	11.166	0.001	0.162	710 000	62.758
Stepwise Linear	4.682	0.121	0.740	320 000	239.063
Fine Tree	2.553	0.002	4.779	450 000	26.730
Medium Tree	2.717	0.002	5.682	470 000	26.534
Coarse Tree	3.267	0.002	7.268	540 000	25.984
Linear SVM	11.140	1.038	0.111	200	70.564
Quadratic SVM	4.944	2.180	2.111	820	47.984
Cubic SVM	2.636	1.898	11.233	8 200	40.853
Fine Gaussian SVM	2.118	0.514	2.698	2 800	40.941
Medium Gaussian SVM	1.838	0.573	2.451	5 800	39.728
Coarse Gaussian SVM	4.167	0.777	3.657	400	48.039
Boosted Trees	7.828	0.785	0.245	160 000	82.042
Bagged Trees	1.855	0.793	6.104	19 000	109.586
Squared Exponential GPR	0.766	9.612	129.476	180	176.084
Matern 5/2 GPR	0.847	2.317	5.750	90	173.816
Exponential GPR	0.728	7.638	6.708	130	176.006
Rational Quadratic GPR	0.806	11.015	114.100	110	176.011
Narrow Neural Network (NNN)	2.297	2.331	0.323	1 100 000	25.142
Medium Neural Network (MNN)	1.615	2.358	5.374	750 000	25.147
Wide Neural Network (WNN)	1.105	2.454	0.957	330 000	25.164
Bi-Layered Neural Network (BNN)	1.686	2.477	13.305	770 000	25.143
Tri-Layered Neural Network (TNN)	3.883	2.511	136.708	730 000	25.146

Table 6-8 shows that the best model for predicting C_S for the VCD mode is the NNN.

Table 6-8: Resulting Ranked Shortlist of Regression Models for Predicting Compliance for VCD Mode

Algorithm	Attributed Score	Accuracy [%]
Narrow Neural Network (NNN)	23.804	97.703
Wide Neural Network (WNN)	18.702	98.895
Medium Neural Network (MNN)	16.707	98.385
Fine Tree	14.492	97.447
Medium Tree	13.766	97.283
Coarse Tree	12.529	96.733

6.2.5 Discussion of the Chosen Models

Table 6-9 summarises the performances of the chosen regression models for the four use cases. All four models have accuracies of 97.703% or higher. The combination of small model sizes (around 25 MB) with the fast prediction speeds (each model running on a single Intel® Core™ i7-6700HQ CPU core @ 2.60 GHz) means computing resource requirements for scaling these models to monitor multiple patients simultaneously are low. For example, assuming a machine uses a core with similar performance, predicting the resistance for a breath that has already been analysed for its feature values could theoretically be achieved with speeds of 610 000 breaths per second. Since the duration of a fully cycled breath could reasonably average above 3 seconds, this means that said single core could monitor 1.83 M patients simultaneously.

Table 6-9: Performance Summary of the Chosen Regression Models

Use Case	Algorithm	RMSE Percentage [%]	Training Speed [Days]	Overfitting Index [%]	Prediction Speed [Obs/s]	Size of Model [MB]
R VCC	Bi-Layered Neural Network	1.610	2.421	3.742	610 000	25.042
R VCD	Bi-Layered Neural Network	1.390	3.386	0.781	940 000	25.043
C VCC	Medium Neural Network	1.963	2.373	1.791	790 000	25.142
C VCD	Narrow Neural Network	2.297	2.331	0.323	1 100 000	25.142

Figure 6-11 exhibits the residual plots for predicting resistance for VCC (a) and VCD (b), and Figure 6-12 for predicting compliance. All models show acceptable target-level accuracy bias.

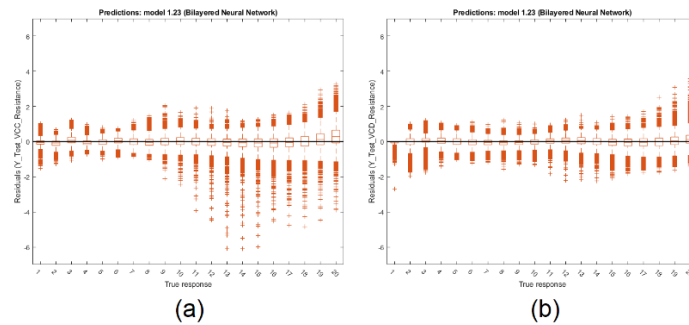


Figure 6-11: Residual Plots for Predicting the Resistance for VCC (a) and VCD (b)

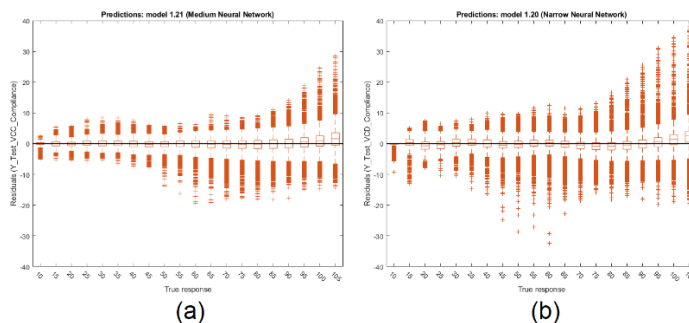


Figure 6-12: Residual Plots for Predicting the Compliance for VCC (a) and VCD (b)

6.3 Deploying the Regression Models

The chosen regression models per use case are deployed and executed on typical mechanical ventilator sessions to validate the project's results. In each case, the session consisted of twenty simulated breaths, either with varying resistance or compliance according to the use case. The patient identity chosen is a 25-year-old male 186 cm in height. The baseline pressure was kept at 5 cmH₂O, tidal volume at 540 mL and the maximum inspiratory flow at 60 L/min for both modes. When validating the varying resistance use cases, C_S is kept at 55 mL/cmH₂O and R_{RS} is linearly swept from 1 to 20 cmH₂O·s/L for the 20 breaths (Figure 6-13 (a) for VCC and (b) for VCD). For the varying compliance use cases, R_{RS} is kept at 4 cmH₂O·s/L, and C_S is linearly swept from 10 to 105 mL/cmH₂O for the 20 breaths (Figure 6-14 (a) for VCC and (b) for VCD).

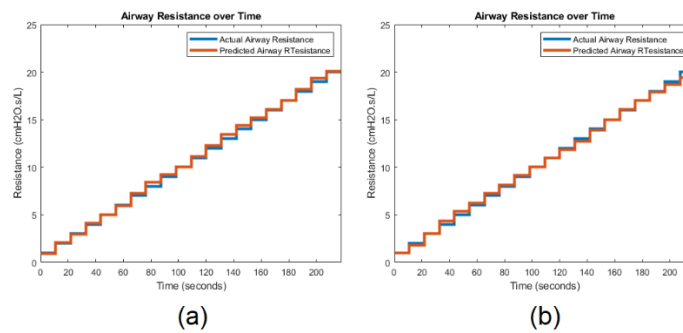


Figure 6-13: Predicted vs Actual Resistance Results for VCC (a) and VCD (b)

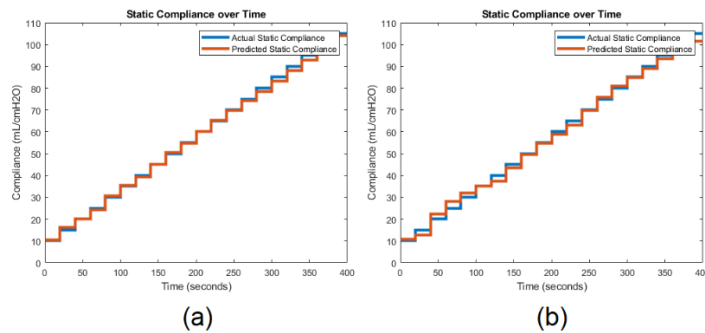


Figure 6-14: Predicted vs Actual Compliance Results for VCC (a) and VCD (b)

Table 6-10 summarises the average RMSE percentages for all four use cases. The local RMSE percentage is calculated with reference to the individual local target values, and the total RMSE percentage, with reference to the total range of the target values. All four simulated use cases produced accuracies (with reference to the total range of the target values) of over 98.22%.

Table 6-10: Local and Total Root Mean Square Error Percentages per Use Case

Use Case	Mean Local RMSE Percentage [%]	Mean Total RMSE Percentage [%]
R VCC	3.10	1.05
R VCD	3.44	1.24
C VCC	2.47	1.01
C VCD	6.04	1.78

6.4 Chapter Summary

This chapter focussed on training machine learning models to predict the patient's respiratory mechanical parameters (airway resistance and static compliance) using the prepared mechanical ventilated breath database of labelled-feature vector pairs.

A regression algorithm set of some of the most popular machine learning algorithms was comprised to create the models. This algorithm set included linear regression algorithms (normal, interactions, robust, and stepwise linear regression), decision tree algorithms (fine, medium, and coarse trees), support vector machine algorithms (linear, quadratic, cubic, fine Gaussian, medium Gaussian, and coarse Gaussian SVM), gaussian process regression algorithms (exponential, squared exponential, Matern 5/2, and rational quadratic GPR), ensemble algorithms (boosted, and bagged trees), and neural networks (narrow, medium, wide, bi-layered, and tri-layered neural network). The regression algorithm set (24 algorithms) was used to train models for four use cases. These four use cases were to separately predict the airway resistance and static compliance for the volume-controlled modes.

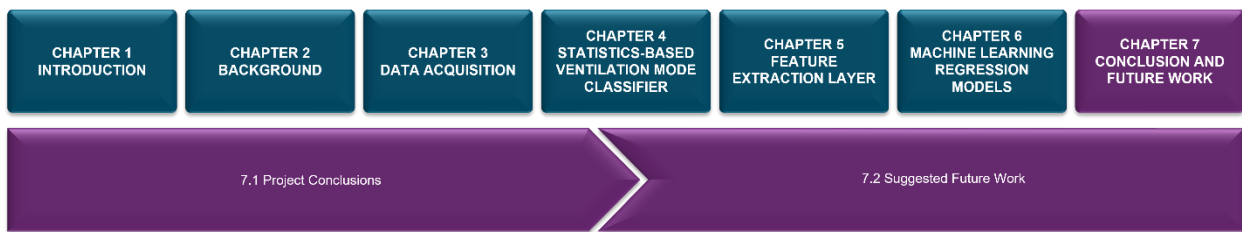
After training all the models (96 models), they were evaluated using five performance parameters to determine which of the 24 models per use case were the best overall models. These five performance parameters were the root mean squared error percentage (no more than 5.00%), training speed (no more than four days), overfitting index (no more than 10.00% deviation), prediction speed (no less than 300 000 obstacles per second), and model size (no more than 55.00 MB). The models that met this criterion were ranked using a scoring system that utilised a ten-fold lesser weight for the once-off training speed performance parameter. The top-ranked models were chosen per use case and are summarised in Table 6-11.

Table 6-11: Performance Summary of the Chosen Regression Models

Use Case	Algorithm	RMSE Percentage [%]	Training Speed [Days]	Overfitting Index [%]	Prediction Speed [Obs/s]	Size of Model [MB]
R VCC	Bi-Layered Neural Network	1.610	2.421	3.742	610 000	25.042
R VCD	Bi-Layered Neural Network	1.390	3.386	0.781	940 000	25.043
C VCC	Medium Neural Network	1.963	2.373	1.791	790 000	25.142
C VCD	Narrow Neural Network	2.297	2.331	0.323	1 100 000	25.142

Finally, these models were deployed by simulating the use cases for a 25-year-old male 186 cm in height, P_0 set at 5 cmH₂O, V_T set at 540 mL, Q_{max} set at 60 L/min, R_{RS} set at 4 cmH₂O·s/L (for variable C_S), and C_S set at 55 mL/cmH₂O (for variable R_{RS}). R_{RS} and C_S were varied from 1 to 20 cmH₂O·s/L and 10 to 105 mL/cmH₂O, respectively. All four simulated use cases produced accuracies (with reference to the total range of the target values) of over 98.22%.

CHAPTER 7 – CONCLUSION AND FUTURE WORK



This chapter summarises the project's conclusions and discusses some ideas for future work.

7.1 Project Conclusions

This project consisted of six main parts, each with its conclusions. In this section, all these conclusions are conveyed and discussed. As a reminder, Chapter 1 is the introductory chapter, Chapter 2 is the background literature, Chapter 3 is about the data acquisition process, Chapter 4 discusses how the statistics-based ventilation mode classifier was developed, Chapter 5 explains the feature extraction layer, and Chapter 6 conveys how the machine learning regression models were trained and evaluated.

7.1.1 Introduction

This chapter concluded that a need persisted in helping pulmonologists manage mechanical ventilation resources more efficiently by automatically and continuously monitoring and logging a patient's respiratory health with ventilation data. The chapter also concluded that delimitations had to be placed on the patient's identity and state and the mechanical ventilation use cases. The patient was chosen to be a 25-year-old male, 186 cm in tall, sedated, intubated, and supine. At most, the ventilation use cases were limited to three ventilation modes. Finally, a delimited methodology was proposed, which is conveyed by the diagram in Figure 7-1

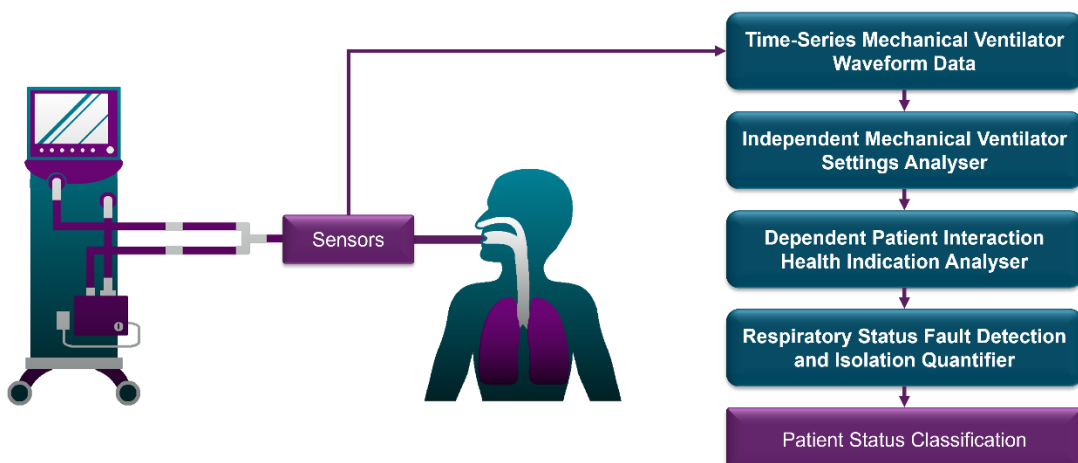


Figure 7-1: Flow Diagram of the Delimited Project Overview

7.1.2 Background

The spontaneous breathing patient uses their abdomen and thoracic muscles to increase the capacity of the lungs, a pressure drop inside the lungs occurs, and equilibrium with the atmospheric pressure is achieved through Boyle's law. Mechanical ventilators leverage the same law to perform mechanical ventilation by applying a positive pressure differential to the patient.

A respiratory system model survey was performed, and the single-compartment RC model proved to have sufficient representative complexity for the project; assuming the patient is sedated, an ETT is used, sub 30 breaths per minute respiratory rates are applied, and airway resistance and static compliance scalar values are sufficient respiratory system health indicators (as in practice).

The standard monitoring outputs used by pulmonologists to examine the patient's health status (the three waveform scalars and the two hysteresis loops) were determined. The waveform scalars comprise the proximal airway pressure (cmH_2O), flow rate (L/min) and volume (mL) over time. The hysteresis loops comprise the pressure-volume and flow-volume loops.

Another survey on the techniques and modes of mechanical ventilation indicated that the three ventilation modes chosen for this project should be the volume-controlled modes (continuous flow (VCC) and decelerating flow (VCD), and the pressure-controlled (PC) mode.

A heuristics survey concluded that the patient's sex, age, and height are used to derive the trachea length and diameter, dead space, functional residual capacity, recommended ETT size, and recommended initial ventilator settings, fully constraining the mechanical ventilator-patient system. To constrain the ventilation mode protocols, the pulmonologist must provide the settings for the respiratory rate, baseline pressure, tidal volume and maximum inspiratory flow for the volume-controlled modes, and peak inspiratory pressure and inspiratory time for the PC mode.

The standard analysing techniques for determining the patient's respiratory status using the standard monitoring outputs were identified. Analysing the outputs without utilising the invasive end-inspiratory hold manoeuvre (needing ethical approval and hardware development) meant that the respiratory mechanical parameters (airway resistance and static compliance) are approximated with the inspiratory resistance and dynamic compliance. These approximations can deviate significantly from the actual respiratory parameters. Therefore, nuance methods are needed that quantify the qualitative changes (due to the varying respiratory state) into features.

Finally, it was concluded that utilising these extracted features from the ventilation data to automatically classify the patient's status would require a regression solution. Therefore, a set of 24 popular regression algorithms was identified for machine learning later.

7.1.3 Data Acquisition

A dataset survey was done to identify existing empirical datasets. However, the datasets did not meet the fidelity requirements, or access for studies by a student was denied. Creating an empirical dataset (real or synthetical) would have consumed too much time, would not have had a satisfactory fidelity resolution, and either require access to patients (ethical approval) or to an appropriate mechanical ventilator (which was unattainable at the time). Therefore, it was concluded that a synthetic dataset would have to be generated and verified using model-based techniques to grant full fidelity, unlimited use cases, and fast recording of clean data.

An existing MATLAB® Simulink® model was drafted and modified to meet the fidelity and representative complexity appropriate for this project. These were to capture and apply the patient's biological identity (i.e., age, sex, and height) and anthropometric data (trachea dimensions, *FRC*, dead space, and appropriate ETT size) to the model. The model was modified to incorporate an ETT as the patient-interface component, variable baseline pressure valve, variable patient mechanical parameters, the variable intensity of a kink in the tubes, a means of performing the end-inspiratory hold manoeuvre, and input options for selecting the ventilation mode (VCC, VCD and PC) and their corresponding parameter settings (respiratory rate, baseline pressure, maximum inspiratory flow, tidal volume, peak inspiratory pressure and inspiratory time).

After that, the mechanical ventilator-patient (MV-P) model was verified qualitatively and quantitatively, and its sensitivity was inspected. The model was qualitatively verified by analysing the pressure component behaviours and the effects of varying the mechanical parameters, and by comparing the shapes of the simulated waveform scalars to actual examples. The model was quantitatively verified by varying the parameters and analysing the results for appropriate outputs. The model's sensitivity was inspected by sweeping the parameters of the components and by comparing deviations when omitting components during certain use cases. The ETT proved to be the only point of significant sensitivity due to turbulent flow, as is the practice case.

After the MATLAB® Simulink® MV-P model was developed and verified, some assumptions were made to scope the theoretically unlimited dataset for the project whilst representing an extensive patient identity set. The assumptions concluded that the generatable dataset for a single MV-P setup could only represent the patient identities deemed appropriate for interfacing with the chosen ETT. Since a 25-year-old male (186 cm in length) was chosen as the identity to be simulated, it resulted in an 8.0 mm inside diameter ETT. The represented patient identity set expanded by sweeping R_{RS} and C_S over extensive ranges, including any patient deemed appropriate to interface with said ETT. Section 3.2.2 implies any man or woman over 16.

The typical ranges of the parameters for the specified patient identity set were determined:

- Baseline Pressure (P_0) – Swept from 0 to 15 cmH₂O (4 levels linearly spaced).
- Tidal Volume (V_T) – Swept from 180 to 750 mL (20 levels linearly spaced).
- Maximum Inspiratory Flow (Q_{max}) – Swept from 10 to 105 L/min (20 levels linearly spaced).
- Peak Inspiratory Pressure (P_{PIP}) – Swept from $P_0 + 5$ to 35 cmH₂O (20 levels linearly spaced).
- Inspiratory Time (T_i) – Swept from 0.5 to 2.4 seconds (20 levels linearly spaced).
- Airway Resistance (R_{RS}) – Swept from 1 to 20 cmH₂O·s/L (20 levels linearly spaced).
- Static Compliance (C_S) – Swept from 10 to 105 mL/cmH₂O (20 levels linearly spaced).

The MV data generator application was adapted to support the parameter sweep functionality, and the model was optimised to generate the required labelled MV dataset (1.92 M breaths). Initially, the average time to simulate, process and store the results was 8.55 seconds per breath (190 days). A few improved application iterations followed, incorporating parallel computing techniques, and storing the data more efficiently into the database by uploading CSV files of about ten million records at a time. This decreased the time per breath to 3.35 seconds (74.44 days).

No access was granted to use the NWU's clusters or to rent other online clusters. Instead, 60 machines housed in one of the NWU's vacant computer laboratories were used for data generation. Generating the 1.92 M breaths took about two days and delivered 168 GB of data (66.7 GB after trimming). Data type conversion by the database reduced the storage to 49 GB. The session settings table was 16 MB, and the extracted MV setting features table was 152 MB.

7.1.4 Statistics-Based Ventilation Mode Classifier

Figure 7-1 lists the development of the independent MV settings analyser as the next step. The first MV setting to determine was the ventilation mode (VCC, VCD or PC). To do so, a statistics-based ventilation mode classifier was developed leveraging standard deviation and coefficient of determination parameters of a smaller dataset (30 000 breaths). The dataset was chosen to have similar parameter ranges but lower resolution. The proposed solution was a hybrid classifier using hard decision boundaries and Kernel probability distribution functions to translate the statistical parameters into ventilation mode probability scores with classification accuracies of 100.00% for VCC, 98.67% for VCD, and 98.86% for PC. The proposed hybrid classifier was evaluated by testing the total dataset of 1.92 M breaths, which resulted in classification accuracies of 99.87% for VCC, 98.75% for VCD, and 98.71% for PC. The overall accuracy is 99.11%, which shows that the proposed hybrid classifier generalises well.

7.1.5 Feature Extraction Layer

The feature extraction layer was developed to determine the ventilator's settings by analysing the waveform data (independent features) and to extract informative features that are indicators of the patient's health status from the waveform data and hysteresis loops (dependent features).

The independent features were extracted with accuracies of 99.11% for the ventilation mode (from the ventilation mode classifier), 98.53% for P_0 , 92.43% for Q_{max} , 93.60% for V_T , 98.47% for P_{PIP} , and 99.15% for T_i . The inaccuracy of Q_{max} is due to the flow-lagging effect of the simulated mechanical valves in the MV-P model, as in the practice case. Also, V_T is dependent on Q_{max} , which explains its relative inaccuracy.

Feature engineering produced six features that quantify qualitative changes in the waveform scalars and hysteresis loops as the respiratory mechanical parameters of the patient vary. These features were extracted from the expiratory phase of the breathing cycle, as this phase is passive and independent of the ventilation mode. The time constant of the volume waveform was extracted, followed by the corresponding flow at that timestamp. The remaining four features were extracted from the flow-volume loop and describe the shape of its renowned scoop curve. These are the scoop's gradient, surface ratio, skewness, and kurtosis features.

Finally, a database was developed to store all the relevant project data (generated and extracted).

7.1.6 Machine Learning Regression Models

Figure 7-1 lists that the project's final step was to develop the respiratory status fault detection and isolation quantifier. This was achieved through training and evaluating machine learning regression models on labelled-feature vector pairs stored in the database. A regression algorithm set (24 algorithms) was used to train models for four use cases; to predict the airway resistance and static compliance for the volume-controlled modes separately. After training all the models (96 models), they were evaluated and ranked using five performance parameters; RMSE percentage, training speed, overfitting index, prediction speed and size of the model. Table 7-1 summarises the results of the top-performing models per use case.

Table 7-1: Performance Summary of the Chosen Regression Models

Use Case	Algorithm	RMSE Percentage [%]	Training Speed [Days]	Overfitting Index [%]	Prediction Speed [Obs/s]	Size of Model [MB]
R VCC	Bi-Layered Neural Network	1.610	2.421	3.742	610 000	25.042
R VCD	Bi-Layered Neural Network	1.390	3.386	0.781	940 000	25.043
C VCC	Medium Neural Network	1.963	2.373	1.791	790 000	25.142
C VCD	Narrow Neural Network	2.297	2.331	0.323	1 100 000	25.142

Finally, these models were deployed by simulating the use cases for a 25-year-old male 186 cm in height, P_0 set at 5 cmH₂O, V_T set at 540 mL, Q_{max} set at 60 L/min, R_{RS} set at 4 cmH₂O·s/L (for variable C_S), and C_S set at 55 mL/cmH₂O (for variable R_{RS}). R_{RS} and C_S were varied from 1 to 20 cmH₂O·s/L and 10 to 105 mL/cmH₂O, respectively. All four simulated use cases produced accuracies (with reference to the total range of the target values) of over 98.22%.

7.1.7 Project Final Result

Figure 7-2 summarises the proposed method behind the delivered solution to this project's problem. Assuming access to filtered time-series waveform data, a ventilation mode classifier predicts the executed ventilation mode (99.11% accuracy). The result is used together with the time-series data to extract independent (MV settings) and dependent features (patient health status indicators) using the mode-specific feature extraction layer. The unlabelled feature vector pair (per breath) is used as input for the corresponding ventilation mode's regression models, which predict the patient's airway resistance and static compliance (over 98.22% accurate). The pulmonologist can then periodically inspect the per-breath logged patient status parameters. Therefore, the primary and first-secondary objective have been accomplished. However, insufficient time rendered the second of the latter as incomplete.

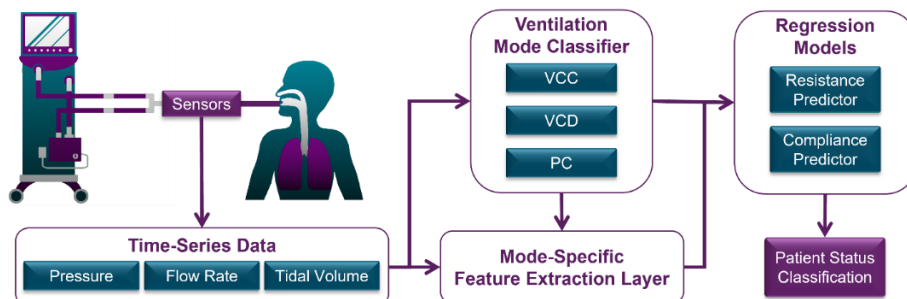


Figure 7-2: Project Final Result Diagram

7.2 Suggested Future Work

Possible future work in the mechanical ventilation health monitoring domain is listed below.

- Develop machine learning (ML) models to predict mechanical parameters for PC mode.
- Optimise and cascade the ML models by using one's output as the next one's extra input.
- Expand the ML models to use patient anthropometric data to include other MV-P setups.
- Use the predicted mechanical parameters to classify the patient's state as ARDS or COPD.
- Develop a fault detection and isolation (*FDI*) system for complications of an active patient.
- Develop an *FDI* system for complications on the MV circuit.
- Develop an automated logging system on an active patient's weaning progress.
- Develop an *FDI* system that recommends optimal adjustment values for the MV settings.
- Develop a sensor device for intercepting the waveform data from existing MVs.
- Develop a scaled version of the project solution with a dashboard for patient prioritisation.

BIBLIOGRAPHY

- [1] M. A. Warner and B. Patel, 'Mechanical ventilation', *Benumof Hagbergs Airw. Manag.*, pp. 981–997, 2013.
- [2] C. F. Haas, R. M. Eakin, M. A. Konkle, and R. Blank, 'Endotracheal Tubes: Old and New', *Respir. Care*, vol. 59, no. 6, pp. 933–955, 2014.
- [3] 'The top 10 causes of death'. <https://www.who.int/news-room/fact-sheets/detail/the-top-10-causes-of-death> (accessed Feb. 22, 2023).
- [4] L. Yu *et al.*, 'Machine learning methods to predict mechanical ventilation and mortality in patients with COVID-19', *PLoS One*, vol. 16, no. 4, p. e0249285, 2021.
- [5] G. Tintinger and A. Engelbrecht, 'Mechanical ventilation in the emergency department', *CME Your SA J. CPD*, vol. 25, no. 3, pp. 118–122, 2007.
- [6] J.-M. Arnal, *Monitoring mechanical ventilation using ventilator waveforms*. Springer, 2018.
- [7] A. R. Carvalho and W. A. Zin, 'Respiratory system dynamical mechanical properties: modeling in time and frequency domain', *Biophys. Rev.*, vol. 3, no. 2, pp. 71–84, 2011.
- [8] G. B. Rehm *et al.*, 'Use of Machine Learning to Screen for Acute Respiratory Distress Syndrome Using Raw Ventilator Waveform Data', *Crit. Care Explor.*, vol. 3, no. 1, 2021.
- [9] E. Emrath, 'The basics of ventilator waveforms', *Curr. Pediatr. Rep.*, vol. 9, no. 1, pp. 11–19, 2021.
- [10] S. R. Wilcox, A. Aydin, and E. G. Marcolini, *Mechanical ventilation in emergency medicine*. Springer, 2021.
- [11] S. Chapman, G. Robinson, J. Stradling, S. West, and J. Wrightson, *Oxford handbook of respiratory medicine*. OUP Oxford, 2014.
- [12] A. A. of Pediatrics, *Pediatric clinical practice guidelines & policies: A compendium of evidence-based research for pediatric practice*. Amer Academy of Pediatrics, 2009.
- [13] J. M. Cairo and others, *Pilbeam's mechanical ventilation: physiological and clinical applications*. Elsevier Health Sciences, 2015.
- [14] P. C. Rimensberger, S. Schulzke, D. Tingay, and B. Von Ungern-Sternberg, 'Pediatric and neonatal mechanical ventilation', *Geneve Springer*, 2015.
- [15] 'Chronic respiratory disease burden - PAHO/WHO | Pan American Health Organization'. <https://www.paho.org/en/enlace/chronic-respiratory-disease-burden> (accessed Feb. 22, 2023).
- [16] 'Average Age by Country 2023'. <https://worldpopulationreview.com/country-rankings/median-age> (accessed Feb. 22, 2023).
- [17] J. Desjardins, 'Mapped: The Median Age of the Population on Every Continent', *Visual Capitalist*, Feb. 15, 2019. <https://www.visualcapitalist.com/mapped-the-median-age-of-every-continent/> (accessed Feb. 22, 2023).
- [18] M. Roser, C. Appel, and H. Ritchie, 'Human Height', *Our World Data*, Oct. 2013, Accessed: Feb. 22, 2023. [Online]. Available: <https://ourworldindata.org/human-height>
- [19] B. Gholami *et al.*, 'Replicating human expertise of mechanical ventilation waveform analysis in detecting patient-ventilator cycling asynchrony using machine learning', *Comput. Biol. Med.*, vol. 97, pp. 137–144, 2018.
- [20] M. J. Tobin, *Principles and practice of mechanical ventilation*. McGraw-Hill Medical, New York, 2013.
- [21] H. Poor, *Basics of mechanical ventilation*. Springer, 2018.
- [22] R. L. Chatburn, *Fundamentals of mechanical ventilation: a short course in the theory and application of mechanical ventilators*. Mandu Press, 2003.
- [23] 'Aerobic Respiration and Anaerobic Respiration - Pass My Exams: Easy exam revision notes for GSCE Biology'. <http://passmyexams.co.uk/GCSE/biology/aerobic-and-anaerobic-respiration.html> (accessed Feb. 22, 2023).
- [24] J. Dunn and M. H. Grider, 'Physiology, Adenosine Triphosphate', in *StatPearls*, Treasure Island (FL): StatPearls Publishing, 2022. Accessed: Feb. 22, 2023. [Online]. Available: <http://www.ncbi.nlm.nih.gov/books/NBK553175/>

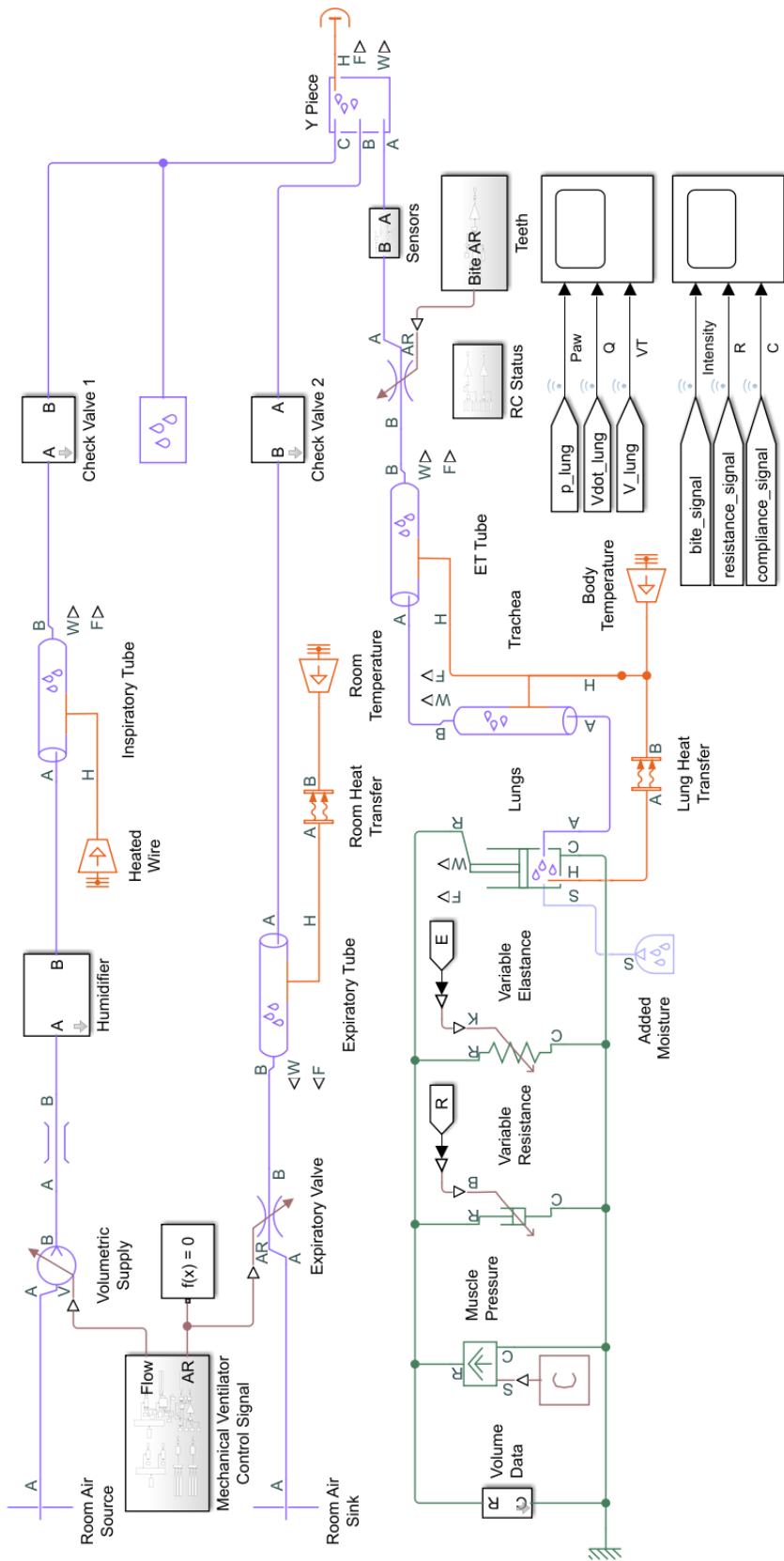
- [25]N. J. Langford, 'Carbon dioxide poisoning', *Toxicol. Rev.*, vol. 24, no. 4, pp. 229–235, 2005, doi: 10.2165/00139709-200524040-00003.
- [26]R. L. Chatburn, 'Understanding mechanical ventilators', *Expert Rev. Respir. Med.*, vol. 4, no. 6, pp. 809–819, 2010.
- [27]J. B. West, *Respiratory physiology: the essentials*. Lippincott Williams & Wilkins, 2012.
- [28]M. Chu *et al.*, 'Respiration rate and volume measurements using wearable strain sensors', *NPJ Digit. Med.*, vol. 2, no. 1, pp. 1–9, 2019.
- [29]J. Landry, BS, and RRT, 'Respiratory Therapy: Formulas, Calculations, and Equations', *Respiratory Therapy Zone*, Dec. 17, 2022.
<https://www.respiratorytherapyzone.com/respiratory-therapy-formulas-calculations/> (accessed Jan. 25, 2023).
- [30]D. Shuttleworth and N. Dodds, 'Ventilators and Breathing Systems', *Maths Phys. Clin. Meas. Anaesth. Intensive Care*, p. 130, 2019.
- [31]P. Ghafarian, H. Jamaati, and S. M. Hashemian, 'A review on human respiratory modeling', *Tanaffos*, vol. 15, no. 2, p. 61, 2016.
- [32]R. Pasteka, J. P. Santos da Costa, N. Barros, R. Kolar, and M. Forjan, 'Patient–Ventilator Interaction Testing Using the Electromechanical Lung Simulator xPULM™ during V/AC and PSV Ventilation Mode', *Appl. Sci.*, vol. 11, no. 9, p. 3745, 2021.
- [33]J. W. Nilsson and S. A. Riedel, *Electric circuits*, 10. ed., Global ed. Boston, Mass.: Pearson, 2015.
- [34]M. Nagarjuna, 'Ventilator waveform analysis [published online July 19, 2016]'. 2016.
- [35]J. Pillow, G. L. HALL, K. E. WILLET, A. H. JOBE, Z. Hantos, and P. Sly, 'Effects of Gestation and Antenatal Steroid on Airway and Tissue Mechanics in Newborn Lambs', *Am. J. Respir. Crit. Care Med.*, vol. 163, pp. 1158–63, May 2001, doi: 10.1164/ajrccm.163.5.9906098.
- [36]A. Rafanan, 'Ventilator waveforms: interpretation [published online August 12, 2014]'. 2016.
- [37]G. T. W. DNAP and D. Scot Pettey, 'Optimizing Mechanical Ventilation During General Anesthesia', *AANA J.*, vol. 88, no. 2, pp. 149–157, 2020.
- [38]M. Meyers, N. Rodrigues, and A. Ari, 'High-frequency oscillatory ventilation: A narrative review', *Can. J. Respir. Ther. CJRT Rev. Can. Thérapie Respir. RCTR*, vol. 55, pp. 40–46, May 2019, doi: 10.29390/cjrt-2019-004.
- [39]'Sedation & Respiratory Depression', *Department of Pediatrics*.
<https://www.pediatrics.wisc.edu/education/sedation-program/sedation-education/sedation-respiratory-depression/> (accessed Feb. 22, 2023).
- [40]P. Szmuk, T. Ezri, S. Evron, Y. Roth, and J. Katz, 'A brief history of tracheostomy and tracheal intubation, from the Bronze Age to the Space Age', *Intensive Care Med.*, vol. 34, no. 2, pp. 222–228, 2008.
- [41]J. S. Sandoz, C. LeBlanc, and D. A. McKim, 'Data downloads for effective noninvasive ventilation in patients with neuromuscular respiratory failure', *Respir. Care*, vol. 59, no. 3, pp. e35–e40, 2014.
- [42]C. D. Smallwood, 'Monitoring big data during mechanical ventilation in the ICU', *Respir. Care*, vol. 65, no. 6, pp. 894–910, 2020.
- [43]R. L. Chatburn, M. El-Khatib, and E. Mireles-Cabodevila, 'A taxonomy for mechanical ventilation: 10 fundamental maxims', *Respir. Care*, vol. 59, no. 11, pp. 1747–1763, 2014.
- [44]R. L. Chatburn and E. Mireles-Cabodevila, 'Closed-loop control of mechanical ventilation: description and classification of targeting schemes', *Respir. Care*, vol. 56, no. 1, pp. 85–102, 2011.
- [45]M. Ghmloush and N. S. Hill, 'Synchronized intermittent mandatory ventilation: time to send this workhorse out to pasture', *Respiratory Care*, vol. 58, no. 11. Respiratory Care, pp. 1992–1994, 2013.
- [46]M. A. Gentile, 'Cycling of the mechanical ventilator breath', *Respir. Care*, vol. 56, no. 1, pp. 52–60, 2011.
- [47]R. S. Campbell and B. R. Davis, 'Pressure-controlled versus volume-controlled ventilation: does it matter?', *Respir. Care*, vol. 47, no. 4, pp. 416–426, 2002.

- [48]N. Rittayamai, C. M. Katsios, F. Beloncle, J. O. Friedrich, J. Mancebo, and L. Brochard, 'Pressure-controlled vs volume-controlled ventilation in acute respiratory failure: a physiology-based narrative and systematic review', *Chest*, vol. 148, no. 2, pp. 340–355, 2015.
- [49]A. Esteban *et al.*, 'A comparison of four methods of weaning patients from mechanical ventilation', *N. Engl. J. Med.*, vol. 332, no. 6, pp. 345–350, 1995.
- [50]C. E. Mathews and R. Unnikrishnan, 'Comparison of Synchronised Intermittent Mandatory Ventilation with Pressure Support versus Assist Control mode of ventilation on time to extubation', *Indian J. Respir. Care*, vol. 6, no. 1, p. 781, 2017.
- [51]A. Abujaber, A. Fadlalla, D. Gammo, H. Abdelrahman, M. Mollazehi, and A. El-Menyar, 'Using trauma registry data to predict prolonged mechanical ventilation in patients with traumatic brain injury: Machine learning approach', *PLoS One*, vol. 15, no. 7, p. e0235231, 2020.
- [52]W. Mi *et al.*, 'Measurement and Analysis of the Tracheobronchial Tree in Chinese Population Using Computed Tomography', *PLOS ONE*, vol. 10, p. e0123177, Apr. 2015, doi: 10.1371/journal.pone.0123177.
- [53]B. E, A. Gc, and F. Rg, 'Dimensions of the normal human trachea', *AJR Am. J. Roentgenol.*, vol. 142, no. 5, May 1984, doi: 10.2214/ajr.142.5.903.
- [54]P. B. Dominelli *et al.*, 'Sex differences in large conducting airway anatomy', *J. Appl. Physiol.*, vol. 125, no. 3, pp. 960–965, Sep. 2018, doi: 10.1152/japplphysiol.00440.2018.
- [55]'Average height for men and women worldwide', *Worlddata.info*.
<https://www.worlddata.info/average-bodyheight.php> (accessed Feb. 22, 2023).
- [56]'Growth Charts - Data Table of Infant Length-for-age Charts', Jan. 11, 2019.
https://www.cdc.gov/growthcharts/html_charts/lenageinf.htm (accessed Feb. 22, 2023).
- [57]'Medical Ventilator with Lung Model - MATLAB & Simulink'.
<https://www.mathworks.com/help/simscape/ug/medical-ventilator-with-lung-model.html> (accessed Jan. 30, 2023).
- [58]O. Kc, A. Gd, E. P, and O. Yy, 'Ideal endotracheal tube placement by referencing measurements on the tube', *Ann. Acad. Med. Singapore*, vol. 25, no. 4, Jul. 1996, Accessed: Feb. 22, 2023. [Online]. Available: <https://pubmed.ncbi.nlm.nih.gov/8893928/>
- [59]C. J. Russian, J. F. Gonzales, and N. R. Henry, 'Suction catheter size: an assessment and comparison of 3 different calculation methods', *Respir. Care*, vol. 59, no. 1, pp. 32–38, 2014.
- [60]'Tracheal tubes explained simply.' https://www.howequipmentworks.com/tracheal_tubes/ (accessed Jan. 30, 2023).
- [61]S. Farrow, C. Farrow, and N. Soni, 'Size matters: choosing the right tracheal tube.', *Anaesthesia*, vol. 67, no. 8, pp. 815–819, 2012.
- [62]C. Nickson, 'Endotracheal Tube (Standard)', *Life in the Fast Lane • LITFL*, Jan. 29, 2019. <https://litfl.com/endotracheal-tube-standard/> (accessed Jan. 30, 2023).
- [63]R. S. Litman and L. G. Maxwell, 'Cuffed versus uncuffed endotracheal tubes in pediatric anesthesia: the debate should finally end', *J. Am. Soc. Anesthesiol.*, vol. 118, no. 3, pp. 500–501, 2013.
- [64]'Endotracheal tube size formula - UpToDate'.
<https://www.uptodate.com/contents/image?imageKey=EM%2F72932> (accessed Jan. 30, 2023).
- [65]R. Isermann, *Fault-diagnosis systems: an introduction from fault detection to fault tolerance*. Springer Science & Business Media, 2005.
- [66]R. Isermann, *Fault-diagnosis applications: model-based condition monitoring: actuators, drives, machinery, plants, sensors, and fault-tolerant systems*. Springer Science & Business Media, 2011.
- [67]G.-Y. Heo, 'Condition monitoring using empirical models: technical review and prospects for nuclear applications', *Nucl. Eng. Technol.*, vol. 40, no. 1, pp. 49–68, 2008.
- [68]M. Nadakatti, A. Ramachandra, and A. S. Kumar, 'Artificial intelligence-based condition monitoring for plant maintenance', *Assem. Autom.*, 2008.

- [69]Y. Cho, N. Bianchi-Berthouze, and S. J. Julier, 'DeepBreath: Deep learning of breathing patterns for automatic stress recognition using low-cost thermal imaging in unconstrained settings', in *2017 seventh international conference on affective computing and intelligent interaction (acii)*, 2017, pp. 456–463.
- [70]I. Marton, A. Sanchez, S. Carlos, and S. Martorell, 'Application of data driven methods for condition monitoring maintenance', *Chem. Eng. Trans.*, vol. 33, pp. 301–306, 2013.
- [71]'Arterial Blood Gas (ABG): What It Is, Purpose, Procedure & Levels', *Cleveland Clinic*. <https://my.clevelandclinic.org/health/diagnostics/22409-arterial-blood-gas-abg> (accessed Jan. 30, 2023).
- [72]D. Lynch-Smith, C. L. Thompson, R. G. Pickering, and J. Y. Wan, 'Education on patient-ventilator synchrony, clinicians' knowledge level, and duration of mechanical ventilation', *Am. J. Crit. Care*, vol. 25, no. 6, pp. 545–551, 2016.
- [73]R. L. Chatburn, 'Classification of ventilator modes: update and proposal for implementation', *Respir. Care*, vol. 52, no. 3, pp. 301–323, 2007.
- [74]B. Enrico, F. Cristian, B. Stefano, and P. Luigi, 'Patient-ventilator asynchronies: types, outcomes and nursing detection skills', *Acta Bio Medica Atenei Parm.*, vol. 89, no. Suppl 7, pp. 6–18, 2018, doi: 10.23750/abm.v89i7-S.7737.
- [75]A. Géron, 'Hands-on machine learning with scikit-learn and tensorflow: Concepts', *Tools Tech. Build Intell. Syst.*, 2017.
- [76]A. Burkov, *The hundred-page machine learning book*, vol. 1. Andriy Burkov Quebec City, QC, Canada, 2019.
- [77]A. C. Müller and S. Guido, *Introduction to machine learning with Python: a guide for data scientists*. O'Reilly Media, Inc., 2016.
- [78]A. Géron, *Hands-on machine learning with Scikit-Learn, Keras, and TensorFlow*. O'Reilly Media, Inc., 2022.
- [79]R. Russell, *Machine Learning: Step-by-Step Guide To Implement Machine Learning Algorithms with Python*. (Knxb), 2020.
- [80]E. Alpaydin, *Introduction to machine learning*. MIT press, 2020.
- [81]'Choose Regression Model Options - MATLAB & Simulink'. <https://www.mathworks.com/help/stats/choose-regression-model-options.html> (accessed Jan. 30, 2023).
- [82]J. P. Mueller and L. Massaron, *Machine learning for dummies*. John Wiley & Sons, 2021.
- [83]'Machine Learning: Validation Techniques - DZone', *dzone.com*. <https://dzone.com/articles/machine-learning-validation-techniques> (accessed Jan. 30, 2023).
- [84]P. Refaeilzadeh, L. Tang, and H. Liu, 'Cross-validation.', *Encycl. Database Syst.*, vol. 5, pp. 532–538, 2009.
- [85]A. W. Moore, 'Cross-validation for detecting and preventing overfitting', *Sch. Comput. Sci. Carnegie Mellon Univ.*, 2001.
- [86]B. Ghojogh and M. Crowley, 'The theory behind overfitting, cross validation, regularization, bagging, and boosting: tutorial', *ArXiv Prepr. ArXiv190512787*, 2019.
- [87]L. Sarlabous *et al.*, 'Development and validation of a sample entropy-based method to identify complex patient-ventilator interactions during mechanical ventilation', *Sci. Rep.*, vol. 10, no. 1, pp. 1–12, 2020.
- [88]A. Abujaber, A. Fadlalla, D. Gammoh, H. Abdelrahman, M. Mollazehi, and A. El-Menyar, 'Prediction of in-hospital mortality in patients on mechanical ventilation post traumatic brain injury: machine learning approach', *BMC Med. Inform. Decis. Mak.*, vol. 20, no. 1, pp. 1–11, 2020.
- [89]S. E. Morton *et al.*, 'Virtual Patient Modeling and Prediction Validation for Pressure Controlled Mechanical Ventilation', *IFAC-Pap.*, vol. 53, no. 2, pp. 16221–16226, 2020.
- [90]Q. A. Ng, N. L. Loo, Y. S. Chiew, C. P. Tan, A. M. Ralib, and M. B. M. Nor, 'Mechanical ventilation monitoring: development of a network data acquisition system', *IFAC-Pap.*, vol. 53, no. 2, pp. 15916–15921, 2020.

- [91] S. Bolourani *et al.*, ‘A machine learning prediction model of respiratory failure within 48 hours of patient admission for COVID-19: model development and validation’, *J. Med. Internet Res.*, vol. 23, no. 2, p. e24246, 2021.
- [92] T. H. Bakkes, R. J. Montree, M. Mischi, F. Mojoli, and S. Turco, ‘A machine learning method for automatic detection and classification of patient-ventilator asynchrony’, in *2020 42nd Annual International Conference of the IEEE Engineering in Medicine & Biology Society (EMBC)*, 2020, pp. 150–153.
- [93] A. Fabregat *et al.*, ‘A Machine Learning decision-making tool for extubation in Intensive Care Unit patients’, *Comput. Methods Programs Biomed.*, vol. 200, p. 105869, 2021.
- [94] L. Zhang *et al.*, ‘Detection of patient-ventilator asynchrony from mechanical ventilation waveforms using a two-layer long short-term memory neural network’, *Comput. Biol. Med.*, vol. 120, p. 103721, 2020.
- [95] S. L. Hyland *et al.*, ‘Early prediction of circulatory failure in the intensive care unit using machine learning’, *Nat. Med.*, vol. 26, no. 3, pp. 364–373, 2020.
- [96] R. L. Chatburn, ‘Computer control of mechanical ventilation’, *Respir. Care*, vol. 49, no. 5, pp. 507–517, 2004.
- [97] F. YALÇINKAYA, M. E. YILDIRIM, and H. ÜNSAL, ‘Pressure-Volume Controlled Mechanical Ventilator: Modeling and Simulation’.
- [98] P. Tamburrano, F. Sciatti, E. Distaso, L. Di Lorenzo, and R. Amirante, ‘Validation of a Simulink Model for Simulating the Two Typical Controlled Ventilation Modes of Intensive Care Units Mechanical Ventilators’, *Appl. Sci.*, vol. 12, no. 4, p. 2057, 2022.
- [99] A. Emig Jr and S. Agili, ‘Plc Controlled Mechanical Ventilator’, in *2006 Annual Conference & Exposition*, 2006, pp. 11–997.
- [100] M. Borrello, ‘Modeling and control of systems for critical care ventilation’, in *Proceedings of the 2005, American Control Conference, 2005.*, 2005, pp. 2166–2180.
- [101] *Understanding Laminar and Turbulent Flow*, (Sep. 08, 2020). Accessed: Jan. 30, 2023. [Online Video]. Available: <https://www.youtube.com/watch?v=9A-uUG0WR0w>
- [102] E. Edge and E. E. LLC, ‘Viscosity of Air, Dynamic and Kinematic’. https://www.engineersedge.com/physics/viscosity_of_air_dynamic_and_kinematic_14483.htm (accessed Jan. 30, 2023).
- [103] K. de S. Kock, B. C. da Rosa, N. Martignago, C. Reis, and R. Maurici, ‘Comparison of respiratory mechanics measurements in the volume cycled ventilation (VCV) and pressure controlled ventilation (PCV)’, *Fisioter. Em Mov.*, vol. 29, pp. 229–236, 2016.
- [104] A. R. P. Ambrozin and A. J. M. Cataneo, ‘Pulmonary function aspects after myocardial revascularization related to preoperative risk’, *Braz. J. Cardiovasc. Surg.*, vol. 20, pp. 408–415, 2005.
- [105] ‘Trustworthy Machine Learning - Kush R. Varshney - Chapter 13: Transparency’. <http://www.trustworthymachinelearning.com/trustworthymachinelearning-13.htm> (accessed Jan. 30, 2023).
- [106] ‘Standard Deviation Formulas’. <https://www.mathsisfun.com/data/standard-deviation-formulas.html> (accessed Feb. 22, 2023).
- [107] A. Kumar, ‘R-squared, R2 in Linear Regression: Concepts, Examples’, *Data Analytics*, Feb. 21, 2022. <https://vitalflux.com/r-squared-explained-machine-learning/> (accessed Feb. 22, 2023).
- [108] ‘Kernel Distribution - MATLAB & Simulink’. <https://www.mathworks.com/help/stats/kernel-distribution.html> (accessed Jan. 30, 2023).
- [109] ‘Regression Learner App - MATLAB & Simulink’. <https://www.mathworks.com/help/stats/regression-learner-app.html> (accessed Jan. 30, 2023).
- [110] ‘Skewness - MATLAB skewness’. <https://www.mathworks.com/help/stats/skewness.html> (accessed Jan. 30, 2023).
- [111] ‘Kurtosis - MATLAB kurtosis’. <https://www.mathworks.com/help/stats/kurtosis.html> (accessed Jan. 30, 2023).

ANNEXURE 1 – SIMULINK MODEL



ANNEXURE 2 – GITHUB REPOSITORY

The GitHub repository that contains all the necessary digital files for the completion of this master's study can be found at https://github.com/TheRealPieterMarx/Masters_2022.git. Access to the repository may be granted upon reasonable request to the student (Mr Pieter Marx – pietermarx.ac@gmail.com) or to the supervisor (Prof H. Marais – henri.marais@nwu.ac.za).

The repository contains the following folders and files:

00_Simulink Model Folder

This folder contains the Simulink® Model and the necessary initiation workspace variables.

01_Mechanical Ventilator Data Generator

This folder contains the MATLAB® Application for generating simulation data.

02_Preprocessing CSV

This folder contains the additional code files for pre-processing the CSV files.

03_Database

This folder contains the SQL™ code for creating the database, MATLAB® Application code for populating the database and the exported databases of the project.

04_Classification Analysis

This folder contains the MATLAB® Applications' code for creating and evaluating the hybrid ventilation mode classifier.

05_Feature Extraction Analysis

This folder contains the MATLAB® Applications' code for analysing the feature extraction for both the independent and dependent features.

06_Machine Learning

This folder contains all the machine learning models that were trained, tested, and compared for determining the best models for deployment.

07_Deployment

This folder contains the MATLAB® Applications' code for deployment of the solution for the automatic classification of patient status based on ventilation data.

ANNEXURE 3 – IFAC WC 2023 SUBMISSION 1589

A conference paper was written and submitted to the International Federation of Automatic Control (IFAC) World Congress (WC) 2023.

Submission number: 1589

Title: Condition Monitoring Of The Mechanically Ventilated Patient

Authors: Pieter Marx*, Henri-Jean Marais

Decision: The submission has been accepted as a discussion paper (i.e., an extended abstract) and for presentation at the 22nd IFAC World Congress, to be held in Yokohama, Japan in July 2023. Unfortunately, it was not accepted as a regular paper.

See the following pages for the submission document.

Condition Monitoring Of The Mechanically Ventilated Patient

Pieter Marx * Henri Marais **

* Unit For Energy and Technology Systems, North-West University,
Potchefstroom, South Africa, 2531

** Unit For Energy and Technology Systems, North-West University,
Potchefstroom, South Africa, 2531 (e-mail: henri.marais@nwu.ac.za)

Abstract: Mechanical ventilation is an invasive procedure for assisting patients with severe respiratory illnesses. The functioning nature of mechanical ventilation may cause the patient to experience adverse effects that are difficult to detect quickly based on standard ventilator equipment outputs. These outputs are typically time-series waveforms associated with varying pressure and flow within the patient-ventilator circuit. Existing techniques that determine patient parameters, such as airway resistance and static lung compliance, are invasive to perform and require highly skilled medical practitioners. Predicting patient parameters automatically from time-series data can improve patient care through targeted protocols and allow limited practitioners to provide care at larger scales. An automated method for identifying the ventilation mode is presented, followed by automatic identification of the patient's airway resistance based solely on time-series data. The latter is a pulmonary parameter that can indicate the patient's clinical status when analysed over time. Initial results show that the mode of ventilation can be determined with an accuracy exceeding 98 %. Once the ventilation mode is predicted, a breath-by-breath analysis of the attached patient's airway resistance can be performed with an accuracy over 98 %, exceeding the ability of human practitioners. These results indicate that monitoring patient parameters directly from time-series data is possible with accuracy exceeding the ordinary skills of practitioners. Additionally, these methods allow the monitoring of several patients remotely, reducing the reliance on highly skilled practitioners.

Keywords: fault diagnosis, supervision, human error, machine learning, condition monitoring

1. INTRODUCTION

Mechanical ventilation generally encompasses all methods of supporting, assisting, or completely supplanting normal human breathing through forced air delivery. Mechanical ventilation (hereafter simply ventilation), although not a new concept, came into sharp relief due to the global Covid-19 pandemic. Large-scale respiratory diseases, such as tuberculosis and the SARS-CoV-2 virus (a common cause of Covid-19), result in more significant amounts of patients requiring ventilation. This, in turn, places high demands not only on equipment and resources but also on medical specialists. It is well reported that the number of qualified ventilation specialists is far outstripped but too little during periods of affecting pulmonary disease flare-ups. Typically, a ventilated patient would be monitored by a pulmonologist with continuous parameter adjustments. Large patient numbers and limited specialists result in parameter adjustment- and tracking errors.

In this paper, background to the ventilation process and standard parameters are provided in Section 2. Also, in Section 2, condition monitoring challenges and patient data generation are discussed. Section 3 deals with the methods used to analyse the ventilation mode and patient parameters based on the time-series data. Finally, the results are presented and discussed in Section 4, with conclusions and recommendations provided in Section 5.

2. BACKGROUND

2.1 Mechanical ventilation

Mechanical ventilation, of the clinical environment, is the process of moving gas to and from the lungs of a patient using a mechanical ventilator. This process contains time-variant parameters; the pressure (cmH₂O), flow (L/min), and volume (mL) of the gas delivered to the patient (Wilcox et al. (2021)). Which of these parameters are dependent, and which are independent, is determined by the ventilation protocol (Shuttleworth and Dodds (2019)). For volume-controlled (VC) modes, the air tidal volume (TV) is delivered by controlling the flow over time. The flow is set to maximum flow (Q_{max}) during the volume-controlled constant flow pattern (VCC), whereas it decelerates from Q_{max} during the volume-controlled decelerating flow pattern (VCD) (Warner and Patel (2013)). In the pressure-controlled (PC) mode, the controlled variable is air pressure, which is set during inspiration at peak inspiratory pressure (PIP) for a set inspiratory time (Ti). In all cases of sedated patients, the exhalation phase is passive and thus driven by the difference between the proximal airway pressure and the positive end-expiratory pressure (PEEP), as well as the respiratory system's state (Poor (2018)). Figure 1 provides a graphical representation of a single breath in each standard control mode.

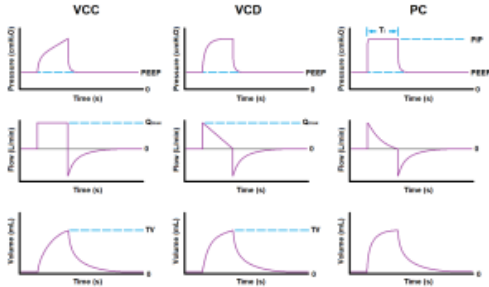


Fig. 1. Graphical representation of the three most common mechanical ventilation modes

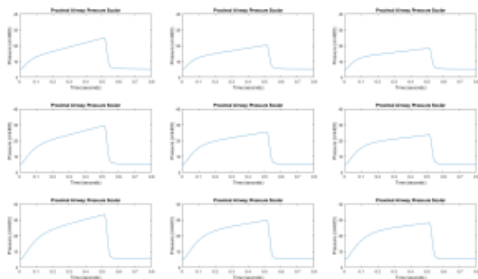


Fig. 2. Graphical illustration of the complexity involved in monitoring patient parameters from time-series data.

2.2 Ventilation data

From a modelling perspective, the human respiratory system can be represented as an RLC-lumped parameter model (Ghafarian et al. (2016)). However, a simplified RC model shows good correlation (Carvalho and Zin (2011)) and is used as such. The patient-ventilator setup will exhibit time variability during ventilation. The patient's respiratory resistance and static compliance changes over time, and the interconnecting ventilator circuit's pipes will cause flow-induced resistance. The change in compliance of the interconnecting ventilator circuit is assumed to be negligible and thus time-invariant.

For illustration purposes, consider the curves in Figure 2. This is a set of nine instances of proximal airway pressure waveforms of a breath, each with a unique combination of static compliance and airway resistance. The compliance and resistance of the respiratory system increase respectively with each column and row, from low to medium to high. On inspection, identifying that the airway resistance has increased, even for a single breath, is a non-trivial task.

2.3 Condition monitoring

In general, condition monitoring is that of a plant or process based on measurements taken from said plant or process (Davies (2012)). In the case of a ventilated patient, the combination of the patient, ventilator-circuit, and the mechanical ventilator itself, forms a single process system. Due to the invariability associated with the ventilator,

monitoring the resistance and compliance of the circuit and patient from the ventilation data becomes the focus.

Data-driven techniques Data-driven techniques leverage large sets of labelled data as input to statistical or machine-learning algorithms (Marton et al. (2013)). Such condition-monitoring applications are increasingly common in industrial processes (Nadakatti et al. (2008)). In the case of the ventilated patient, obtaining an existing data set which is sufficiently large and properly labelled is nearly impossible. Although datasets containing patient parameters and treatment protocols are available (Ng et al. (2020); Hyland et al. (2020); Sandoz et al. (2014); Smallwood (2020)), the fidelity of the data is insufficient. Typically, only a ventilation mode and possibly some clinical parameters are noted, if any. Currently, it is uncommon for ventilators to record data for later analysis. Therefore, obtaining actual lung resistance and compliance data in addition to the ventilation data can only be reasonably accomplished by employing an autopsy. Thus, a model-based methodology is more viable.

Model-based techniques Model-based techniques use analytic methods (Isermann (2011)) to determine if deviations are present. Typically, such methods are well suited for simulation and the subsequent adjustment of parameters. Utilising this approach makes it possible to excite anomalous behaviour that might pose a safety risk if obtained by other means. A sufficiently detailed model comprising a human respiratory and mechanical ventilation system is thus needed.

3. METHODOLOGY

3.1 Simulation model

An analysis of the literature indicates that the following parameters are critical in the application of mechanical ventilation:

- Patient clinical diagnosis (Chapman et al. (2014))
- Patient biological data (Farrow et al. (2012))
- Anthropomorphic data (Chatburn (2003))
- Ventilator operating parameters (Chatburn et al. (2014))

The clinical diagnosis would mandate mechanical ventilation and, as such, falls outside the scope of this work. Since the biological data can be leveraged to determine standard anthropomorphic parameters such as tracheal diameter, which in turn determines the diameter of a suitable endotracheal tube, amongst others (Bigatello et al. (2010)), certain simplifying assumptions are made in this work:

- Patient is a 25-year-old male, 186 cm in length
- Patient is fully sedated
- Ventilation protocol is volume-controlled with a constant flow pattern (VCC)

The assumptions simplify the patient model as much as possible and provide initial estimates of suitable ventilation settings and endotracheal tube diameters (Russian et al. (2014)). The selected ventilation protocol is exceedingly standard in clinical practice.

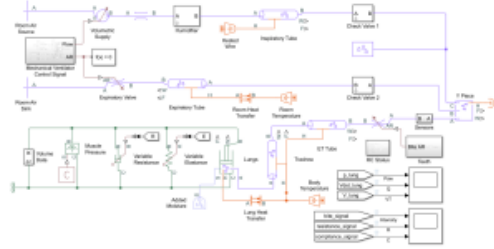


Fig. 3. A MATLAB® Simulink® model of a mechanically ventilated patient

These simplifying assumptions are used with an enhanced MATLAB® Simulink® model (shown in Figure 3) to generate a dataset with known ventilation and patient parameters (based on The MathWorks (2022c)).

A simulation model could simulate the variables over a more extensive range of values than expected in clinical practice without endangering consequences. This is advantageous when considering the deviating behaviour of machine learning models at the edges of data sets. In line with this work's purposes, the patient's airway resistance was simulated from 1 to 20 cmH₂O·s/L. This provided a database of 640 000 breaths per ventilation mode.

3.2 System overview

The overall concept is illustrated in Figure 4, where the patient-ventilator setup generates waveforms for the associated pressure, flow rate, and volume scalars. The ventilation mode and extracted features are used to develop regression models for the patient's airway resistance and static compliance. Finally, a patient status classification is made.

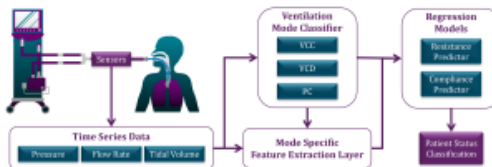


Fig. 4. Overall representation of system architecture

3.3 Mode classification

Referring to Section 2, VCC, VCD, and PC are the three standard ventilation modes. Since all three modes deliver an air volume to the patient by following predefined protocols that only manipulate proximal airway pressure or flow rate over time, establishing which protocol was implemented does not require the volume waveform and is thus excluded from Figure 5 (Arnal (2018)).

The proposed mode classification technique extracts two statistical parameters from a breath cycle. The first is a standard deviation (STD) parameter, and the second is a coefficient of determination (R^2) parameter from the pressure- and flow rate waveforms (indicated in Figure 5).

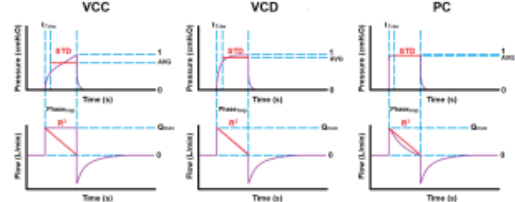


Fig. 5. Classification of ventilation modes

The pressure waveform is first offset and normalised; the mean is used to calculate the STD parameter. Then, a straight line is fitted through two points; the first is the initial maximum flow rate achieved, and the second is the zero-flow point directly after the inspiratory phase. This reference line is used to calculate the R^2 parameter. Generating boxplots of these statistical parameters indicates that R^2 alone can identify VCC entirely with a decision boundary of 0.254 (see Figure 6). In both cases, the ranges of the VCD and PC modes overlap (inspect Figure 7), and decision boundaries of non-overlapping areas were leveraged. Finally, STD Kernel probability distribution functions (PDFs in Figure 8) were leveraged to predict the rest of the instances for the remaining confusion area (The MathWorks (2022b)).

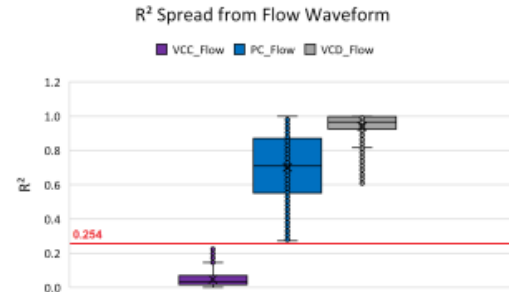


Fig. 6. Analysis of variability in flow parameter

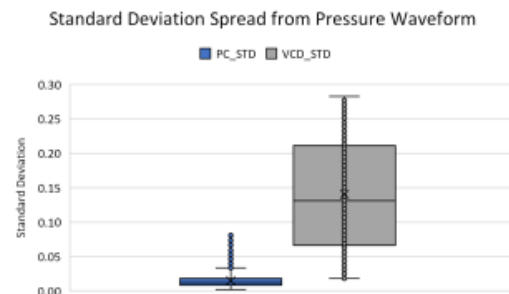


Fig. 7. Analysis of variability in pressure parameter

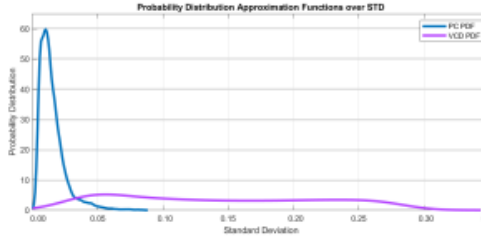


Fig. 8. Kernel probability distribution functions (PDFs)

3.4 Lung resistance

A ventilated patient's airway resistance is expected to vary over time as the patient either recovers or deteriorates. To investigate indicators thereof, the airway resistance in the model can be swept from 1 to 20 cmH₂O·s/L. The range of swept values exceed expected clinical values to account for statistical regression methods (Ambrozin and Cataneo (2005)). Cyclical operations are commonly analysed graphically from hysteresis loops. This is also the case with the flow-volume loop (Mason et al. (2010)). In Figure 9, the shape and size of the curves vary as the lung resistance is varied (only VCC implemented).

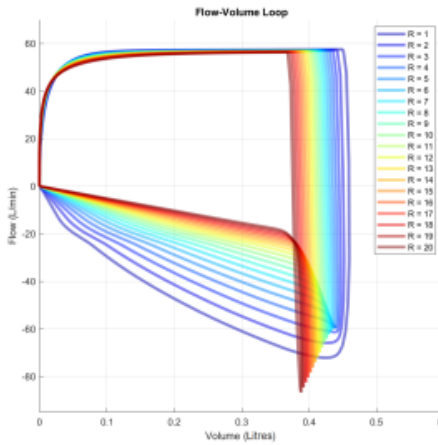


Fig. 9. Flow-volume loop of swept airway resistance

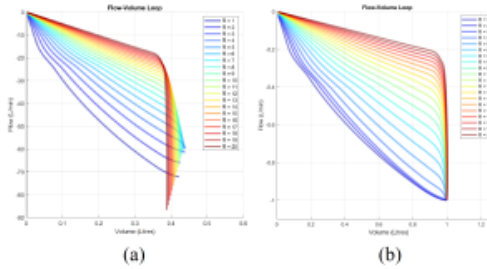


Fig. 10. Flow-volume loops of (a) isolated exhalation phase and (b) normalised version

The features extracted per breath for training the regression models for airway resistance prediction consist of types that are independent (informative of the nature of applied ventilation) and dependent (informative of the status of the respiratory system). The former type is the settings of the ventilator for VCC mode: respiratory rate, PEEP, maximum flow rate and tidal volume (Tobin (2013)). The latter type consists of features describing the shape of the waveforms during the exhalation phase: volume time constant, flow at one time constant, a ratio of the area under the flow-volume loop, gradient- (extracted from the isolated expiratory phase version represented by Figure 10 (a)), skewness-, and kurtosis of the flow-volume loop (from the normalised version of the loops depicted in Figure 10 (b)).

3.5 Regression models

These informative features were extracted from 640 000 unique labelled breath instances. The set of feature-label pairs was randomly divided into two subsets of equal size: a training set and a test set. The training set was used to train different regression model algorithms, which were validated using five cross-validation folds from the same set to protect the models from over-fitting Refaeilzadeh et al. (2009). These were 24 different algorithms comprising linear regression models, trees, SVM-, GPR- and neural network models (The MathWorks, 2022a). After the models were trained, they were all tested with the testing set, and a scoring system was applied to identify the overall best algorithms. The criteria used for evaluation were accuracy, degree of over-fitting, model size, prediction speed, accuracy bias to intervals over the prediction range and training time.

4. RESULTS AND DISCUSSION

4.1 Mode classification

The proposed mode classifier was applied to 640 000 unique breaths per ventilation mode. The classifier performance results are summarised in the confusion matrix in Table 1.

Table 1. Mode classification confusion matrix

Modes	Predicted	VCC	VCD	PC
Actual	Total = 1.92 M	639 922	641 377	638 701
VCC	640 000	639 922	0	78
VCD	640 000	0	631 067	8 933
PC	640 000	0	10 310	629 690

The true positive and false positive percentages were recorded in Table 2. All ventilation modes had true positive results of 98.99 %. VCC had 0.00 %, VCD 1.61 %, and PC 1.41 % false positives. All cases mistaken for VCD were PC. 99.13 % of the cases mistaken for PC were VCD, and the rest were VCC.

Table 2. Mode classification performance

Mode	% True Positives	% False Positives
VCC	99.99	0.00
VCD	98.60	1.61
PC	98.39	1.41

4.2 Proximal airway resistance

The criteria for the scoring system were implemented with strict cut-off boundaries. The accuracy had to be more than 95 %, the degree of overfitting less than 10 %, the model size less than 55 MB, the prediction speed more than 300 000 obstacles/s (obs/s), and the training time less than four days. This resulted in four remaining models: a bi-layered neural network (BNN), medium tree, fine tree and coarse tree (performance summary in Table 3).

Table 3. Top regression models results

Model Type	ACC [%]	Overfit [%]	Size [kB]	Speed [obs/s]	Training [s]
BNN	98.39	3.74	25 643	610 000	209 170
Medium Tree	96.95	3.14	27 405	540 000	142
Fine Tree	97.00	2.91	27 666	440 000	157
Coarse Tree	96.61	4.26	26 545	590 000	141

Further inspection of the interval-dependent accuracies of Figure 11 (neural network model) and that of Figure 12 (represent tree models) showed that the BNN model had less accuracy bias over the range of the target values. Therefore, the BNN had a more stable performance and was chosen as the best overall model for implementation.

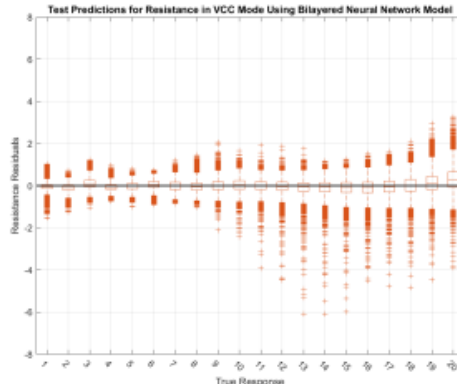


Fig. 11. Prediction accuracy of bi-layered neural network

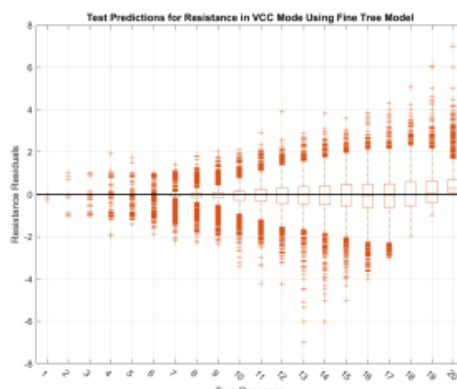


Fig. 12. Prediction accuracy of fine tree method

A simulated use-case of the model was performed for a 25-year-old sedated male on VCC mode with a height of 186 cm. The ventilator settings were set at appropriate values: PEEP was set at 5 cmH₂O, tidal volume at 540 mL and the maximum flow rate held at 60 L/min (Cairo et al. (2015)). The static compliance of the patient was kept constant at 55 mL/cmH₂O, and the airway resistance was swept from 1 to 20 cmH₂O·s/L. The feature extraction layer analysed the waveforms, and the features were provided as input to the BNN model. Figure 13 shows that the airway resistance predictions were plotted with each breath's target values over time. Further analyses showed that the mean local RMSE percentage was 3.10 %, and the mean total RMSE percentage was 1.05 %.

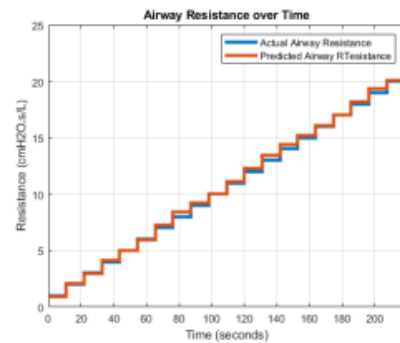


Fig. 13. Patient resistance prediction accuracy

5. CONCLUSION

The proposed method for monitoring the condition of the mechanically ventilated patient was designed and implemented as a data-driven solution. The method required a large, high fidelity, labelled data set, which was obtained employing simulated model-based techniques using a MATLAB® Simulink® model. A total of 1.92 million unique breath instances were simulated using parameter sweeps (640 000 per ventilation mode). The proposed condition monitoring method consisted of a ventilation mode classifier and an airway resistance predictor. The former could make classifying predictions with accuracies over 98 % for VCC, VCD and PC modes. The latter was implemented by training different regression models, which were compared to identify the best solutions. From the set of models trained and tested, the BNN had the best performance overall with an accuracy of over 98 % and was implemented on a typical use case. The use case was to make airway resistance predictions on breaths with varying resistances from 1 to 20 cmH₂O·s/L. The mean total RMSE of the predictions was 1.05 %.

From these results, data-driven condition monitoring techniques for mechanically ventilated respiratory health status are not only feasible but show great promise in performance. Future work will consist of a static compliance predictor, introducing patient feature variability, incorporating parameter predictions for the other ventilation modes, scaling the solution to monitor multiple patients simultaneously, and inspecting the possibility of expanding condition monitoring to active patients.

REFERENCES

- Ambrozin, A.R.P. and Cataneo, A.J.M. (2005). Pulmonary function aspects after myocardial revascularization related to preoperative risk. *Brazilian Journal of Cardiovascular Surgery*, 20, 408–415.
- Arnal, J.M. (2018). *Monitoring mechanical ventilation using ventilator waveforms*. Springer.
- Bigatello, L.M., Alam, H., and Allain, R.M. (2010). *Critical care handbook of the Massachusetts General Hospital*. Lippincott Williams & Wilkins.
- Cairo, J.M. et al. (2015). *Pilbeam's mechanical ventilation: physiological and clinical applications*. Elsevier Health Sciences.
- Carvalho, A.R. and Zin, W.A. (2011). Respiratory system dynamical mechanical properties: modeling in time and frequency domain. *Biophysical reviews*, 3(2), 71–84.
- Chapman, S., Robinson, G., Stradling, J., West, S., and Wrightson, J. (2014). *Oxford handbook of respiratory medicine*. OUP Oxford.
- Chatburn, R.L. (2003). *Fundamentals of mechanical ventilation: a short course in the theory and application of mechanical ventilators*. Mandu Press.
- Chatburn, R.L., El-Khatib, M., and Mireles-Cabodevila, E. (2014). A taxonomy for mechanical ventilation: 10 fundamental maxims. *Respiratory care*, 59(11), 1747–1763.
- Davies, A. (2012). *Handbook of condition monitoring: techniques and methodology*. Springer Science & Business Media.
- Farrow, S., Farrow, C., and Soni, N. (2012). Size matters: choosing the right tracheal tube. *Anaesthesia*, 67(8), 815–819.
- Ghafarian, P., Jamaati, H., and Hashemian, S.M. (2016). A review on human respiratory modeling. *Tanaffos*, 15(2), 61.
- Hyland, S.L., Faltys, M., Hüser, M., Lyu, X., Gumbisch, T., Esteban, C., Bock, C., Horn, M., Moor, M., Rieck, B., et al. (2020). Early prediction of circulatory failure in the intensive care unit using machine learning. *Nature medicine*, 26(3), 364–373.
- Isermann, R. (2011). *Fault-diagnosis applications: model-based condition monitoring: actuators, drives, machinery, plants, sensors, and fault-tolerant systems*. Springer Science & Business Media.
- Marton, I., Sanchez, A., Carlos, S., and Martorell, S. (2013). Application of data driven methods for condition monitoring maintenance. *Chemical engineering transactions*, 33, 301–306.
- Mason, R.J., Broaddus, V.C., Martin, T.R., King, T.E., Schraufnagel, D., Murray, J.F., and Nadel, J.A. (2010). *Murray and Nadel's Textbook of Respiratory Medicine E-Book: 2-Volume Set*. Elsevier Health Sciences.
- Nadakatti, M., Ramachandra, A., and Kumar, A.S. (2008). Artificial intelligence-based condition monitoring for plant maintenance. *Assembly Automation*.
- Ng, Q.A., Loo, N.L., Chiew, Y.S., Tan, C.P., Ralib, A.M., and Nor, M.B.M. (2020). Mechanical ventilation monitoring: development of a network data acquisition system. *IFAC-PapersOnLine*, 53(2), 15916–15921.
- Poor, H. (2018). *Basics of mechanical ventilation*. Springer.
- Refaeilzadeh, P., Tang, L., and Liu, H. (2009). Cross-validation. *Encyclopedia of database systems*, 5, 532–538.
- Russian, C.J., Gonzales, J.F., and Henry, N.R. (2014). Suction catheter size: an assessment and comparison of 3 different calculation methods. *Respiratory care*, 59(1), 32–38.
- Sandoz, J.S., LeBlanc, C., and McKim, D.A. (2014). Data downloads for effective noninvasive ventilation in patients with neuromuscular respiratory failure. *Respiratory Care*, 59(3), e35–e40.
- Shuttleworth, D. and Dodds, N. (2019). Ventilators and breathing systems. *Maths, Physics and Clinical Measurement for Anaesthesia and Intensive Care*, 130.
- Smallwood, C.D. (2020). Monitoring big data during mechanical ventilation in the icu. *Respiratory Care*, 65(6), 894–910.
- The MathWorks, I. (2022a). Choose regression model options. [urlhttps://www.mathworks.com/help/stats/choose-regression-model-options.html](https://www.mathworks.com/help/stats/choose-regression-model-options.html). [Online; accessed 9-November-2022].
- The MathWorks, I. (2022b). Kernel distribution. [urlhttps://www.mathworks.com/help/stats/kernel-distribution.html](https://www.mathworks.com/help/stats/kernel-distribution.html). [Online; accessed 9-November-2022].
- The MathWorks, I. (2022c). Medical ventilator with lung model. [urlhttps://www.mathworks.com/help/simscape/ug/medical-ventilator-with-lung-model.html](https://www.mathworks.com/help/simscape/ug/medical-ventilator-with-lung-model.html). [Online; accessed 9-November-2022].
- Tobin, M.J. (2013). *Principles and practice of mechanical ventilation*. McGraw-Hill Medical, New York.
- Warner, M.A. and Patel, B. (2013). Mechanical ventilation. *Benumof and Hagberg's airway management*, 981–997.
- Wilcox, S.R., Aydin, A., and Marcolini, E.G. (2021). *Mechanical ventilation in emergency medicine*. Springer.

ANNEXURE 4 – ENLARGED FIGURES

As a precaution for illegibility of detail in certain figures, this annexure contains enlarged figures.

The following figures are enlarged:

Figure 7-3: Thesis Structure of the Chapters and Sections per Chapter

Figure 7-4: The Three Most Common Modes for Controlled Ventilation: Volume-Controlled Constant Flow Mode (a), Volume-Controlled Decelerating Ramp Flow Mode (b) and Pressure-Controlled Mode (c)

Figure 7-5: The Schematic Diagram of The RC Subsystem Block

Figure 7-6: The Schematic Diagram of The Teeth Subsystem Block

Figure 7-7: Schematic Diagram of The Constant Flow Mechanical Ventilator Control Signal Subsystem

Figure 7-8: Schematic Diagram of The Decelerating Flow Mechanical Ventilator Control Signal Subsystem

Figure 7-9: Kernel Fitted Functions of the Coefficient of Determination Statistical Parameter for the VCC (a), VCD (b) and PC (c) Ventilation Modes

Figure 7-10: Kernel Fitted Functions of the Standard Deviation Statistical Parameter for the VCC (a), VCD (b) and PC (c) Ventilation Modes

Figure 7-11: 3D Distribution Graphs of the False Negative Predictions for the VCC Mode

Figure 7-12: 3D Distribution Graphs of the False Negative Predictions for the VCD Mode

Figure 7-13: 3D Distribution Graphs of the False Negative Predictions for the PC Mode

Figure 7-14: Boxplots of Baseline Pressure Feature for VCC (a), VCD (b) and PC (c)

Figure 7-15: Boxplots of Maximum Inspiratory Flow Feature for VCC (a) and VCD (b)

Figure 7-16: Boxplots of Tidal Volume Feature for VCC (a) and VCD (b)

Figure 7-17: Boxplots of Inspiratory Time Feature for PC

Figure 7-18: Boxplots of Peak Inspiratory Pressure Feature for Baseline Pressures of 0 cmH₂O (a), 5 cmH₂O (b), 10 cmH₂O (c) and 15 cmH₂O (d)

Figure 7-19: Normalised Segments of Flow-Volume Loops of Varying Resistance for VCC (a) and VCD (b)

Figure 7-20: Entity Relationship Diagram of the Database

Figure 7-21: Response Plots for Bi-Layered Neural Network (a), Medium Tree (b) and Linear SVM (c)

Figure 7-22: Predicted vs Actual Plots for Bi-Layered Neural Network (a), Medium Tree (b) and Linear SVM (c)

Figure 7-23: Residual Plots for Bi-Layered Neural Network (a), Medium Tree (b) and Linear SVM (c)

Figure 7-24: Predicted vs Actual Resistance Results for VCC (a) and VCD (b)

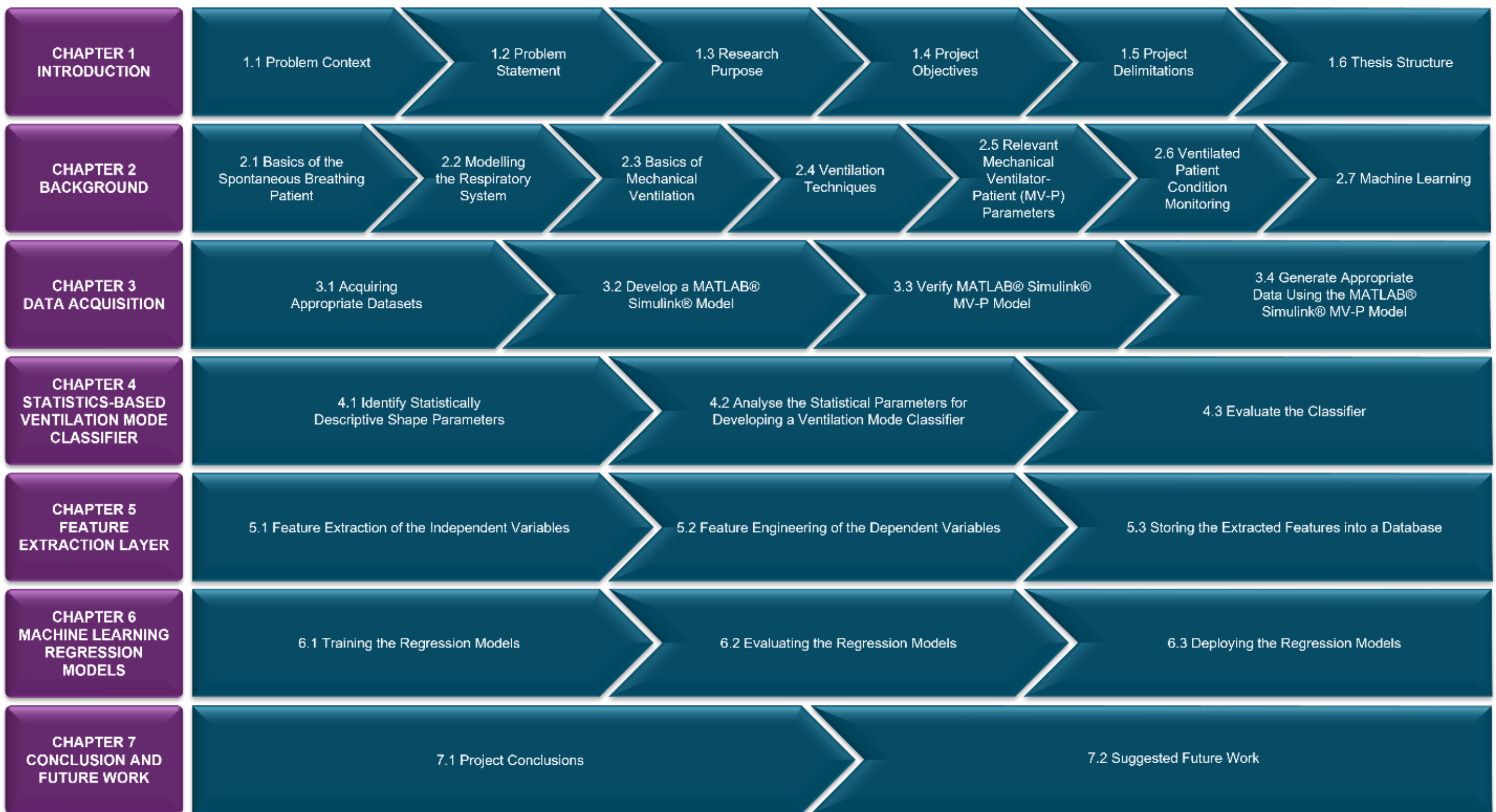


Figure 7-25: Thesis Structure of the Chapters and Sections per Chapter

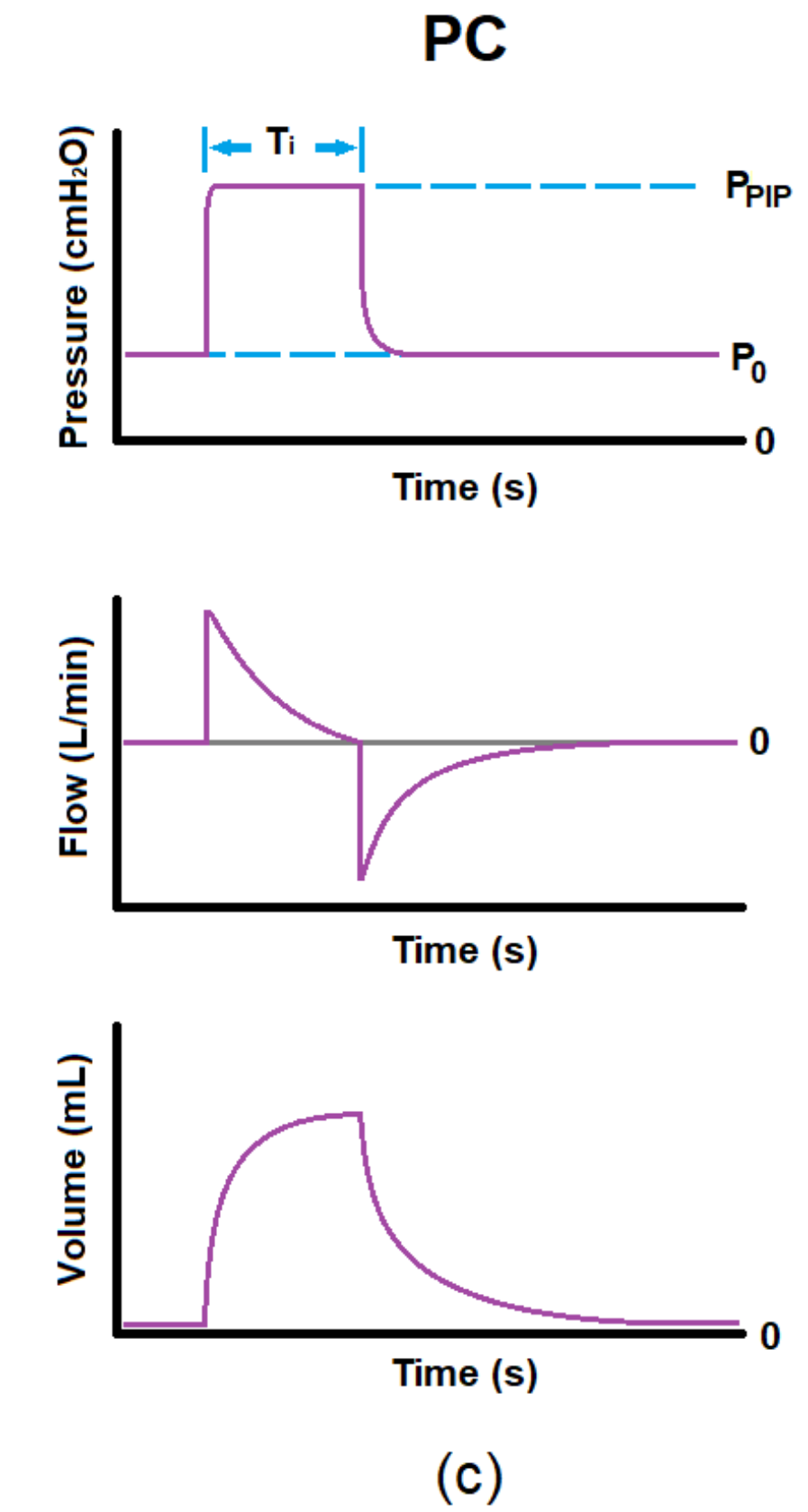
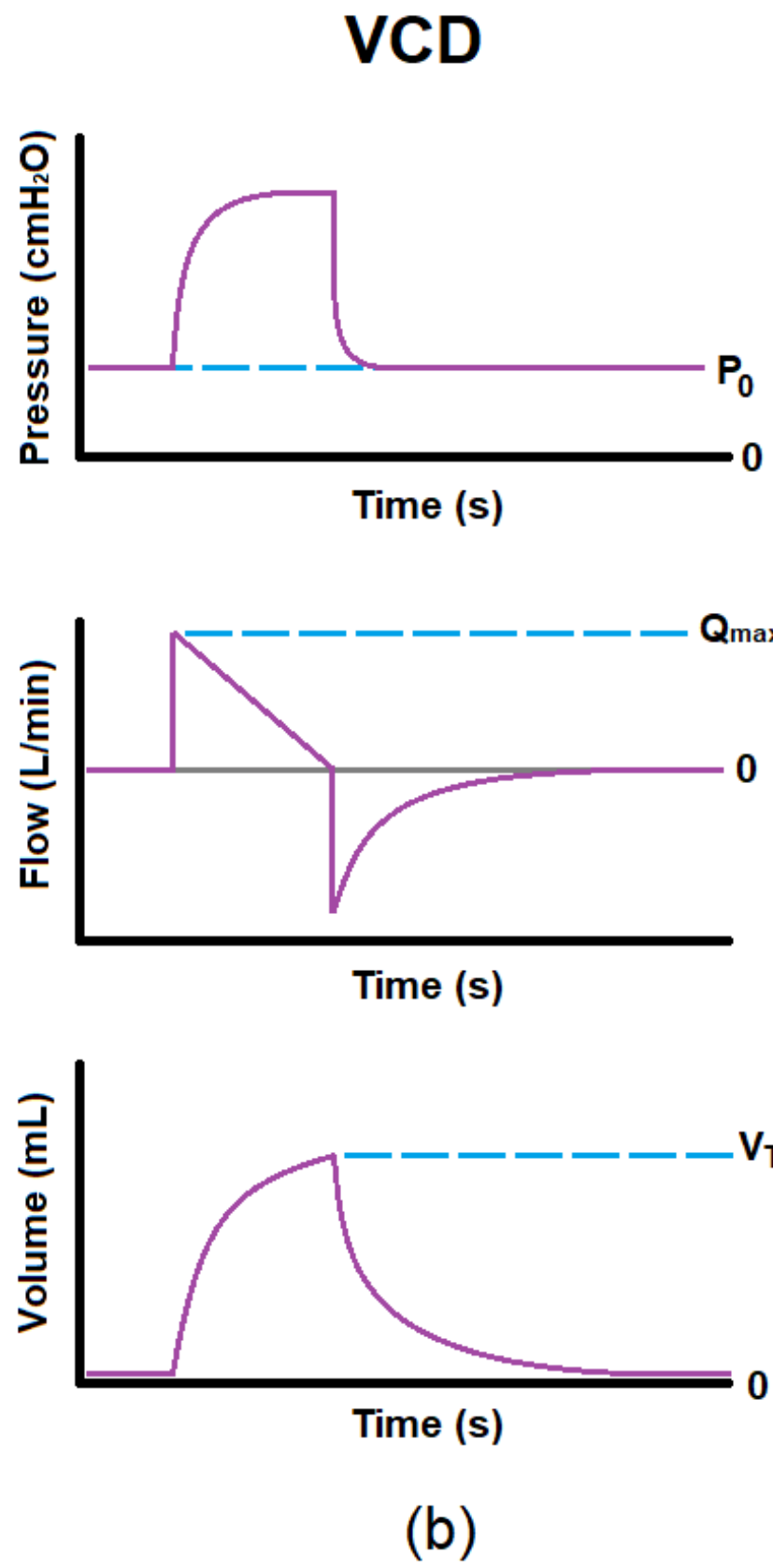
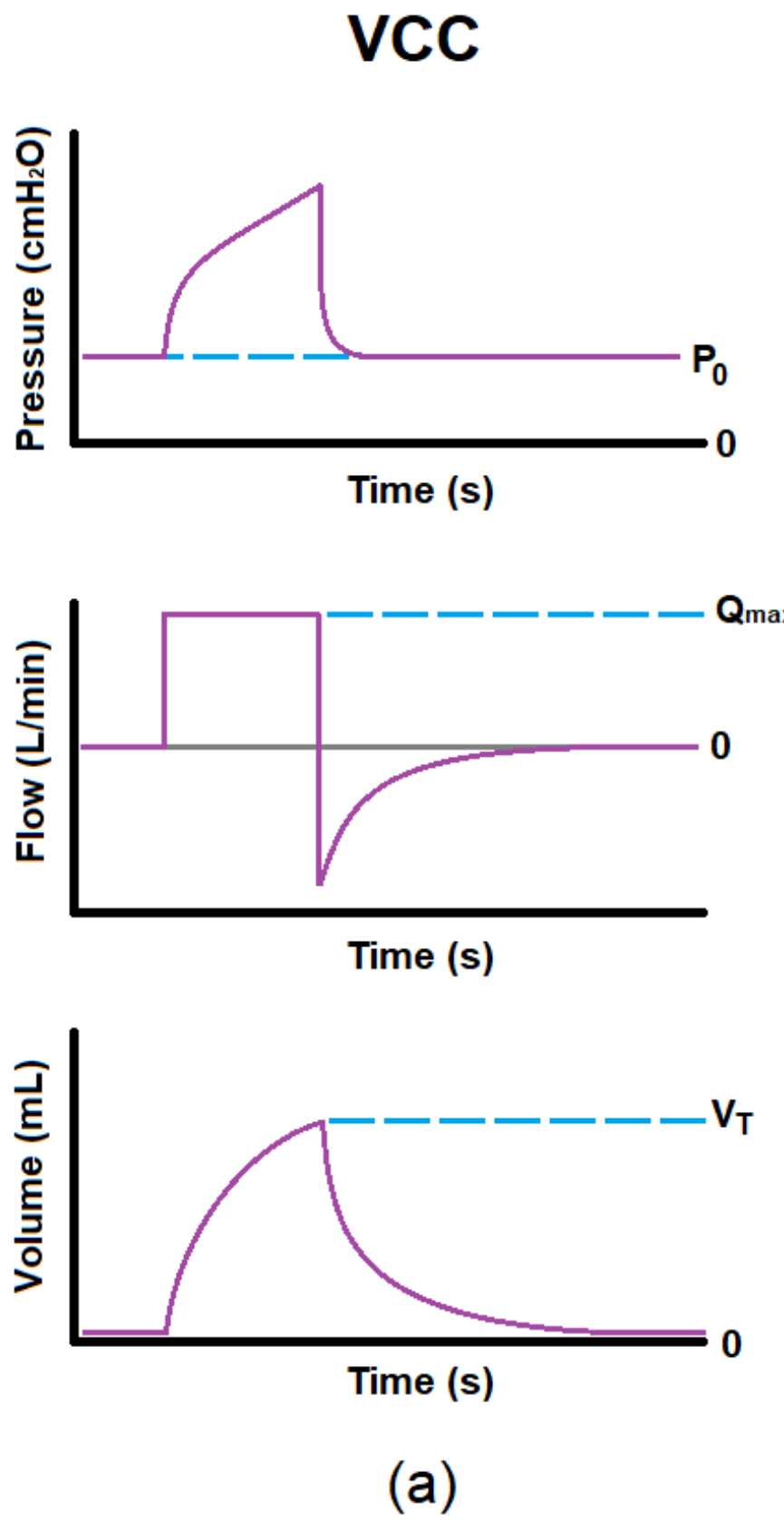


Figure 7-26: The Three Most Common Modes for Controlled Ventilation: Volume-Controlled Constant Flow Mode (a), Volume-Controlled Decelerating Ramp Flow Mode (b) and Pressure-Controlled Mode (c)

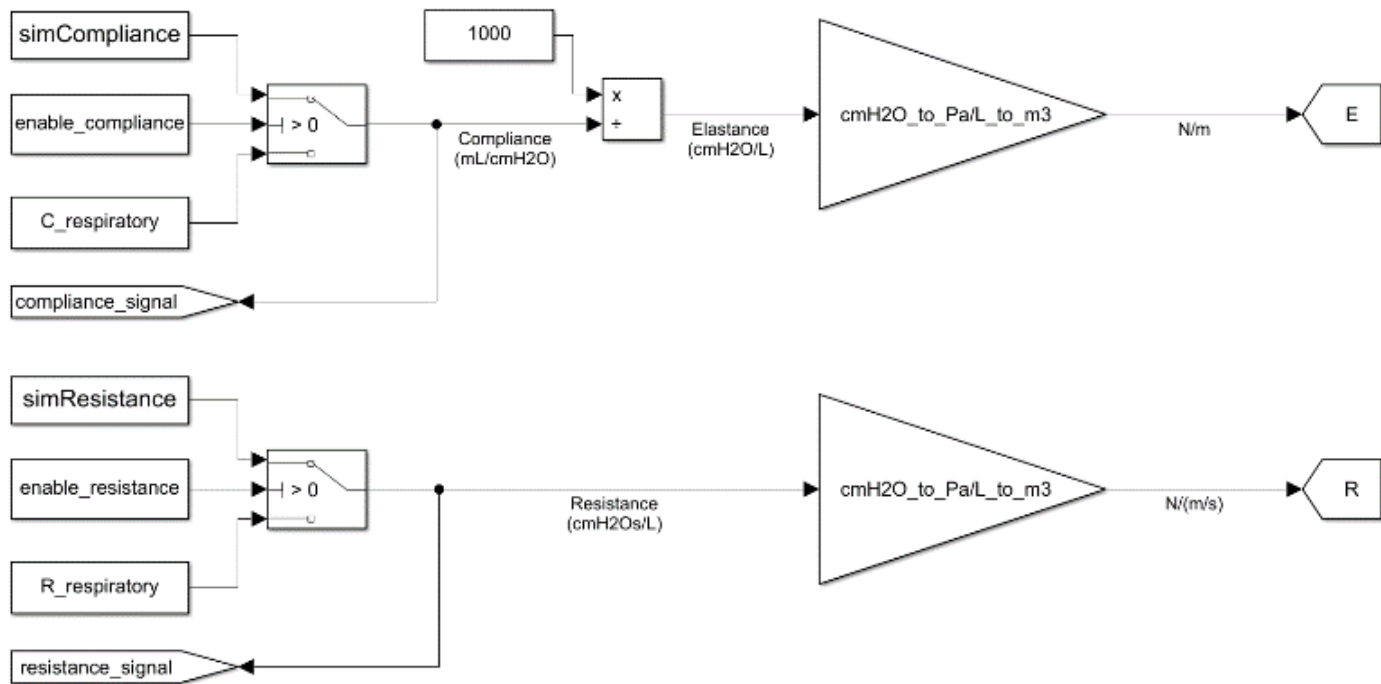


Figure 7-27: The Schematic Diagram of The RC Subsystem Block

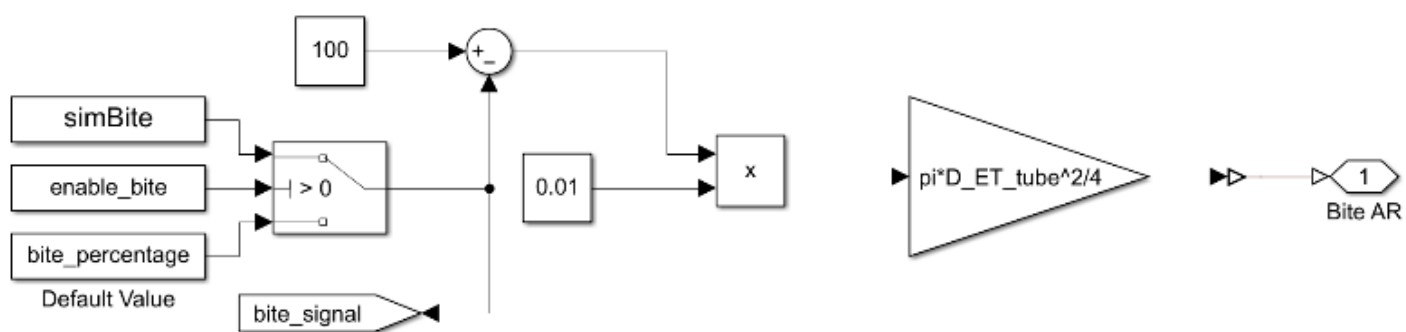


Figure 7-28: The Schematic Diagram of The Teeth Subsystem Block

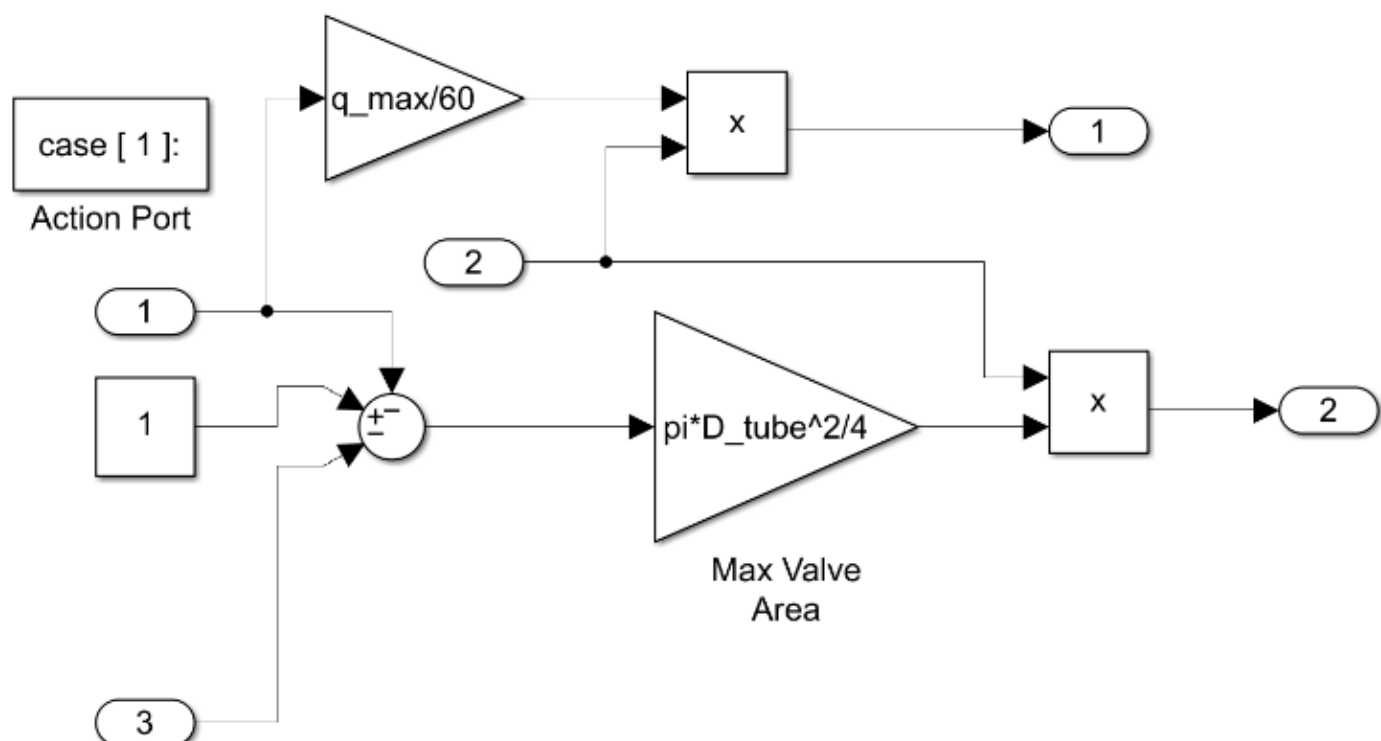


Figure 7-29: Schematic Diagram of The Constant Flow Mechanical Ventilator Control Signal Subsystem

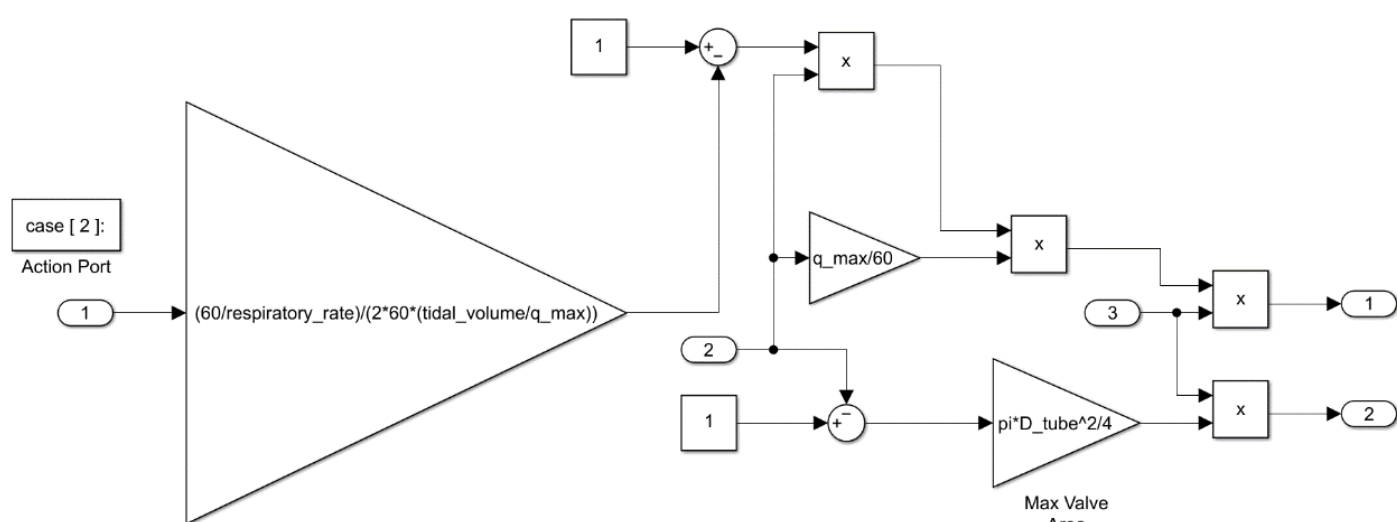


Figure 7-30: Schematic Diagram of The Decelerating Flow Mechanical Ventilator Control Signal Subsystem

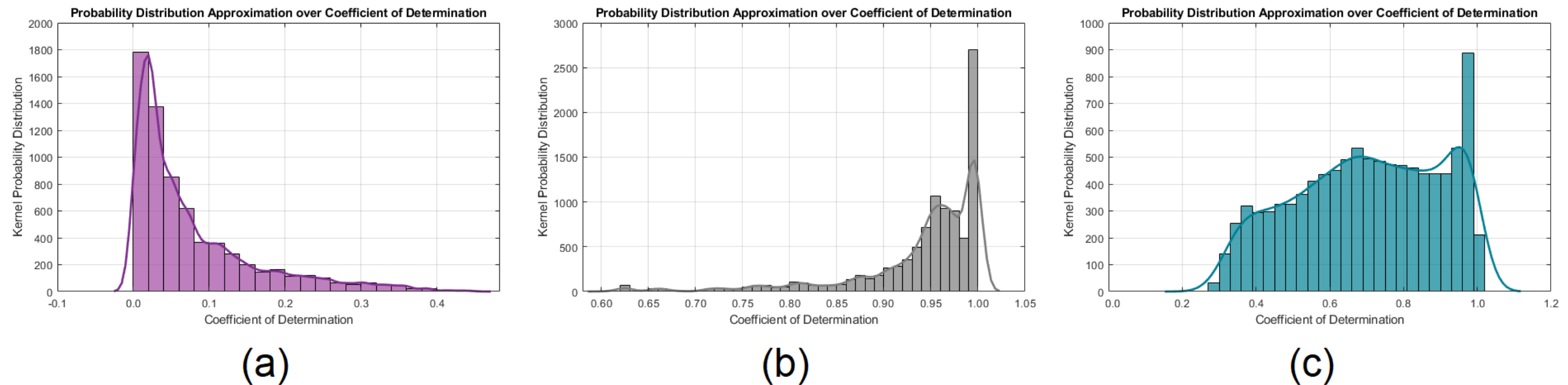


Figure 7-31: Kernel Fitted Functions of the Coefficient of Determination Statistical Parameter for the VCC (a), VCD (b) and PC (c) Ventilation Modes

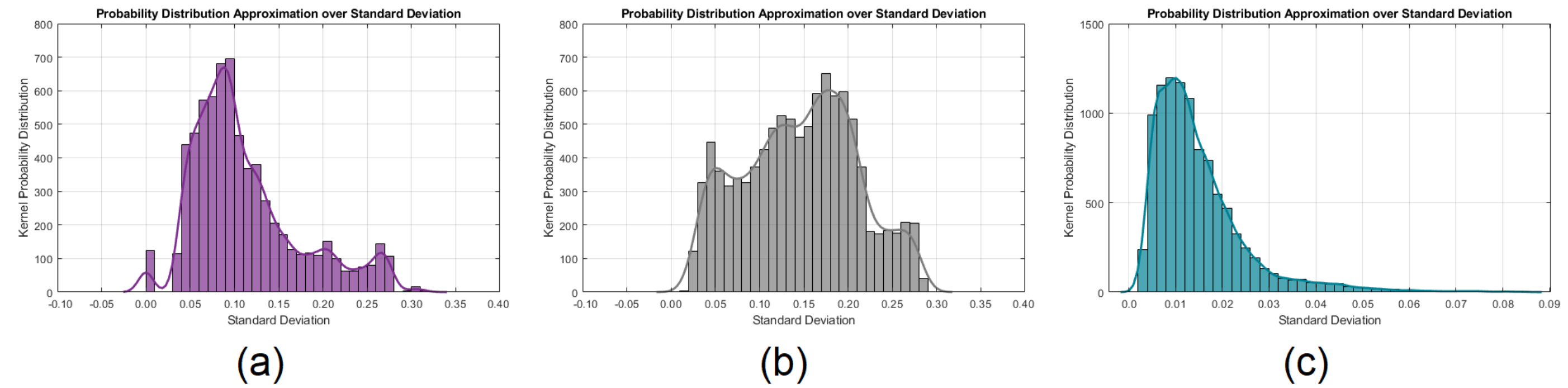


Figure 7-32: Kernel Fitted Functions of the Standard Deviation Statistical Parameter for the VCC (a), VCD (b) and PC (c) Ventilation Modes

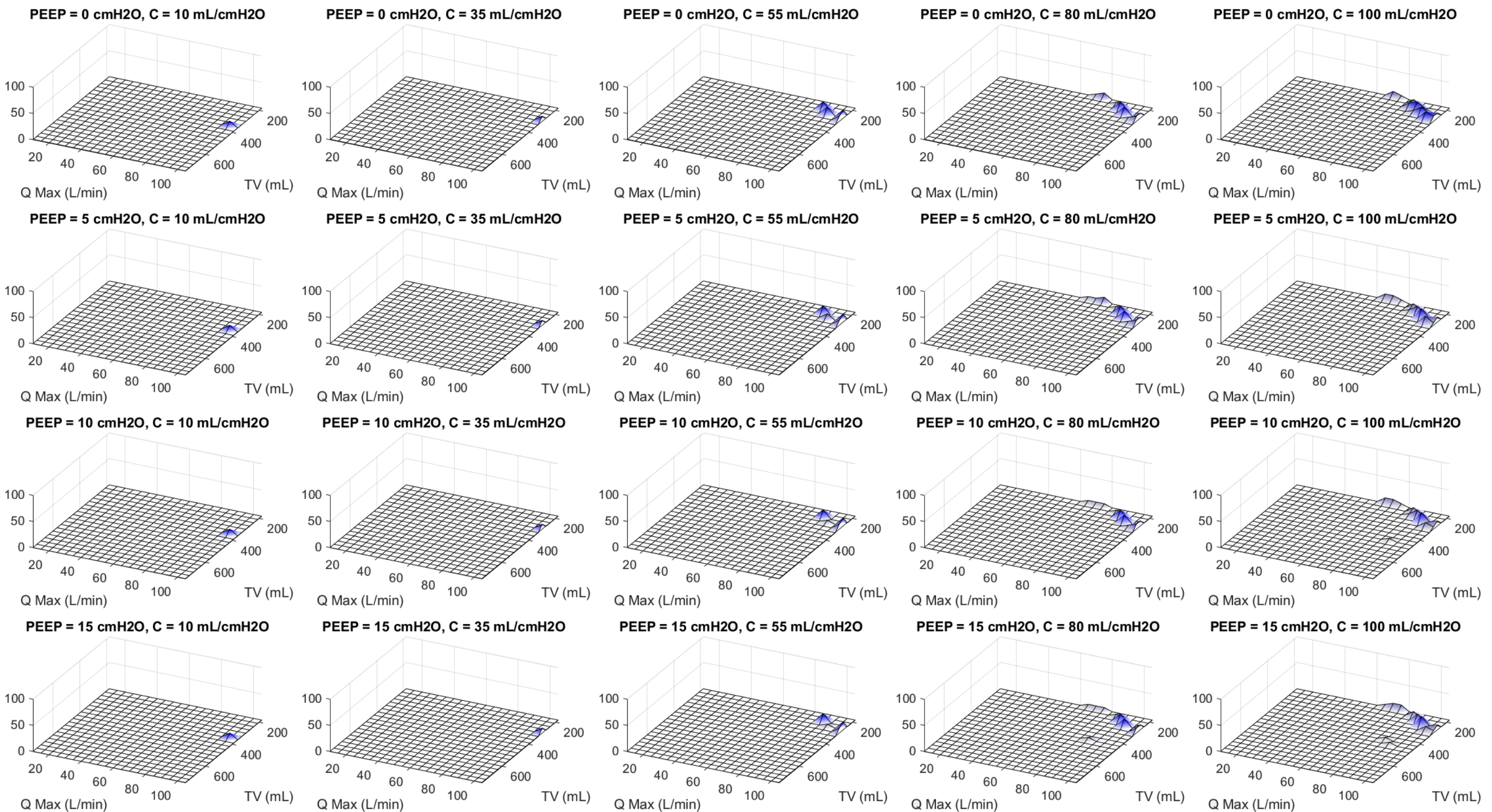


Figure 7-33: 3D Distribution Graphs of the False Negative Predictions for the VCC Mode

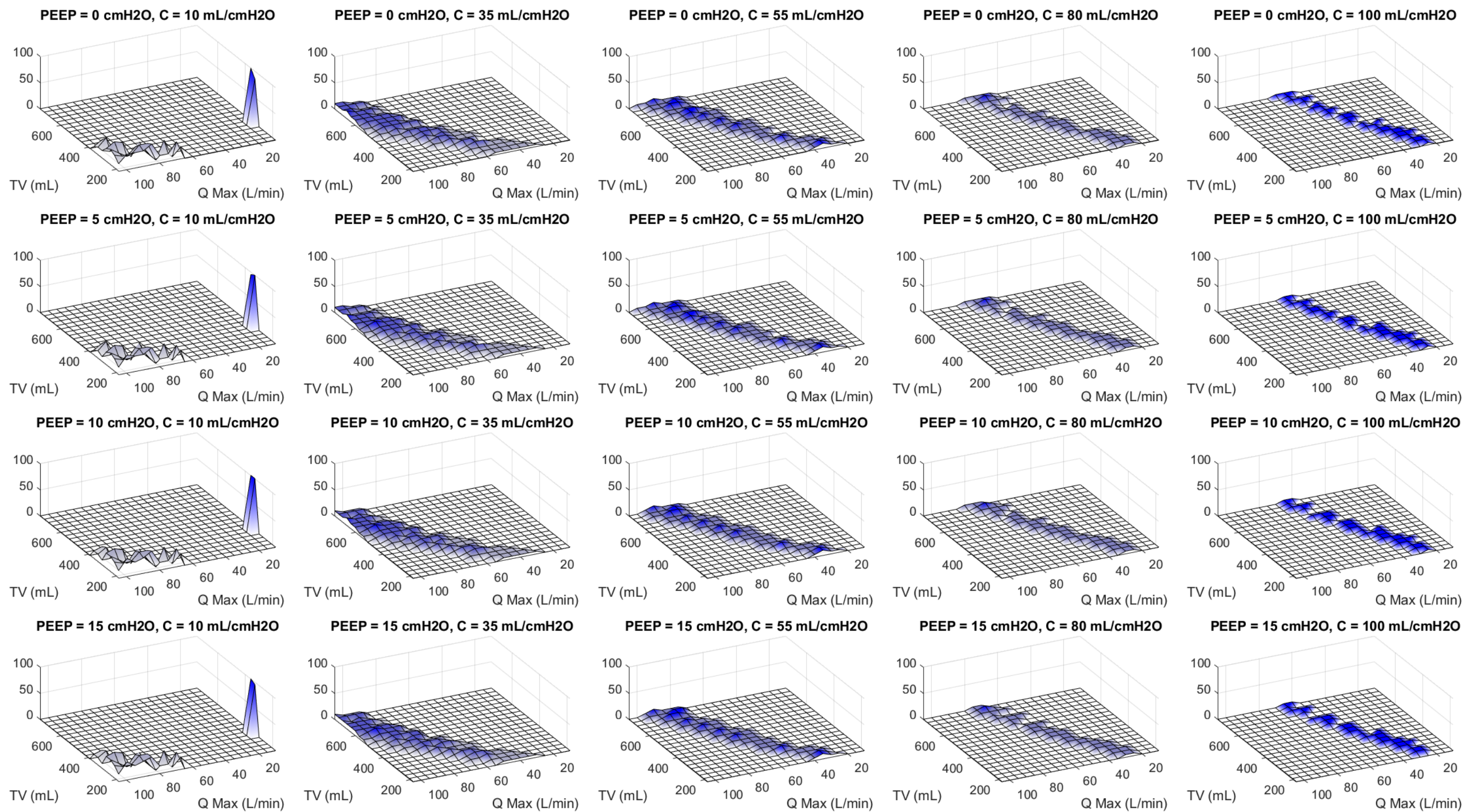


Figure 7-34: 3D Distribution Graphs of the False Negative Predictions for the VCD Mode

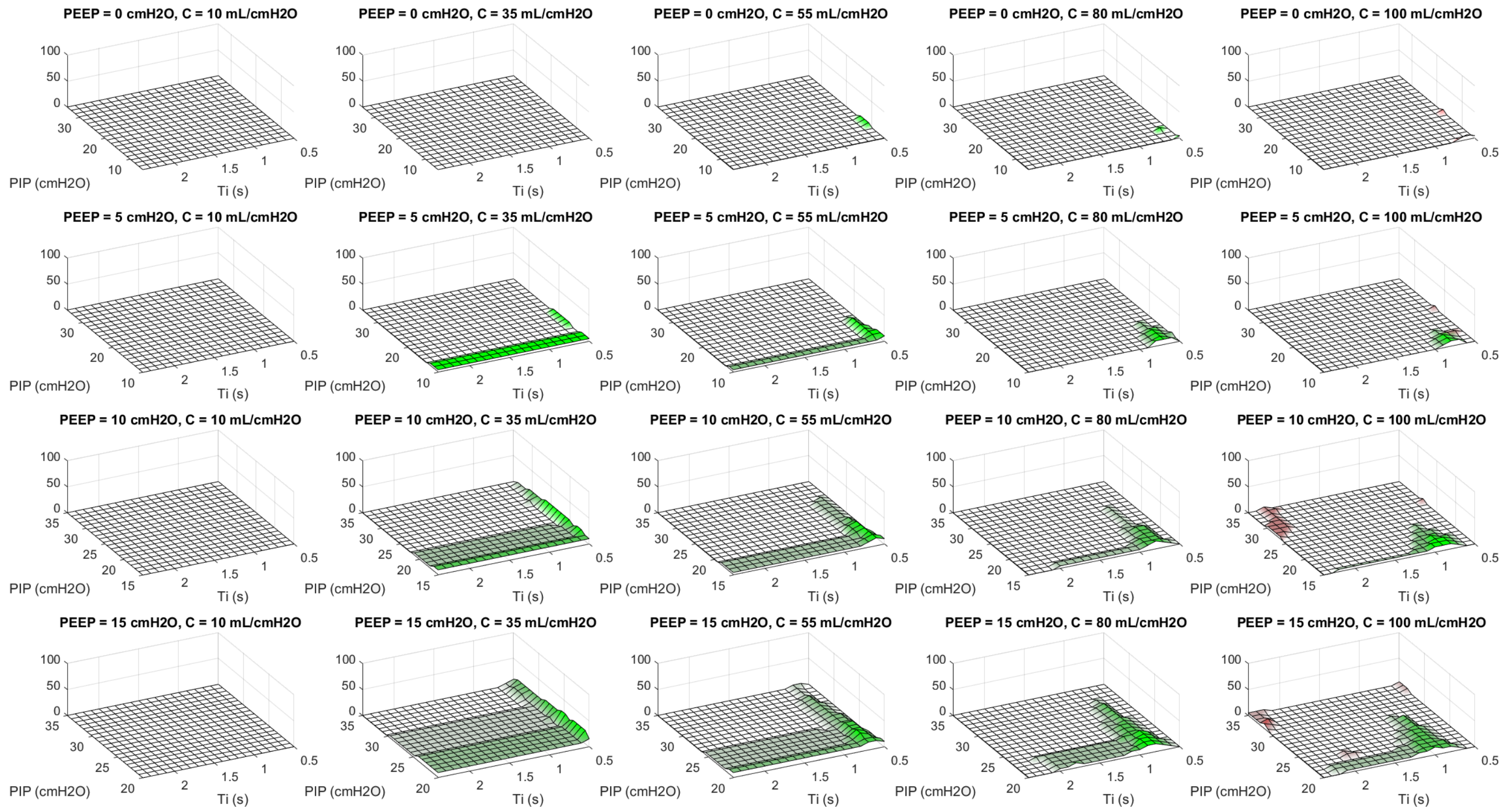


Figure 7-35: 3D Distribution Graphs of the False Negative Predictions for the PC Mode

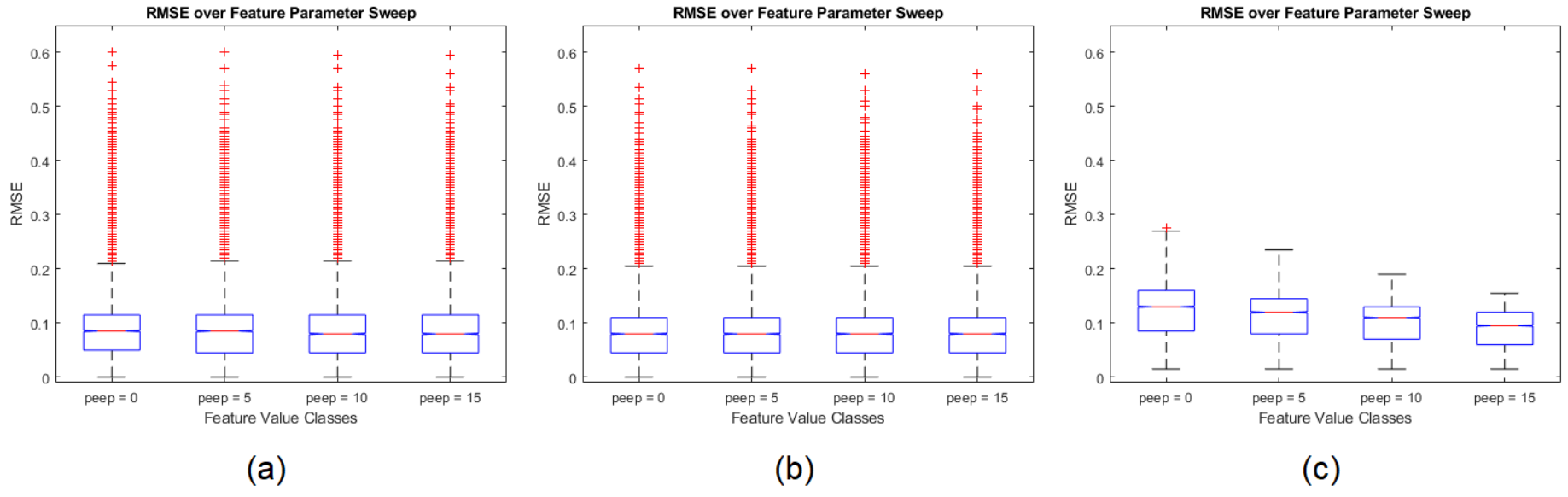


Figure 7-36: Boxplots of Baseline Pressure Feature for VCC (a), VCD (b) and PC (c)

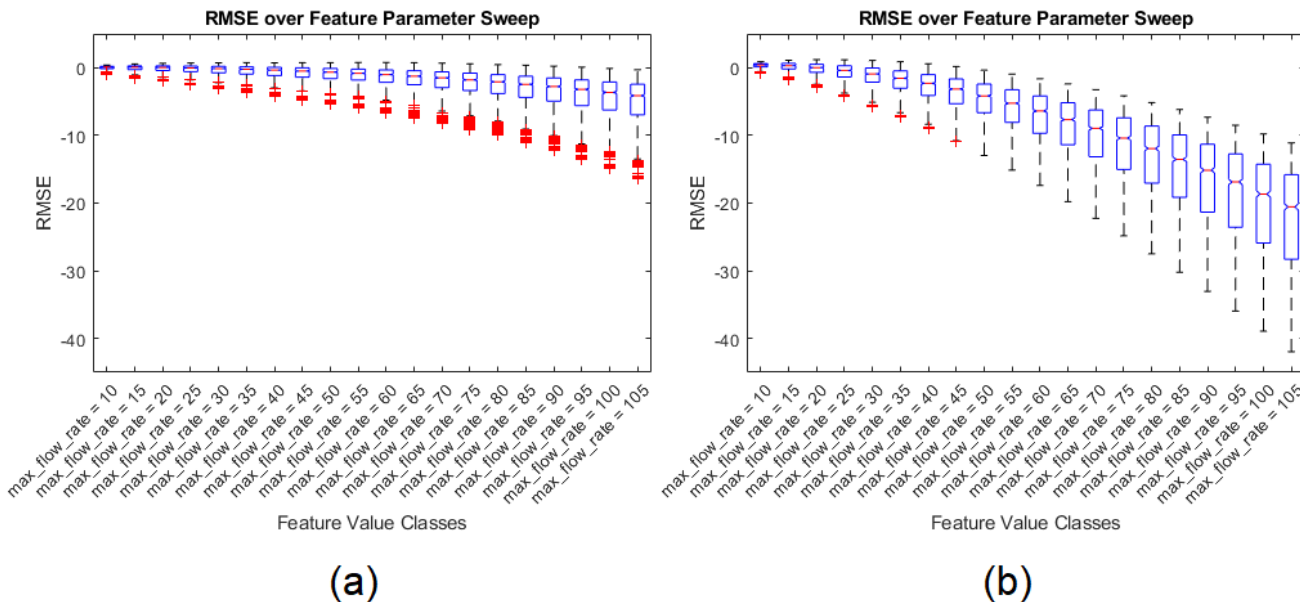


Figure 7-37: Boxplots of Maximum Inspiratory Flow Feature for VCC (a) and VCD (b)

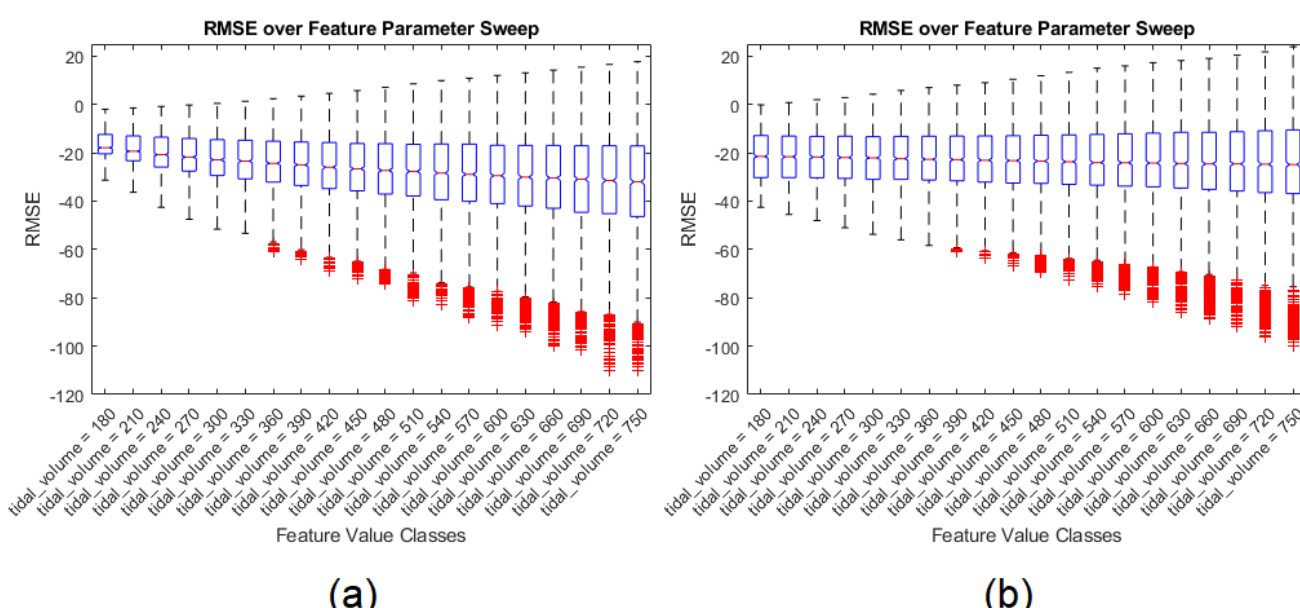


Figure 7-38: Boxplots of Tidal Volume Feature for VCC (a) and VCD (b)

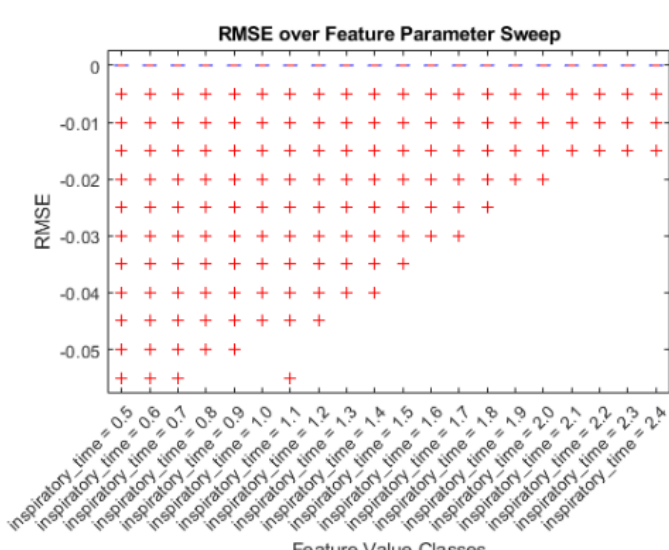


Figure 7-39: Boxplots of Inspiratory Time Feature for PC

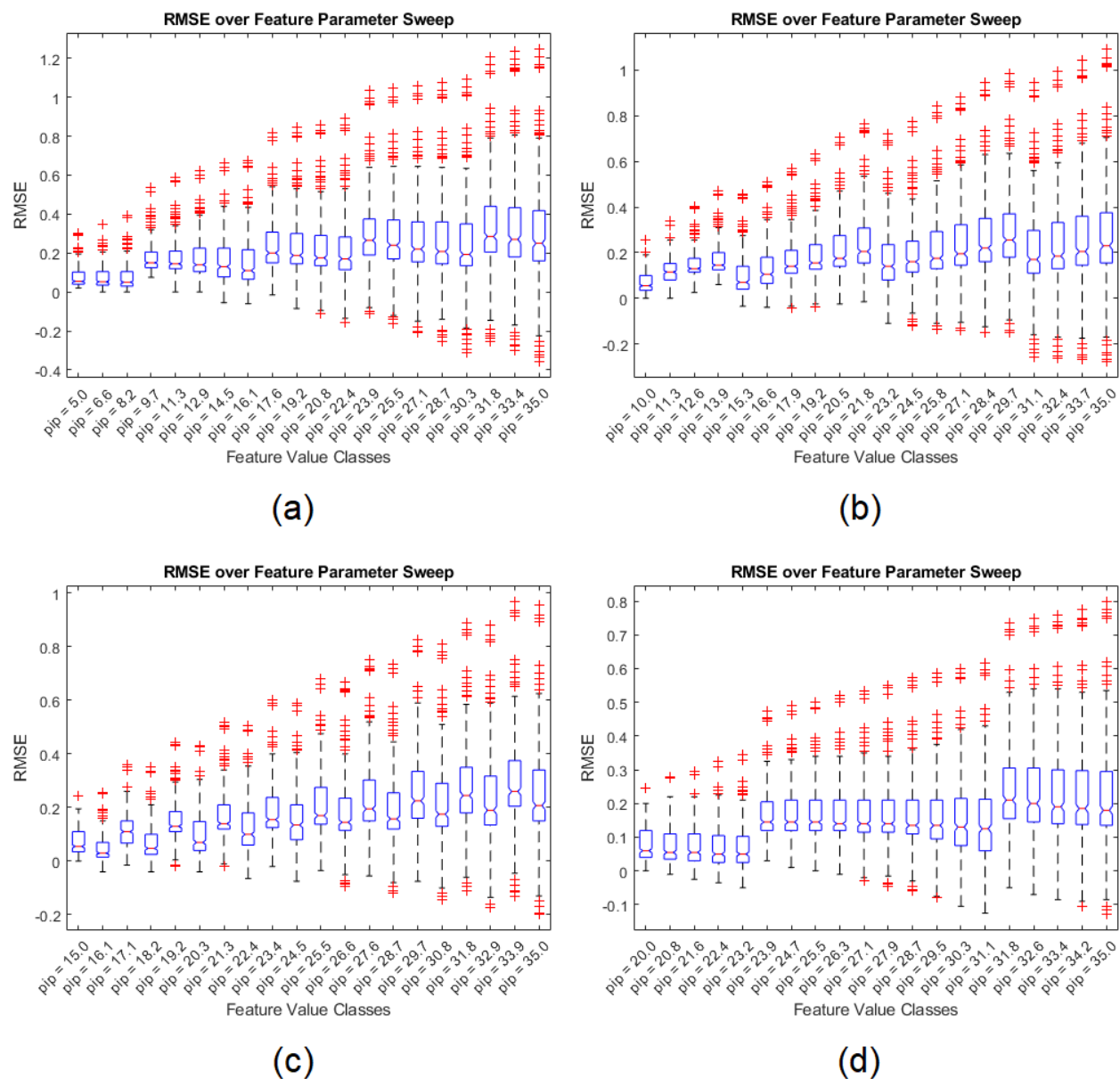


Figure 7-40: Boxplots of Peak Inspiratory Pressure Feature for Baseline Pressures of 0 cmH₂O (a), 5 cmH₂O (b), 10 cmH₂O (c) and 15 cmH₂O (d)

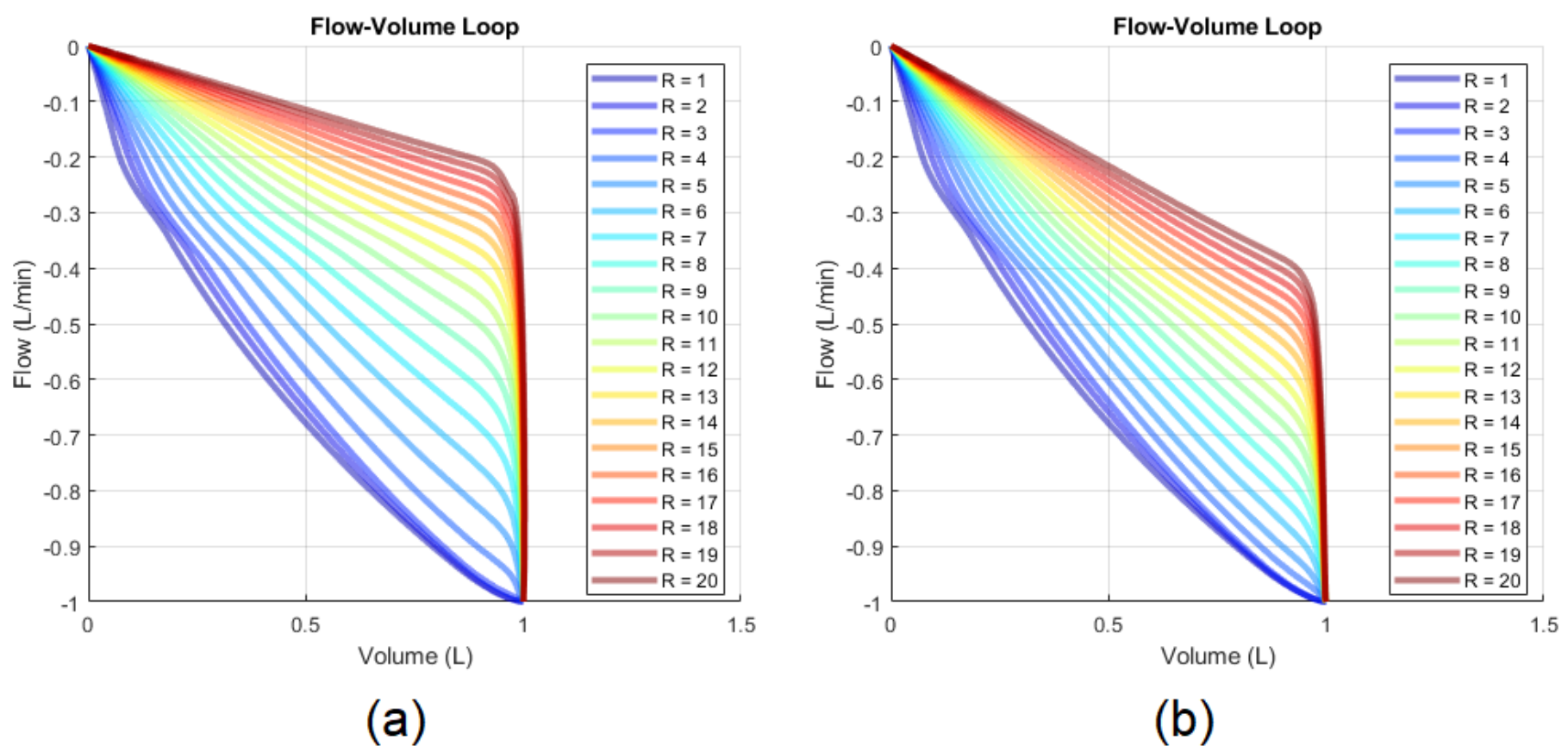


Figure 7-41: Normalised Segments of Flow-Volume Loops of VCC (a) and VCD (b)

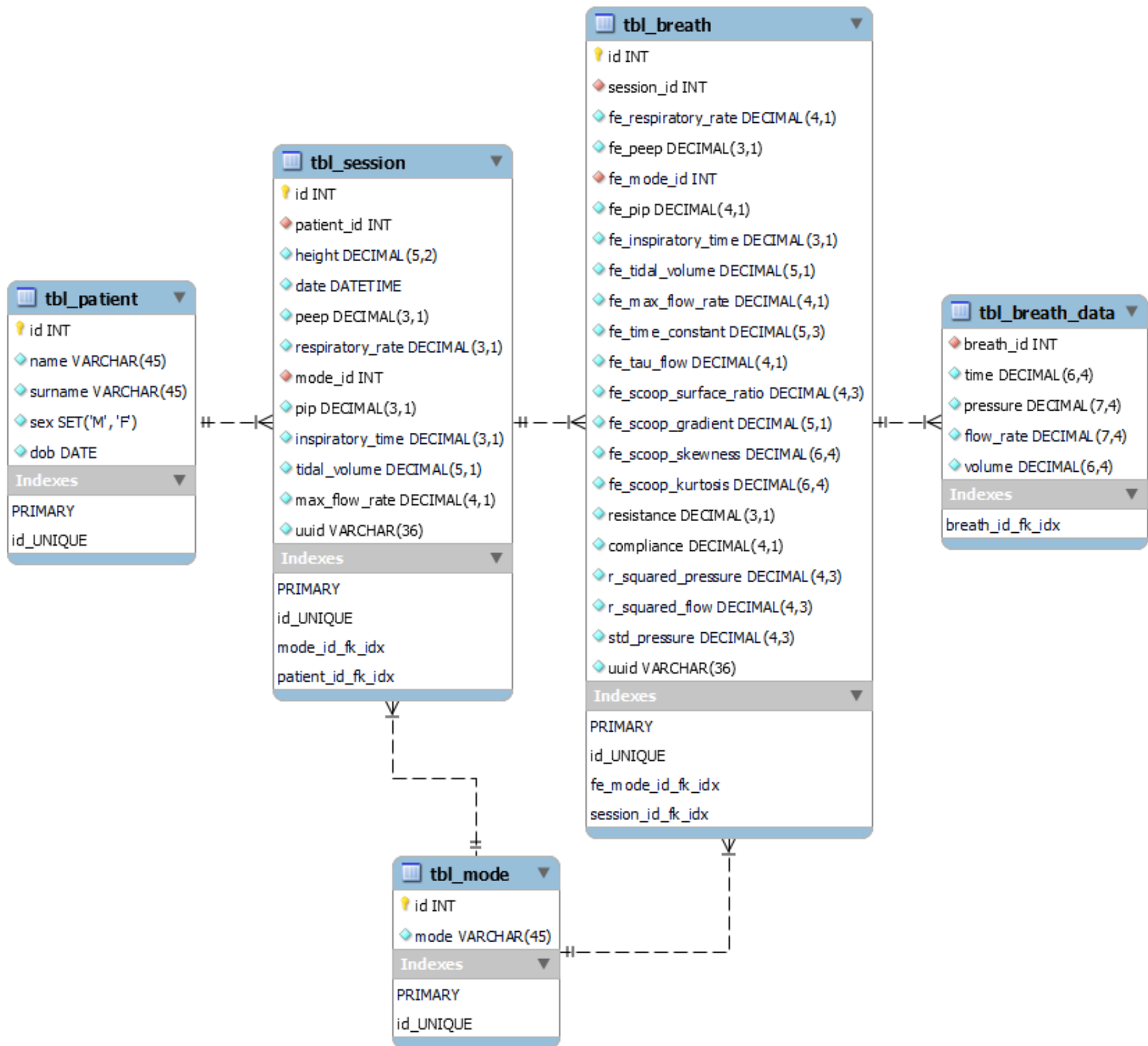


Figure 7-42: Entity Relationship Diagram of the Database

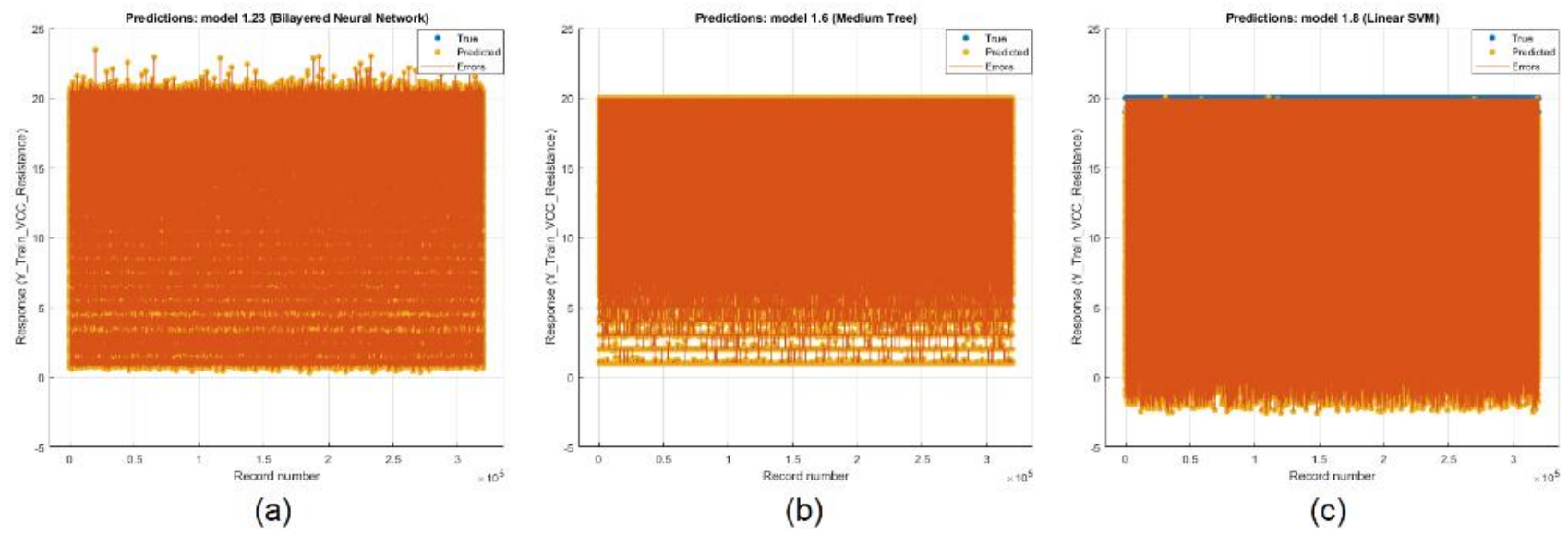


Figure 7-43: Response Plots for Bi-Layered Neural Network (a), Medium Tree (b) and Linear SVM (c)

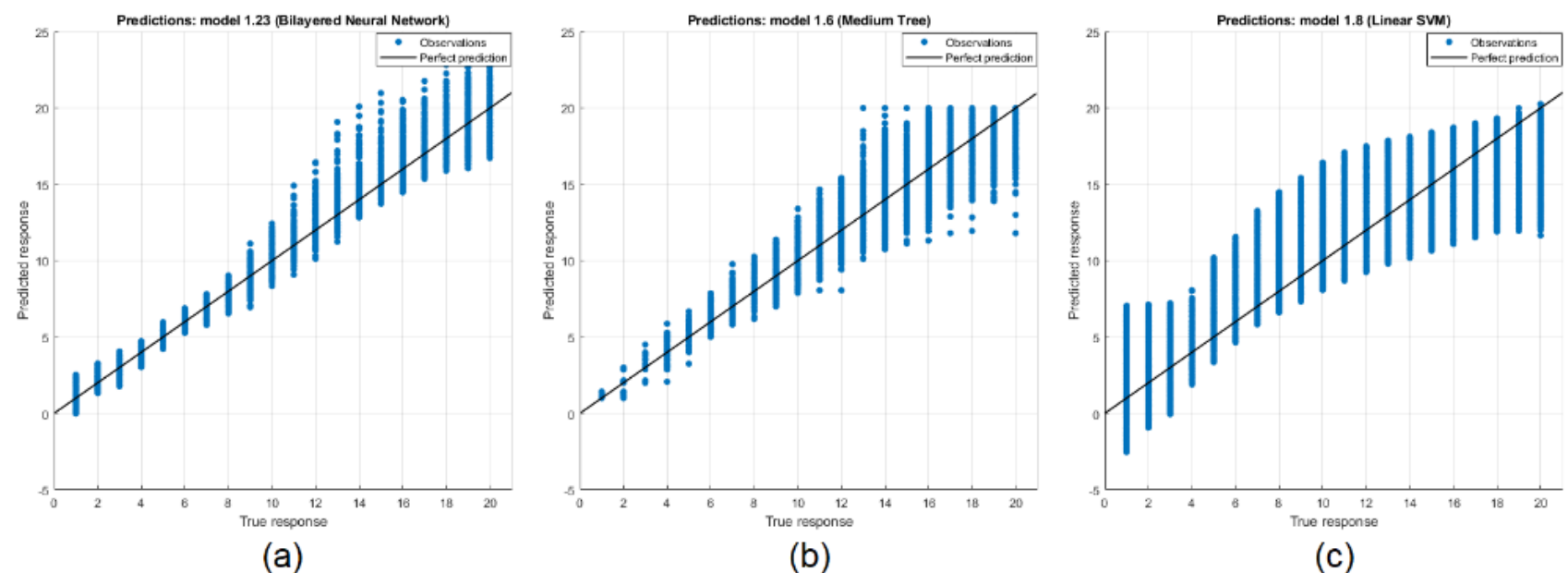


Figure 7-44: Predicted vs Actual Plots for Bi-Layered Neural Network (a), Medium Tree (b) and Linear SVM (c)

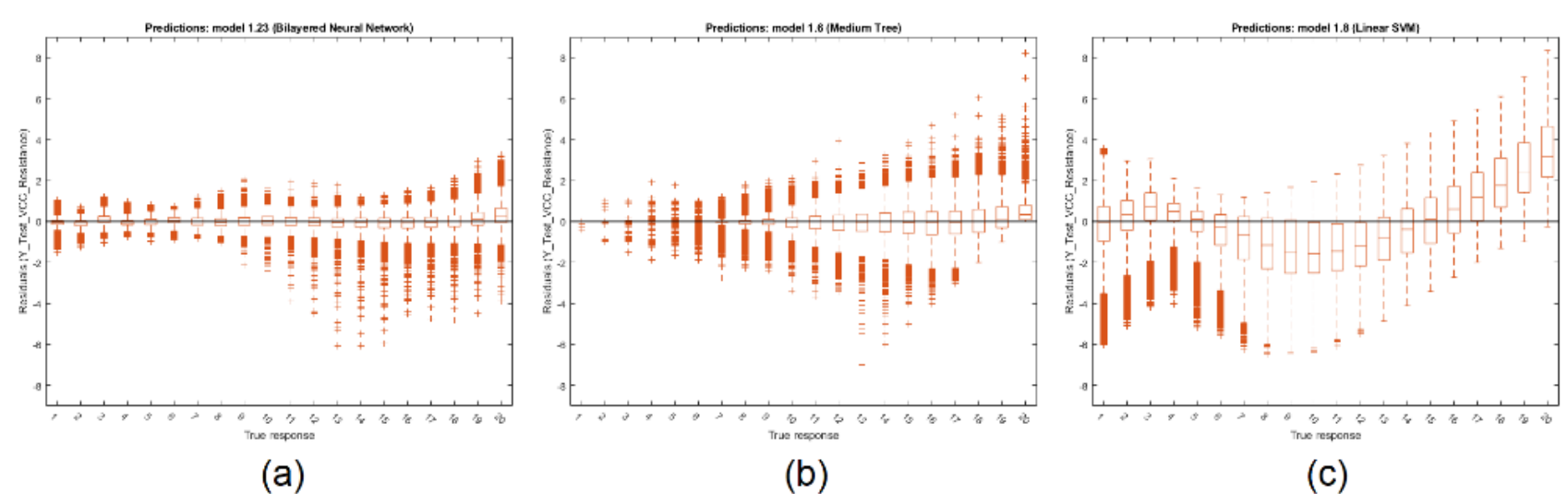


Figure 7-45: Residual Plots for Bi-Layered Neural Network (a), Medium Tree (b) and Linear SVM (c)

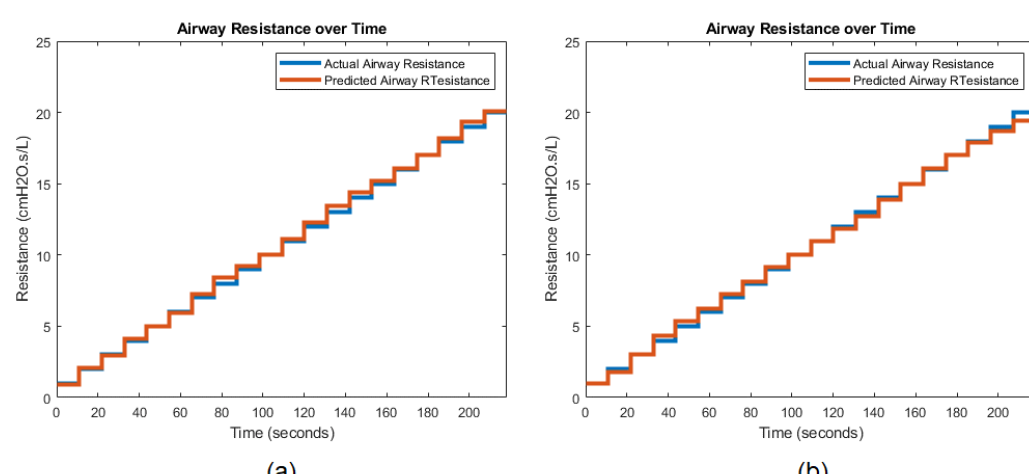


Figure 7-46: Predicted vs Actual Resistance Results for VCC (a) and VCD (b)